PILE BEHAVIOUR SUBJECT TO EXCAVATION-INDUCED SOIL MOVEMENT IN CLAY

ONG EK LEONG, DOMINIC

NATIONAL UNIVERSITY OF SINGAPORE

2004

PILE BEHAVIOUR SUBJECT TO EXCAVATION-INDUCED SOIL MOVEMENT IN CLAY

ONG EK LEONG, DOMINIC
(B. E. (*Hons.*), UWA)

A THESIS SUBMITTED
FOR THE DEGREE OF DOCTOR OF PHILOSOPHY
DEPARTMENT OF CIVIL ENGINEERING
NATIONAL UNIVERSITY OF SINGAPORE
2004

Acknowledgements

I would like to convey my heartfelt gratitude to my supervisors, Professor Chow Yean Khow and Associate Professor Leung Chun Fai for their advice, guidance, encouragement and patience shown to me over these years. Their valuable effort and time dedicated to this research are appreciated. Sincere thanks are also extended to Dr. Ting Wen Hui and Mr. Tai Lee Yoon for their confidence and belief placed in me in scaling greater heights in career and life. Their words of wisdom are greatly appreciated.

The research scholarship and financial support granted by the National University of Singapore (NUS) to make this research a reality and success are acknowledged. Special thanks are also extended to Mr. Shen Rui Fu (Professional Officer), Mr. Loo Leong Huat, Mr. Wong Chew Yuen, Mr. Tan Lye Heng, Mr. Choy Moon Nien, Mr. Shaja Khan, Mdm. Jamilah bte Mohd. (Laboratory Officers), Mr. Cheang Wai Lum, Mr. Cheng Ch'ng Yih, Mr. Lim Joo Kai, Dr. Lim Ken Chai, Dr. Goh Teik Lim, Dr. Wong Wai Kit, Mr. Leong Kam Weng, Ms. Zhang Xi Ying and Mr. Ran Xia (fellow Research Scholars and good friends) for making this journey of a lifetime more exciting, smooth, meaningful, colourful and less painful. A special thank you is also extended to Ms. June Ngo for her support and kind assistance in the compilation of this thesis.

I believe no words can describe the amount of patience, understanding and sacrifices made by my loving parents, brother and sister as well as my grandparents and relatives in seeing me through this research. You are the ones who have gone through thick and thin with me so that this lifetime dream of mine can be fulfilled. As such, I am now immortalising my heartfelt warmth, love and gratitude to you all in this thesis. I hope I have made you all proud!

Table of Contents

CHAPTER 3 EXPERIMENTAL SET-UP AND PROCEDURES

Summary

Centrifuge model tests have been conducted to study the effects of excavation-induced soil movement on the behaviour of a single pile and pile groups behind stable and collapsed walls in clay. The experiment results reveal that for an excavation in front of a stable retaining wall, the induced maximum bending moment and deflection on a single pile occur some time after the final excavation depth has been reached. On the other hand, the pile behaviour behind a collapsed wall is noted to be also time dependent but the responses depend on the degree of wall instability. After a critical excavation depth/time, the soil is observed to "flow" around the pile and the development of tension cracks and active wedge failure slip plane behind the wall exert significant influences on the pile responses.

It is found that as the number of piles in a group increases, the induced pile bending moment would reduce. Moreover, the peripheral piles in a group would experience larger bending moment than the interior piles as the former are more exposed to the moving soil. It is found that by capping a pile group, the piles would experience a smaller deflection at the expense of a large negative bending moment along the pile shaft. In addition, the behaviour of the rear piles is influenced by the front piles via the connecting pile cap.

A numerical model developed at the National University of Singapore is employed to back-analyse the centrifuge test data. The key parameters required by the numerical model include lateral free-field soil movement, subgrade modulus and limiting soil pressure. The numerical model provides a fair prediction of the induced pile bending moment, shear force, deflection and soil pressure profiles if the soil movement is not significant. For piles subject to large soil movement, the model can

predict the induced pile bending moment if the appropriate limiting soil pressure is adopted.

A field case study of full-scale instrumented pile group has also been carried out so that the responses of the pile group due to excavation-induced soil movement can be studied. Owing to heavy rainfall, an unintended failure of the excavation had occurred and this led to the failure of the pile group. The field data complements the experimental and numerical studies to provide further understanding of pile group behaviour subject to large lateral soil movement.

Keywords: Centrifuge model, Bending moment, Deflection, Free-field soil movement, Soil flow, Limiting soil pressure, Time dependent behaviour.

Nomenclature

$(EI)_{cap}$	Pile cap bending rigidity
$[F_s]$	Soil flexibility matrix
$[K_p]$	Assembled stiffness matrix of all the beam elements forming the piles
$[K_s]$	Stiffness matrix of soil
$\{P_p\}$	Vector of pile-soil interaction forces acting on pile
$\{P_s\}$	Vector of pile-soil interaction forces acting on soil
$\{y_o\}$	Vector of lateral soil movements at the pile nodes in the absence of piles
$\{y_p\}$	Vector of pile deflections
$\{y_s\}$	Vector of soil deformations at pile nodes
A	Cross sectional area
b	Breath/width
C_c	Compression index
C_s	Swelling index
c_u	Undrained shear strength
d	Depth of wall toe
D	Measured deflection
d’	Depth from compression zone to centroid of compression steel
D_i	Initial deflection at onset of cracking
E_c	Young’s modulus for concrete
E_pI_p	Pile bending rigidity
E_s	Young’s modulus of soil
E_{st}	Young’s modulus of steel
$f’_c$	Characteristic strength of concrete
f_{ct}	Tensile strength of concrete in flexure or modulus of rupture of concrete
f_{ij}	Flexibility coefficient denoting the lateral deformation of the soil at node i due to a unit pile-soil interaction lateral force acting at node j
f_{max}	Maximum pile head deflection
g	Gravitational field
G_s,	Specific gravity of soil
h	Thickness of pile cap
I_{cr}	Fully cracked moment of inertia

I_e	Effective moment of inertia
I_g	Gross moment of inertia
I_{uncr}	Uncracked moment of inertia
k	Coefficient of permeability
K	Limit yield pressure coefficient
K_a	Active earth pressure coefficient
k_c	Pile cap reduction factor
k_h	Modulus of subgrade reaction of soil
k_hd	Soil stiffness per unit length of pile
K_{onc}	Lateral earth pressure coefficient at rest for normally consolidated clay
K_{ooc}	Lateral earth pressure coefficient at rest for overconsolidated clay
K_p	Passive earth pressure coefficient
k_s	Soil movement moderation factor
K_T	Ratio of the measured total horizontal stress to measured total vertical stress
l	Pile element length
M	Slope of critical state line in q-p' space
M_{cr}	Pile cracking moment
M_{max}	Maximum pile bending moment
M_{ult}	Ultimate pile bending moment capacity
N	Total number of nodes
p'	Mean effective stress
P_s	Lateral force of soil acting on pile
p_s	Lateral soil pressures
P_{sj}	Pile-soil interaction lateral force acting at node j
p_y	Limiting soil pressures,
q_c	Cone resistance
R	Registration ratio between measured and applied vertical stress of a Total Stress Cell (TSC)
x	Distance of pile behind the wall
y	Distance from the centroid of the section to the extreme fibre in tension
y_o	Lateral soil movement
y_{oi}	Lateral soil movement at node i in the absence of piles
y_s	Soil deformation at the pile-soil interface
y_{si}	Lateral soil deformation at pile-soil interface at node i

Z	Section modulus
z_p	Depth of pivot point
Γ	Location of critical state line in compression plane
α	Coefficient as a function of excavation depth
β	Coefficient as a function of excavation depth
ε_c	Strains in compression
ε_t	Strains in tension
ϕ’	Effective friction angle
κ	Slope of unloading-reloading line in ν:ln p’ plane
λ	Slope of normal compression line in ν:ln p’ plane
ν	Poisson’s ratio
σ_h	Total horizontal stress
σ_h’	Effective horizontal stress
σ_v	Total overburden pressure
σ_v’	Effective overburden pressure
ψ	Curvature of pile

List of Figures

List of Tables

CHAPTER ONE

INTRODUCTION

1.1 BACKGROUND

The scarcity of land in Singapore has led engineers to maximize the utilization of underground space. Many of Singapore's underground infrastructures such as Mass Rapid Transit (MRT) tunnels and underground car parks are situated close to existing buildings. Buildings and infrastructures are normally supported by pile foundations to transfer the structural loads to the lower and more competent subsurface strata, especially in areas where soft marine clay is found in the upper soil layers. In many cases, these pile foundations are designed primarily to sustain vertical loads only. An existing pile foundation may experience additional bending moment due to excavation-induced lateral soil movement if a deep excavation is carried out nearby. Some typical scenarios of piles subjected to lateral soil movement include the followings:

(a) Piles used for slope stabilization [Fukuoka (1977), Sommer (1977) and Kalteziotis et al. (1993)].

(b) Piles supporting a bridge abutment near an embankment [De Beer and Wallays (1972), Schmidt (1977), Hull and McDonald (1992)].

(c) Piles adjacent to an excavation [Finno et al. (1991), Poulos and Chen (1997) and Chandrasekaran et al. (1999)].

An assessment of the magnitude of induced bending moment in the above cases is important to ensure the structural integrity of the pile is maintained. There are cases

whereby piles are purposely designed to restrain or limit lateral soil movement such as those installed for landslide prevention. For slope stabilization or landslide prevention purposes, piles are deliberately heavily reinforced so that they can withstand the lateral soil pressures exerted by the moving soil mass.

In urbanized areas where existing buildings and infrastructures are built very close to one another, any nearby excavation will cause a reduction of horizontal earth pressure on the side of excavation, leading to soil movement behind the retaining wall towards the cut. Besides that, the relief of vertical pressure due to excavation may also cause basal heave. The basal heave and the inward soil movement often cause ground subsidence around the excavation. If the excavation is carried out below the ground water level and if the coefficient of permeability of the soil is relatively high, the seepage-induced consolidation and drawdown may also cause problems (Lee et al., 1993). Owing to such phenomena in excavation works, excessive soil deformation in the retained soil can pose a serious threat to the retaining structure and nearby existing structures supported on pile foundations. Moreover, in low-lying areas around Singapore, the soil deposits consist of the marine member of the Kallang Formation. This soft marine clay typically has an undrained shear strength that varies with depth and sometimes less than 25 kPa. As such, the stability of a retaining structure supporting such soft marine clay is often problematic and can also induce significant ground movement behind the excavation.

Lateral soil movement would induce additional bending moment and deflection on adjacent existing piles and can have detrimental effects on existing pile foundations. If the excavation is very deep, such as that for the construction of a multi-storey basement car park or an underground subway station, the problem can become a very delicate issue. The shaft friction of the pile, which helps to carry the vertical load

imposed by the structures, will be reduced due to the reduction of the confining pressure around the piles as a result of ground deformation and settlement caused by the excavation.

Several case histories have been reported on pile foundations whose structural integrity has been threatened as a result of additional bending moment caused by excavation-induced lateral soil movement. Finno et al. (1991) described a case where a tie-back excavation was performed in granular soils. Despite being supported by a tie-back sheet pile wall, some pile caps had deflected by as much as 65 mm towards the excavation. This might induce additional bending moment on the pile group.

Poulos (1997) described a bizarre case history where an office building had to be demolished due to massive ground deformation. A nearby unsupported excavation had caused the office building to tilt excessively. Maximum settlement of about 900 mm was detected at one corner of the building. The horizontal movement at the top of the building was reported to be about 1.2 m. Grouting was carried out to arrest the settlement but was unsuccessful. Back-analysis was conducted and the results revealed that the pile structural capacity had been exceeded. Eventually, it was decided to demolish the entire office building in order to prevent possible collapse.

In view of the grave hazards associated with excavation near existing structures, it is vital for geotechnical engineers to develop a good understanding of pile behaviour due to excavation-induced lateral soil movement. Recently, researchers like Chen and Poulos (1997) as well as Chow and Yong (1996) have developed theoretical approaches to predict the pile responses in such situations. Design charts have also been established by Poulos and Chen (1996, 1997) to estimate the pile responses near an unstrutted and a strutted excavation.

It may not be economically viable in practice to conduct large-scale instrumentation and monitoring programs just to study the response of piles due to excavation. An alternative way is to conduct centrifuge model experiments whereby artificial gravitational field is employed to replicate the increasing stress with depth as experienced by the ground in the field. Under a well-controlled environment, centrifuge experiments provide the flexibility and repeatability that cannot be achieved in field tests. Researchers like Springman et al. (1991) and Stewart et al. (1994a) have successfully modelled and investigated bridge abutment pile behaviour due to embankment loading.

At the National University of Singapore (NUS), Shen (1999) performed centrifuge tests to investigate the behaviour of single piles and two-pile groups subject to excavation-induced lateral soil movement in dense sand. Lim (2001) extended the experiments to study the behaviour of two, four and six-pile groups in dense sand. The above experiments provided a fundamental insight to explain the pile behaviour subject to excavation-induced soil movement in sand.

1.2 OBJECTIVES OF STUDY

Soft clay is commonly found in Singapore and many other coastal cities around the world and its characteristics are very different from those of sand. The earlier studies at NUS on pile behaviour due to excavation-induced soil movement in sand are extended to that in clay in the present study. The objectives of the present study are as follows:

a) To carry out centrifuge model tests to study the behaviour of piles behind a stable retaining wall and a retaining wall that subsequently collapses as it is believed that the pile behaviour is affected by the stability of the retaining wall,

which in turn determines the degree of deformation of the retained soil, rates of progressive lateral wall movement and dissipation of excess negative pore water pressure over time. Theoretically, the stress state of the soil should vary after the start of excavation and as such, this research is dedicated to experimentally study these time-dependent variables on the behaviour of piles embedded in such soil.

b) To interpret the behaviour of free-head single pile as well as free-head and capped-head pile groups when subject to excavation-induced soil movement from the centrifuge test results. It is important to demonstrate using experiments to provide a fundamental understanding on how deforming soil over time would provide various stabilizing mechanisms, such as arching effect, in the presence of a single pile as well as various types of pile group configurations.

c) To evaluate the ability of an existing numerical model developed at NUS to back-analyse the centrifuge test results so that a better understanding of pile-soil behaviour can be achieved. It is hoped that this back-analysis would shed some light on the (i) ratio of undrained shear strength (c_u) to limiting soil pressure (p_y), (ii) validity of measured free-field soil movement to be used in the back-analysis and (iii) the effect of pile cap fixity on the back-analysed results. Hence, this exercise also serves to calibrate the existing numerical model and also to complement the previous studies carried out on pile behaviour subject to excavation-induced soil movement in sand.

d) To carry out a field case study on a pile group nearby an excavation and to compare the field observations with the predictions made from the existing numerical model. It is hoped that through this field study, the assessment of the

development of moment of inertia of the pile and the pile bending moment capacity, issues which are of great importance but are often given less attention by practicing engineers, would be addressed. This field study would also serve to complement the understanding developed in (a), (b) and (c) above so that a comprehensive research that encompasses centrifuge experiments, numerical back-analyses and practical field case study can be achieved wholesomely.

1.3 OUTLINE OF THESIS

The outline of this thesis is as follows:

a) Chapter 2 presents an overview of the causes of lateral soil movement and existing research studies similar to the present research, with special emphasis on the pile behaviour subject to excavation-induced lateral soil movement.

b) Chapter 3 highlights the centrifuge experiment set-up and procedure. Some new and improved instrumentation techniques such as non-contact laser displacement transducers for measuring pile head deflection are described. The effects of simulating an excavation using the method of draining a heavy fluid of equal unit weight as the soil it replaces are also discussed in detail.

c) Chapter 4 discusses the centrifuge experiment results of the short and long term behaviour of a single pile behind a stable wall and a wall that subsequently collapses.

d) Chapter 5 presents centrifuge test results of 2-, 4- and 6-pile groups behind a stable wall and a wall that subsequently collapses. The behaviour of free- and capped-head pile groups as well as the soil deformation patterns surrounding the piles are discussed in detail. In addition, the wall and soil deformation

behaviour as well as the time dependent pile responses during and after excavation are discussed.

e) Chapter 6 presents and discusses the comparison between centrifuge test results and back-analysed numerical predictions obtained using an existing program developed at NUS. The importance of input soil properties is discussed with particular emphasis placed on the undrained soil strength and the limiting soil pressures. The effect of rotation of the pile head on the performance of the pile group is also presented.

f) Chapter 7 presents the results of a large-scale field test on a 4-pile group nearby an excavation. Comparisons between the predicted pile behaviour using an existing numerical method and the field observations are made.

g) Chapter 8 concludes the findings of the present study.

CHAPTER TWO

LITERATURE REVIEW

2.1 INTRODUCTION

Lateral soil movement would induce additional bending moment and deflection on adjacent pile foundation. If the induced bending moment is unaccounted for in the design, structural integrity of the piles may be compromised. Hence, it is of great importance to understand the effects of lateral soil movement on piles. Generally, lateral soil movement may be caused by embankment loading, unstable or creeping slopes, tunnelling and excavation. The methods, effects and difficulties faced in investigating the behaviour of piles subject to lateral soil movement will be reviewed in detail in this chapter. The review is presented in the first half of this chapter and divided into three main sections; namely, (a) field studies, (b) theoretical predictions and (c) laboratory experiments. In addition, the effects of soil "flow" and its associated limiting soil pressure on piles are presented. Methods of simulating excavation at high-g level and the stability of excavation over time are also reviewed.

2.2 FIELD STUDIES

A good number of field case histories to study the effects of soil movement on piles have been reported. These studies will be reviewed briefly in this section.

2.2.1 De Beer and Wallays (1972)

De Beer and Wallays (1972) reported a field test at Zelzate, Belgium to study the influence of a sand embankment on instrumented test piles shown in Figure 2.1. Four test piles were installed at the toe of the embankment. One of the piles was a steel tube of 900 mm diameter and 28 m in length with wall thickness of 15 mm. The other three piles were reinforced concrete piles of diameters 600 mm, 450 mm and 350 mm. The length of the reinforced concrete piles was 23.2 m. Only the steel pile and the 600-mm diameter reinforced concrete pile were fully instrumented to measure the pile stresses and strains, deflection and soil displacement. The soil profile, which was predominantly sand, is shown in Figure 2.2 together with the measured horizontal movement of the soil due to the embankment construction. The maximum soil movement was about 60 mm near the ground surface and decreased rapidly with depth. A maximum bending moment of 280 kNm was developed in the pile shaft. As the pile head had been rigidly restrained, the observed pile head deflection was negligible. However, a maximum pile deflection of about 20 mm was noted at about 5 m depth. It was further observed that as the computed factor of safety decreases due to increasing embankment height and hence greater lateral soil movement at the embankment toe, greater pile bending moment was observed. Therefore, it has been demonstrated from this case study that soil movement would induce additional bending moment and deflection in adjacent piles.

2.2.2 Marche (1973)

Marche (1973) discussed the results of a reported loading test in Amsterdam. The load test set-up is given in Figure 2.3. Three steel test piles, each consisting of an open rectangular section and a length of 12.5 m, were driven at 5 m centre-to-centre spacing into peat, clay and sandy clay and founded on the firm sand stratum. The pile

head was restrained using a structural beam at the ground level. The embankment was built with each height increment of 5 m. The displacement of the pile head was prevented by means of struts propped at the ground level against a concrete beam supported by 8 raking piles in front of the embankment. The stresses in the piles were measured by strain gauges. The maximum induced bending moment recorded as a function of the pile distance is shown in Figure 2.4. Figure 2.5 shows the displacements induced in the underlying stratum after each height increment of 5 m. The results indicated that the pile bending moment increased with increasing distance between the embankment toe and the pile. In addition, the displacements of the pile and soil were not significantly different. It was concluded that the reaction frame did not successfully prevent the soil movement, which had induced additional bending moment onto the test pile. It is observed that relatively large negative bending moment was developed in pile head when the pile was restraint by the ground beam.

2.2.3 Hannick and van Tol (1988)

Hannink and van Tol (1988) reported that 41 terrace houses at the north side of a quay in Rotterdam, the Netherlands, have been subjected to large lateral soil movement, some as much as 2.5 m since 1958. The cause of the lateral soil movement was due to an unstable quay nearby. As a result, the piles supporting the terrace houses had deflected to such an extent that complete failure was feared. It was also reported that the maximum rate of soil displacement was about 0.10 m/year. The cross section of the quay is shown in Figure 2.6. Figure 2.7 details the magnitude of the lateral displacements experienced by some of the houses for a period of up to 4 years. It was concluded that the foundation piles offered no resistance against the creeping quay and that the stresses in the foundation piles had far exceeded the allowable values. It was feared that the foundation piles would soon experience complete failure unless

remedial measures were taken immediately. This case study highlights the importance of designing piles to withstand horizontal soil movement.

2.2.4 Coutts and Wang (2000)

Coutts and Wang (2000) instrumented six 1200-mm diameter bored piles supporting a vehicle viaduct to obtain the pile responses when the tunnel boring machine (TBM) approached or moved away from the instrumented piles. The piles for the viaduct were already constructed before the start of the tunnelling process. The instrumentation programme consists of in-pile and in-soil inclinometers and vibrating wire strain gauges. The layout of the instruments is shown in Figure 2.8. Anticipating that the ground surrounding the tunnel would deform, the bored piles were heavily reinforced to increase their bending moment and tension capacities. Typical reinforcement consisted of 20 T25 longitudinal bars with T16 link at 175 mm centres over the top 20 to 30 m of the piles. The results revealed that the maximum forces and stresses were recorded when the TBM was directly adjacent to the piles.

The measured maximum bending moments and the moment as percentage of design working moment are shown in Table 2.1. The results revealed that the piles underwent bending in directions both parallel and perpendicular to the line of the tunnels. In general, the maximum bending moments were recorded at invert and crown levels. Approximately 91% and 59% of the design working axial load and bending moment, respectively, of the pile had been reached due to the tunnelling process alone. Had the piles not been adequately reinforced to cater for the anticipated additional bending moment due to tunnelling, they would have been substantially damaged, even before the full load of the viaduct superstructure was imposed on the piles. However, despite many inclinometers had been installed in the ground, no soil movement data was presented. The importance of pile-soil interaction is highlighted in this case study.

Significant additional pile bending moment and deflection can be expected due to a tunnelling process nearby.

2.2.5 Poulos (1997)

A well-documented field case study on the effects of excavation on nearby pile foundations was presented by Poulos (1997). Poulos (1997) reported the failure of piles supporting a building due to excessive ground movement arising from an uncontrolled and unsupported excavation close to one corner of the building. The project involved the construction of three buildings; namely, an office block, a hotel and a shopping centre in Indonesia. A nearby building had to be demolished due to the continual increase in settlement that caused it to tilt. Poulos summarized the available geotechnical and foundation data for the project and evaluated the various possible causes of settlement. The plan of the project and the borehole locations are shown in Figure 2.9. The borehole information is shown in Figure 2.10. The foundations for the buildings consisted of cast-insitu piles, 0.5-m nominal shaft diameter and 20 m in length. Vertical and lateral load tests were carried out and the piles generally performed satisfactorily.

Both the office and hotel buildings were completed and no undue settlement was noted. Subsequently, piling work for the shopping centre building was undertaken between the two completed buildings. At the same time, an excavation adjacent to the shopping centre was carried out for the placement of a ground tank. The excavation was unsupported and extended to depth of 4 m. Before the excavation was completed, massive ground movement was observed. The contractor decided to stop the excavation and subsequently backfilled the excavated ground. The backfilling process took about three months.

During backfilling, the soil was merely dumped into the excavated ground without proper compaction. Consequently, the nearby ground continued to move towards the excavation over a period of two months. This resulted in a large area (approximately 36 m by 22 m) surrounding the excavated area being affected by soil settlement. The office building was found to have tilted towards the shopping centre site with a maximum settlement of about 900 mm. The horizontal movement at the top of the building was reported to be about 1.2 m. In view of this, grouting was carried out to arrest the settlement but this remedial action was unsuccessful. Eventually, it was decided to demolish the office building in order to prevent possible collapse. Nevertheless, no substantial movement was observed at the hotel site where the ground was undisturbed. However, substantial movement was observed for the newly installed free head piles for the shopping centre. The piles, which were located about 2 to 3 m from the line of excavation, had moved more than 1 m towards the excavation. Besides that, settlement of about 50 to 60 mm was also noted for these piles.

Numerical analysis was also carried out to further study the effects of excavation on the piles. The analysis revealed that the pile head movement increased with increasing soil movement until the soil movement reached about 200 mm. It was postulated that at this stage, the soil might have just flowed past the pile and thus the pile did not experience any further movement. Figure 2.11 shows the maximum bending moment induced on the pile due to soil movement. A maximum bending moment of about 380 kNm had developed. For these piles having an unrestrained head, the maximum deflection occurred at the pile head while the maximum bending moment and shear occurred at a pile shaft elevation near the base of the soft soil layer. The maximum bending moment calculated from the numerical analysis was then compared with the structural capacity of the pile section. Figure 2.12 shows the

computed axial force and bending moment in the pile and clearly reveals that the structural capacity of the pile section is far exceeded, even for the case where ultimate steel and concrete strengths are used.

Figure 2.13 compares the maximum bending moment and axial load computed from the horizontal soil movement acting on the capped pile of the office building with the structural capacity of the pile section. Again, the pile capacity was found to have been far exceeded.

There was sufficient evidence to suggest that the failure of the pile foundations was directly associated with attempts made to carry out an unsupported excavation near the existing office building and shopping centre. It was also suggested that horizontal movement caused by such excavation could have caused overloading and eventual structural failure of the piles supporting the building. However, the mechanisms of large strain soil deformation behaviour on adjacent piles due to excavation have not been fully understood. Owing to such detrimental effects of an excavation on existing pile foundations, the present research project is deemed necessary so that a better understanding on pile-soil interaction can be obtained.

2.3 THEORETICAL STUDIES

Bransby and Springman (1996) studied the short term behaviour of pile groups subjected to lateral pressure caused by the deformation of a clay layer under an adjacent surcharge load using a three-dimensional finite element method. The clay was modelled with three different constitutive models namely; elastic, plastic and Cam Clay. The pile group was represented by linear elastic elements. The sand was modelled using Mohr-Coulomb elastic-plastic soil with an associated flow rule. The results were then compared with centrifuge test data. It was reported that the results

were in good agreement, although the finite element analyses over-predict the pile group displacements at small surcharge loads. Nevertheless, it had shed some light on problems involving passive lateral loading on piles as well as understanding the behaviour of soil-pile interaction. However, its use is still rather limited in practice due to the computation time required for the analysis, unless specific quantities had to addressed, which are not capable to be modeled in 2-D simulations.

Stewart et al. (1994a) presented empirical design charts based on centrifuge test data to determine the maximum pile bending moment and pile head deflection as a function of the relative soil-pile stiffness and the current loading level based on limited field data and centrifuge results.

Poulos (1994) developed design charts with the provision of maximum positive and negative bending moments, lateral pile head deflection, axial force and axial pile head deflection of a pile within an embankment. They were called the “CPI” charts. In this method, the piles were assumed to be installed after the embankment had been constructed. The bending moment and deflection developed in such piles might be substantially less than those developed in piles installed before the construction of embankment.

De Beer and Wallays (1972) presented a simple empirical formula to calculate the horizontal pressure acting on a pile when an embankment was being constructed. In order to calculate the induced bending moment, assumptions had to be made concerning the lateral support of the piles. The proposed method was very rough and the aim was to obtain an estimate of the maximum bending moment. This method could not be used to estimate the bending moment profile along the pile and hence, the pile has to be reinforced over the whole length for the calculated maximum bending

moment. Furthermore, this method is only applicable if a large factor of safety is used for the overall stability of the embankment.

Mroueh and Shahrour (1999) carried out a study on the influence of construction of shallow tunnels on pile foundations using the finite element program PECPLAS. The soil behaviour was assumed to be governed by an elastic-perfectly plastic constitutive relation based on Mohr-Coulomb criterion with a non-associated flow rule. The numerical modelling was carried out in two stages. In the first stage, an axial load was applied. The second stage involved the construction of the tunnel in the proximity of the pile. A free-field condition (i.e. without the presence of the pile in the ground) was also analysed. The results revealed that the presence of the pile reduced the settlement of the ground by about 50 %. Figures 2.14(a) and (b) show that the pile lateral movement and the development of bending moment are very much dependent on the distance between the tunnel face and the pile axis. The influence of the position of the pile tip with regard to the tunnel axis was also observed to be very much related. As tunnelling could cause inevitable soil movement, the consequence was that the pile internal forces tend to increase and sometimes certain section of the pile tended to exceed the section capacity of the pile, as illustrated in Figure 2.15. This is an important finding and is in line with the objective of the present research, which focuses on pile behaviour subject to excavation-induced soil movement.

Poulos and Chen (1996, 1997) described a two-stage analysis involving finite element and boundary element methods to study pile responses due to excavation-induced lateral soil movement, focusing on unsupported and braced excavation in clay. In the simplified form of boundary element analysis, the pile was idealized as an elastic beam and the soil as an elastic continuum, but with limiting pressure at the pile-soil interface to allow considerations of local failure of the soil adjacent to the pile. In

the finite element method, the computer program AVPULL was used for the analysis. The soil was modelled as an elasto-plastic material, governed by the Tresca failure criterion and a non-associated flow rule. The computed lateral soil movement from the finite element analysis was then used as input to the boundary element program to determine the pile responses. The predicted maximum pile bending moment and deflection showed fair agreement with existing measured field data. However, the boundary element method has a major limitation that it can be only performed on a single pile and a group with non-identical free-head piles, but cannot handle capped pile groups.

Free-field displacements are motions of the soil that occur at a distance from the pile such that the displacements are not affected by the presence of the pile. A free-field soil displacement method, in which a pile was represented by beam elements and the soil was idealized using the modulus of subgrade reaction, was proposed by Chow and Yong (1996). The magnitude of soil movement profile serves as input for the method. With this idealization, non-homogeneous soil can be easily treated. This approach requires the knowledge of the pile bending stiffness, distribution of lateral soil stiffness and the correct limiting soil pressure acting on the pile with depth. Comparisons with available well-documented case histories suggest that the method gives reasonable prediction of the general behaviour of pile foundations experiencing lateral soil movement. This numerical method will be used to back-analyse the centrifuge results in the present study.

Byrne et al. (1984) proposed a simple method of analysis by modifying the conventional laterally loaded pile problem to predict the pile responses due to lateral free-field soil displacements. The method involved representing the stiffness of the soil with non-linear springs, with the outer ends of these springs attached to the free-field

so that a movement of the free-field resulted in a deflection of the pile. The governing differential equation for the pile was solved by iteration so that the bending moment, shear force and deflection of the pile could be estimated. However, this method does not consider the continuity of the soil and depends on an accurate input of the spring stiffness and the magnitude of free-field soil displacements. As such, a more reliable and efficient method is necessary to consider the various types of soil profiles common in practice.

Viggiani (1981) derived dimensionless solutions for the ultimate lateral resistance of a pile in a two-layer cohesive soil profile, in which six possible failure modes were suggested. Piles whose yield moment was larger than the bending moment acting upon them were considered as rigid piles, and three possible soil failure modes were proposed. Another three possible failure modes were proposed for more flexible piles, whose yield moment was smaller than the bending moment acting upon them. A pile-soil contact pressure distribution was assumed for each failure mode and the shear force and bending moment in the piles were derived by satisfying force equilibrium conditions accordingly. These solutions are limited to cohesive soil only, can only be applied to the ultimate state and are confined to a simplified representation of the distribution of soil movement with depth. However, a more versatile approach, which overcomes these deficiencies, has been described by Poulos and Davis (1980) by making use of a simplified form of boundary element analysis to obtain the solution. Therefore, the method proposed by Viggiani (1981) has limited use in practice.

Chen and Poulos (1997) presented a theoretical procedure for analyzing pile responses subjected to lateral soil movement. The pile lateral responses are computed using a boundary element analysis, utilizing the specified free-field soil movement profile. It is concluded that this method gives reasonable good estimation of the pile

responses after comparing the results with model tests and published case histories. Nevertheless, this method is only accurate for relative small soil movement. Relatively large soil movement can also be expected during excavation in practice and therefore, it is necessary to have a versatile method capable of predicting the pile responses regardless of the magnitude of the soil movement.

2.4 LABORATORY STUDIES

A good number of laboratory studies on the effects of soil movement on piles have been reported. These studies are divided into 1g model and centrifuge tests and will be reviewed in this section.

2.4.1 1g model tests

Fukuoka (1977) reported a small-scale model study with an instrumented pile installed in an iron box filled with soil. The model pile had a rectangular cross-section and was instrumented with strain gauges along the shaft. The iron box had dimensions of 100 mm x 200 mm in plan view. A jack was used to apply a uniform soil movement to the upper portion of the model pile. The study showed that the pile deflection profile was dependent on the flexural rigidity of the pile. This finding is important to this research so that care will be taken during the fabrication of the instrumented model piles.

Matsui et al. (1982) carried out a model study on piles subject to soil movement in both clay and sand. The test equipment consisted of three parts, an air pressure control device, a main body of the apparatus and recording systems as shown in Figure 2.16. The main model consisted of a soil container box with the model pile and a laterally loading system. The interior dimension of the steel box measured 600

mm long, 300 mm wide and 300 mm deep. The deforming soil around the piles could be viewed through a strengthened glass plate. The soil in the box could be horizontally moved by providing different pressure through the loading systems. The experimental results were then compared to theoretical predictions, whereby a reasonable match was obtained. However, there was no explicit mention on how a vertical confining was applied in the experiment. Since this experiment was done in a 1g environment, it is suspicious if the stress-dependent soil properties that vary with depth are correctly accounted for.

A series of small-scale laboratory tests on single instrumented model piles embedded in calcareous sediments undergoing lateral movement were reported by Poulos and Chen (1995b). The main part of the test apparatus consisted of a testing vessel, made of steel sheet with dimensions of 450 mm wide, 565 mm long and 700 mm deep as shown in Figure 2.17. The vessel was equipped with steel plates capable of rotating and creating a triangular soil movement profile. Instrumented aluminium piles with different diameters of 25 mm, 35 mm and 50 mm were used. It was found that under a constant soil density, the maximum pile bending moment was dependent on the pile head fixity condition, the ratio of pile embedded length in the upper moving soil layer to the pile length in the lower stable soil layer, pile diameter and pile stiffness. Normalised expressions for pile bending moment caused by different amounts of soil displacements were also derived. Boundary element analyses showed good prediction of the experimental results. The same apparatus was used by Chen and Poulos (1997) to study pile groups subjected to a linearly varying distribution of horizontal soil movement with depth. Tests were conducted on groups of free-head piles and groups of piles connected by a rigid cap. The extent of the group effect was

found to be dependent on a number of factors, including the position of the pile in the group, the pile spacing, the number of piles and the head fixity condition.

2.4.2 Centrifuge experiments

A good number of studies have been done on the centrifuge to examine the effects of lateral soil movement caused by embankment loading on piles supported bridge abutments in soft clay deposits. When an embankment on soft clay forms an approach to a piled bridge abutment, time dependent movement within the clay may induce significant lateral loading and deflection on the piles. In severe cases, structural distress to the piles may be detected. Embankment loading on the piled bridge abutments on soft clay is probably the most widely centrifuge experiments done to date to study pile behaviour subjected to lateral soil movement; see for example Springman et al. (1991), Stewart et al. (1994a, 1994b), Bransby and Springman (1997) and Ellis and Springman (1998).

Springman et al. (1991) carried out a series of centrifuge tests to investigate the effect of surcharge loading on a single row of free-headed piles and on a pile group. A parametric study was also carried out to investigate the effect of different pile spacings for the free-headed piles with two types of head fixity and three foundation layouts. In prototype scale, the sub-soil condition consisted of a 6 to 8 m thick soft clay underlain by 8 to 10 m of sand. The instrumented model piles were made of aluminium tubes with 12.7 mm diameter and wall thickness of 1.219 mm. The embankment was modelled by means of a normal surcharge load, controlled by an inflatable latex bag at the location of the proposed embankment. The centrifuge data was used to verify or to complement the theoretical and numerical solutions such as SIMPLE and SLAP and reasonable agreement had been achieved. Bransby and Springman (1997) attempted to investigate the behaviour of pile groups when adjacent surcharge loads were applied

over a clay layer using the same method as Springman et al. (1991). The pile cap was in contact with the surface of the deforming soil and interaction was detected, in addition to the soil-pile interaction, as shown in Figure 2.18. Two types of model tests were conducted, namely a normal foundation and a buttonholed foundation with piles surrounded by an annulus of bentonite in the deforming soil layer. Comparison between the two sets of results revealed that buttonhole foundations reduced the lateral pile group deflection due to passive lateral pile loading. Stewart et al. (1994a, 1994b) reported a series of centrifuge tests on piled bridge abutment shown in Figure 2.19. Responses of flexible piles, pile rake and embankment geometry were the main focus. A sand hopper was designed to construct the embankment in-flight in stages. It was found that the factor of safety of the constructed embankment was critical in determining the response of the piles. Ellis and Springman (2001) carried out similar tests in the centrifuge and subsequently attempted to predict the responses of pile group using finite element analyses. A sand hopper was used to simulate the embankment construction. Vertical drains were used to speed up the consolidation process. Multi-filament polyester strings were twisted to diameter of 1.5 mm (150 mm prototype scale) to simulate vertical drains. It was noted that the lateral displacement of the clay underneath the embankment generated shear stress on the interface with the fill material. The underside of the pile cap also attracted this form of ‘shear transfer’ loading, which was predominantly the result of undrained shearing. Soil arching effect was also noted, thus causing additional lateral loading on the pile group and the FEM analyses were particularly useful in identifying this phenomenon. It was then concluded that the agreement between the centrifuge results and the FEM analyses were good. Even though the research projects described above were done to study the effects of embankment loading on adjacent pile foundations, the modelling principles

and methodologies are quite similar and thus can be used as a preview, guide and checklist for the present study to ensure the successful execution of centrifuge experiments to study the pile behaviour subject to excavation-induced soil movement.

Almeida et al. (1985), Davies and Parry (1985), Ismes and Taylor (1991) and Bujang et al. (1991, 1993) shed some light on the time dependent behaviour of clay during and after the construction of an embankment without piles. This may be useful especially in understanding the time dependent effect of excess pore water pressure on pile behaviour. Bransby and Springman (1997) studied this phenomenon by observing the pile behaviour throughout their experiments and reported that the pile bending moment, shear force and lateral soil pressure varied with time. Nonetheless, no further investigation into the time dependent pile behaviour has been done. The research has highlighted that the time dependent pile behaviour may be associated to the dissipation of excess of pore water pressure. As such, the present research will investigate this further for the case of excavation.

Loganathan et al. (2000) carried out centrifuge experiments on single pile and pile group subject to tunneling-induced ground deformation in clay shown in Figure 2.20. The tunnel diameter was controlled and reduced by pumping away the oil in the annulus between the inner core and the membrane to simulate ground loss. Tunnel depths were then varied in each test to assess the influence of tunnel depth on ground movement and pile responses. The results revealed that the induced maximum pile bending moment and ground loss could be described by a near linear relationship. As such, it was postulated that an elastic analysis can be performed to predict pile behaviour induced by tunnelling if the ground loss value was less than 5%. Besides that, the induced pile bending moment and lateral deflection of adjacent piles may be critical when the tunnel central line is located at or near the pile tip level. From the

studies, it has also been shown that any lateral soil movement and settlement caused by tunnelling could induce bending moment and axial forces on an adjacent pile. The measured ground movement generally compared well with the analytical solutions presented.

At the National University of Singapore (NUS), centrifuge model tests have been carried out by Shen (1999) and Lim (2001) to study the responses of a single pile and pile groups due to excavation-induced soil movement in sand. It was reported that the induced bending moment on the piles increased with excavation depth. However, when the wall collapsed resulting in large lateral soil movement, the induced bending moment did not increase accordingly. It was postulated that the sand just flowed around the pile without exerting any additional load on the piles after the wall had failed. Lim (2001) also pointed out that if clay was used instead of sand, the pile bending moment and deflection reduced over time in the case of a collapsed wall. This sets the platform for the present research to study the time dependent behaviour of a single pile in clay subject to lateral soil movement in clay.

Thus far, it has been observed from the above literature review that additional induced bending moment on existing pile foundations can arise from lateral soil movement, be it due to embankment loading or tunnelling. If some cases, additional induced pile bending moment can be so large that the pile ultimate bending moment capacity is exceeded. Besides embankment loading and tunnelling, lateral soil movement can also arise due to excavation. However, not much studies on the effects of excavation in clay on existing pile foundations have been done when compared to embankment loading. Therefore, this highlights the importance and necessity to perform an in-depth research on the behaviour of piles subject to excavation-induced

soil movement to complement existing findings based on research on embankment loading.

2.5 CENTRIFUGE MODELLING OF EXCAVATION

In the preceding sections, existing field, theoretical and laboratory studies on pile behaviour due to lateral soil movement have been reviewed. As the present study involves a centrifuge model study on pile behaviour due to excavation-induced soil movement, existing methods of modelling of excavation in the centrifuge will be reviewed in this section. Centrifuge modelling is deemed to be more attractive to study soil excavation. Being a small scale model it is relatively inexpensive to perform and the tests can be repeated under controlled and well-instrumented conditions. Thus the behaviour of the retaining wall and associated ground movement can be examined thoroughly.

2.5.1 Methods of simulating excavation

Generally, there are three methods to simulate excavation in centrifuge model tests. In the first method, the model excavation is carried out at 1g and the centrifuge model is then subjected to increasing centrifugal acceleration until the retaining wall fails. The second method involves replacing the excavation area with a heavy liquid of equal unit weight as the soil at 1g. The release of the heavy fluid, typically Zinc Chloride ($ZnCl_2$) solution, simulates the progress of excavation. Such a method has been used by Katakami et al. (1998), Bolton and Powrie (1987, 1988) in Cambridge, Lee (1995), Wei (1997), Shen (1999) and Lim (2001) in NUS. The third method utilizes an in-flight excavator to perform the excavation process. This method has been used by Kimura et al. (1994) and Kongsomboon (2002).

2.5.2 Lateral soil pressure due to $ZnCl_2$

The lateral earth pressure due to $ZnCl_2$ is different from that due to soil and hence requires further consideration. Bolton and Powrie (1987) discounted the high in-situ lateral earth stresses in an overconsolidated clay deposit (for example, London clay) as they postulated that the slurry trench phase of the diaphragm wall construction was certain to alter them significantly, as observed by Powrie (1985). It was also postulated that the boundary stresses were approximately consistent with that imposed by the $ZnCl_2$ solution after reconsolidation in the centrifuge. In addition, Powrie (1986) noted that the measured bending moment measured in a more flexible wall embedded in overconsolidated clay during the reconsolidation stage was relatively small, indicating that $K_o = 1.0$ was quite closely achieved behind a more flexible wall, similar to the K_o value imposed by the $ZnCl_2$ liquid.

The important findings from these researchers increase the confidence level of modelling excavation using $ZnCl_2$ since it has been recognized that for overconsolidated clay, the effect of substituting it with $ZnCl_2$ for the purpose of excavation does not necessarily adversely affect its initial stress condition prior to excavation after the reconsolidation stage in a centrifuge environment.

2.5.3 Soil condition during and after excavation

Bolton and Powrie (1987) studied the collapse of diaphragm wall embedded in overconsolidated clay. Subsequently, the study was extended to the behaviour of diaphragm walls in overconsolidated clay prior to wall collapse (Bolton and Powrie, 1988). In both series of experiments, the excavation process was simulated by the draining of $ZnCl_2$.

Bolton and Powrie (1987) established that unpropped walls usually require large embedment depths for stability. Tension cracks would occur between the retained

soil and wall after excavation. It was observed that the flow rate of water flooding the tension cracks determined the rate of soil movement. As the passive resistance of the clay was not sufficient to sustain the full height flooded cracks, the wall started to fail by rotation at a pivot slightly above the wall toe. However, if the soil remained in contact with the wall, the development of large negative pore water pressure or suction in the soil next to the wall could maintain short term equilibrium of the wall. Subsequently, the failure mechanism of the wall was governed by the rate at which the soil could shear or slide along the rupture surfaces. The boundaries of significant soil movement and ruptures lied about 45^{o} drawn from the base of the wall, indicating an undrained failure. The phenomenon of progressive wall failure was also highlighted, as the local slippages that occurred on the rupture surfaces tended to reduce the height of the retained soil and thus increased stability. However, the suctions generated in the soil during and after excavation caused an initial increase but subsequent gradual decrease in soil strength. These two processes continued to occur as the wall tilted progressively during and after excavation, leading to the time dependent effect analogous to observations noted by Stewart (1992) as well as Bransby and Springman (1997) in their research on behaviour of piles adjacent to an embankment.

Bolton and Powrie (1988) presented the behaviour of diaphragm wall in clay prior to collapse using the same excavation method. Based on the measurements of soil displacement vectors during excavation, kinematically admissible strain fields were derived to idealize the soil behaviour in terms of uniformly deforming triangles. The mobilization of shear strain was also measured and displacements calculated during and after excavation using an appropriate assumed idealized strain field.

From the review, it can be surmised that soil deformation behaviour associated with excavation includes the development of tension cracks, generation of negative

pore water pressure, progressive failure, significant soil movement and ruptures surfaces of 45^{o} from the base of the wall. Therefore, with prior knowledge of the deformation behaviour of the wall and the retained clay, anticipation of specific observations from the author's experiments can be easily and readily made so that consistency in observations between existing and new findings can be achieved.

2.6 ESTABLISHED FINDINGS

At this juncture, the findings from existing studies relevant to the present study are summarised. Stewart (1992) as well as Bransby and Springman (1997) reported time dependent pile behaviour in their centrifuge modelling of pile groups adjacent to a piled bridge abutment. Stewart (1992) observed the increase in pile bending moment over time occurred essentially under undrained conditions due to a number of factors, which would lead to an increase in subsoil displacement. These factors are redistribution of pore water pressure, progressive shearing, stress redistribution and local soil consolidation around the piles. Bransby and Springman (1997) further reported that the increase in pile bending moment over time (see Figures 2.21 and 2.22) was due to the pile-soil-pile interaction, which led to an increase of average total stress around the front row piles and a decrease of total stress around the back row piles. It was also reported that as the clay consolidated further under the surcharge load, further lateral soil movement and pore water pressure redistribution were noted, hence the increase in pile bending moment (see Figure 2.23), shear forces and lateral pile pressure. Since the present study involves excavation in clay, which is critical in the long-term, it would be interesting to investigate the presence of any time dependent pile or soil behaviour.

The effects of soil flow on slope stabilizing piles have been reported by Ito and Matsui (1975). They established that plastic soil flow velocity and viscosity are important parameters in studying the visco-plastic soil behaviour and this concept is distinctly different from soil plastic deformation. These two parameters would significantly influence the undrained loading on a pile when a soil mass flows past the piles. They showed that the soil pressure acting on the piles increased with increasing product of soil flow velocity and viscosity (see Figure 2.24) when all other parameters are held constant. However, these parameters are notoriously difficult to measure. Nevertheless, it is important to acknowledge that the theory of plastic flow has been attempted to back-analyse field results but without much success.

Randolph and Houlsby (1984) analyzed the limiting pressure on a circular pile loaded laterally in a cohesive soil using cavity expansion theory. Their results compared well with the exact calculation of load acting on a long cylindrical pile which moved laterally through an infinite medium, where the soil was modelled as a perfectly plastic cohesive material with shear strength independent of the current total stress level. Randolph and Houlsby (1984) further reported that as the pile was pushed laterally through the soil, a region of high mean stress would occur in front of the pile and a region of low stress behind the pile. Therefore, the soil would flow around the pile from front to back. Characteristic meshes are used to represent the slip lines or planes on which the maximum shear stress occurs for the extreme cases for smooth pile ($\alpha = 0$) and for fully rough pile ($\alpha = 1.0$) as shown in Figure 2.25. Soil “flow” and its associated limiting soil pressure are important phenomena in the study of geotechnical failure conditions and this will be referred to in the author’s experiment involving a collapsed wall.

Maugeri et al. (1994) reported that by using the measured soil movement profiles obtained from inclinometers, bending moment and shear forces could be computed. A reduction of soil movement must be considered in this case because of the interaction between the rows of piles and the moving soil itself. By reducing the soil movement by 60% due to the reinforcing effect of the piles in the moving soil, better prediction of pile bending moment and shear forces could be obtained. It was also mentioned that since the moving soil had generally yielded, the numerical prediction would not be significantly affected by the soil subgrade modulus, especially when the magnitudes of soil displacements were considerable. The more important parameter in this case would be the limiting soil pressure. It has been shown that free-field soil movement far from the instrumented piles may often give excessive soil movement, which may be unrealistic to be used in order to predict the behaviour of a closely spaced pile group, as the reinforcing and arching effect of the pile group are often neglected. Therefore, further research into such pile-soil-pile interaction would definitely be of interest and will be addressed in the present research.

Chen and Martin (2002) used the 2-D finite difference analysis program FLAC to simulate soil plastic flow around pile group. It is a common knowledge that the arch that forms around the pile group provides a stabilizing mechanism against landslide. The numerical results revealed that the formation and shape of the arching zone are functions of pile arrangement, relative pile/soil displacement, pile shape, interface roughness and the soil dilation angle. The arching effect was explained using the pile load-displacement curves, which give the magnitudes of stresses that are transferred from the soil to the piles.

In addition, the analyses also showed the development of plastic zones around the piles and the eventual failure modes at the pile/soil interface. It was concluded that

the development of soil arching is limited by the pile spacing. For cohesionless soils, lower ultimate lateral forces were observed on the piles with closer spacing. However, for closer spaced piles in cohesive soils, the ultimate lateral forces acting on the piles were higher. Nonetheless, it was also concluded that no significant group effect would occur if the pile spacing exceeds four pile diameters. Group effects were also noted to be more pronounced for cohesionless soils than for cohesive soils. As the work of Chen and Martin (2002) is purely numerical in nature, there is no proof to show the existence of such phenomenon. Therefore, it would be of interest to investigate further if such phenomenon actually exists and will be subsequently addressed in the present research.

2.7 LIMITING SOIL PRESSURE ON ACTIVE AND PASSIVE PILES

It is evident from the preceding section that the limiting soil pressure on the pile is crucial. The limiting soil pressure deserves greater attention and will be reviewed in detail in this section. Many researchers have proposed single, average values or lumped limiting soil pressure/undrained shear strength (p_y/c_u) ratios for estimating limiting soil pressure on piles due to moving soils. De Beer (1977) defined passive piles as piles subjected to lateral soil movement and active piles as conventionally laterally loaded piles. The limiting soil pressure adopted by various researchers is listed in Table 2.2. It is evident that a wide range of p_y/c_u ratios for laterally loaded piles (active piles) and piles subjected to lateral soil movement (passive piles) have been proposed. Careful study of the proposed p_y/c_u ratios in Table 2.2 reveals some contradictions by several researchers. For example, Poulos and Chen (1997) proposed that the limiting soil pressure on an active pile is similar to that of a passive pile. Poulos and Davies (1980) proposed that for the case of a laterally loaded

pile in a purely cohesive soil, the ultimate lateral resistance or limiting pressure, p_y, increases from 2 c_u at the surface to 8 to 12 c_u at a depth of about three pile diameters and remains constant for greater depths.

It was further illustrated by Poulos and Davies (1980) that when p_y becomes constant, lateral failure involves a plastic flow of soil around the pile. On the other hand, Broms (1964a) proposed that this ultimate soil resistance or limiting soil pressure, p_y, for a cohesive soil can be further simplified and to account for the near ground effect for design purposes. The result is a limiting soil pressure distribution of zero from the ground surface to a depth, z of 1.5 pile diameters and a constant value of 9 c_u below this depth. However, the limiting soil pressure of 9 c_u has also been adopted by some researchers in their analyses of piles subject to lateral soil movement caused by embankment loading (Goh et al., 1997) and excavation (Poulos and Chen, 1997), even though the former is a loading process while the latter is an unloading process. However, other researchers like Viggiani (1981), Maugeri et al. (1994) and Chow (1996) proposed that the limiting soil pressure on a passive pile is much lower than that of an active pile. Therefore, in view of such contrasting p_y/c_u ratios adopted for a passive pile, one of the aims of the present study is to evaluate the p_y/c_u ratio for piles subject to excavation-induced soil movement.

2.8 SUMMARY

It has been illustrated in the literature review that lateral soil movement can induce considerable bending moment on adjacent pile foundations. If the piles have not been designed to withstand these additional induced bending moment, the structural integrity of the piles may be threatened. Nevertheless, most of the earlier studies are related to landslide stabilization using piles and effects of embankment loading on

nearby piles supported bridge abutments. However, not many studies have been done to investigate the pile behaviour behind an excavation. This could be due to the fact that excavations are normally carried out close to an existing structure. As such, it is impossible to instrument an existing pile foundation that is already in place to study its behaviour. Therefore, physical modelling involving centrifuge experiments are deemed attractive as the behaviour of an existing pile foundation subject to excavation-induced soil movement can be studied in detail under a well-controlled laboratory environment.

Excavation involves creating a large void in the ground, where the soil close to the excavation would move towards the cut. As such, the soil behind the wall may yield much more than the relatively stable soil further behind the wall. If the piles are capped in a group with some piles located in the yielded zone and some piles located in the stable zone, the different stress levels in the soils may affect the overall performance of the pile group. In addition, owing to the alleviation of the overburden pressure as a result of excavation, the horizontal confining soil pressure also reduces (Katakami et al., 1998) due to stress relief. Therefore, the limiting soil pressure may be exceeded when the excavation results in relatively large strain soil deformation. Such soil deformation behaviour is different from that due to embankment loading, landslides or tunnelling. The effects of excavation, such as soil deformation, seepage due to ground water drawdown and progressive wall movement may affect the behaviour of the piles close to an excavation. As such, a more detailed study involving the behaviour of piles subject to excavation-induced soil movement in clay is necessary.

It is also important to realize from the literature review that relatively few attempts have been made to investigate the pile behaviour subjected to active and passive loadings. The limiting soil pressure proposed by Poulos and Davies (1980) and

Broms (1964a) for a laterally loaded pile (active) have been used for the analyses of passive piles subjected to lateral soil movement caused by embankment loading (Goh et al., 1997) and excavation (Poulos and Chen, 1997), even though the former is a loading process while the latter is an unloading process. The main reason many researchers tried to relate limiting soil pressure to the methods proposed by Poulos and Davies (1980) and Broms (1964a, b) is because of its simplicity of use. Therefore, in the present study, the applicability and validity of the method proposed by Poulos and Davies (1980) and Broms (1964a) to excavation will also be investigated.

It is a common practice to use two-dimensional plane strain finite element method to predict pile responses due to excavation. Precautionary measures must be taken to smear the strength and stiffness properties of the pile over a unit width. Therefore, a correct choice of equivalent flexural rigidity is desired in order to correctly predict the pile responses when subject to lateral soil movement. The drawback of this method is that, if the piles are smeared in plane strain, the phenomenon of plastic soil "flow" could not be readily captured in the two-dimensional analysis. For this reason, a centrifuge study or three-dimensional analysis is deemed more suitable to model the plastic flow of soils.

As far as the author is able to ascertain, there has not been any reported centrifuge experiments done to investigate the behaviour of piles located behind a stable and collapsed retaining wall in an unstrutted excavation in a normally consolidated clay. In the case of a collapsed wall, the phenomenon of soil flowing past the pile and subsequently, the alleviation of soil pressure on the pile as well as the prediction of the soil pressure acting on the pile prior to soil flow have apparently not been studied. For these reasons, an in-depth centrifuge study into the behaviour of pile subject to excavation-induced soil movement in clay is deemed appropriate.

Table 2.1 Maximum bending moments and moment as percentage of design working moment (Coutts and Wang, 2000)

Pier number	Pile number	Max M_{xx} (kNm)	Percentage of design working moment (%)	Max M_{yy} (kNm)	Percentage of design working moment (%)
11	1	-176.6	16	492.1	44
	2	-677.4	60	506.6	45
14	1	561.0	40	502.2	36
	2	527.3	38	820.4	59
20	1	610.8	39	249.0	16
	2	-289.5	19	237.4	15

Table 2.2 Values of p_y/c_u for single piles

Reference	**K value**	**Method of analysis**	**Situation**	**Type of loading on pile**
Chen and Poulos (1994)	11.4 for piles near a cut	2-D FEM	Similar to piles used for landslide stablisation	Passive
Viggiani (1981)	2.8-4 (sliding soil) 8 (stable soil)	Empirical	Piles used for landslide stabilisation	Passive
Maugeri et al. (1994)	3.33 (sliding soil); 6.26 (stable soil	Empirical, field data	Piles used for landslide stabilisation	Passive
Chow (1996)	3-4 (sliding soil); 8-12 (stable soil)	Empirical, numerical	Piles used for landslide stabilisation	Passive
Poulos and Chen (1997)	9	Empirical	Piles adjacent to an excavation	Passive
Goh et al. (1997)	9	Empirical	Single pile adjacent to embankment	Passive

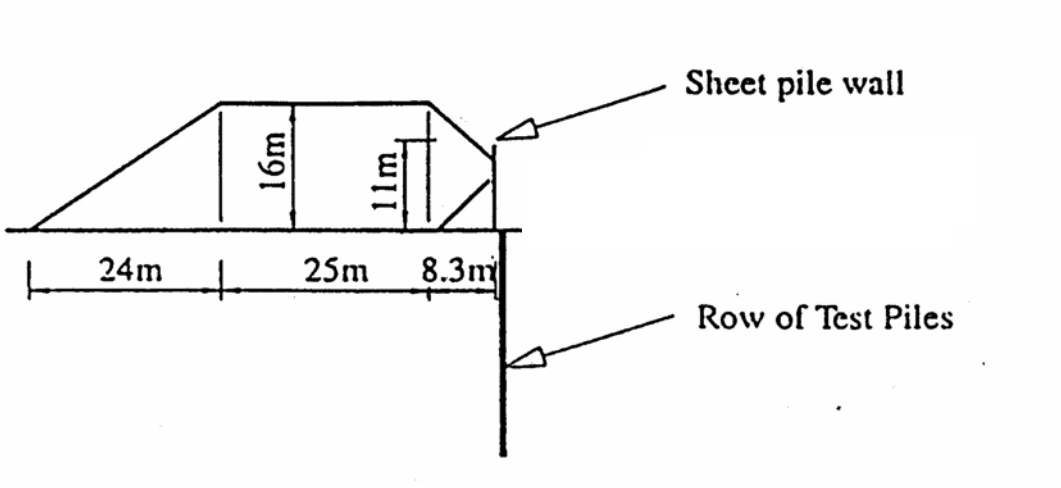

Figure 2.1 Test set-up at Zelgate, Belgium (after De Beer and Wallays, 1972)

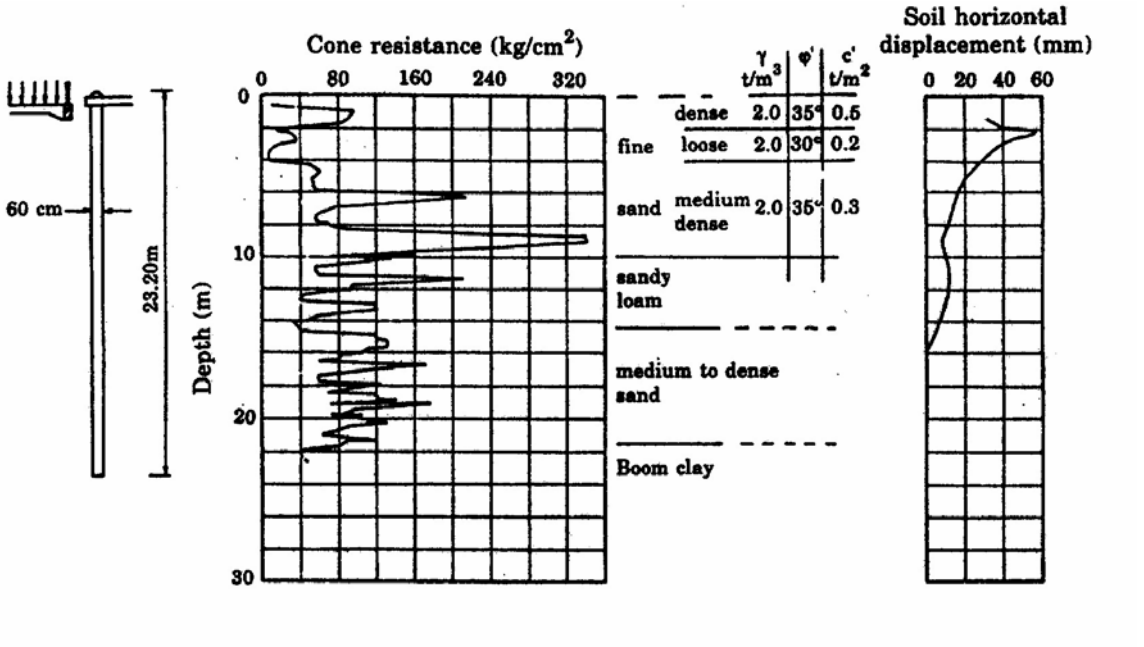

Figure 2.2 Soil profile and measured data for 600 mm diameter reinforced concrete pile (after De Beer and Wallays, 1972)

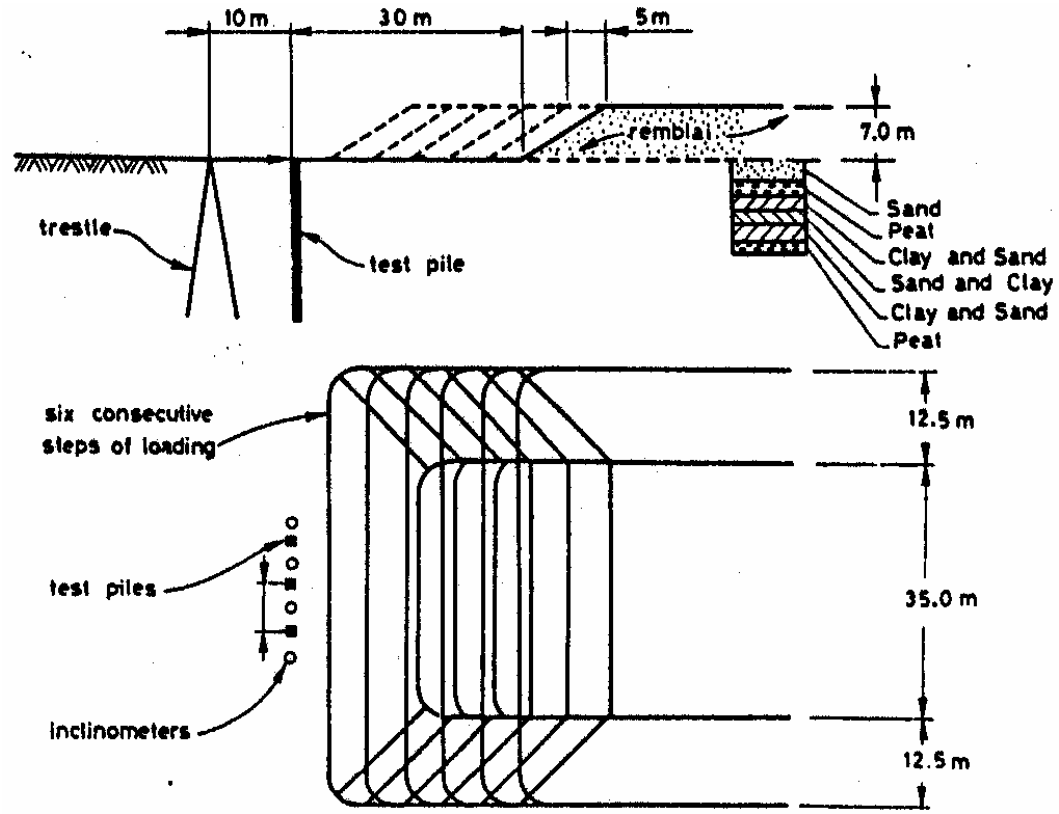

Figure 2.3 Loading test set-up at Amsterdam (after Marche, 1973)

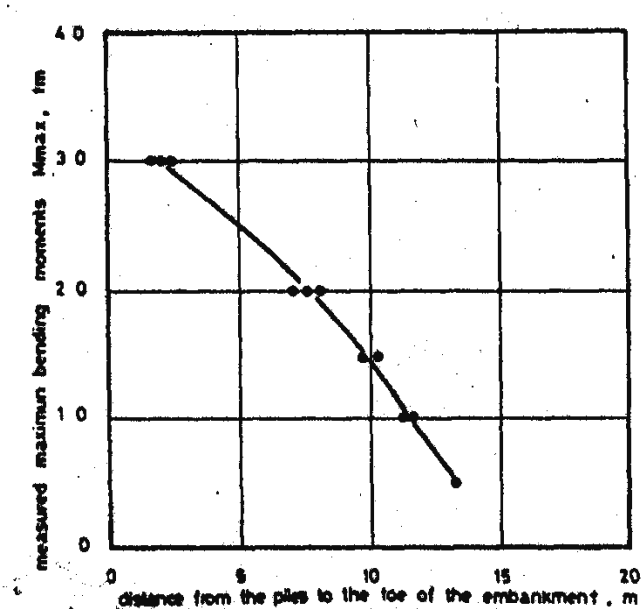

Figure 2.4 Measured maximum bending moments in piles (after Marche, 1973)

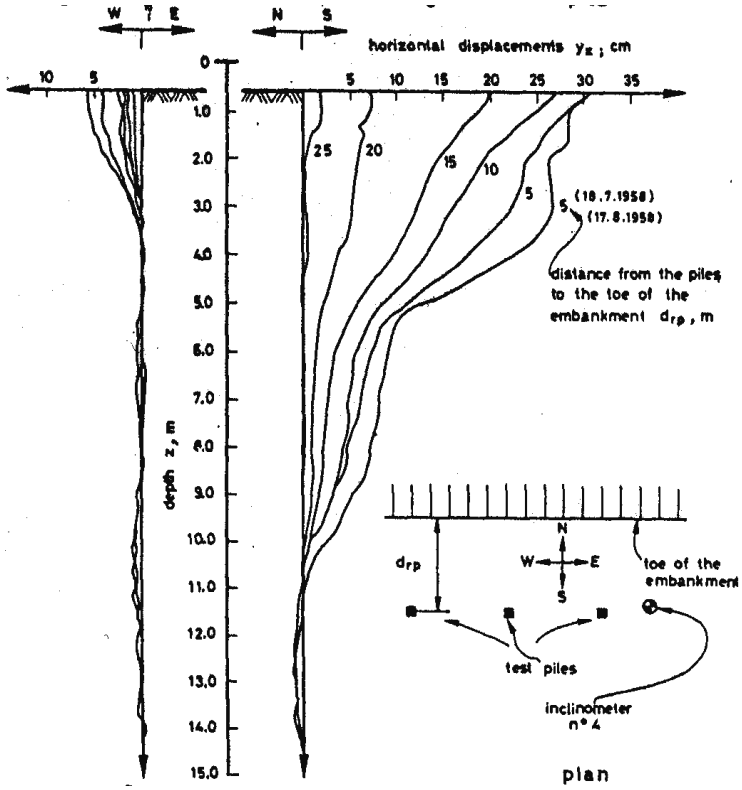

Figure 2.5 Measured pile horizontal displacements (after Marche, 1973)

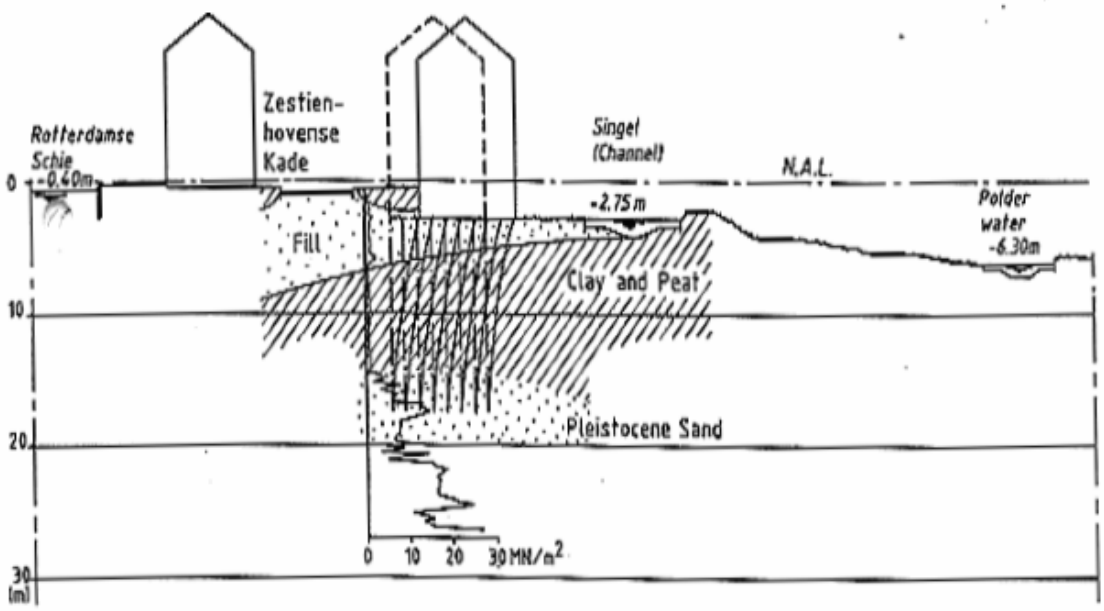

Figure 2.6 Cross-section of the quay (after Hannink and van Tol, 1988)

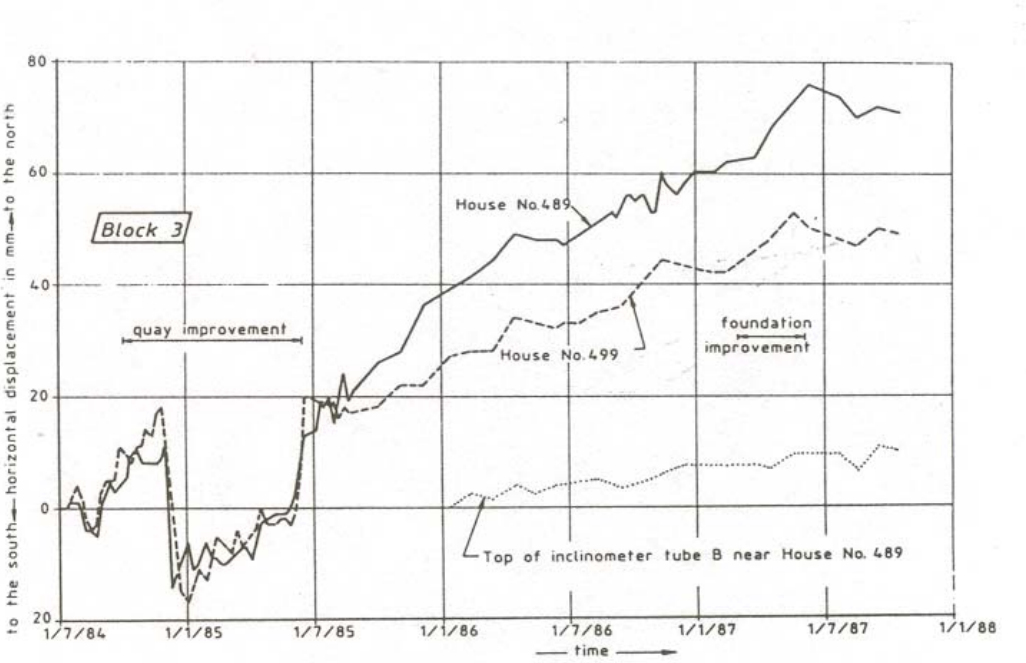

Figure 2.7 Horizontal displacements of Block 3 (after Hannink and van Tol, 1988)

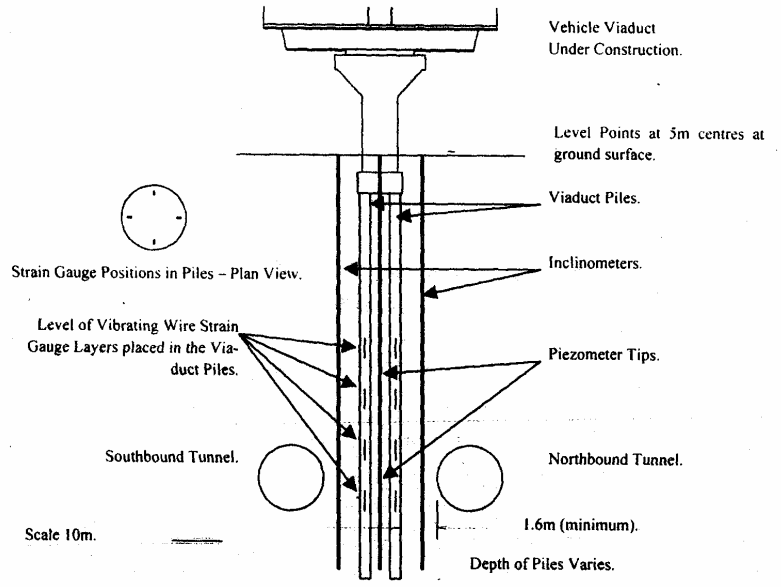

Figure 2.8 Viaduct, pile and tunnel layout (after Coutts and Wang, 2000)

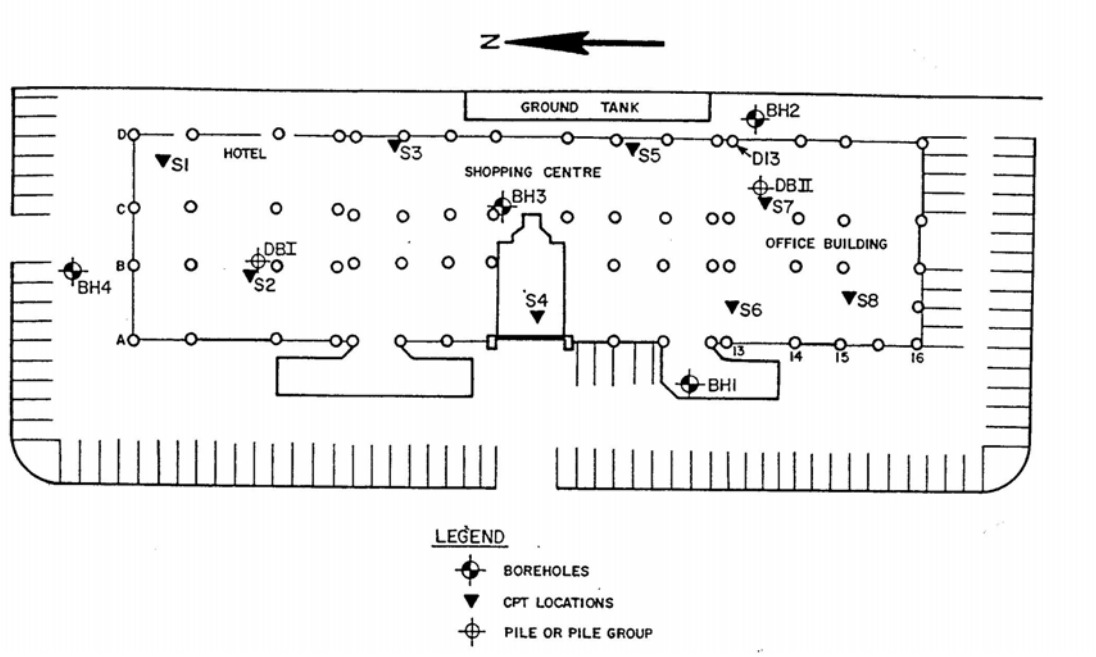

Figure 2.9 Plan of the project and the borehole locations (after Poulos, 1997)

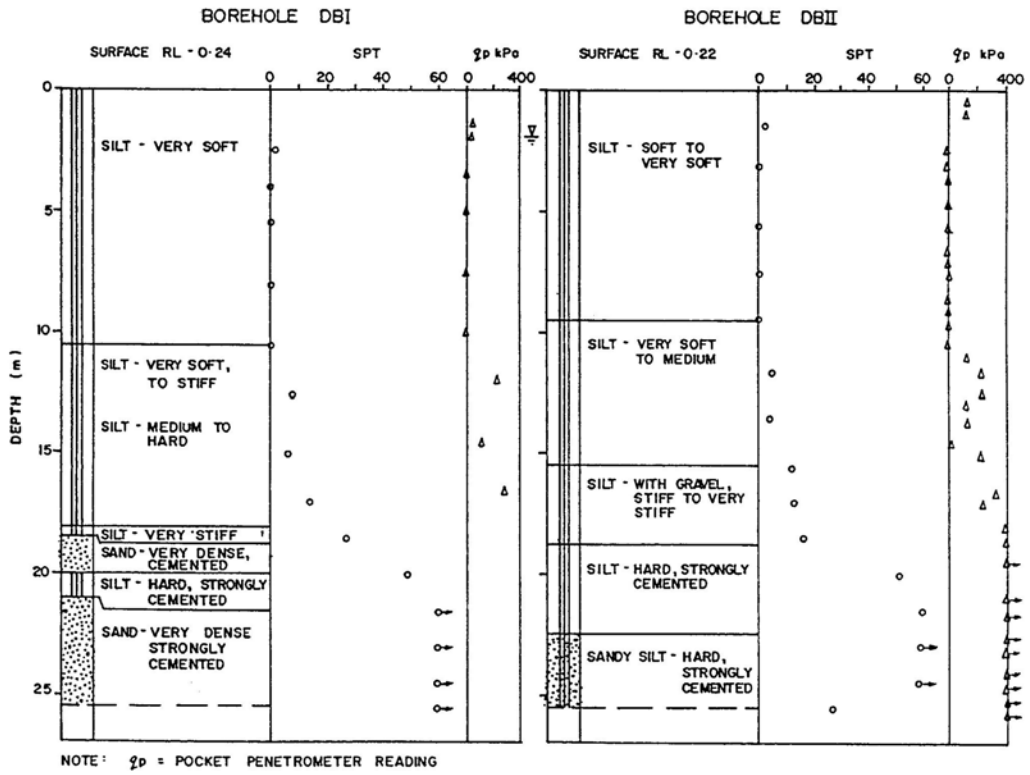

Figure 2.10 Borehole information (after Poulos, 1997)

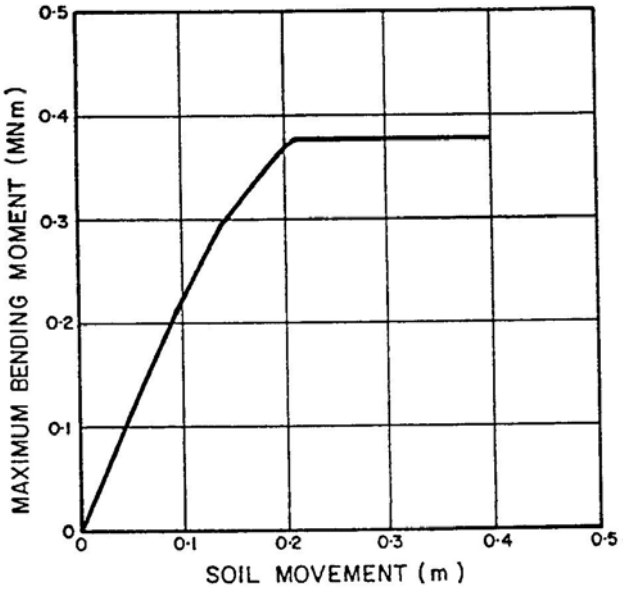

Figure 2.11 Maximum pile bending moment (after Poulos, 1997)

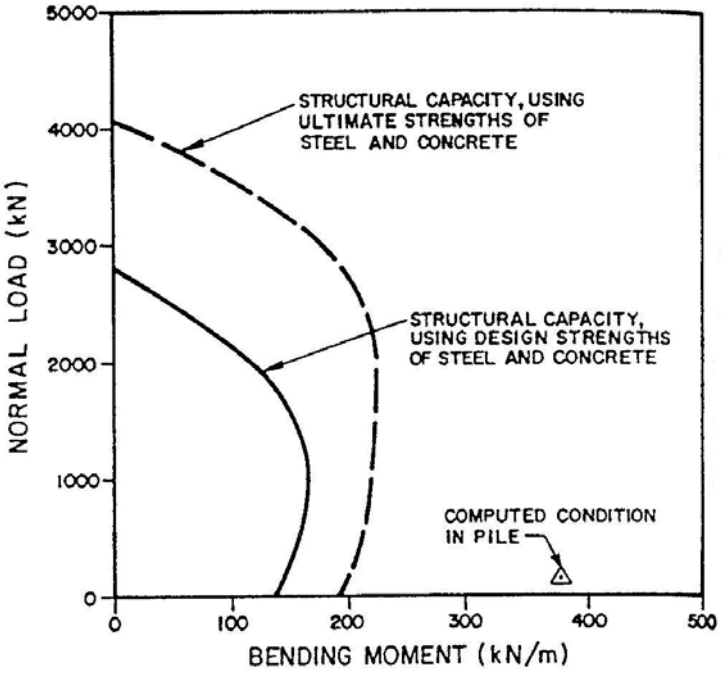

Figure 2.12 Structural capacity of shopping centre piles (after Poulos, 1997)

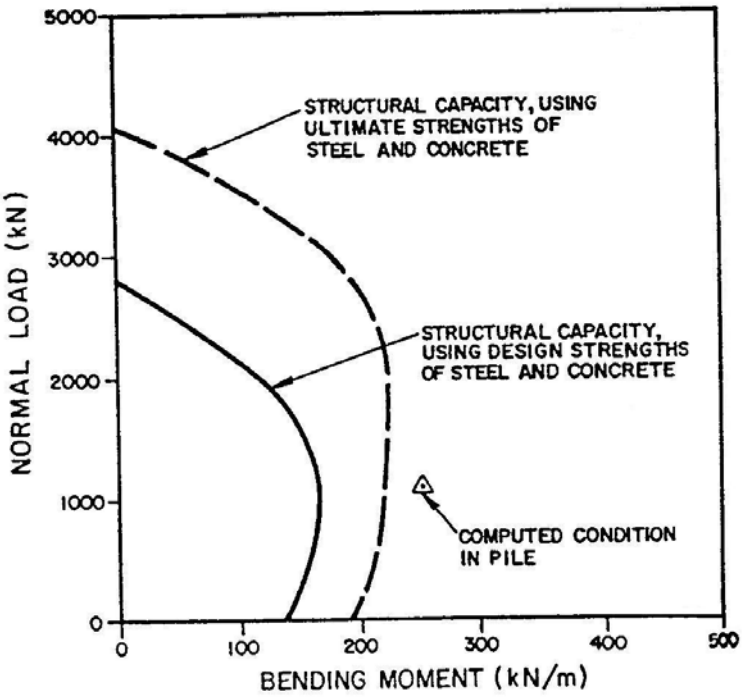

Figure 2.13 Structural capacity of office building piles (after Poulos, 1997)

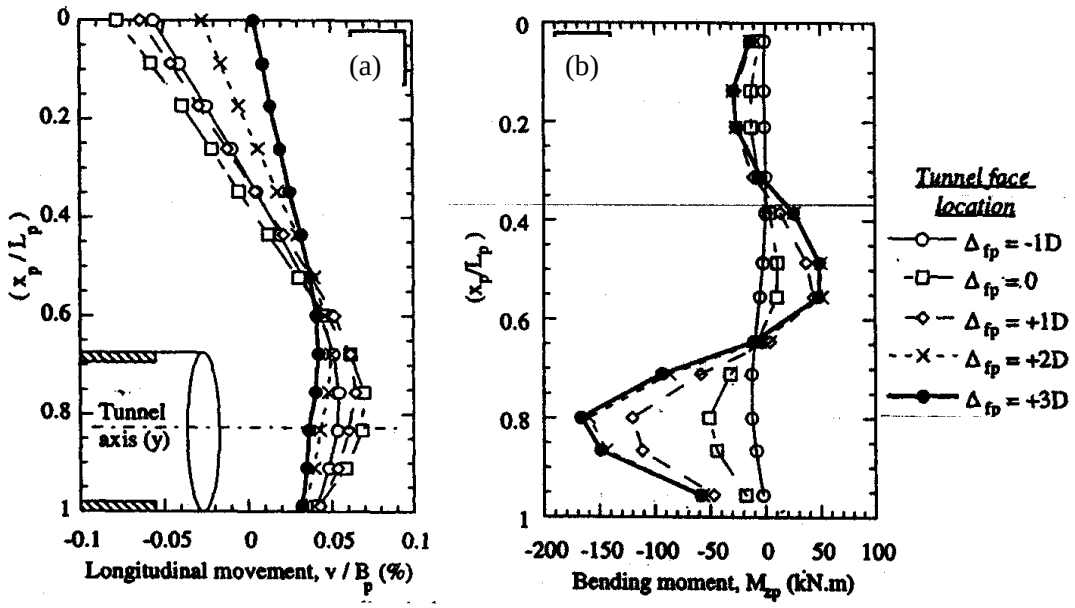

Figure 2.14 (a) Pile movement and (b) development of bending moment in pile due to tunnelling (after Mroueh and Shahrour, 1999)

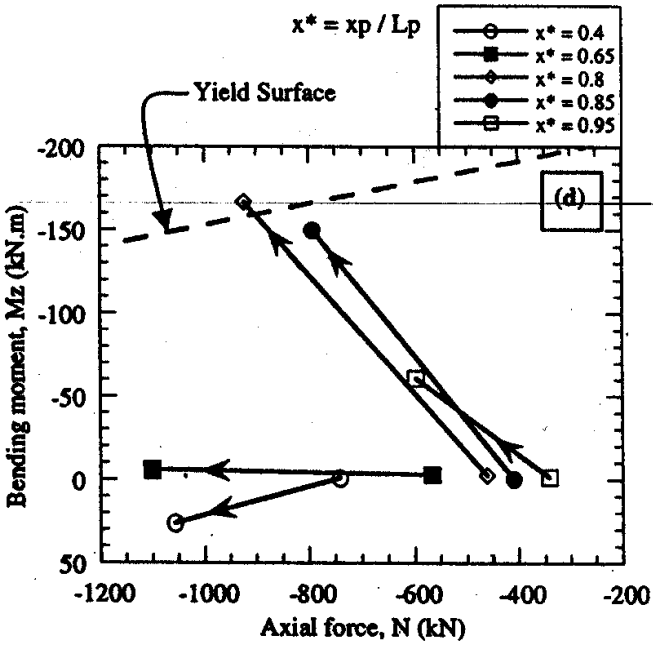

Figure 2.15 Certain section of pile capacity is exceeded due to effect of tunnelling (after Mroueh and Shahrour, 1999)

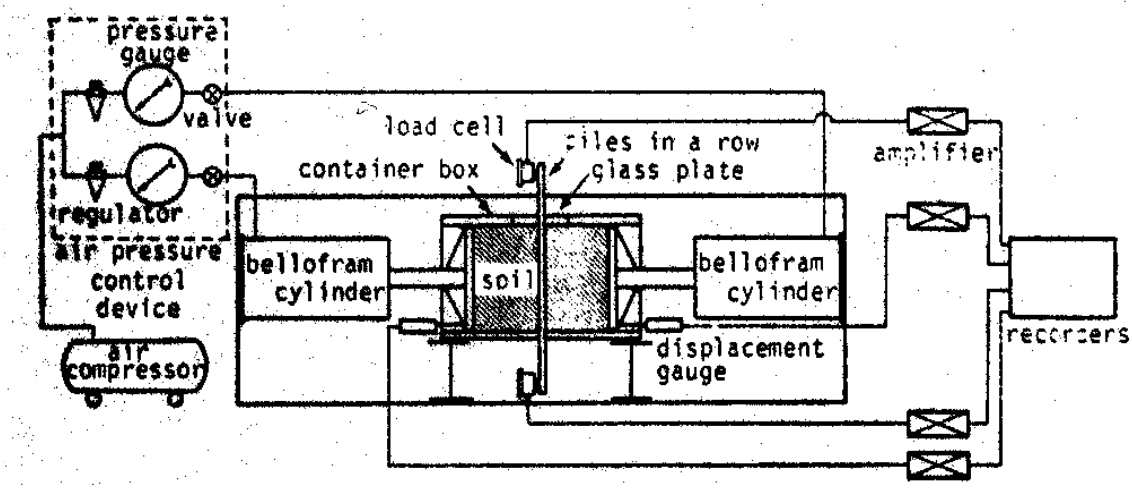

Figure 2.16 Experiment set-up (after Matsui et al., 1982)

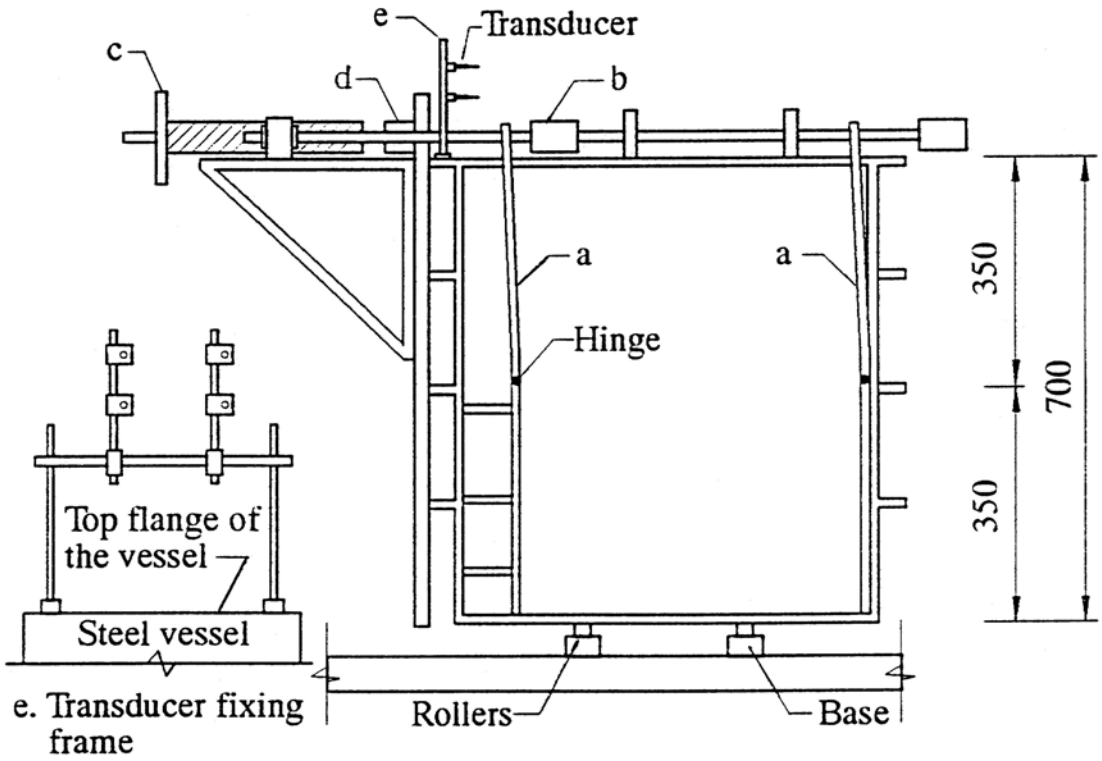

Figure 2.17 Elevation view of testing vessel (after Poulos and Chen, 1995b)

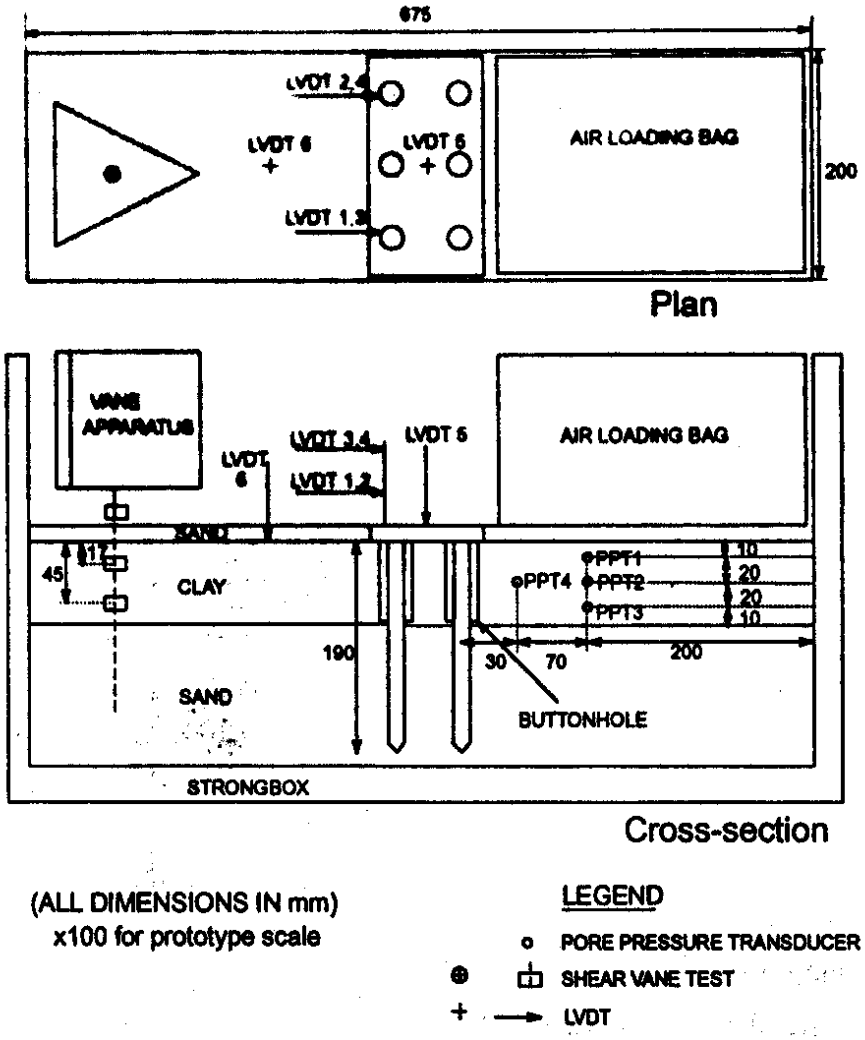

Figure 2.18 Centrifuge experiment set-up – piled bridge abutment (after Bransby and Springman, 1997)

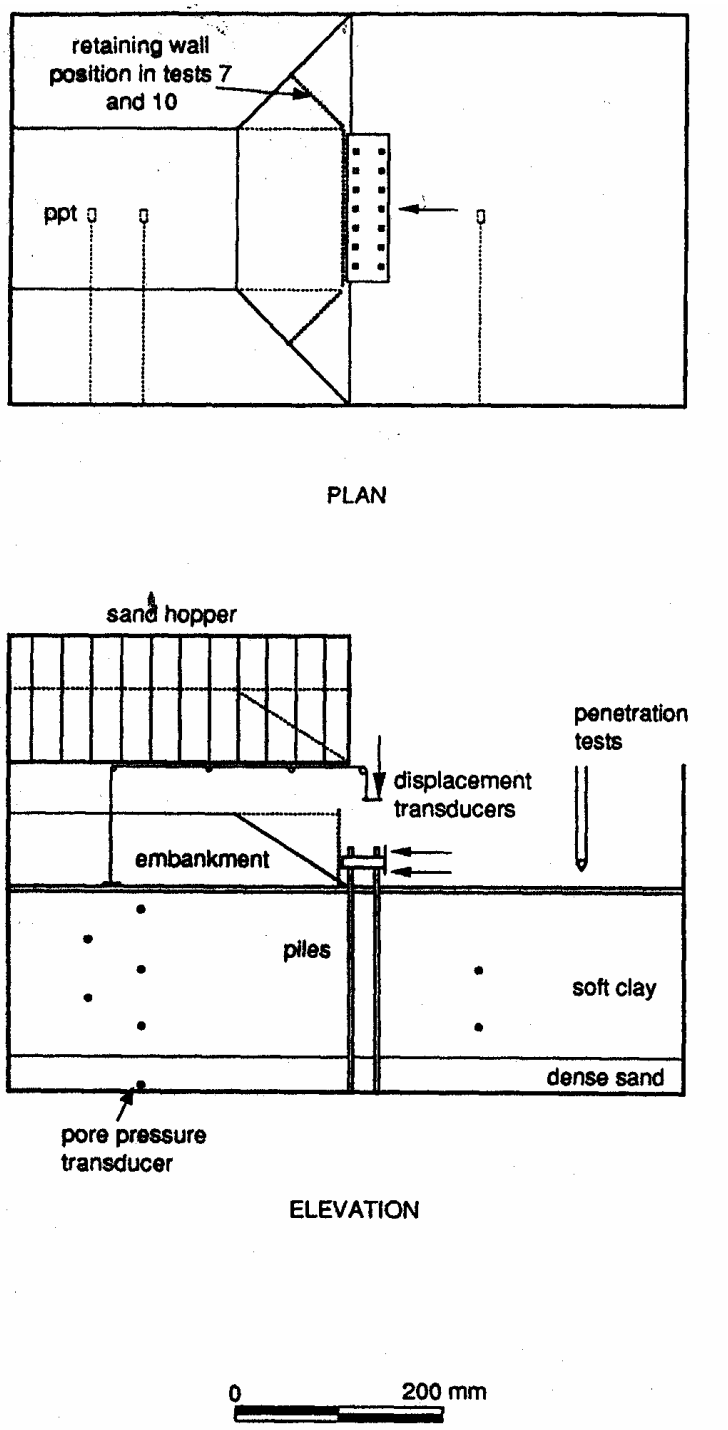

Figure 2.19 Centrifuge experiment set-up – piled bridge abutment (after Stewart et al., 1994b)

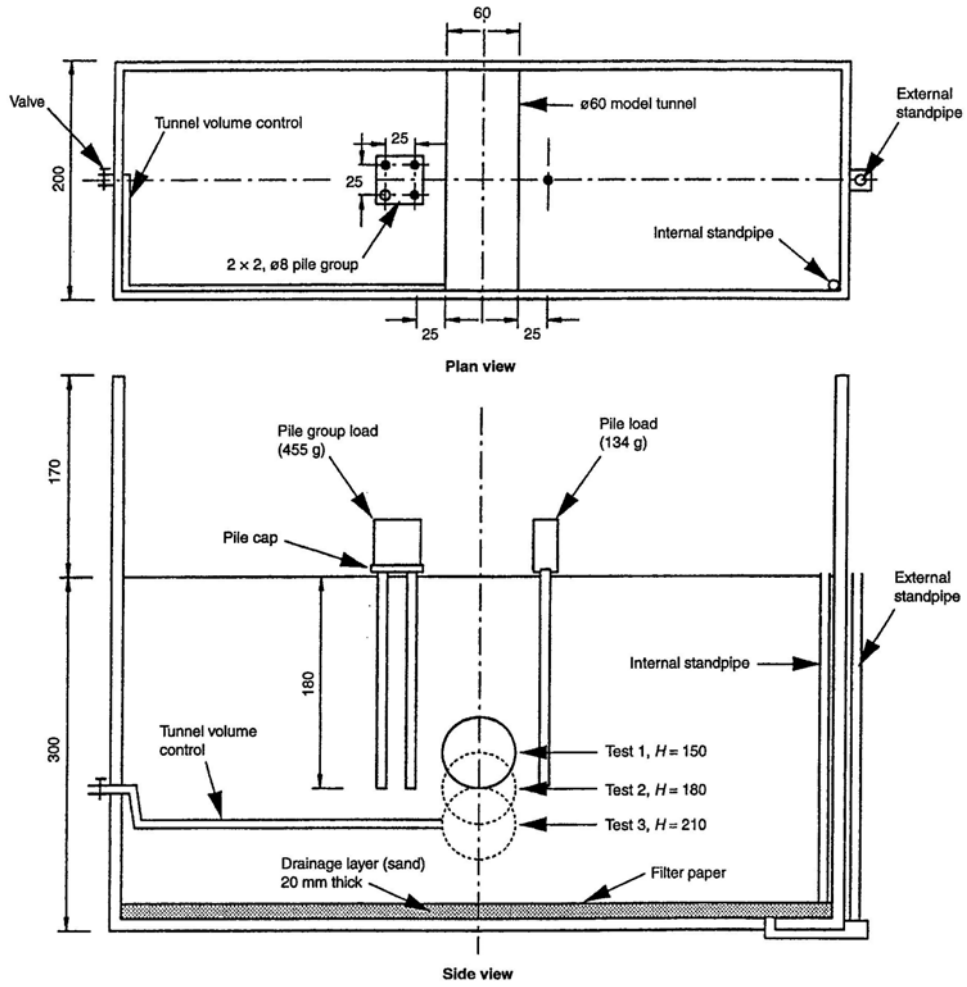

Figure 2.20 Centrifuge experiment set-up - tunnelling, dimensions in mm (after Loganathan et al., 2000)

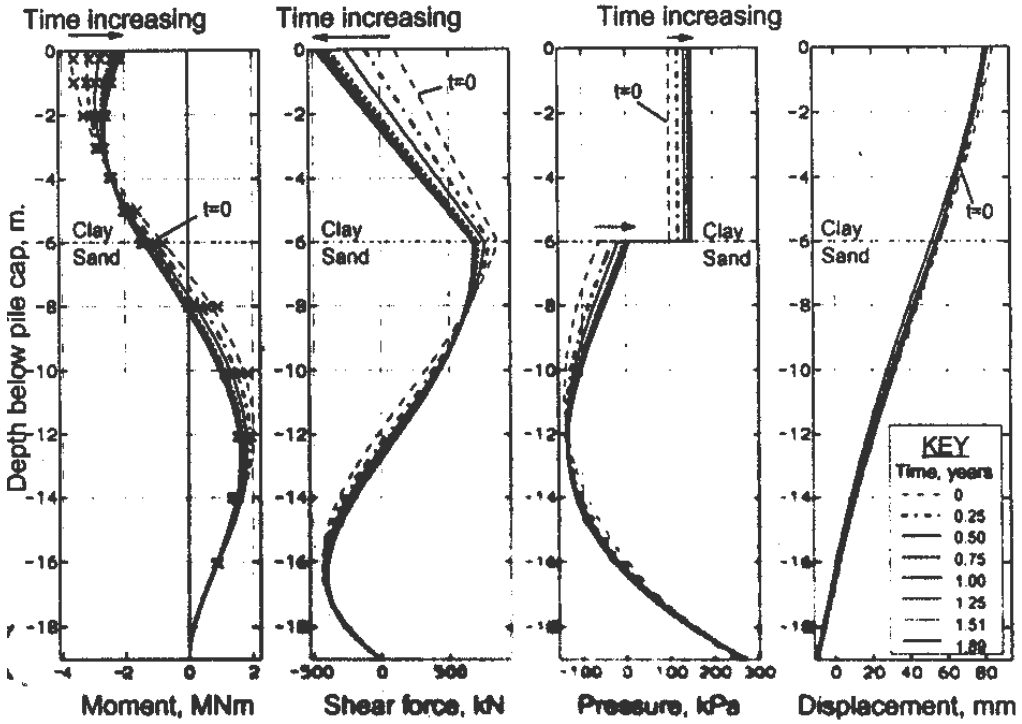

Figure 2.21 Front row pile behaviour with time (after Bransby and Springman, 1997)

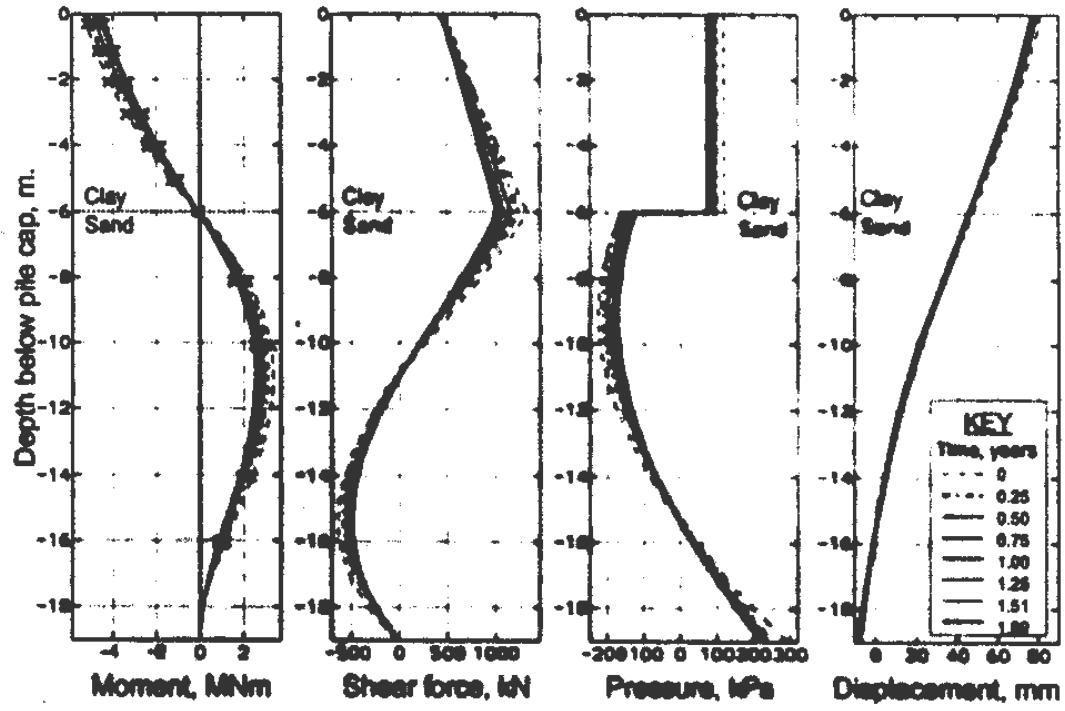

Figure 2.22 Back row pile behaviour with time (after Bransby and Springman, 1997)

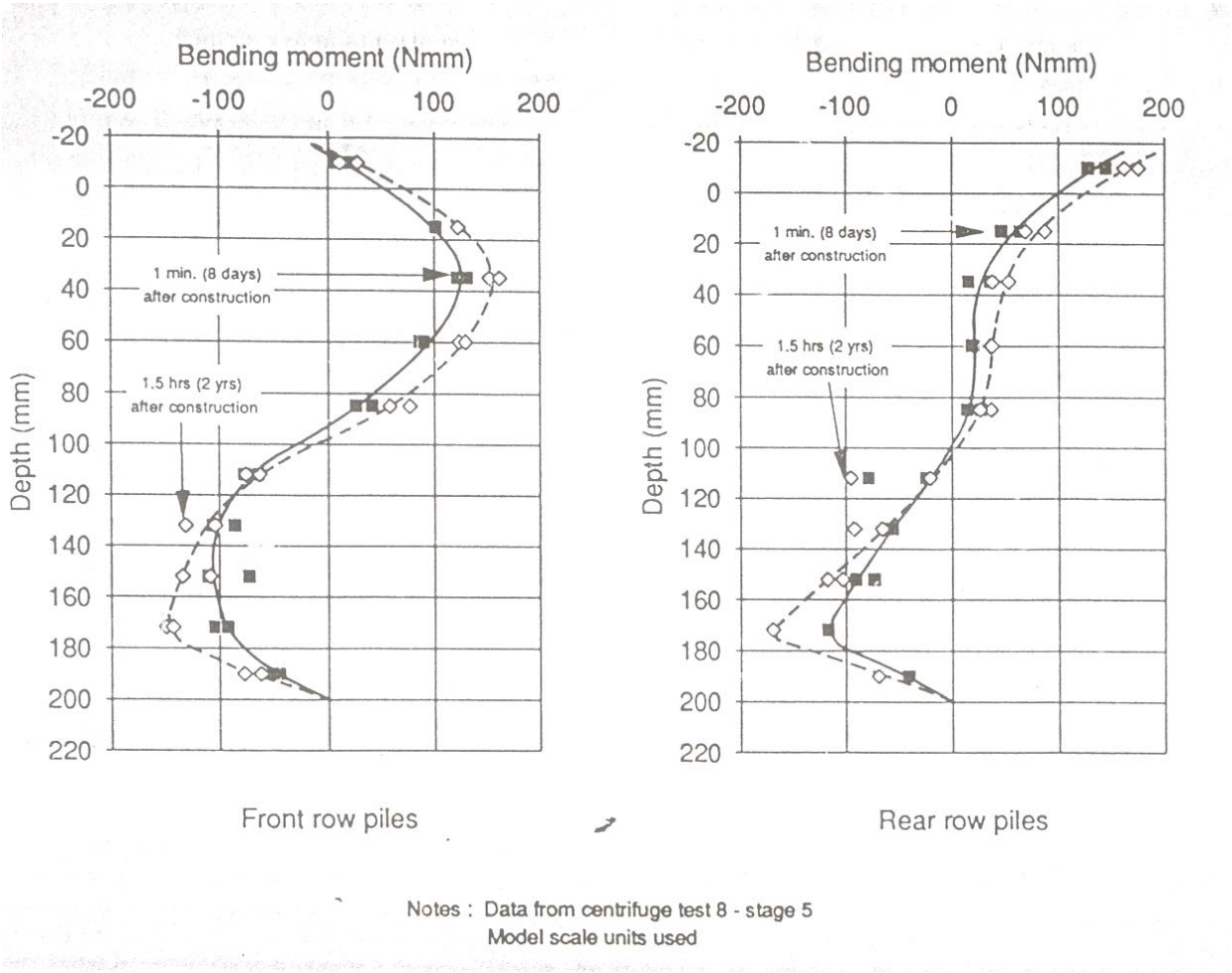

Figure 2.23 Variation of pile bending moment profiles with time (after Stewart, 1992)

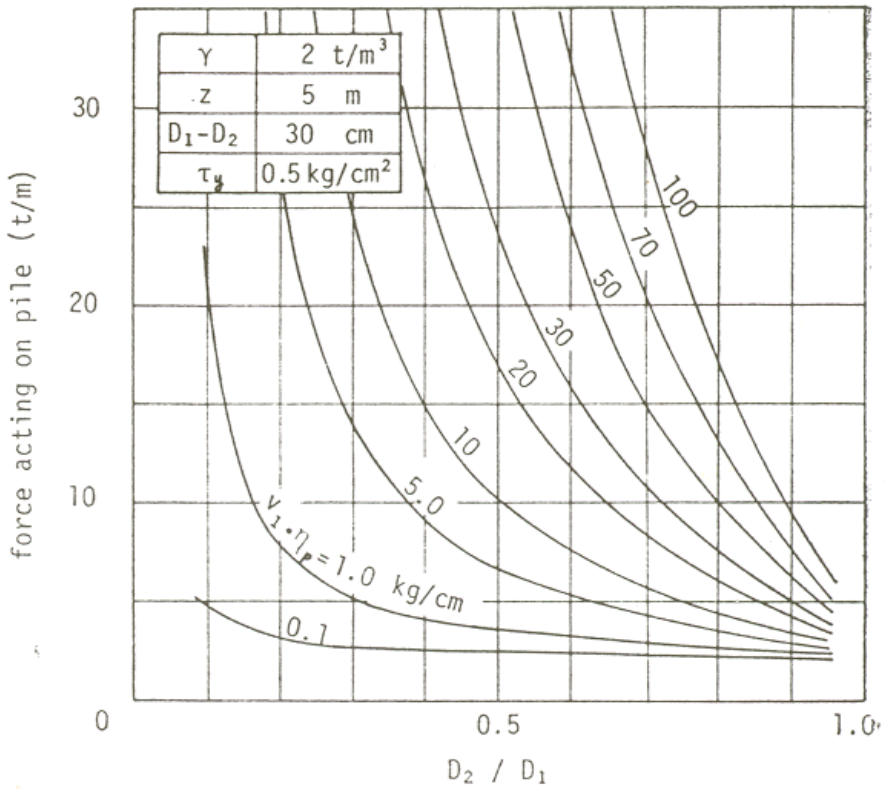

Figure 2.24 The effect of product of flow velocity and plastic viscosity ($v_p \cdot \eta_p$) on the theory of plastic flow (after Ito and Matsui, 1975)

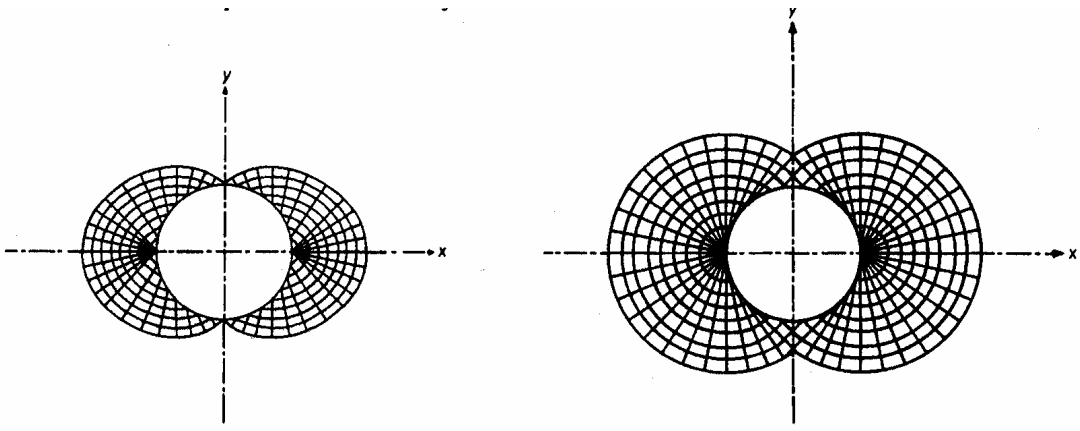

Figure 2.25 Example of a characteristic mesh at $\alpha = 0$ (fully smooth) and $\alpha = 1.0$ (fully rough), respectively (after Randolph and Houlsby, 1984)

CHAPTER THREE

EXPERIMENTAL SET-UP AND PROCEDURES

3.1 INTRODUCTION

This Chapter presents the model set-up package, model pile and pile cap as well as model wall. This is then followed by the test procedures, and the preparation of clay. In order to enable acquisition of consistent and high quality data from centrifuge experiments, a good understanding of the working behaviour of miniature transducers and probing tools such as the linear variable displacement transducers (LVDTs), pore pressure transducers (PPTs), total stress cells (TSCs), non-contact laser potentiometers, in-flight bar penetrometer (T-bar) and the automated enhanced image processing system have to be established. The effects of simulating an excavation using the method of draining a heavy fluid of equal unit weight of the soil it replaces are also discussed in detail.

3.2 CENTRIFUGE MODELLING

3.2.1 Centrifuge modelling principles

In geotechnical engineering, full-scale field tests are considered not viable because they are expensive, time-consuming and inconvenient. The inability to control the test conditions and soil properties in the field makes it unattractive because

parametric studies cannot be carried out. On the other hand, physical model tests may be attractive since the soil properties can be artificially controlled. Nevertheless, the drawback is that laboratory model tests could not duplicate the non-linearity characteristics of soil whose behaviour is highly stress dependent. Hence the data obtained cannot be extrapolated to the soil behaviour in the field. However, this drawback can be solved by subjecting the model tests to an artificially enhanced gravitational field N times the Earth's gravity, whereby the prototype stress levels can be reproduced in the model tests. Hence, the model test results can then be used to interpret the prototype behaviour in a rational manner.

As mentioned by Craig (1995), the first English language publication on centrifuge modelling in geotechnical engineering was presented at the First International Conference on Soil Mechanics and Foundation Engineering at Harvard in 1936. Since then, centrifuge modelling technology has improved so rapidly that it has become a versatile tool in geotechnical engineering to study problems such as deep excavations and tunnelling works, embankment and slope stability, land reclamation as well as shallow and deep foundations amongst others.

In physical model studies, it is seldom possible to replicate precisely all details of the prototype and some approximations have to be made (Taylor, 1995). For example, the most common question is that how can centrifuge modelling be justified if the soil particles are not reduced in size by a factor of N. Therefore, it is sensible to develop guidelines on the critical ratio between a major dimension in the model to the average grain diameter to minimise the problems of particle size effects. Ovesen (1979) compared centrifuge and prototype results and showed that when the ratio of foundation diameter to grain size was less than about 15, some deviations of results were noted. Tatsuoka et al. (1991) considered the ratio of particle size to shear band

width. Nevertheless, the important point is to recognize this fact and to carry out further centrifuge model tests to assess its significance in the problem being studied.

Particle size effect is usually significant for coarse-grained soils but is much less so for clayey and other fine-grained soils (Zeng and Lim, 2002). In the present study, the top kaolin clay layer and the underlying fine sand layer are used to model the ground. Therefore, the particle size effects are unlikely to affect the findings significantly. One of the advantages of centrifuge modelling in the present study is that the consolidation time of the clay can be significantly expedited.

A well-known issue caused by centrifugal acceleration is the variation of centrifuge acceleration field in the model and its effects on the vertical stress at the centre of a model with depth (Zeng and Lim, 2002). In the present study, the ratio of the height of model ground (250 mm, model scale) to the radius of centrifuge arm (1871 mm) is about 13%, which is slightly over the 10% recommended by Schofield (1980). However, potential errors resulted from the ratio of 13% is considered to be insignificant.

3.2.2 Centrifuge scaling relationships

The scaling relationship between a small-scale centrifuge model and its full-scale prototype can be derived by dimensional analysis or from consideration of the governing differential equations (Taylor, 1995). The centrifuge model test results in the present study are related to their prototype scale by appropriate scale factors as shown in Table 3.1.

3.2.3 NUS geotechnical centrifuge

Figures 3.1 and 3.2 show the NUS centrifuge facilities. The NUS centrifuge has a capacity of 40 000g-kg and operates up to a maximum g-level of 200g. This implies that the allowable payloads at 200g and 100g are 200 kg and 400 kg, respectively. The structure of the centrifuge is based on the conventional dual swing platform design. The model package is normally loaded onto one of the swing platforms with the opposing platform counter balanced by either counterweights or another model package with identical weights. When the centrifuge is spinning, the distance from the axis of rotation to the base of the platform is 1.871 m. The centrifuge is driven by a hydraulic motor, which is capable of delivering up to about 37 kW of power. The swing platform has a working area that measures 750 mm x 700 mm and a headroom of 1180 mm. A stack of electrical slip rings is mounted at the top of the rotor shaft for signals and power transmission between the centrifuge and the control room.

DC voltage is transmitted through the slip rings to the transducers mounted on the centrifuge or the model package from the control room. Likewise, registered signals from the transducers are then transmitted via slip rings. The signals are first filtered by an amplifier system at 100 Hz cut-off frequency to reduce interference or signal noise pick-up through the slip rings. The amplified signals are then collected by a data acquisition system at a regular interval in the control room. A software called Dasylab is used to process the signals whereby the signals are smoothened by using a block average. Two closed circuit cameras, which are mounted on the centrifuge, enable the entire in-flight process to be monitored in the control room. The NUS centrifuge is described in detail in Lee at al. (1991) and Lee (1992).

3.3 EXPERIMENTAL SET UP

Figure 3.3 shows the experimental set-up of the present study. All the tests were carried out at 50g in the present study. It should be noted that pore pressure transducers (PPTs) are present in all the tests performed, but total stress cells (TSCs) are only placed in selected number of tests.

3.3.1 Model container

The model container weighs 100 kg and is made of stainless steel. The internal dimensions measure 540 mm in length, 200 mm in width and 470 mm in height. The front face of the container consists of a 60 mm thick perspex window, which enables the whole testing process to be monitored by an image processing camera system mounted in front of the container. The back face of the container consists of a steel plate, which is strengthened by stiffeners. This enables the container to withstand high gravitational force during centrifuge flight. The main body of the container comprises a base and two side walls forming a U-shape structure. The two front and back faces are secured to the main body of the container by means of bolts and nuts. Water tightness is ensured by bolting all connected faces with rubber seals or gaskets in between. A specially designed valve to drain the zinc chloride solution ($ZnCl_2$) via a polyethylene tube is located at the bottom, left-hand corner of the back face.

3.3.2 Model pile

The model pile was fabricated from a hollow square aluminium tube with an outer dimension of 9.53 mm and a wall thickness of 3.18 mm. Ten pairs of strain gauges were glued on opposite faces of the model pile at a vertical interval of 25 mm as shown in Figure 3.4. The strain gauges would be connected to a TDS-200 strain meter or data logger, mounted on-board the centrifuge. The strain meter would

transmit digitized data, which would be acquired by the data acquisition system in the control room.

Strain gauges of model Kyowa KFG-1-120-C1-23 are used. Each strain gauge has a resistance of 120 Ω and a gauge factor of 2.1.The strain gauges were glued to the surface of the model pile using an adhesive of type Kyowa CC-33A after the pile surface had been roughened and cleaned with acetone. A coating agent of type Kyowa KE48RTV was used to ensure that the strain gauges are water-proofed and to ensure proper connection between the strain gauge and the electrical wires. After that, a thin layer of epoxy was applied to the entire length of the pile to ensure the strain gauges and all connections were waterproof. The final width of the pile measures 12.6 mm or 630 mm in prototype scale. The total length of the model pile is 350 mm with a soil embedment depth of 250 mm or 12.5 m in prototype scale. The calibrated bending rigidity, EI of the model pile is 2.2 x 10^5 kNm^2 at 50g. This is equivalent to a 600-mm diameter Grade 35 bored pile or a 610-mm diameter steel pipe pile with 12.7 mm wall thickness.

The strain gauges were calibrated to measure the pile bending moment. The pile was properly cushioned and then clamped to a table edge in such a way that the pile shaft was cantilevered from the table edge. The instrumented pile was connected to a strain meter for data acquisition. Known dead weights were then hung at the tip of the pile so that the strain gauges at every level along the pile shaft would respond (in units of microstrain, με) according to the bending moment induced by the dead weights. The known weights were increased in steps after the strain meter had acquired each corresponding set of data measured by the strain gauges. The measured strain gauge readings were then printed out from the strain meter so that the relationship between microstrain, με (registered by the strain gauges) and the induced pile bending

moment (result of hanging dead weights at the tip of the cantilevered pile) could be established. Two appropriate faces of the instrumented square pile were calibrated. As such, during centrifuge experiments, the microstrain readings acquired from the data acquisition system can be readily related to its corresponding bending moment from the scaling relations of centrifuge modelling shown in Table 3.1. Typical calibration charts for the instrumented pile used in the centrifuge tests are shown in Figures 3.5 and 3.6.

3.3.3 Model pile cap

The model pile cap is made of aluminium. Three types of pile caps were fabricated for the 2-, 4- and 6-pile group configurations. The thickness of the pile cap is 20 mm or 1.0 m thick in prototype scale. The pile caps were specifically designed to enable each pile in the group to be tightened individually using clamps in both directions. These clamps are attached to the main connecting pieces of the pile caps by means of bolts. Figure 3.7 shows the pile caps used in this study.

This is a much improved design compared to previous pile caps done in NUS (Lim, 2001) as the rotation or movement of the pile-pile cap connection can be minimized. However, it is believed that since the width of each pile is not exactly identical to the slot width in the pile cap due to workmanship, some degree of rotation or movement might still be present. Nonetheless, extra precautionary measures have been employed to minimize such rotation or movement, such as by using clamps lined with rubber pads to ensure better grip. The prototype pile cap bending rigidity for the 2- and 4-pile groups is 1.2×10^7 kNm^2 and 2.0×10^7 kNm^2, respectively. For the 6-pile group, the pile cap bending rigidity depends on the configuration of the piles facing the excavation. If the 6-pile group consists of 3 rows of 2 piles per row (2 piles x 3 rows) facing the excavation, the prototype EI of the pile cap is 2.0×10^7 kNm^2 (similar to the

4-pile group case). However, in a 6-pile group of 3x2 configuration, the EI of the cap is 3.6 x 10^7 kNm^2.

3.3.4 Model retaining wall

The model retaining wall is simulated using a 3 mm thick aluminum plate. The prototype bending rigidity is 24 x 10^3 kNm^2/m at 50g, which is equivalent to a FSP IIA sheet pile. The total embedded length of the wall is 160 mm or 8 m at 50g.

3.3.5 Pore pressure transducers

Druck PDCR81 miniature pore pressure transducers (PPT) were used to monitor the variations in pore water pressure during the centrifuge tests. Before each test was carried out, the PPTs were de-aired using a vacuum machine to release any trapped air bubbles in the PPTs to prevent acquisition of inaccurate readings. Each PPT comes with its own manufacturer's calibration factor and this must be incorporated into the calculation of pore water pressure.

3.3.6 Total stress transducers

The behaviour of total stress cells (TSCs) has to be understood fully as they are more sensitive than the pore water pressure transducers. Their presence in the clay will affect their own readings due to adjacent soil arching, surrounding soil saturation level and pore water pressure, presence of supporting backing plates and thickness of silicone rubber as waterproofing material applied to their bodies. It has been demonstrated by many researchers that difficulties arise when measuring normal stress accurately in a soil medium due to arching and grain size effects on the active diaphragms of the total stress transducers (see for example, Weiler and Kulhawy, 1982 and Dewoolkar et al., 1998). It is well known that a stiff diaphragm will attract stress

to itself causing over-prediction of soil stress and a flexible diaphragm will shed stress from its active face, resulting in under-prediction.

Lee et al. (2002) carried out various tests in different loading conditions to evaluate the performance of miniature total stress transducers (Entran EPL-D12) embedded in clays. The most applicable experiment from Lee et al. (2002) with regards to the present study is the self-weight loading test of saturated normally consolidated kaolin clay at high-g. They found that the registration ratio, R (ratio between the measured and applied vertical stress) is under-registered and ranges from 0.8 to 0.95 (Figure 3.8) over two consecutive loading-unloading cycles at high-g. Nonetheless, this range of R values is considered much closer to unity as compared to other loading cases like the 1g tests and tests done with dry kaolin powder, as reported by Lee et al. (2002).

Juneja (2003) further showed that the increased stiffness of a normally consolidated kaolin clay, as compared to that of kaolin slurry, was insufficient to lead to a significant increase in stress arching. Besides that, it was also reported that total stress transducers installed with backing plates would register higher R values than those without the presence of such backing plates. It had also been shown that the thinner, long aluminium backing plate would serve to lower the transducer aspect ratio (0.04), thus reducing the effect of stress concentration on the transducer (Weiler and Kulhawy, 1982) as compared to the short aluminium plate (aspect ratio of 0.2) and the perspex plate (aspect ratio of 0.09). In practice, the long aluminium plate could be used to maintain the transducer orientation during insertion into the model ground. However, it has to be recognised that any insertion of miniature transducers into a model ground may interfere with the soil flow during consolidation, but such an effect can be greatly reduced by keeping the width of the plate to a minimum.

The miniature total stress transducers would have to be waterproofed using silicone rubber before it could be used in the saturated clay. Lee et al. (2002) reported that the thicker the waterproofing silicon rubber, the lower would be the registration ratio, R as shown in Figure 3.9. Nonetheless, the transducers that were embedded in clay subjected to high-g all recorded higher R values than those at 1g. Figure 3.9 suggests that if silicon rubber had not been used as waterproofing coating, the R value would have been greater than 0.95.

The ratio of the measured total horizontal stress to the measured total vertical stress, K_T, as presented by Lee et al. (2002), is shown in Figure 3.10. By using Jaky's (1948) relation of K_o = 1-sin ϕ', where K_o is the lateral coefficient of earth pressure at rest, ϕ' is the effective friction angle and measured bulk unit weight of about 15 kN/m^3, K_T = 0.85, 0.84 and 0.82 for ϕ' = 26^o, 29^o and 32^o, respectively. Lee et al. (2002) showed that the measured values of K_T are rather consistent with Jaky's K_o values.

Juneja (2003) reported that the calibration factors of the total stress transducers provided by the manufacturer are in close agreement with the measured loading and unloading calibration factors. This implies that the manufacturer's calibration factors can be used directly and confidently with a correction factor of between 0.8 and 0.95 such that the under-registration of the measured output readings of the total stress transducers can be corrected.

All necessary precautions and findings described by Lee et al. (2002) and Juneja (2003) have been strictly adhered to in the present study to ensure proper and correct installation of the total stress transducers.

3.3.7 Non-contact laser displacement transducers

NAIS micro laser sensors LM10 (model ANR1250) were used to measure the pile head movement during and after excavation process. This sensor has a centre point distance (distance between sensor and target) of 50 mm and a measurable range of ±10 mm within the centre point distance. The light source comes from a laser diode and has a wave length 685 nm and beam dimension of 0.6 mm x 1.1 mm at the centre point distance. It has a maximum linearity error of ±0.5% on aluminium. This translates to a linear error of 0.25 mm at prototype scale. The laser sensors must be warmed up for about 30 minutes before being put to active usage.

The laser sensor has three main components, namely, the sensing body, the relay cable and the controller/display unit. The sensing body houses the laser diode and its function is to emit laser beam upon connected to a power supply of 24V DC. The relay cable connects the sensing body to the DC power supply. The controller/display unit is used to control and set the measuring limit of the sensor. A display window on the unit shows the measurement data as voltage signal.

Calibration was carried out by securing a 100-mm Linear Variation Displacement Transducer (LVDT) to the sensing body of the laser sensor. The LVDT was connected to a voltmeter so that the voltage could be displayed digitally. The LVDT could take up to a maximum of 10 V. Hence, a direct relationship between displacement and voltage could be established, i.e. 1 V per 10 mm movement of the LVDT. The laser sensor has a specified optimum range of measurement to ensure accuracy of the readings. However, readings outside this optimum range can still be measured by the laser sensor but to a lesser accuracy. Therefore, calibration is ensured to lie only within this optimum range (for example, see Figure 3.11). As such, the LVDT serves as an indication or a ‘ruler’ for the calibration of the laser sensor.

The output voltage reading on the laser sensor display unit varies with the displacement. Each set of readings of the LDVTs and the laser sensors were recorded at every specified displacement intervals so that correlation between displacement and voltage could be established. The calibrated charts for the two laser sensors used in the centrifuge tests are shown in Figures 3.12 and 3.13.

3.3.8 Kaolin clay

The kaolin clay used in the present study has a liquid limit (LL) of 80 %, plastic limit (PL) of 40 % and hence a plasticity index (PI) of 40 %, and a specific gravity, G_s, of 2.65. The compression index, C_c and swelling index, C_s are 0.64 and 0.13, respectively. The coefficient of permeability of normally consolidated kaolin at a consolidation pressure of 100 kPa is about 1.36×10^{-8} m/s. The effective internal friction angle, ϕ', is 25^o Kaolin clay has critical state parameters λ of 0.27, average κ of 0.06, Γ of 3.265 and M of 1.02. The ratio of undrained shear strength, c_u, to the effective overburden pressure for the normally consolidated clay is typically between 0.20 and 0.30.

3.3.9 Sand

The sand that underlies the clay in each test serves as a stiff material for wall and pile embedment as well as for drainage purpose. The sand used is Toyoura sand, which is described in detail by Shen (1999). It has a mean grain size of 0.26 mm, uniformity coefficient of 1.3 and specific gravity, G_s, of 2.645. The maximum and minimum density of the sand is 16.17 kN/m^3 and 13.10 kN/m^3, respectively. Under a confining pressure of between 50 and 100 kPa, the peak internal friction angle is about 43^o.

3.4 EXPERIMENTAL PROCEDURES AND ASSESSMENT

Standard or repetitiveness of experimental procedure is very important as it determines the reliability of reproducing similar soil stress state in each experiment. Both clay and sand were used in the present experiments. The thicknesses of the sand and clay layers depend on the requirement of each experiment. Besides that, the assessment of retained soil stress immediately prior to excavation at the reconsolidation stage as well as the evaluation of the effectiveness of the image processing system in this study are also presented.

3.4.1 Preparation of model ground

All kaolin clay samples tested were normally consolidated with a layer of overconsolidated crust. Standard preparation procedure was adopted to ensure repetitive reproduction of the model ground with similar stress distribution in each test. The kaolin powder was mixed with water at a water content of 120% in a de-airing mixer to produce uniform clay slurry as shown in Figure 3.14. Simultaneous mixing and de-airing could be done at the same time and thus the clay preparation time is cut down. De-airing is important as it ensures that the clay slurry is fully saturated. De-airing also helps to free trapped air bubbles. This process normally took about 4 to 5 hours.

The four walls of the container were greased to reduce the soil-wall friction during testing. Subsequently, the model container was filled with water before the sand was rained down from a height of 600 mm. This ensures that the sand is saturated and is uniformly formed at the bottom of the model container. Depending on the requirement of the experiments, the thickness of sand may vary between 40 mm to 130 mm. This will be further discussed in Chapter 4.

A sheet of filter paper was then placed on top of the sand to prevent direct contact between the sand and the clay that would be placed subsequently. This is to ensure that the sand will not be "contaminated" and thus can be re-used after each test. The kaolin slurry was then placed carefully under water to avoid trapping of air bubbles until the desired height was reached. Two pore pressure transducers (PPTs), which had been de-aired, were embedded in the kaolin slurry. As the kaolin slurry was initially very soft, it was left in the container to consolidate under its own weight overnight. Subsequently, a 17 kg plate measuring 520 mm long, 190 mm wide and 60 mm thick was placed on top of the slurry to stiffen it for a couple of days. Then, the sample was placed on a loading frame for further 1-D consolidation under a loading pressure of 20 kPa.

3.4.2 Self-weight consolidation

When the kaolin clay had fully consolidated under a 20 kPa pressure, two linear variation displacement transducers (LDVTs) were installed on the clay surface. The LVDTs were supported by a gantry, which was bolted to the edge of the model container. After that, the model container was placed on the centrifuge swing platform and spun up to 50g for about 6 to 7 hours to allow the kaolin clay to consolidate under its own weight to obtain a normally consolidated sample. The dissipation of excess pore water pressure was monitored by the PPTs embedded in the kaolin clay.

The ground surface settlement was monitored by the LDVTs. When the LVDTs register negligible changes, the centrifuge was spun down and the model container was removed from the platform. In doing so, a 2.8-m (prototype scale) thick layer of stiff overconsolidated crust is obtained so that instrumentation work can be carried out easily. Had this overconsolidated crust not been there, instrumentation

work would be very difficult, as the soft clay would collapse easily. However, much of the clay remained normally consolidated.

3.4.3 Excavation and installation of model pile at 1g

After consolidation under 50g, the kaolin clay became stiffer and thus more manageable. The back face of the model container was then removed so that additional PPTs could be embedded at pre-determined positions.

A polyethylene tube, which would be used to drain off the zinc chloride from the latex bag, was fastened through the valve at the bottom corner of the back face. The valve was then tightened so that the 'O' rings would expand and squeeze against the polyethylene tube to ensure water tightness. One end of the polyethylene tube was connected to the bottom of the latex bag while another end was connected to a solenoid valve fixed onto the top of a stainless steel container. The solenoid valve, as shown in Figure 3.15, was controlled by a 24V DC power supply. When power was supplied during flight, the valve would open to release the zinc chloride solution in-flight.

The stainless steel container would be used to contain the drained zinc chloride during in-flight excavation. After this was done, the back face was bolted back to the main body of the container. Subsequently, the model wall and model pile were installed at 1g by jacking them into the clay using a guide to ensure that it was installed vertically as shown in Figure 3.16.

Excavation was then carried out at 1g. The clay was carefully removed to minimize ground disturbance. The removed clay was replaced by zinc chloride solution in a latex bag. The density and height of the zinc chloride solution were made identical to those of the clay that had been removed.

3.4.4 Placement of soil markers

The front perspex face of the model container was then removed to place markers on the kaolin clay with the aid of a template at 20 mm grid as shown in Figure 3.17. The markers were used to track the soil movement during and after the excavation process so that the magnitude of soil movement could be quantified.

3.4.5 Instrumentation of model ground and model pile

Subsequently, a series of LVDTs and a pair of non-contact laser displacement transducers were installed and supported from a gantry fastened to the edges of the model container as shown in Figure 3.18. The LVDTs were used to measure the ground settlement behind the excavation.

The pile head deflection during and after the excavation was monitored by the two non-contact laser transducers. Owing to the size of the laser transducers, it was not possible to measure them at the ground level. Since the pile head deflection was measured at two elevations along the free standing portion of the model pile above the ground, it is possible to calculate the pile head deflection at the ground level by linear interpolation. Figure 3.18 shows the plan view of the package set-up complete with the necessary instrumentation.

3.4.6 Preparation for data acquisition

Two personal computers in the control room were used to acquire the data. A computer software called Dasylab was used in the first computer to acquire readings from the PPTs and LVDTs. The second computer was used to run the image processing system so that images could be captured during the experiments and also to acquire the strain gauge readings from the on-board data logger after the experiment. The sampling rate for both computers was 3 seconds. The time on both the computers

were synchronized so that the PPT, LVDT and the strain gauge readings could be simultaneous. The data acquisition system was checked to be working properly before the start of each centrifuge experiment. All wired connections and bolts were ensured to be tightly secured. After checking, the data acquisition system was triggered to start acquiring data just before the centrifuge was activated. The image processing system was activated when excavation was to be carried out. The completed centrifuge package is shown in Figure 3.2. Finally, the model package was spun up to 50g for the reconsolidation of soil.

3.4.7 Assessment of in-flight simulation of excavation using $ZnCl_2$

When zinc chloride solution ($ZnCl_2$) is used as a substitute for the excavated soil, stress inequilibrium will occur initially due to different lateral stresses imposed by the soil and the liquid. It should be noted that in-flight excavation was only carried out when there were no further recorded changes in the consolidation settlement and pore water pressure values. In an undrained condition, the soil stresses can be characterized by its lateral earth pressure coefficient, K_T, which is the ratio of the total horizontal to the total vertical stresses in the soil (Holtz and Kovaks, 1981). Therefore, this K_T value is deemed appropriate to describe the soil total stresses prior to the start of excavation process.

In order to study the stress state of the retained soil prior to excavation, two total stress cells (TSCs) were embedded at depths 1.5 m (TSC 1) and 3.5 m (TSC 2) at a distance of 0.5 m behind the wall. It is also very important to embed corresponding pore water pressure transducers (PPTs) close to the TSCs so that the effective stresses of soil can be calculated. Owing to soil settlement during the high-g reconsolidation, the image processor is used to capture the soil images over specified intervals so that subsurface settlement can be measured. When the settlement at the location of the

TSCs is known, corrections can then be made to the embedded depths of the TSCs, which are expected to settle together with the consolidating soil (Lee et al., 2002).

Since the unit weight of the clay is known and the height of the water table above the ground surface can be measured by two PPTs on the ground surface, the total, σ_v, and effective overburden pressure, σ_v', can be calculated. Besides that, the lateral earth pressure coefficients at rest for a normally consolidated, K_{onc}, and overconsolidated, K_{ooc}, clay layer can be calculated as follows:

$$K_{onc} = 1 - \sin(\phi') \qquad \text{(Jaky, 1948)} \qquad (3.1)$$

$$K_{ooc} = K_{onc}(OCR)^{\sin(\phi')} \qquad \text{(Mayne and Kulhawy, 1982)} \qquad (3.2)$$

Therefore, the effective horizontal stress, σ_h' can be calculated since K_o and σ_v' are already known. The pore water pressure, u, can also be calculated since both σ_h' and σ_h (directly measured from TSCs) are known as well. This calculated pore water pressure is then compared to the measured values from the PPTs and is shown in Figure 3.19. Since both the measured and calculated pore water pressure show fair agreement, it can be safely deduced that the TSCs are reliable in measuring the total stresses in the soil in this study.

Figure 3.20 shows that immediately after 50g has been achieved during the spinning up process, the average lateral earth pressure coefficient (TSCs 1 and 2), K_T, of the retained soil is about 1.49. Since the K_T value for the $ZnCl_2$ is 1.0, wall and soil movement towards the excavation are inevitable as shown in Figure 3.21. After about 2 hours (model time) of reconsolidation, the K_T values of TSCs 1 and 2 would decrease due to dissipation of pore water pressure.

With the subsequent reduction in the differences of K_T values over time, the wall and soil movement would eventually reduce too. Therefore, after about 3 hours (model time) of high-g reconsolidation, stress and hydrostatic equilibrium is checked

based on the changes in the K_T values. Figure 3.22 shows that for 30 days (prototype scale) prior to excavation, the K_T values are indeed consistent and shows minimal fluctuation, suggesting an undrained hydrostatic equilibrium condition. At this stage, the average K_T value measured on the retained soil is about 1.13, which is only slightly higher than the value of 1.0 due to the $ZnCl_2$. As such, movement was expected to be negligible at this stage. This is consistent with the observation that no further wall or soil movement was noted by the image processing system. Subsequently, in-flight draining of the $ZnCl_2$ from the rubber bag to simulate excavation was ready to be carried out.

When both excess pore water pressure and ground settlement behind the wall showed negligible changes over time, the power supply controlling the solenoid valve would be switched off so that the $ZnCl_2$ could be released to depict excavation at 50g. In prototype scale, the simulated excavation rate was 0.6 m per day. All data acquired and still images captured would be stored as temporary files in the computers and could be retrieved after the experiment.

From this assessment, it has been shown that under an undrained condition, the K_T value of an overconsolidated (OC) layer is higher than that of a normally consolidated (NC) layer. The K_T value of an OC layer is generally higher than unity, while the K_T value of a NC layer is lower than unity after 3 hours of reconsolidation (model time). This implies that if the $ZnCl_2$ depth is equal or less than the depth of the OC layer at the retained side, the average K_T value would not differ significantly from unity. Satisfactory stress equilibrium can hence be achieved at both sides of the wall immediately prior to excavation.

3.5 IMAGE PROCESSING SYSTEM

Image processing techniques have been used by Allersma (1991) and Davies and Jones (1998). The image processing system used in NUS consists of a high resolution camera, a lighting system, an on-board computer mounted on the centrifuge and a command computer in the control room. This image processing system is capable of capturing live images of the soil movement during an in-flight centrifuge test via a remote control function.

3.5.1 High resolution camera

A CV-M1 2/3" CCD Progressive Scan High Resolution Camera was mounted in front of the perspex window of the model container. The resolution of the images captured using this camera is over a million pixels. However, the accuracy of soil movement measurement depends on the size of the image captured; the smaller the area of interest, the better is the accuracy. For a high resolution image, the size of an image of about 100 mm x 100 mm can produce a pixel-to-pixel spacing of less than 0.1 mm.

3.5.2 Lighting system

An appropriate lighting system is important in producing sharp and clear images, as shown in Figure 3.23. Two spot lights, each with a 50 W halogen bulb, were positioned on a cross bar at a specific distance in front and parallel to the model container to achieve the best lighting effects. When the centrifuge was in operation, the florescent lights inside the centrifuge enclosure were turned off. This would greatly enhance the quality of the images captured.

3.5.3 On-board and command computers

The on-board computer mounted on the centrifuge was capable of sustaining high gravitational force without being damaged. The computer consists of a solid-state hard disk, which is a collection of solid-state semi-conductors to provide fast access time as compared to a conventional hard disk. Since the hard disk of the computer was specially designed and built, it provided greater resilience to physical vibration, shock and extreme temperature fluctuations. All captured images were stored in this on-board computer.

Both the on-board computer and the command computer in the control room were loaded with three different types of software, namely, PCVision, PcAnyWhere and Optimas.

PCVision is capable of buffering images between the camera and host PC system to enhance the quality of the images. This feature allows faster transfer of images as well as simultaneous acquisition and processing of data. The memory of the on-board computer also assures that the images will not be lost during transfer of files from hard disk to system memory or vice-versa.

PcAnyWhere enables the on-board computer to be manually controlled by the command computer in the control room so that image capturing can be activated at any time during a centrifuge test. Wireless communication between the two computers can be established either via an "internet" mode or a "direct" mode. In the "internet" mode, the communication between the two computers is via the Internet TCP/IP protocol, whereby each computer is identified by its unique allocated IP address and communication is automatically established via the internet. Any intermittent network instability, which may occur unexpectedly, will inevitably interfere with the controlling operation. Owing to this risk involved, the "direct" mode is preferred.

In the "direct" mode, the computer is connected directly to the on-board computer using a "cross" type network cable. By this configuration, the command computer in the control room establishes a "direct" connection with the on-board computer. This "direct" mode works in a more self-contained and robust environment, and will not be affected by any internet connectivity problem. This "direct" remote sensing method of communication is used for all the centrifuge tests.

Once the connection between the two computers is established, the command computer in the control room can virtually take control of the on-board computer. Hence, the image capturing process can be activated anytime at the user's will.

3.5.4 Assessment of effectiveness of image processing system

The image processing method is used to track the soil markers so that the soil movement due to excavation can be quantified. If necessary, this method can also be extended to measure the deflection profile of the wall since the wall has also been permanently marked with black dots at a specified interval as shown in Figure 3.23. The image processing software, Optimas, is used for live capturing of the desired images during in-flight centrifuge operation manually or at a specified time interval automatically. Optimas also enables calibration of distance between two fixed points in terms of pixel prior to the analysis. Pixel can be thought of as the small discrete elements that together constitute an array of element known as image and the value of a pixel is the average luminance value of an image.

Since the number of pixels for each set of pictures taken after each centrifuge test is unique, a standard calibration method is necessary. Unless the focusing distance between the image processing camera and the model container in each centrifuge test can be consistently maintained to be exactly identical, variation in the number of pixels is due to occur. For this calibration purpose, two fixed points exactly 20 mm apart

from centre-to-centre were placed on the inside perspex screen at the same focusing distance as the soil markers so that this calibration points would be captured in every still image. These two points serve as reference points to convert pixel distance into a linear measuring unit. These reference points were located above the retained soil as shown in Figure 3.23. In this research, the average calibration factor obtained using this method is about 0.22 mm per pixel.

In order to assess the effectiveness of the image processing system, two methods of measuring the surface settlement are adopted. The first method is the direct measurement of the surface settlement using LVDTs at various distances behind the wall. The second method involves measuring the subsurface settlement by tracking the vertical movement of the soil markers at various depths using the image processing method.

A typical reconsolidation stage of a centrifuge test is used for this purpose. Figure 3.24 shows the settlement measured by both these methods over time. It is observed that the measured total sub-soil settlement agrees well with the direct measurement of the surface settlement using LVDTs. In view of this, the image processing analysis can be considered a competent and reliable method to measure the soil movement in the present study.

3.5.5 Post-processing of images

For the post-processing of the images, Optimas offers a powerful function of "Motion Analysis" whereby the movement of the points of interest in a series of images can be tracked using a pre-defined co-ordinate system. The movement of the points of interest can be established as the pixels of the images are converted into a linear measuring unit if the calibration is known.

The results of soil movement can be readily exported from Optimas to Excel spreadsheet for further manipulation. After the necessary calculations were done in Excel, the final results of soil movement were plotted in vectors and contours for easy visualization using a plotting software called Surfer version 7.0. Basically, the input parameters are the magnitudes and direction of the movement of the beads analyzed using Optimas. The computer software, Surfer, could be used to interpolate the soil movement in areas where the beads were not present, for example, at locations in in-between the beads.

Table 3.1 Scaling relation of centrifuge modelling

Parameter	**Prototype**	**Centrifuge model at Ng**
Linear dimension	1	1/N
Area	1	$1/N^2$
Volume	1	$1/N^3$
Density	1	1
Mass	1	$1/N^3$
Acceleration	1	1/N
Displacement	1	1/N
Strain	1	1
Energy	1	$1/N^3$
Stress	1	1
Force	1	$1/N^2$
Time (creep)	1	1
Time (dynamics)	1	1/N
Time (seepage)	1	$1/N^2$
Flexural rigidity, EI	1	$1/N^4$
Axial rigidity, EA	1	$1/N^2$
Bending moment	1	$1/N^3$

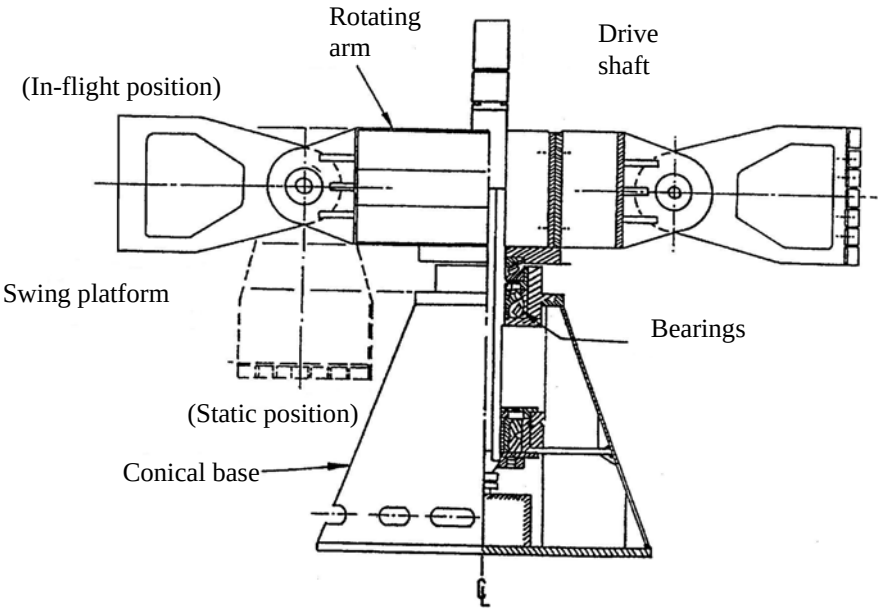

Figure 3.1 Elevation view of the NUS centrifuge

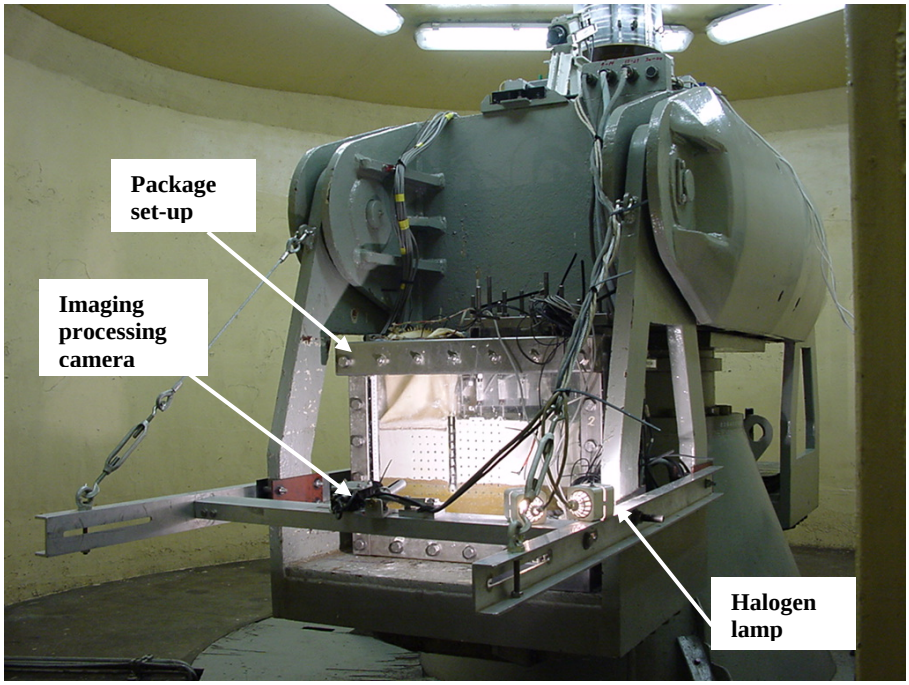

Figure 3.2 Centrifuge package set-up with lighting system and image processing camera

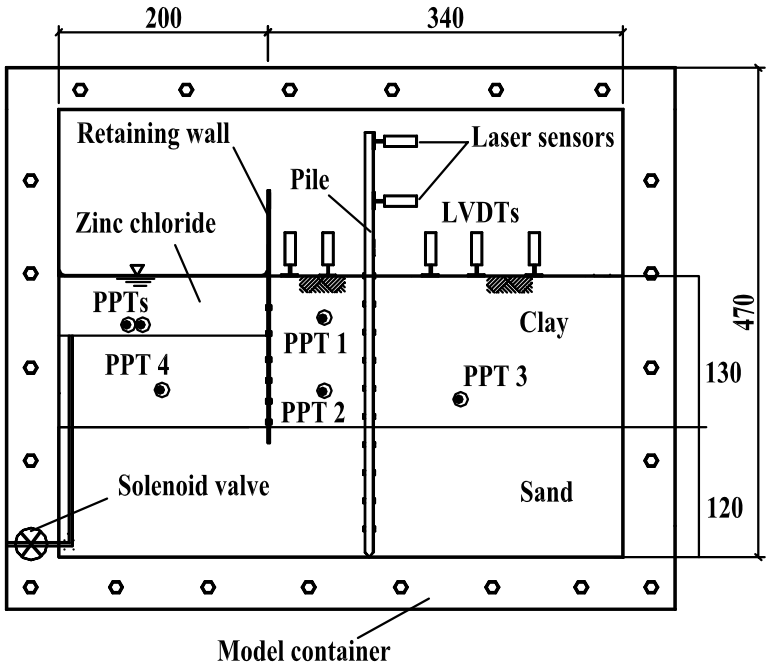

Figure 3.3 Experiment set-up of the present study

Figure 3.4 A partially completed and a completed model pile

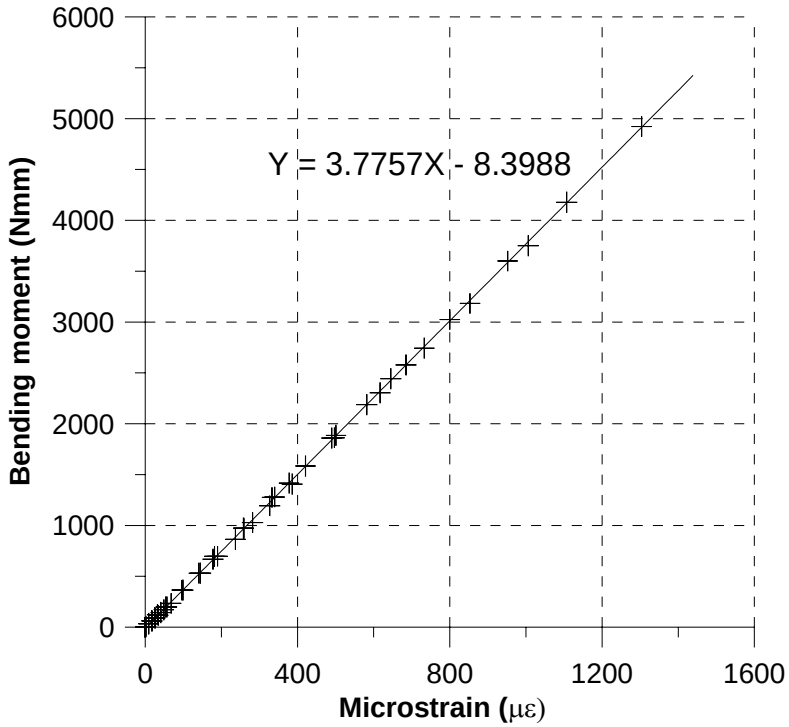

Figure 3.5 Typical calibration chart for the instrumented pile (Face A)

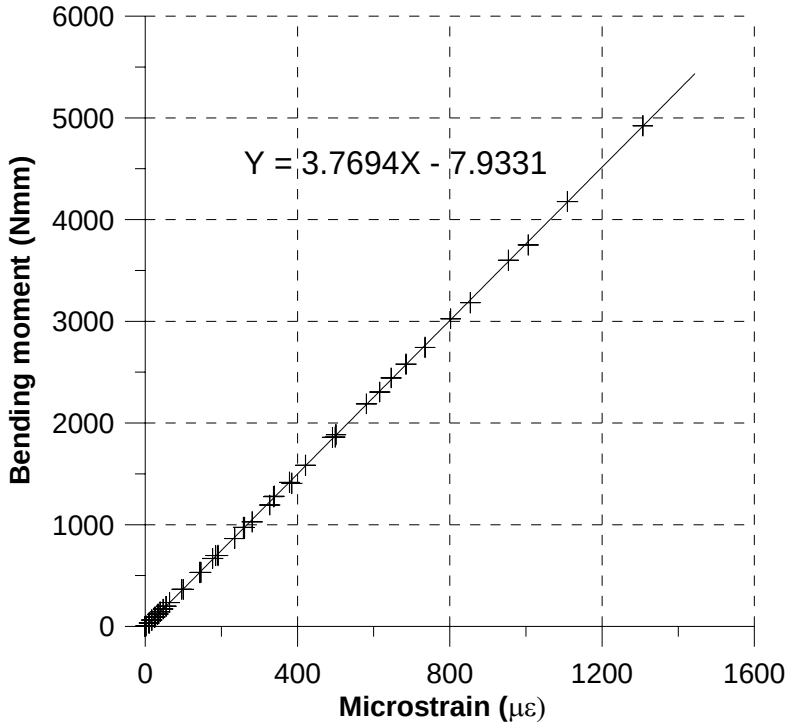

Figure 3.6 Typical calibration chart for the instrumented pile (Face B)

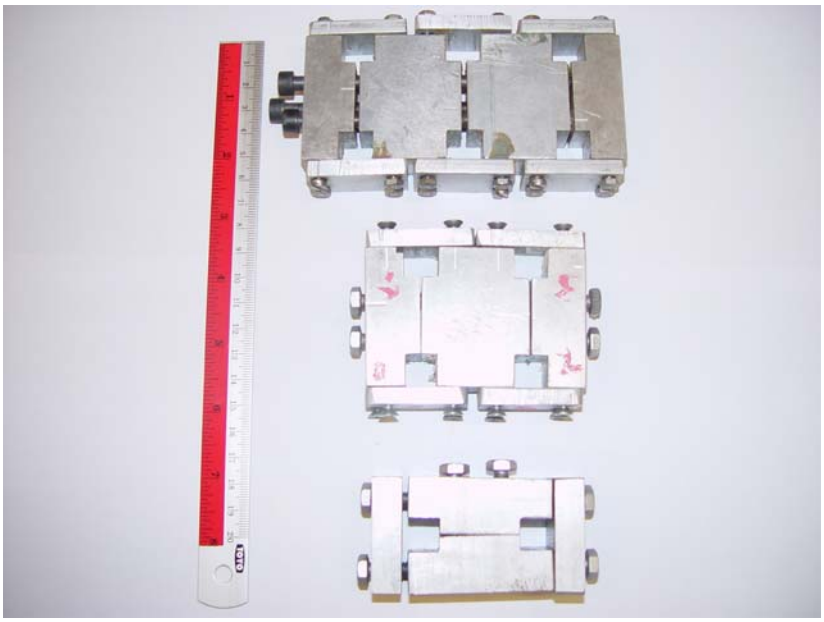

Figure 3.7 Pile caps that can be clamped in both directions

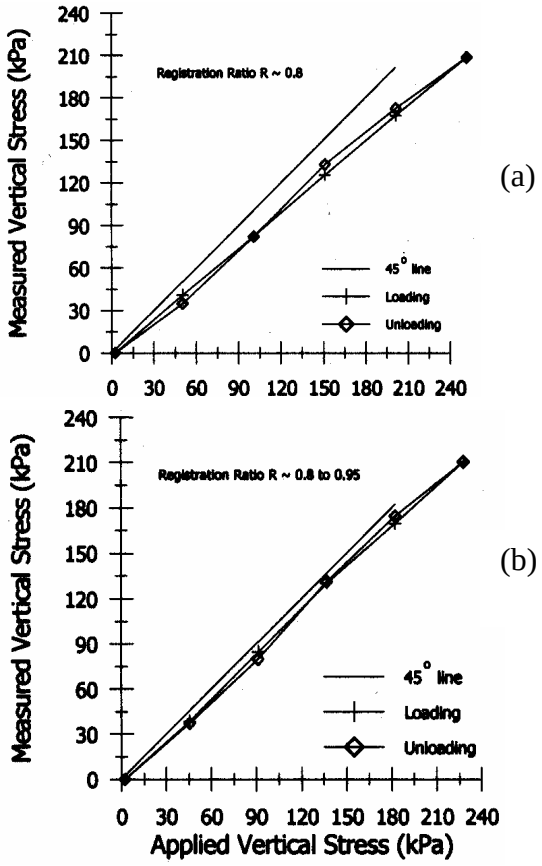

Figure 3.8 Measured and applied vertical stress over 2 consecutive loading unloading cycles at high-g (a) Cycle 1 (b) Cycle 2 (after Lee et al., 2002)

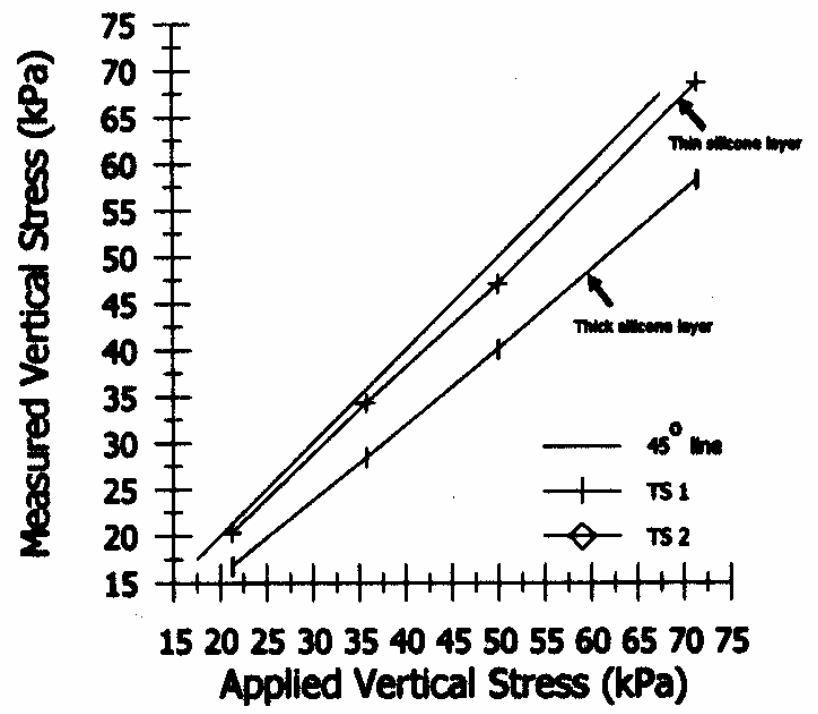

Figure 3.9 Measured and applied vertical stress over 2 consecutive loading unloading cycles at high-g (a) Cycle 1 (b) Cycle 2 (after Lee et al., 2002)

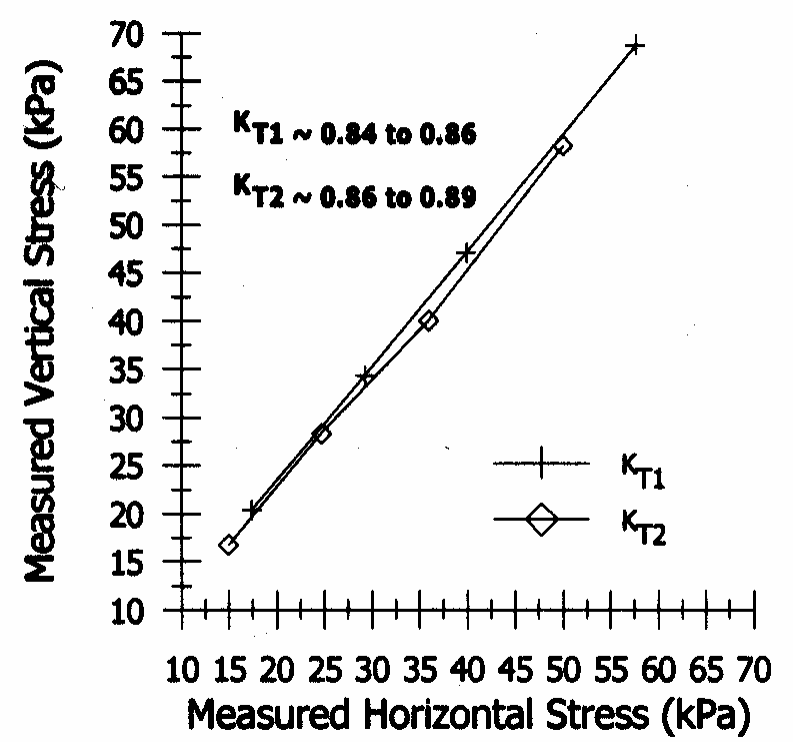

Figure 3.10 Variation of measured vertical and horizontal stress at high-g (after Lee et al., 2002)

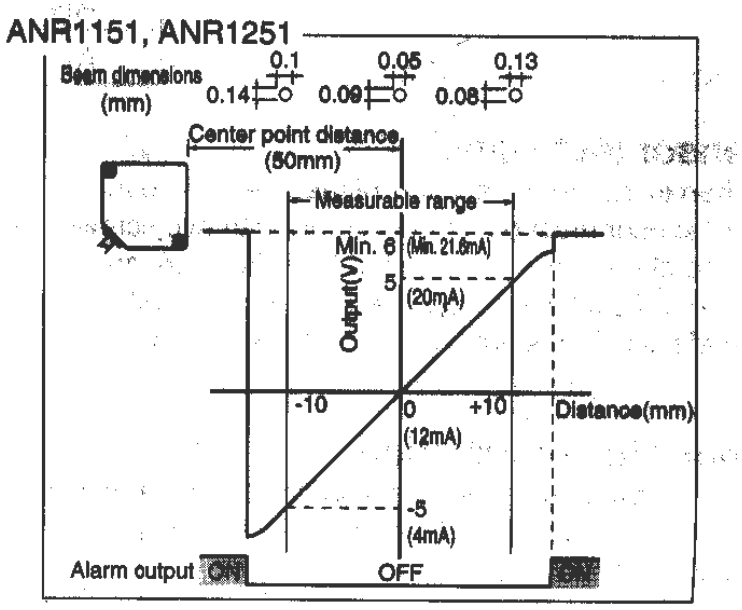

Figure 3.11 Typical optimum measuring range of a laser sensor

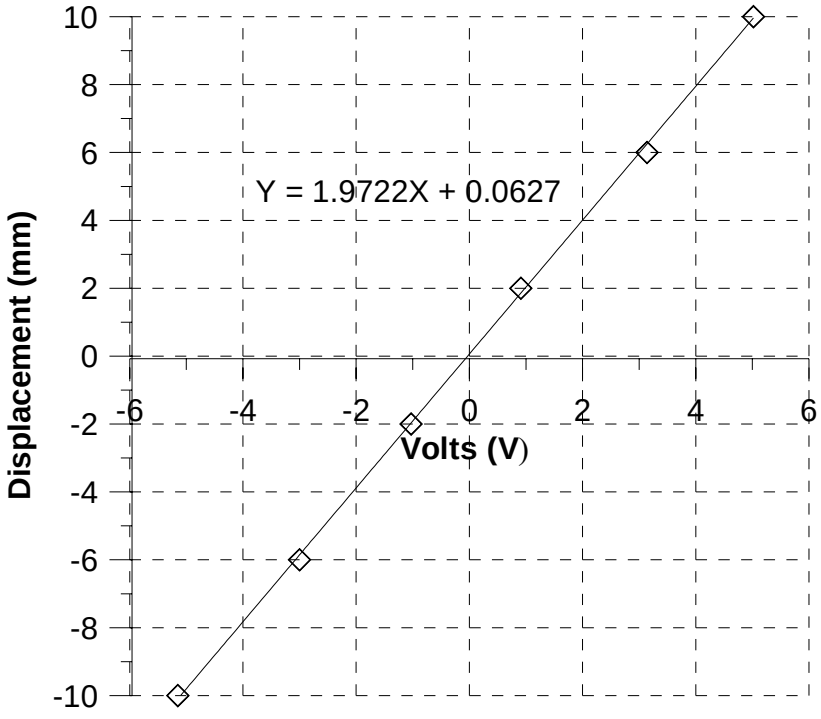

Figure 3.12 Typical calibration chart for laser sensor A

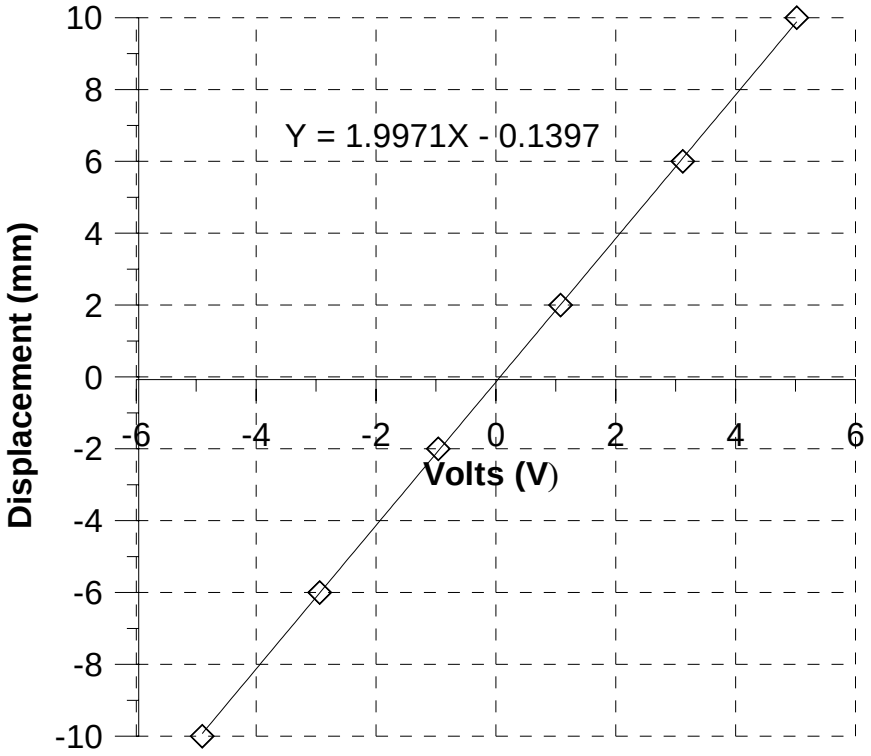

Figure 3.13 Typical calibration chart for laser sensor B

Figure 3.14 De-airing mixer used to mix and de-air kaolin clay

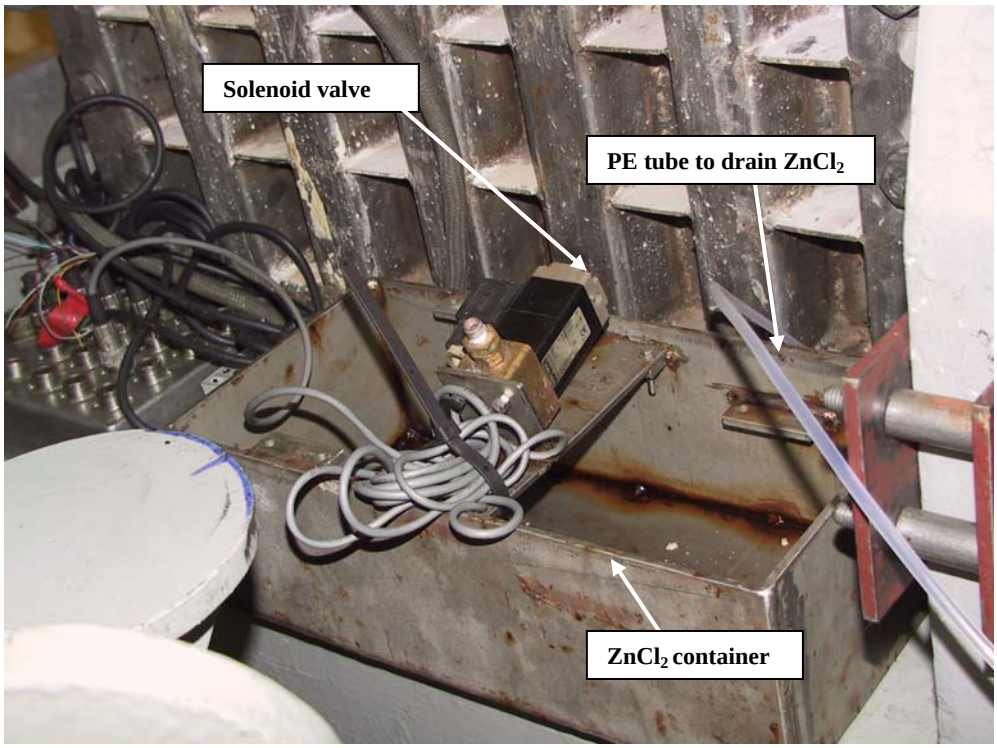

Figure 3.15 Solenoid valve and stainless steel container behind the model container

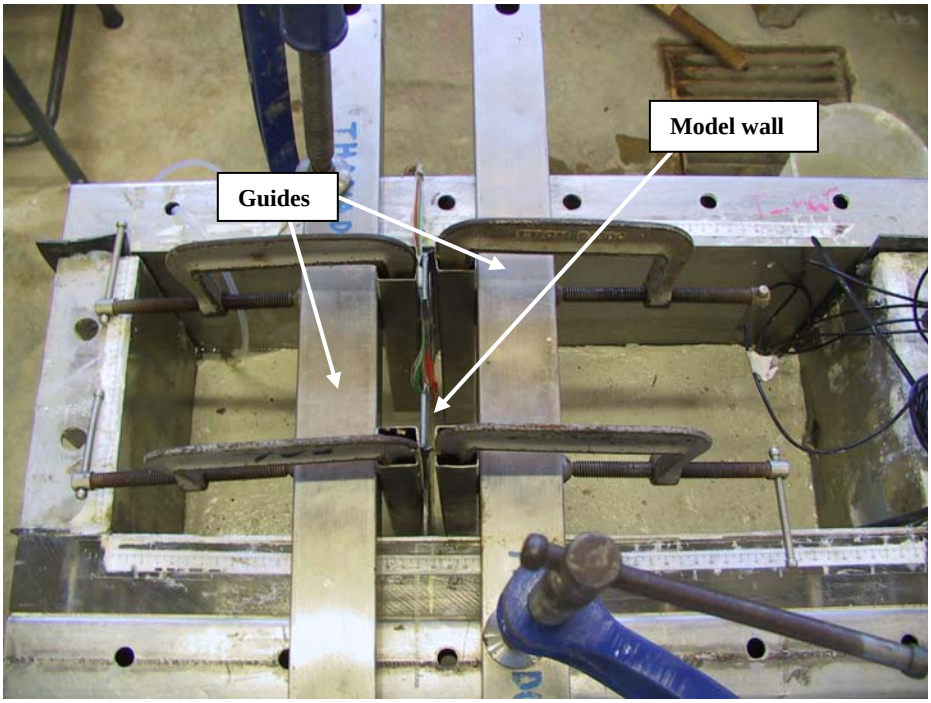

Figure 3.16 Installation of model wall using guides to ensure verticality

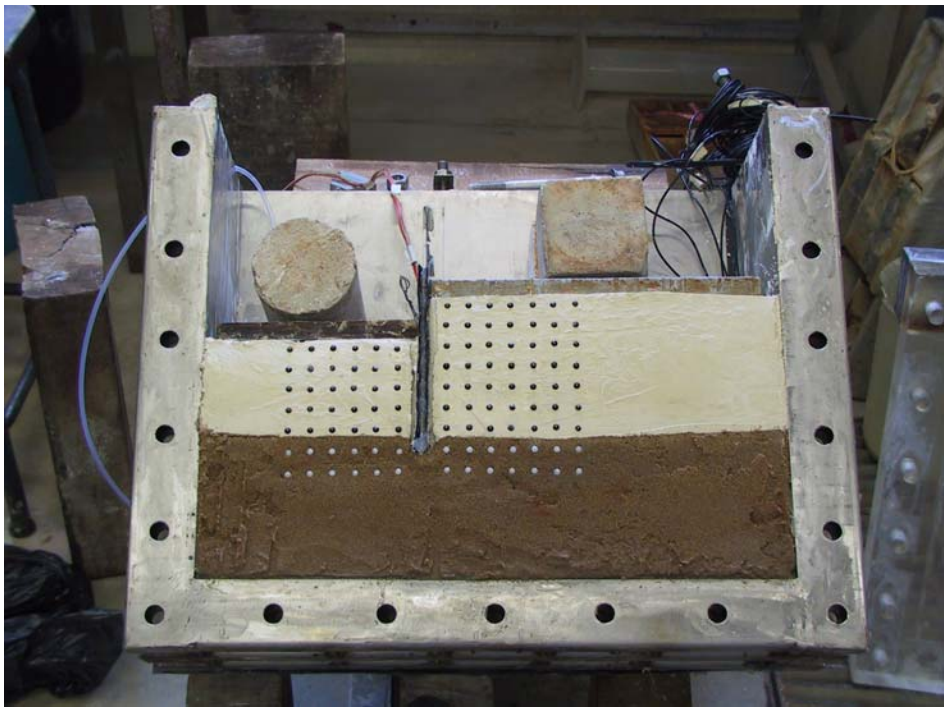

Figure 3.17 Placement of markers on soil to track soil movement

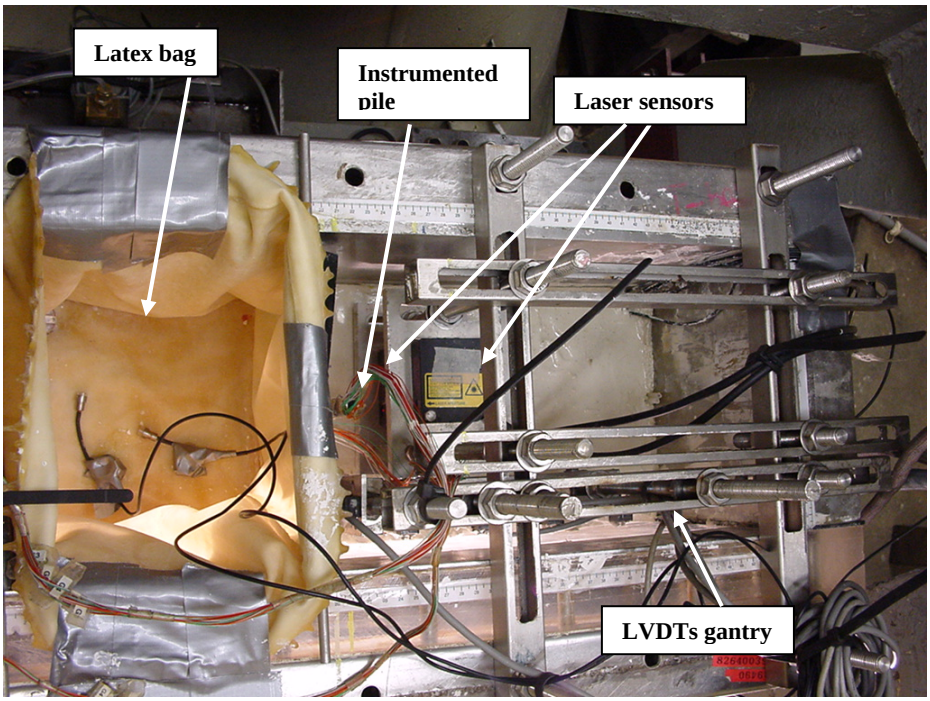

Figure 3.18 Plan view showing the instrumentations installed on the model container

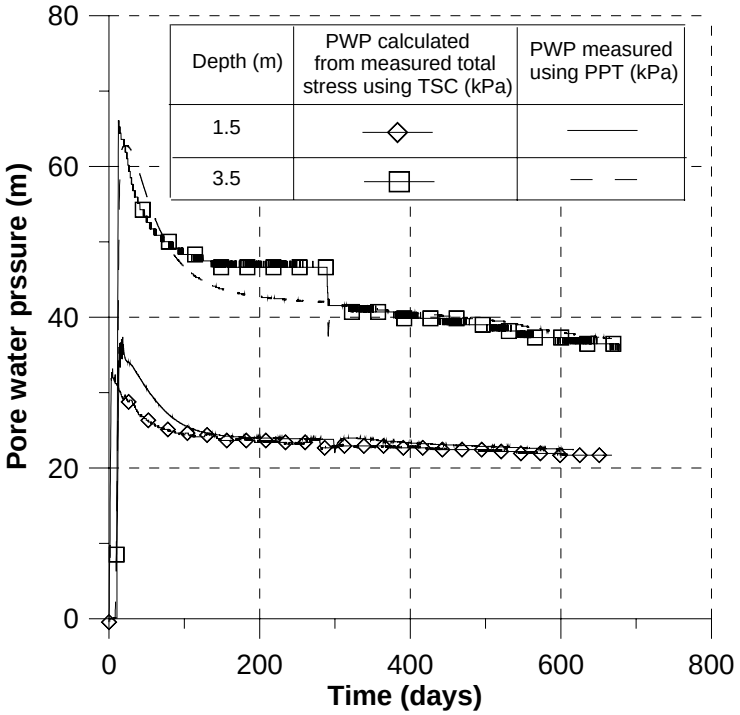

Figure 3.19 Calculated pore water pressure from TSCs compared with that measured from the PPTs (water table approximately 0.5 m above clay surface)

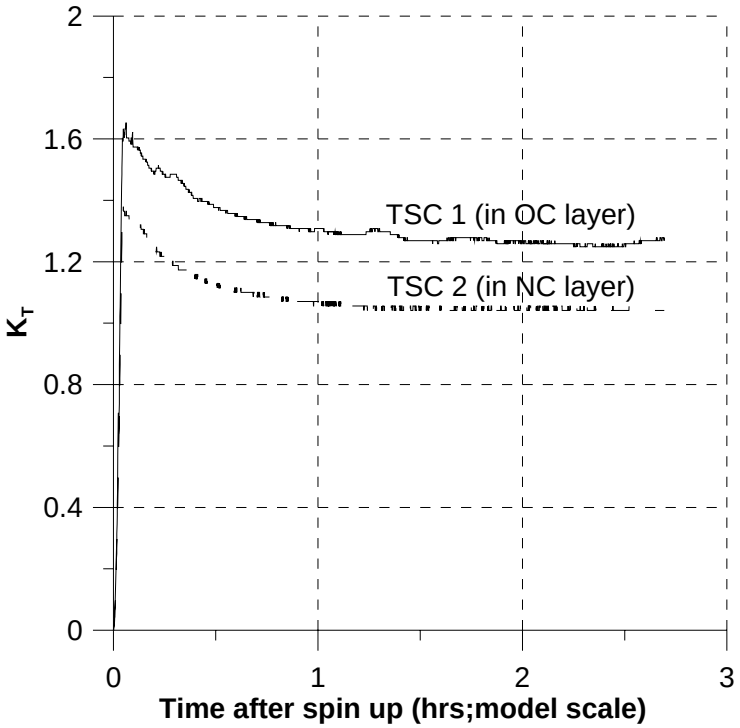

Figure 3.20 Measured K_T value during reconsolidation of clay

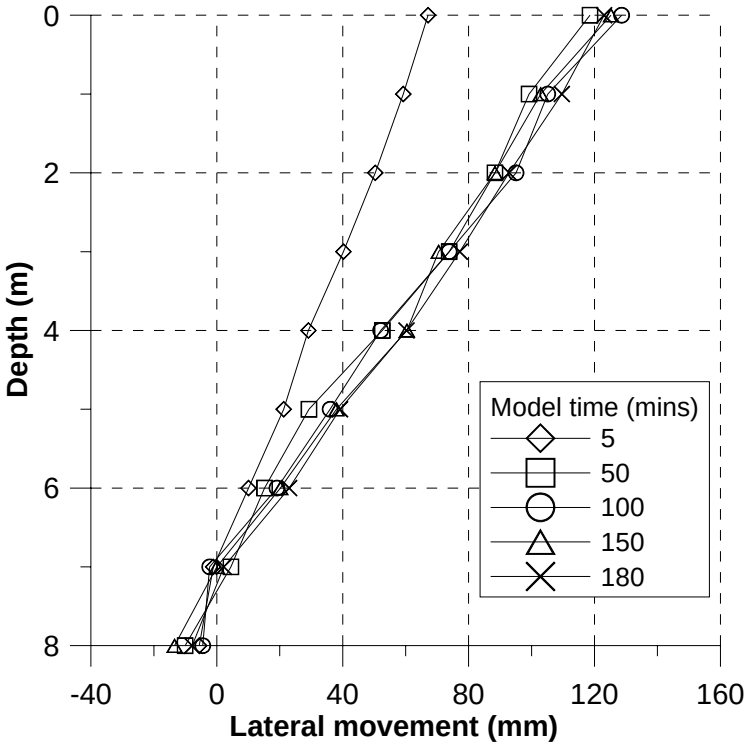

Figure 3.21 Measured wall deflection profile during reconsolidation

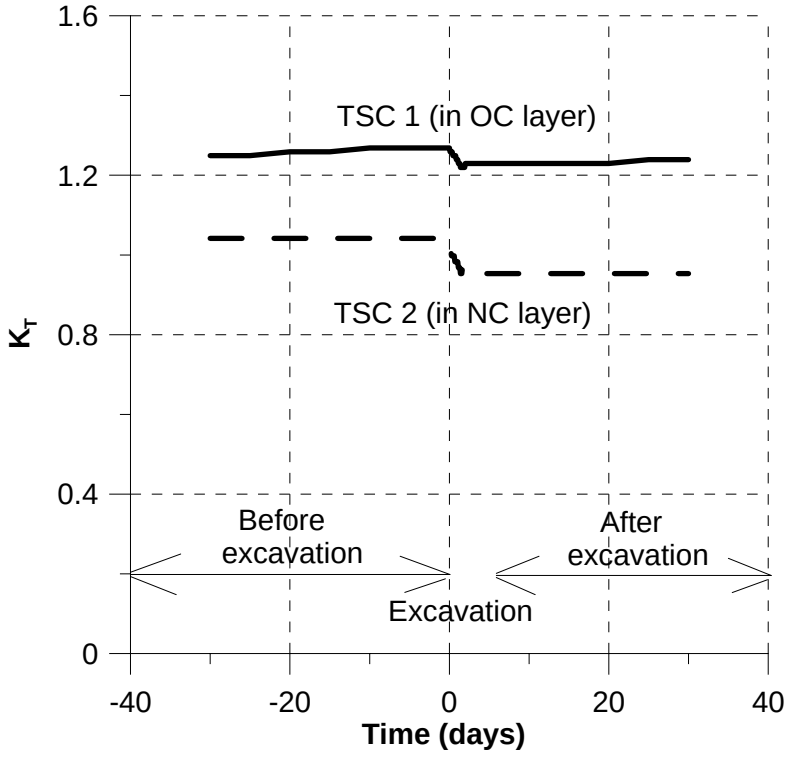

Figure 3.22 Measured K_{total} 30 days before and after excavation (0 days denotes start of excavation)

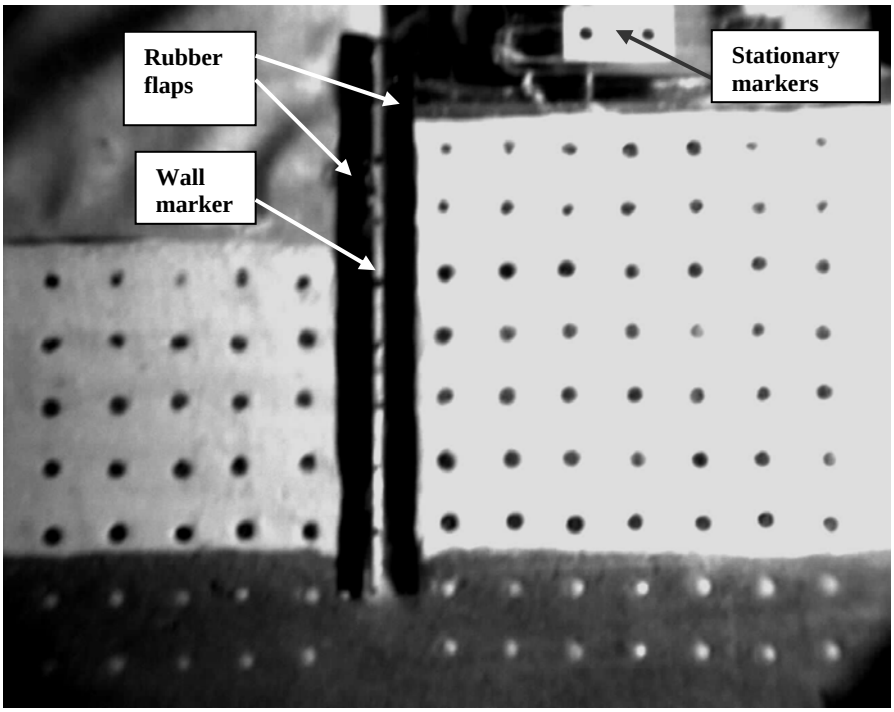

Figure 3.23 Sharp and clear image captured using the image processing camera

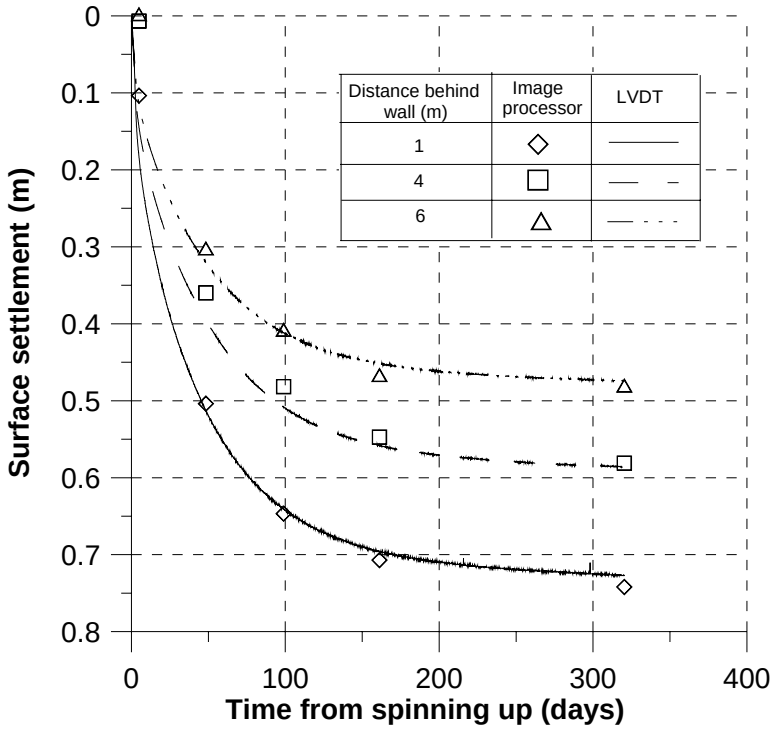

Figure 3.24 Comparison of ground settlement measured using image processor and LVDTs

CHAPTER FOUR

BEHAVIOUR OF SINGLE PILE ADJACENT TO EXCAVATION IN CLAY

4.1 INTRODUCTION

As reported in Chapter 2, only limited case studies and laboratory tests have been carried out to investigate the pile responses due to an adjacent excavation in clay. To obtain a better understanding on the effects of excavation on a nearby pile foundation, centrifuge tests are carried out in the present study. The first test series involved a free head single pile behind a wall that remained stable after excavation. In the subsequent second test series, the excavation was made deep enough so that the wall would subsequently fail to fully appreciate the pile responses under this extreme circumstance.

The failure of retaining wall is defined as the onset of excessive wall deflection. During and after completion of soil excavation in front of the wall, the ground surface settlement trough behind the wall, subsurface soil movement and pore water pressure in the soil, wall and induced pile head deflection as well as bending moment profiles along the pile were monitored regularly. This chapter reports the results of the abovementioned centrifuge tests.

4.2 TEST PROGRAM

All the centrifuge tests were performed at 50g. Unless otherwise stated, the test results are presented in prototype scale hereinafter. The complete test program of single pile is shown in Figure 4.1. The single pile in Tests 1, 2, 3 and 4 are located 1, 3, 5 and 7 m behind the retaining wall, respectively. In these tests, the excavation depth is 1.2 m and the single pile is socketed 6 m into the lower sand layer. The pile toes are rested directly on the base of the model container. Tests 1, 2, 3 and 4 represent cases where the wall remains stable after excavation.

Tests 5, 6 and 7 were carried out to study the pile behaviour behind a marginally stable wall and a wall that subsequently collapses. In order to induce significantly large wall movement upon excavation, either the excavation depth is greater and/or the height of the underlying sand layer is reduced as compared to the earlier stable wall test series. In these tests, the pile is located 3 m behind the retaining wall.

4.3 EQUILIBRIUM ANALYSES FOR WALL STABILITY

A refined limit equilibrium analysis, (Bolton and Powrie, 1987) based on permissible stress fields was used to calculate the required wall embedment below the dredged line. In the analysis, the active and passive zones switch about a pivot point so that the unpropped wall could satisfy the conditions of both moment and force equilibrium This method is capable of giving a more reasonable prediction of wall failure than other widely used method such as “fixed earth support” method. Figure 4.2 shows the limit equilibrium of forces on the retaining wall. The depth of wall toe, d, and the depth of pivot point, z_p, are determined by solving both the horizontal force

and moment equilibrium equations simultaneously. The equation of equilibrium of horizontal forces is given as:

$$(h+d)^2\left[\gamma+(K_p-1)\gamma_r'\right]-(h+z_p)2\gamma_r'(K_p-K_a)-d^2\left[\gamma+(K_a-1)\gamma_e'\right]-z_p^2\gamma_e'(K_p-K_a)=0 \quad (4.1)$$

The equation of moment equilibrium about the wall crest is given as:

$$(h+d)^3\left[\gamma+(K_p-1)\gamma_r'\right]-(h+z_p)^3\gamma_r'(K_p-K_a)-d^2\left(\frac{3h+2d}{2}\right)\left[\gamma+(K_a-1)\gamma_e'\right]-z_p^2\left(\frac{3h+2z_p}{2}\right)\gamma_e'(K_p-K_a)=0 \quad (4.2)$$

where $\gamma_r'=\gamma-\gamma_w\left(\frac{2d}{h+2d}\right)$, $\gamma_e'=\gamma-\gamma_w\left(\frac{2(h+d)}{h+2d}\right)$ and γ is the bulk unit weight of clay. The active and passive earth pressure coefficients are K_a = (1-sinϕ')/(1+sinϕ') and K_p = (1+sinϕ')/ (1-sinϕ'), respectively. By substituting the soil bulk unit weight, γ, of 16.5 kN/m^3 and effective friction angle, ϕ', of 25^o and by iteration, Eqs. (4.1) and (4.2) can be solved simultaneously to yield d = 3.4 m and z_p = 3.2 m. Thus, a required wall embedment depth of 3.4 m is needed to maintain limit equilibrium of the retaining wall. To safeguard the wall against failure, a factor of safety of 2 is used and hence an embedment depth of 6.80 m below the dredged level.

For Test 5, the excavation depth is 1.8 m while the wall is embedded 6.5 m through the clay layer and 1.5 m into the underlying sand layer. The calculated factor of safety using the limit analysis is 1.46 and hence the wall is considered marginally stable. To model a cantilever retaining wall that eventually fails after excavation as in Test 6, the entire wall is embedded in clay. This is commonly known as a floating wall. For an excavation depth of 1.8 m, the calculated factor of safety is 0.95. Tests 6 was done to illustrate the importance of wall toe embedment into the underlying sand layer. To simulate a catastrophic wall failure case as in Test 7, the wall and soil conditions are the same as those in Test 5 but with a much greater excavation depth of 2.8 m.

4.4 IN-FLIGHT EXCAVATION

In-flight excavation was simulated by draining zinc chloride ($ZnCl_2$) solution from the rubber bag. The density of $ZnCl_2$ is 16.5 kN/m^3 and is identical to that of the clay. The simulated excavation rate is about 0.6 m per day, which is compatible to a medium scale excavation work. At this excavation rate, the change in pore water pressure caused by the release of lateral stress can be comfortably captured in this study. This is important because when the soil is unloaded, it will cause a drop in pore water pressure. If the excavation is carried out too fast, subsequent dissipation of excess negative pore water pressure and seepage effects over a longer time may conceal this drop.

4.5 IN-FLIGHT BAR PENETROMETER TESTS

A bar penetrometer or T-bar was used to estimate the undrained shear strength profile of the clay. The T-bar was first developed in the University of Western Australia and had been proven to be more advantageous than cone penetrometer and vane shear apparatus (Stewart and Randolph, 1991). It is an ideal tool to be used for clay since it combines the advantages of the cone penetrometer, which gives a continuous profile of strength and the vane shear device, which gives direct measure of shear strength.

Besides that, the bar factor, N_b, has a strong theoretical basis (Randolph and Houlsby, 1984) and its value may be chosen with confidence (usually around 10.5) as opposed to the cone penetrometer where the cone factor is dependent on OCR and the measured cone resistance is dependent on stress level (Stewart and Randolph, 1991). A particular application for the bar penetrometer is for laterally loaded piles. The test measures the ultimate soil pressure acting on the bar and thus, a direct comparison to

the ultimate lateral pile capacity may be made. The schematic diagram of a bar penetrometer is shown in Figure 4.3.

Figure 4.4 shows the undrained shear strength, c_u profiles for the kaolin clay tested under 50g at 1.5 m and 3.0 m behind a stable wall before and after excavation. Figure 4.5 shows the clay c_u profiles at 3.0 m behind the wall before and after the collapse of the wall in tests involving wall failure. Figures 4.4 and 4.5 reveal the presence of a 2.8 m thick lightly overconsolidated crust above the normally consolidated clay. It is also evident that the undrained shear strength of the clay prior to excavation increases with depth and can be readily described by:

$$\frac{c_u}{p_o'} = 0.29 OCR^{0.85} \tag{4.3}$$

where p_o' is the effective overburden pressure and OCR is the overconsolidated ratio. An important observation was noted. When in-flight T-bar tests were carried out for the stable wall test series, a drop in the c_u values was noted for clay at 1.5 m behind the wall only (see Figure 4.4). For clay at 3.0 m behind the wall, the c_u values did not reduce much. This is so because the clay experiences greater deformation nearer to the wall. However, if the wall collapsed after excavation, the c_u profile at 3.0 m behind the wall would reduce due to large soil deformation at the location.

4.6 SINGLE PILE BEHAVIOUR BEHIND A STABLE WALL

This section reports the results for Tests 1, 2, 3 and 4 where the retaining wall remains stable throughout the tests. The final excavation depth is 1.2 m and only free-head single piles are studied. The test results are presented in prototype scale according to relevant scaling principles. The following sign conventions have been adopted in the

present study. The deflection of the pile towards the excavation side is regarded as positive. The pile shaft curvature towards the excavation side is also taken as positive.

4.6.1 Test results

The test with pile at 3 m behind the retaining wall (Test 2) is used to illustrate the general trend of the results. Two pore water pressure transducers or PPTs were placed at the bottom of the latex bag to monitor the variation of the $ZnCl_2$ pressure during in-flight excavation. Figure 4.6 shows the variation of $ZnCl_2$ pressure and excavation depth over time. The excavation depth increases fairly linearly over time and it took about 2.0 days to reach an excavation depth of 1.2 m. This corresponds to an excavation rate of 0.6 m/day.

Figures 4.7(a) to (c) show the variations of excavation depth, wall head deflection and pile head deflection at ground level with time, respectively. It should be noted that the wall and pile head deflections at the ground level are derived by the linear geometry of the two displacement readings obtained along the free-standing portion of the wall and the pile, respectively. As the development of excavation depth and wall head deflection with time for the 4 tests are essentially identical, only a typical set of test data are shown in Figures 4.7(a) and (b) for clarity.

Figure 4.8 shows the measured ground surface settlement troughs at different times. These troughs are derived from several displacement transducers placed at various distances behind the wall. As expected, the magnitude of soil movement decreases with increasing distance from the wall. It is noted that after completion of excavation, the soil continues to settle with time with the rate of increase decreasing with time. However, between the completion of excavation to the end of test (about 350 days in duration), the incremental soil settlement is noted to be higher further away from the wall than those nearer to the wall. Such long term settlement behind the

wall after excavation is similar to those observed by Bolton and Powrie (1987). This observation will be further discussed later.

Figure 4.9(a) shows the induced bending moment profile along the pile at different times for Test 2 with the pile located at 3 m behind the wall. The induced bending moment is noted to increase with excavation depth and the maximum bending moment is located at about 7.5 m below the ground. After completion of excavation, the bending moment along the pile continues to increase for some time. The bending moment reaches the respective maximum values at about 50 days after completion of excavation and after which it decreases with time. This phenomenon will be explained in greater detail in the next section. The induced shear force and soil pressure profiles along the pile can be derived from the first and second derivatives of the bending moment profiles, respectively. This is achieved by fitting a fourth order spline function between successive data points. On the other hand, the pile deflection profile can be obtained by integrating the spline function for the bending moment profiles twice with two specified boundary conditions in the double integration. The first condition is the measured pile head displacement and the second is zero pile toe rotation.

By specifying the above specific boundary conditions, the use of the extremely sensitive pile head rotation in the double integration process that may considerably affect the accuracy of the end results could be avoided. Figures 4.9(b), (c) and (d) show the derived pile shear force, deflection and lateral soil pressure profiles, respectively. Similar to the bending moment profile, the pile shear force, deflection and soil pressure profiles reach the respective maximum values about 50 days after excavation and after which they reduce slightly with time. This is expected as the shear force, deflection and lateral soil pressure profiles are derived from the measured pile bending moment profiles.

The development of maximum induced pile bending moment along the pile with time for all the 4 tests is shown in Figure 4.7(d). The elevation of the maximum induced pile bending moment is noted to be the same for all the 4 tests. As mentioned earlier, for Test 2 with the pile located at 3 m behind the wall, the maximum induced bending moment reaches its peak value about 50 days after completion of excavation as observed earlier and after which the bending moment decreases slightly with time. For Test 1 with the pile located very close to the wall at 1 m away, the trend is similar except that the peak value of maximum bending moment is reached 4 days after the completion of excavation, respectively. It has to be acknowledged that the approximate time for the pile bending moment to reach a maximum value is solely based on this research for a given set of boundary conditions and may not be applicable to a general case.

On the other hand, for Tests 3 and 4 with the pile located further away from the wall at 5 m and 7 m away, respectively, the maximum bending moment is observed to increase continuously with time. Figures 4.7(c) and (d) clearly show that the induced pile bending moment and deflection reduce considerably with increasing distance between the pile and the wall. It is also evident from Figures 4.7 to 4.9 that the movements of the wall, the soil and the pile as well as the induced pile bending moment are dependent upon excavation depth and time. Further evaluation of the time dependent responses of the pile, the soil and the wall are examined in the next section.

Figure 4.10 shows the maximum induced pile bending moment at various excavation depths obtained from the tests. It is evident that the maximum bending moment reduces exponentially with increasing distance of pile from the retaining wall. The maximum pile head deflection also shows an exponential reduction in magnitude with increasing distance of pile from the retaining wall, as illustrated in Figure 4.11.

The maximum pile bending moment, M_{max}, in this case, can be expressed generally as an exponential function:

$$M_{max} = \alpha e^{\beta x} \tag{4.4}$$

where x is the distance of pile behind the wall and α and β are functions of excavation depth, d. From the test data for an excavation whose maximum depth is 1.2 m, α and β can be established as:

$$\alpha = (125d + 125)d \tag{4.5}$$

$$\beta = 0.15d - 0.58 \tag{4.6}$$

The data fitted using the exponential function is also shown in Figure 4.10.

Likewise, the maximum pile head deflection, f_{max}, can also be expressed using a similar exponential function:

$$f_{max} = \alpha e^{\beta x} \tag{4.7}$$

It is established that α and β for pile head deflection can be expressed as:

$$\alpha = 27.5d \tag{4.8}$$

$$\beta = 0.25d - 0.62 \tag{4.9}$$

Figure 4.11 also shows the exponential function data expressed by Eqs. (4.7) to (4.9). The ability of the test data to be consistently described by such functions shows the consistency in performing these centrifuge experiments and thus, increases the level of confidence of the quality of data acquired.

In order to further illustrate the progressive deformation of the soil near to the excavation, total stress cells (TSCs) were used. From the onset of excavation, the soil will progressively depart from the totally undrained assumption and approaches the partially drained condition over time until a totally drained condition is achieved. The mobilization of the lateral earth pressure coefficient, K from an initially K_o condition to or approaches the K_a condition is measured by the two TSCs described earlier in

Chapter 3. TSCs 1 and 2 are located 1.5 m and 3.5 m below ground level, respectively. The K_T values prior to excavation as described in Chapter 3 are not meaningful anymore since K_T caters for a totally undrained condition. Therefore, effective stress parameters have to be used instead. The coefficient of lateral earth pressure at rest, K_o, can be determined, since σ_v' and σ_h' can be calculated as σ_h and u are measured by the TSCs and PPTs, respectively. Immediately prior to excavation, the measured K_o values for TSCs 1 and 2 are approximately 0.78 and 0.68, respectively. By using $\phi' = 25^o$ and OCR = 2.0 in Eqs. (3.1) and (3.2), the calculated K_o values for TSC 1 and TSC 2 are 0.78 and 0.58, respectively. Therefore, relatively good agreement is shown between the measured and calculated K_o values. As excavation progresses, the K_o values drop and the mobilized K values for TSCs 1 and 2 at the end of excavation are about 0.64 and 0.63, respectively as shown in Figure 4.12. It is intuitively correct that the drop in TSC 1 to be greater than TSC 2 as the soil movement is greater near the surface of the ground. When the mobilized K values are plotted over time after the excavation as shown in Figure 4.13, it is observed that the K value for TSC 2 approaches the failure condition described by the coefficient of active soil pressure, K_a, whose value is calculated to be 0.406. This illustrates the progressive shearing of the soil over time.

4.6.2 Evaluation of time dependent pile responses

4.6.2.1 Pore water pressure

Figure 4.14 shows the changes in excess pore pressure in the soil within the first 30 days of a typical test. The locations of the 4 PPTs are shown in Figure 3.3. It should be noted that adjustments have been made to the readings of PPTs 1, 2 and 3. Owing to water evaporation during the course of the centrifuge tests, the first adjustment accounts for the continuous drop in the ground water level that is measured

by 2 PPTs placed on the ground level. The second adjustment accounts for the continuous downward movement of PPTs 1, 2 and 3 as they settle together with the soil. The subsurface soil movement is estimated by comparing the different high-resolution photographs taken during the tests. The method of estimating soil movement will be described in the next section. Figure 4.14 reveals that negative excess pore pressure has developed during excavation. For PPTs 1, 2 and 3 that are located behind the wall, negative excess pore pressure develops and increases with excavation depth and then dissipates with time after the excavation has been completed. This observation reveals that there is stress relief in the soil and hence the soil and the wall continue to move with time after excavation.

Figure 4.15 shows the excess pore pressure responses for the entire test duration. The excess negative pore pressure behind the wall has fully dissipated within 30 days after the completion of excavation, as indicated by the readings of PPTs 1, 2 and 3. PPT 4, which is embedded in front of the wall and at 2.5 m beneath the excavation base, experiences some fluctuations in readings. The rise in the excess pore pressure over time in front of the wall reveals that significant seepage has taken place from the retained side to the excavated side of the wall through the underlying permeable sand layer.

4.6.2.2 Subsurface soil movement

The above excess pore pressure responses reveal that the soil behavior is time dependent and the soil continues to move with time due to dissipation of excess pore pressure. To further investigate the time dependent phenomenon, the subsurface soil movement is examined in detail in this section. Figure 4.16(a) shows selected photographs of soil markers taken at different times of Test 2 (pile located 3 m from the wall) using the high-resolution image-processing camera. By comparing the

position of the soil markers from the photographs using a commercial computer software, the soil movement vectors could be derived and shown in Figure 4.16(b). It is noted that relatively large subsurface soil movement starts to occur beyond an excavation depth of 1 m. This observation is consistent with the corresponding large increase in the bending moment and pile deflection when excavation depth exceeds 1 m, as shown in Figures 4.9(a) and 4.9(c), respectively. Figure 4.16(b) further reveals that the soil deformation increases significantly as the wall moves and the zone of relative significant soil movement extends deeper with increasing wall movement. The significant soil deformation zone is confined to an approximate triangular area behind the wall bounded by a line of about 45^{o} to the vertical. This observed soil deformation zone is somewhat similar to that observed by Bolton and Powrie (1988). The size of the zone increases with time after the completion of excavation. Figure 4.17 shows a photograph of the top view of the ground surface taken after a test. It reveals the occurrence of fissures within the deformation zone of the ground surface.

To further examine the phenomenon of progressive soil movement, the soil movement vectors can be translated to shear strains defined using the method proposed by Ou et al. (2000). The shear strain provides a quantitative measure on the degree of soil shearing. Figure 4.16(c) shows the measured shear strains of the clay at different stages. Upon completion of excavation, the development of shear strain is confined to within 4 m of the wall. Within 50 days after the completion of excavation, the shear strains have propagated further and deeper due to progressive wall movement as shown in Figure 4.7(b).

The development of shear strains around the pile is consistent with the concept of characteristic meshes in a plastically deformed cohesive soil proposed by Randolph and Houlsby (1984). Menzies (1997) established that in such a case, the soil

surrounding the piles would experience a reduction in strength and shear modulus. It is believed that this scenario applies to the soils within the soil deformation zone in the present study. Therefore, for a pile with a substantial portion of it lying within this largely plastically deformed soil region, there would be a relaxation of the induced pile bending moment once the soil within the deformation zone has weakened. At 300 days after the completion of excavation, the main plastic deformed soil region extends to a depth of about 2 m and a width of 2 m behind the wall. This observation is consistent with the post-excavation soil strength measurements shown in Figure 4.4 whereby the soil at 1.5 m behind the wall has significantly weakened after excavation while the soil at 3 m behind the wall remains practically undisturbed.

Figure 4.16(c) also reveals that for piles located further away from the wall, the magnitudes of shear strains around the piles would be considerably smaller than those located closer to the wall. Hence, majority of the soil surrounding the piles have not weakened. This helps to explain the progressive increase in pile bending moment for Tests 3 and 4 over time shown in Figure 4.7(d).

Figure 4.18 shows the measured free-field lateral soil movement profiles at different locations and times derived from the photographs of soil markers of a typical test where no piles are present. As expected, the magnitudes of lateral soil movement are noted to reduce with increasing depth and distance away from the wall. Figure 4.18 also reveals that the soil continues to move after completion of excavation. These soil movement profiles will be used as part of the input parameters for all the numerical back analyses presented in Chapter 6.

4.7 SINGLE PILE BEHAVIOUR BEHIND A COLLAPSED WALL

Tests 5, 6 and 7 were conducted to investigate the behaviour of a single pile behind a marginally stable wall, a collapsed wall and a totally collapsed wall, respectively. Details of the test configuration are given in Figure 4.1.

4.7.1 Wall and soil deformations

The wall deflection profiles at different times obtained from Tests 5, 6 and 7 as well as Test 2 from the stable wall test series are shown in Figure 4.19. In all cases, the maximum wall deflection is at the ground level since it is a cantilever wall. The maximum wall defection for Test 5 is 0.5 m, which is 2.5 times that of 0.2 m recorded for Test 2. Figure 4.19(b) reveals that the wall deflection within the underlying sand layer is relatively small, illustrating the 'key-in' effect of the wall in the underlying dense sand layer. In Test 6, the wall is essentially 'floating' entirely in the soft clay layer. Hence it is significantly less stable and the maximum wall deflection of 1.2 m is much larger than that of Test 5. In this test, the whole wall is noted to tilt about the toe of the 'floating' wall, as shown in Figure 4.19(c). Test 7 involves the most severe case with the same wall embedment condition as that of Test 5 but a significantly larger excavation depth of 2.8 m. The wall 'key-in' effect in the dense sand layer disappears when excavation depth exceeds 1.4 m. As expected, the wall deflection in Test 7 is by far the most severe with a maximum wall deflection of 2.7 m at the ground level, as shown in Figure 4.19(d). Similar to the stable wall test series, the wall deflection is noted to be time dependent, whereby the wall would continue to deflect after completion of excavation. Nevertheless, the rate of increase in the wall tilt decreases over time.

Figure 4.19 shows that at the same excavation depth of 1.2 m, the wall deflection profile obtained from Test 7 is significantly larger than that of Test 5, which

is in turn considerably larger than that of Test 2. This observation differs from the expected situation in the field whereby for the same soil and wall conditions, the wall deflection is expected to be very similar under the same excavation depth. The differences in the wall deflection profile in the 3 tests are attributed to the use of zinc chloride liquid to simulate in-flight soil excavation. In Test 2, the liquid in the latex bag has been completely drained out as the maximum excavation depth of 1.2 m has been reached. When the excavation depth reaches 1.2 m in Test 5, there is 0.6-m high liquid below the 1.2 m depth remaining in the latex bag while in Test 7, there is 1.6 m of liquid left in the bag. As the liquid below 1.2 m depth does not offer any shear resistance to the moving wall, the wall deflection is hence the largest in Test 7, followed by Test 5 and then Test 2. It is believed that while such shortcoming would cause discrepancies in the wall and pile responses in the intermediate excavation stages for the 3 tests, the results obtained at the maximum excavation depth for each test are valid and still useful for the understanding of pile responses behind a collapsed retaining wall.

In all tests, the tilted wall causes the clay behind the wall to settle and the ground settlement continues to increase over time after the completion of excavation, as shown in Figure 4.20. It is noted that the ground surface settlement for Test 6 is about twice as large as that of Test 5. As the wall head in Test 7 has deflected by a massive 2.7 m, the ground surface settlement behind the wall is hence very large as well, with an observed maximum settlement of almost 1.6 m at 1.5 m behind the wall, as shown in Figure 4.20(d). It is observed that the post-excavation settlement troughs are very much time dependent, especially for the cases with significantly large wall movement and ground settlement. For the stable and marginally stable wall cases (Figures 4.20(a) and (b)), the gradient of the ground surface settlement trough close to

the wall is not as significant as those observed for the collapsed wall cases (Figures 4.20(c) and (d)). This could be attributed to the formation of failure wedge behind the wall for the latter cases.

4.7.2 Pile responses

Figure 4.21 shows the development of bending moment profiles with excavation depth and time for Tests 2, 5, 6 and 7. Similar to the relative magnitudes of wall and soil movements reported earlier, the induced maximum bending moment on the pile increases significantly from the case of stable wall (Test 2), marginally stable wall (Test 5), collapsed wall (Test 6) to totally collapsed wall (Tests 7). Owing to differences in the excavation depth and wall stability, the elevation of maximum bending moment varies with the highest elevation at 7.5 m for the stable wall case to the lowest elevation of 9 m for the totally collapsed wall case. Similar to the stable wall test series, the post-excavation pile responses are clearly time dependent.

Figure 4.22 shows the variation of induced pile head deflection and maximum pile bending moment with logarithmic of time. It was reported in Section 4.6.1 that for a pile located 3 m behind a stable retaining wall in clay (i.e. Test 2), the post-excavation pile responses increase with time and reach their peak values 50 days after the completion of excavation after which the pile responses decrease with time. Figure 4.22 reveals that the induced pile responses for the marginally stable wall (Test 5) are similar to that of the stable wall except the magnitudes of the pile responses are considerably larger due to a greater excavation depth.

However, the induced pile responses behind the two collapsed walls are significantly different. In Test 6 with a collapsed wall, the maximum induced pile head deflection and bending moment are significantly larger than those of Test 5 due to wall instability. Figure 4.22(b) shows that the induced maximum pile bending moment

reaches a peak value of 238 kNm at the onset of wall collapse at an excavation depth of 1.4 m. Thereafter the induced maximum pile bending moment decreases with time and upon reaching the maximum excavation depth of 1.8 m, the maximum bending moment reduces to 185 kNm, a reduction of 22 % from its peak value. The post-excavation bending moment continues to reduce with time with the observed bending moment reducing to about 80 kNm at the end of the test. On the other hand, the pile head deflection (Figure 4.22(a)) remains practically unchanged for some time after the wall collapse.

In Test 7 with a totally collapsed wall, the maximum induced pile bending moment reduces after reaching its first peak value at an excavation depth of 1.2 m and then remains fairly constant with increasing excavation depth. However, the bending moment increases again once the excavation depth exceeds 2 m until the final excavation depth of 2.8 m, as shown in Figure 4.22(b).

The pile head deflection responses over time show a similar trend as the pile bending moment. Despite greater excavation depth, the pile head deflection observed in Test 7 is less than that in Test 6 (Figure 4.22(a)). The above suggests that the underlying dense sand layer has restrained the lower part of the pile from severe movement and rotation during and after the wall collapse. Figure 4.22 further reveals that the induced maximum pile bending moment and deflection for Test 7 are significantly larger than those of Test 5.

4.7.3 Evaluation of pile responses due to soil deformation

During the tests, photographs of soil markers were taken through the perspex window of the model container using a high resolution camera. Figures 4.23(a) and (b) show the photographs of side elevation of the experiment at maximum excavation depth for Tests 5 and 6, respectively. By comparing the photographs against those

prior to excavation using a commercial computer software, the soil movement vectors can be obtained and also shown in Figure 4.23. It is noted that the soil deformation patterns for Test 5 are similar to those observed for Test 2 in Section 4.6.2. For Test 6 involving a collapsed wall, massive soil movement is detected and tension cracks can clearly be seen in the soil behind the wall, as shown in Figure 4.23(b). A photograph of the ground surface taken from the top after Test 6 shown in Figure 4.24 reveals that there is soil "flowing" around the pile. This observation is somewhat similar to the characteristic mesh of the deformed soil on a laterally loaded pile described by Randolph and Houlsby (1984).

Figure 4.25 shows a photograph of the side elevation of the experiment at maximum excavation depth for Test 7. From the series of photographs taken at different periods, two stages of soil failure are noted. The first stage involves the development of tension cracks in front of the pile, similar to the observations described earlier for Test 6. It is believed that the tension cracks that develop in front of the pile could have reduced the soil-pile interface contact and this leads to a reduction in the transmission of full soil pressure onto the pile.

Figure 4.22 reveals that for Test 7, the pile head deflection and bending moment remain fairly constant from the excavation depth of 1.2 m to 2 m. It is postulated that during this stage, the increase in soil pressure due to increasing soil movement on the pile arising from increasing excavation depth is just about balanced by the reduction in soil pressure on the pile due to the development of tension cracks. Upon further soil excavation, the second failure stage commences as the tension cracks further propagate and the active failure wedge is then prominently developed resulting in very large soil movement in front of the pile. With this, the soil mass behind the pile starts to press onto the pile again and causes the pile head deflection and bending

moment to increase again. After the wall has completely collapsed, the entire failure wedge slides and separates itself from the remaining soil mass, resulting in a significant reduction in the induced bending moment and deflection onto the pile. The vectors of significant soil movement in front and behind the retaining wall at the end of excavation for Test 7 are also shown in Figure 4.25. The formation of failure wedge in front of the pile is clearly evident as denoted by the longer soil movement vectors. As expected, soil heave is noted in front of the wall upon wall collapse.

Figures 4.26(a) and (b) shows the measured free-field lateral soil movement profiles of Tests 5, 6 and 7 derived from the high resolution photographs of soil markers. These will be used as the input data for the subsequent numerical back analyses presented in Chapter 6.

The variations of pile head deflection and free field soil movement at different depths at the pile location with time for Tests 5, 6 and 7 are shown in Figures 4.27(a), (b) and (c), respectively. For Test 5 involving a marginally stable wall, the soil starts to move ahead of the pile when the excavation depth exceeds 0.9 m. For Tests 6 and 7 involving collapsed walls, the soil starts to move ahead of the pile at a relatively shallow excavation depth of 0.6 m, after which the difference between the soil and pile movement becomes more significant with increasing excavation depth. When the excavation depth exceeds about 1.0 m, relatively large free-field soil “flow” is observed and this is consistent to the soil “flow” phenomenon observed in Figure 4.24. The development of soil “flow” and tension cracks is thought to have prevented the transmission of additional soil pressure onto the pile and hence the drop in pile bending moment as noted in Figure 4.22(b).

4.8 COMPARISON OF SINGLE PILE BEHAVIOUR IN SAND AND CLAY

Shen (1999) performed centrifuge tests on single free headed piles in sand with piles at 1 m, 3 m, 5 m, 7 m and 9 m behind a wall that remains stable with excavation depth of 4.5 m. He also carried out two tests involving single piles at 2 m and 4 m behind a wall that subsequently collapsed with excavation depth of 6.0 m. The pile condition is identical to the present study. Some similarities and differences could be drawn between the behavior of a single pile behind a stable and collapsed wall in both clay and sand.

4.8.1 Similarities

In the case of a stable wall in both clay and sand, the induced maximum pile bending moment and maximum pile head deflection reduce exponentially with increasing distance of pile behind the wall. The location of maximum pile bending moment for both clay and sand tests is at 7.5 m.

4.8.2 Differences

The most distinct difference of single pile behaviour is that the piles in clay, the induced pile bending moment would gradually increase over time for piles located further (at 5 m and 7 m) behind the wall, whereas for the tests in sand, the pile bending moment remain essentially unchanged, irrespective of pile distance from the wall, as established by Shen (1999). This is due to the fact that for sand, the excess pore water pressure generated during excavation would have already been dissipated after the completion of the excavation and hence, there is insignificant time dependent pile behaviour. Time dependent pile behaviour in clay could be seen as the effect caused by the progressive wall and soil deformations over time.

In the case of collapsed wall, tests carried out in clay display tension cracks and soil “flow” when wall movement is excessive. For piles in sand, when the soil movement becomes excessive, the sand particles would slide on top of one another and “flow” past the pile.

Test	Plan	Elevation	Parameter (m)	Pile head condition	Wall condition
1	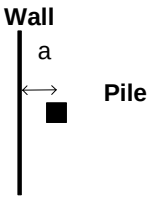	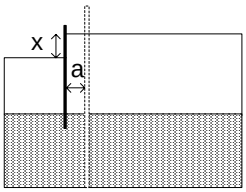	a = 1 x = 1.2	Free	Stable wall
2	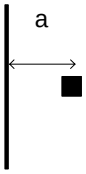	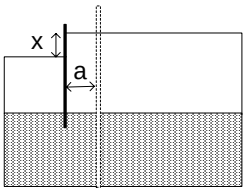	a = 3 x = 1.2	Free	
3	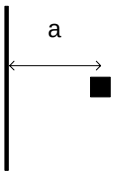	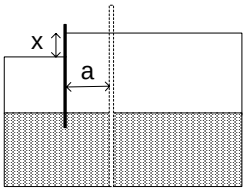	a = 5 x = 1.2	Free	
4	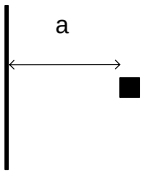	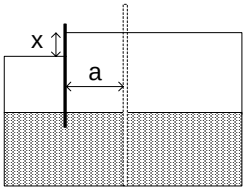	a = 7 x = 1.2	Free	
5	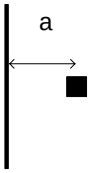	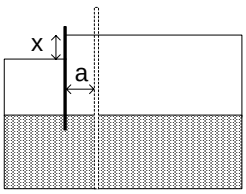	a = 3 x = 1.8	Free	Marginally stable wall
6	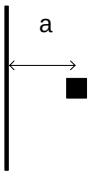	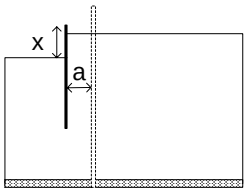	a = 3 x = 1.8	Free	Collapsed wall
7	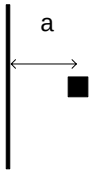	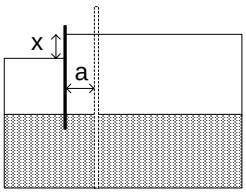	a = 3 x = 2.8	Free	Totally collapsed wall

■ Instrumented pile

Figure 4.1 Test program of single pile

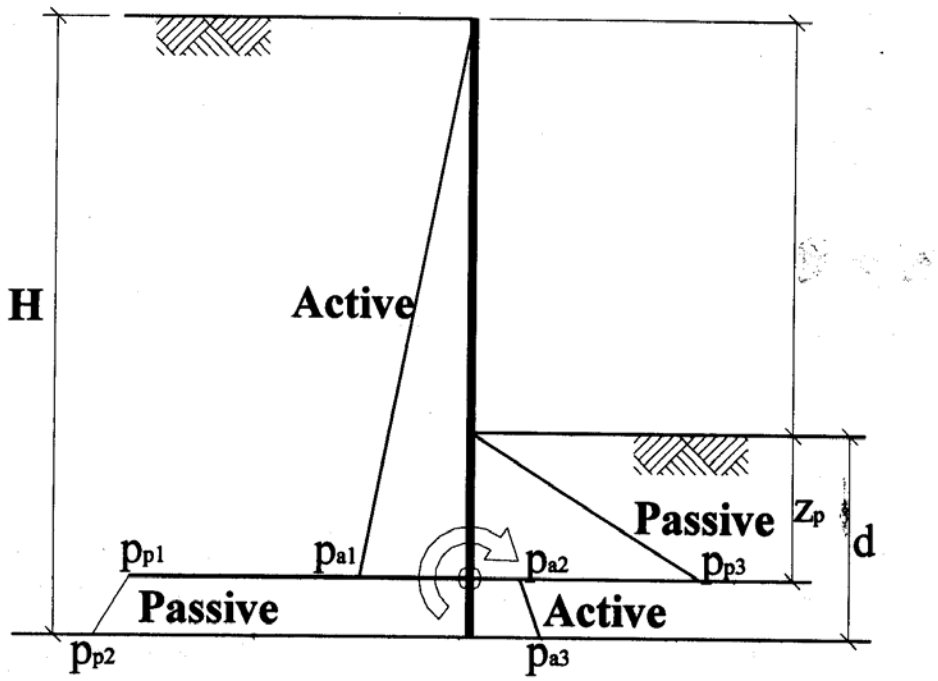

Figure 4.2 Limit equilibrium analysis of retaining wall (after Bolton and Powrie, 1987)

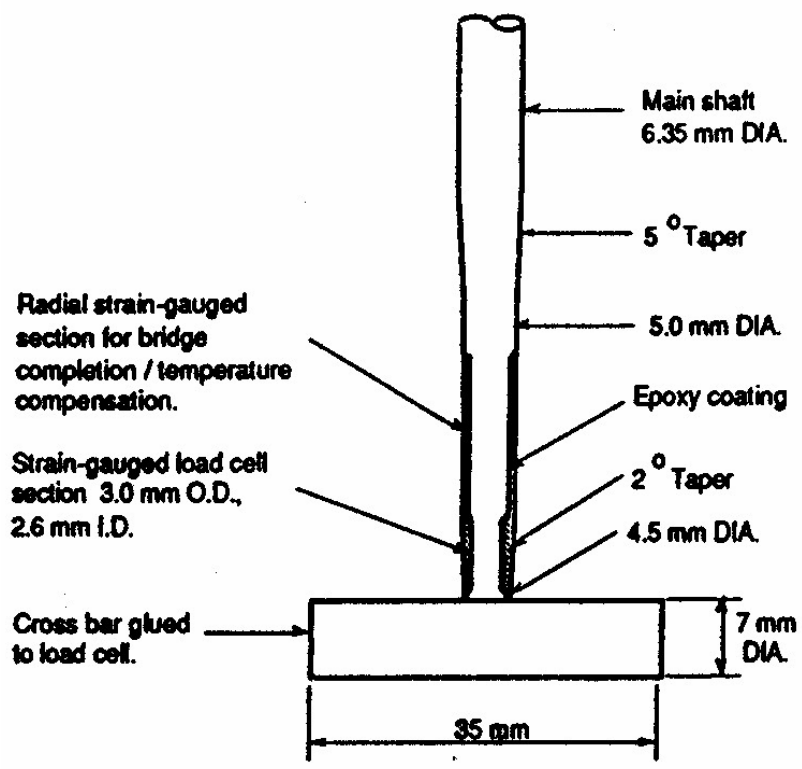

Figure 4.3 Bar penetrometer or T-bar (after Stewart and Randolph, 1991)

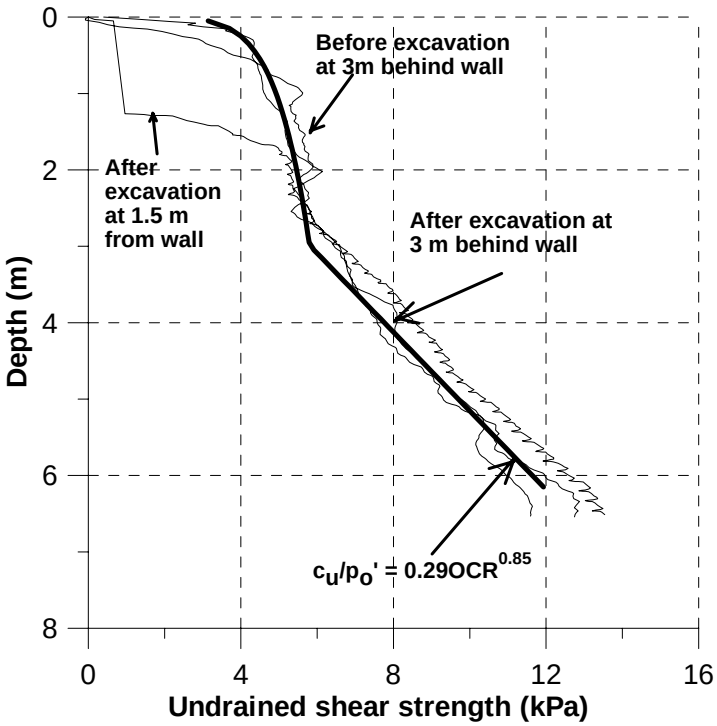

Figure 4.4 Measured undrained shear strength profiles for tests involving a stable wall

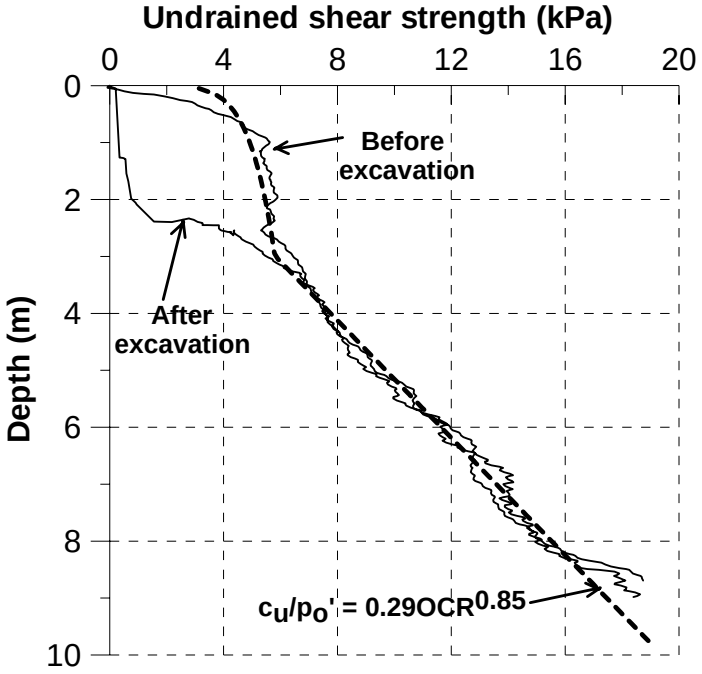

Figure 4.5 Measured undrained shear strength profiles for tests involving a collapsed wall

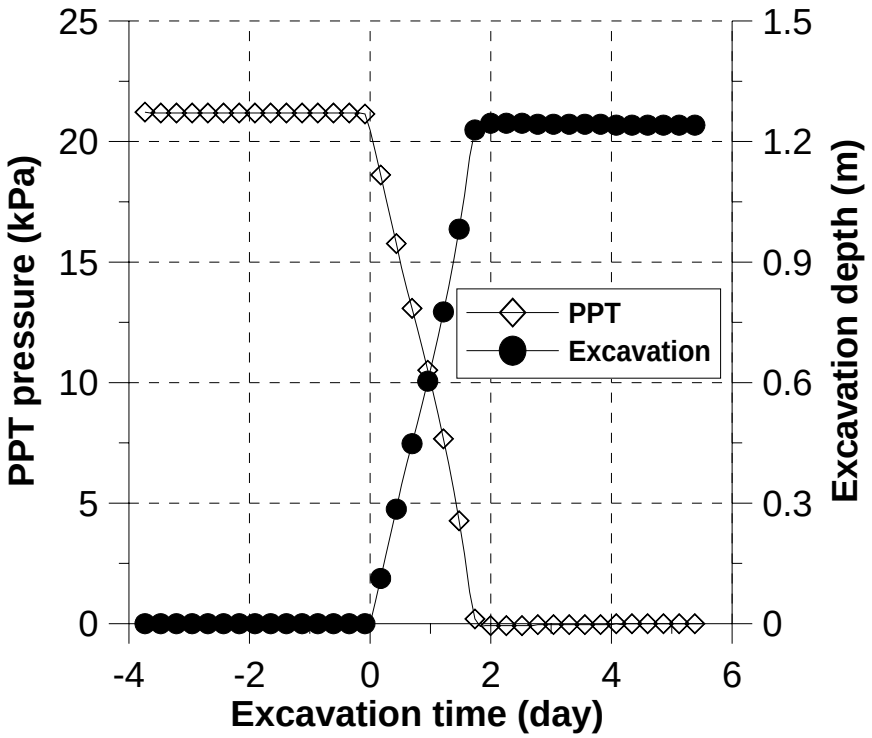

Figure 4.6 Variations of $ZnCl_2$ and excavation depth with time

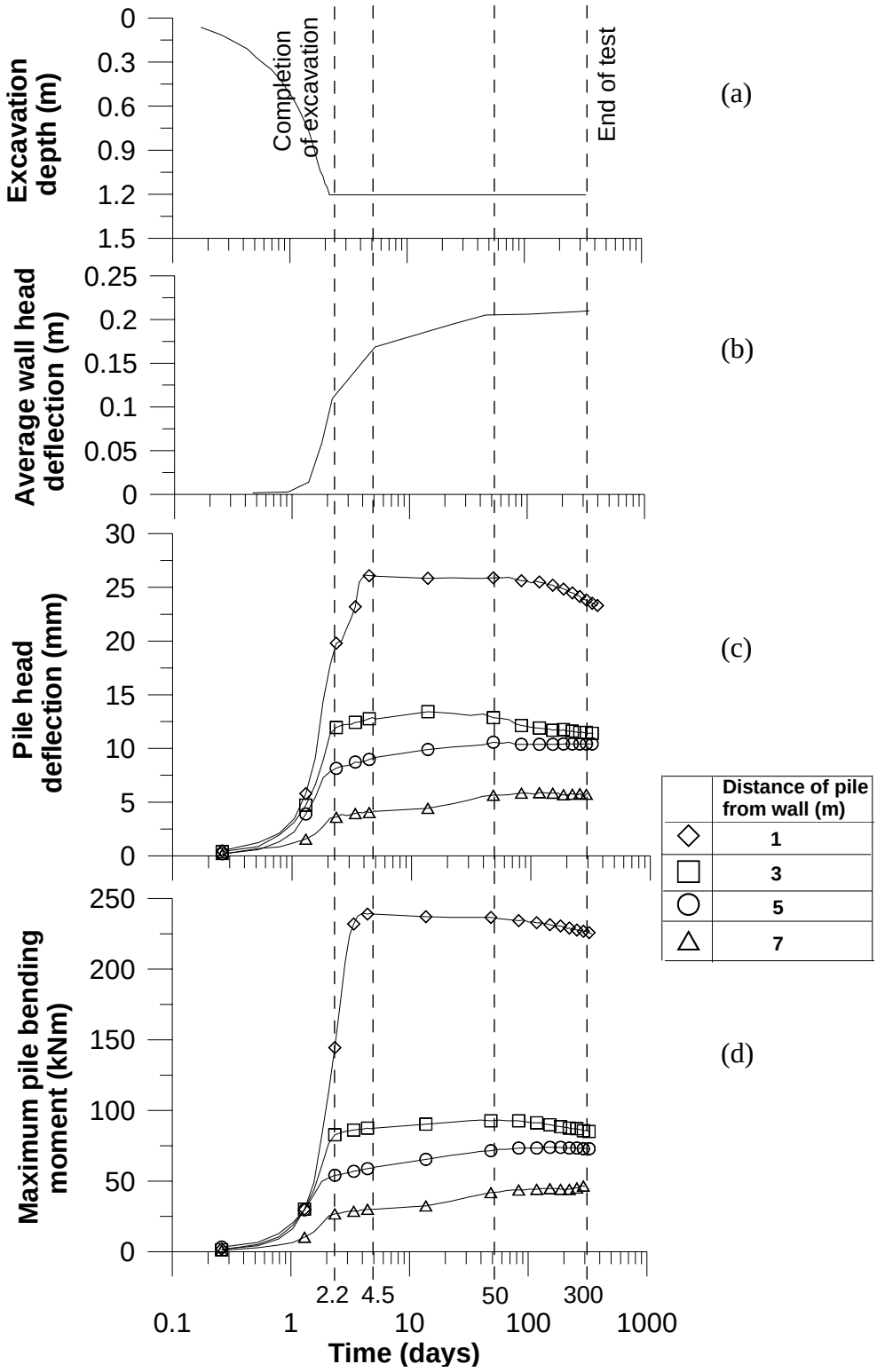

Figure 4.7 Variations of (a) excavation depth, (b) average wall head deflection, (c) induced pile head deflection and (d) induced maximum pile bending moment with time

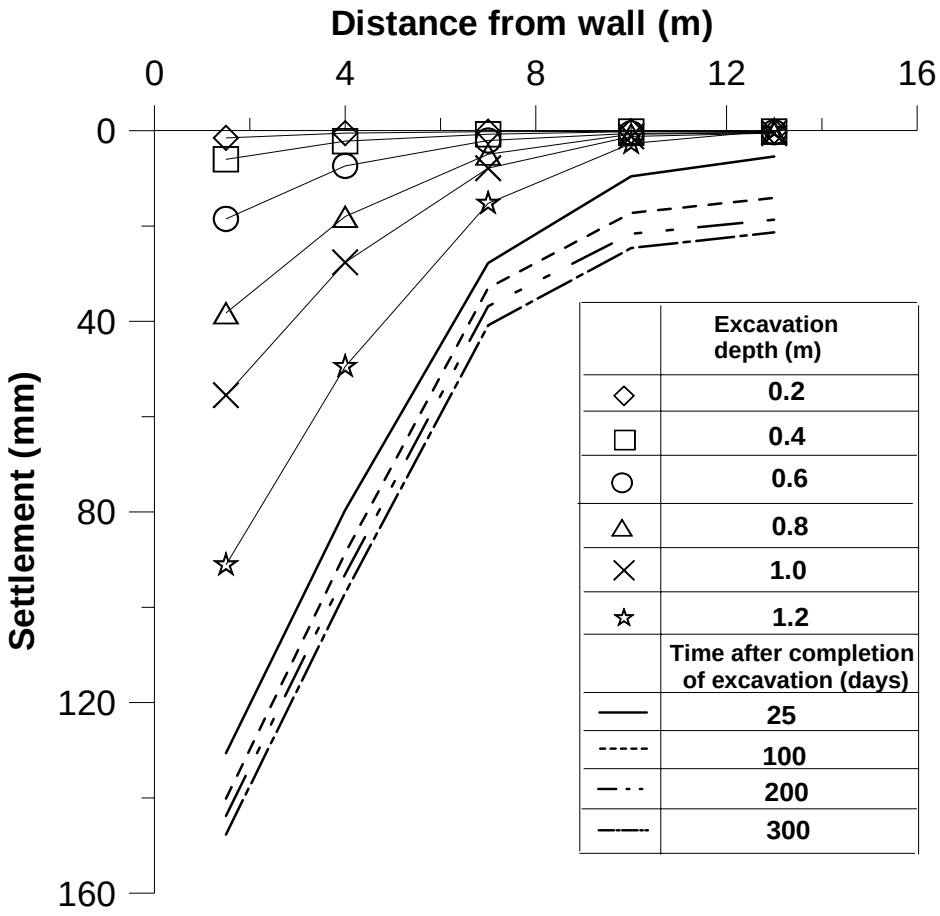

Figure 4.8 Surface settlement troughs during and after excavation

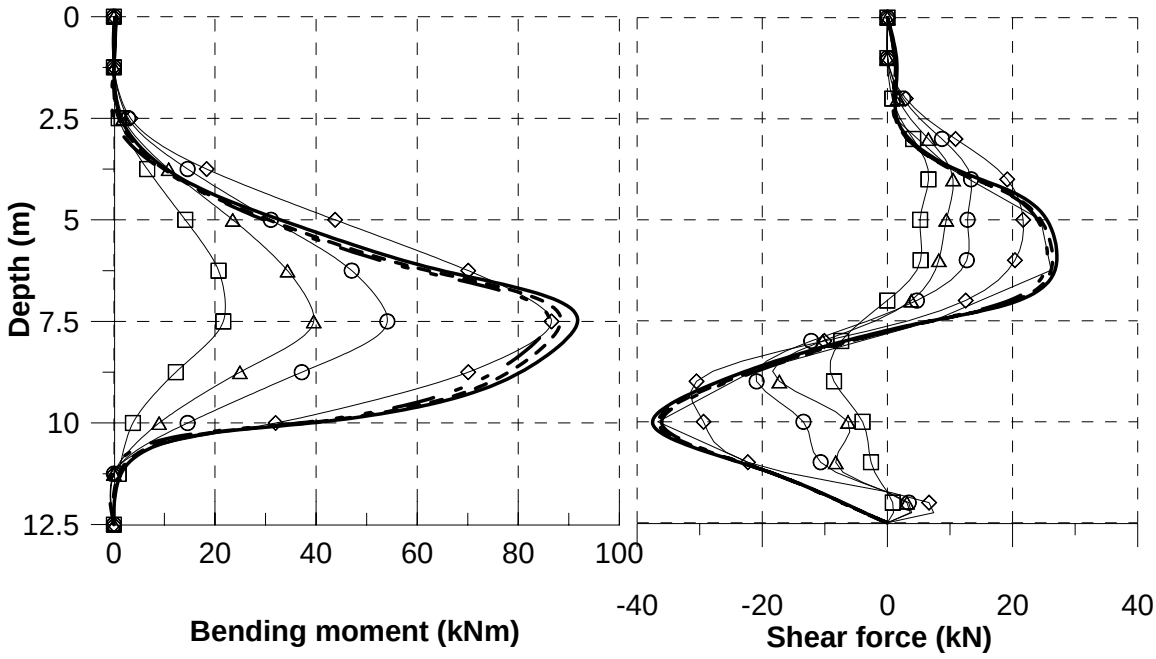

(a) (b)

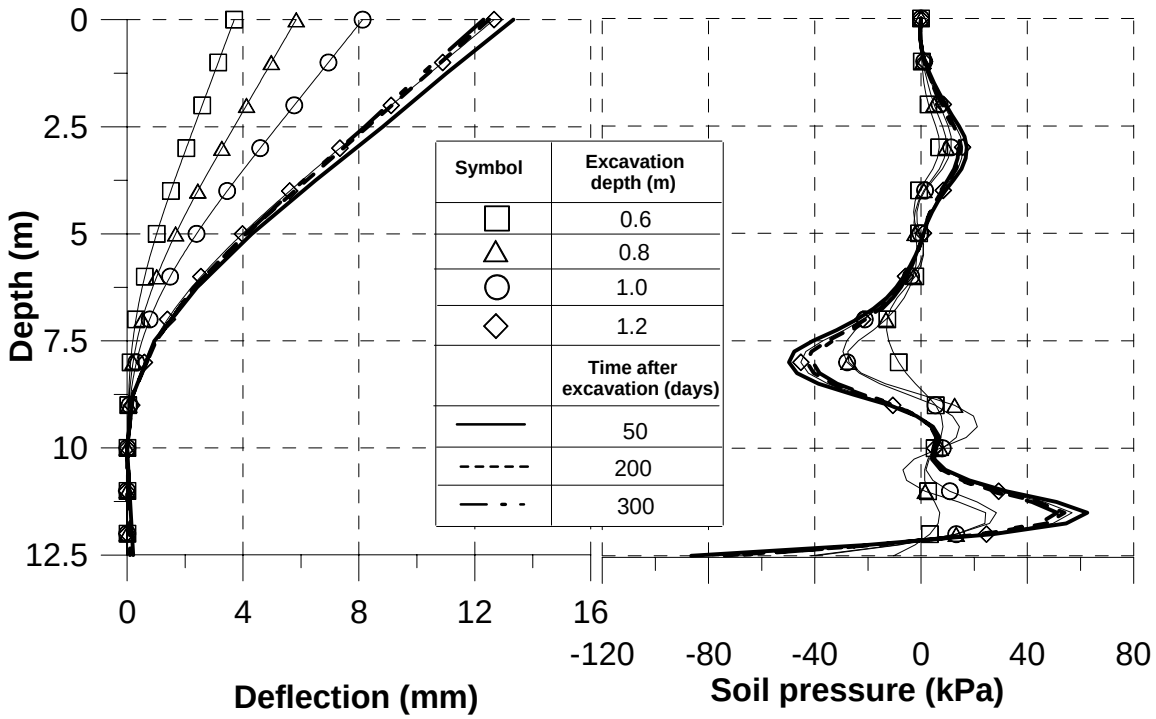

(c) (d)

Figure 4.9 Measured pile (a) bending moment, (b) shear force, (c) deflection and (d) soil pressure profiles for Test 2

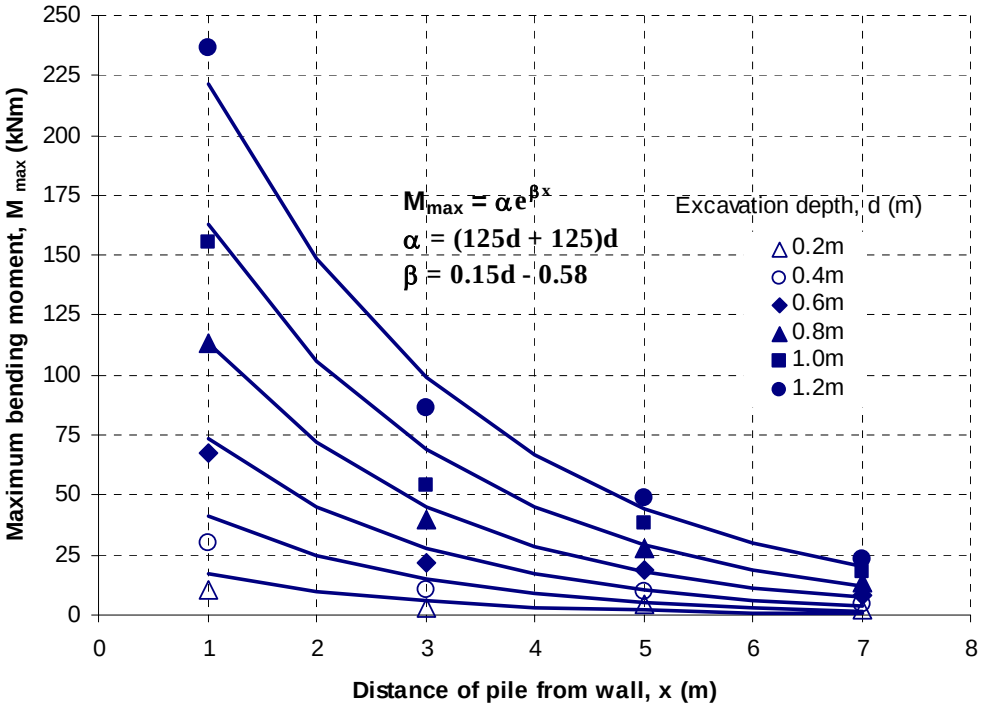

Figure 4.10 Variation of maximum pile bending moment and distance of pile behind retaining wall

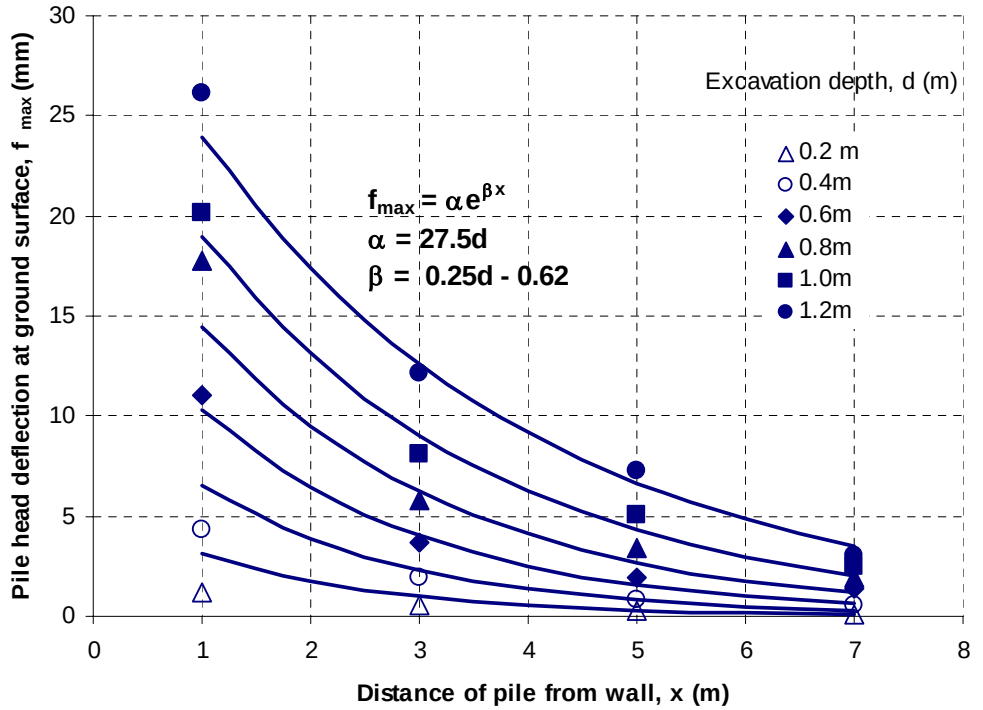

Figure 4.11 Variation of maximum pile deflection and distance of pile behind retaining wall

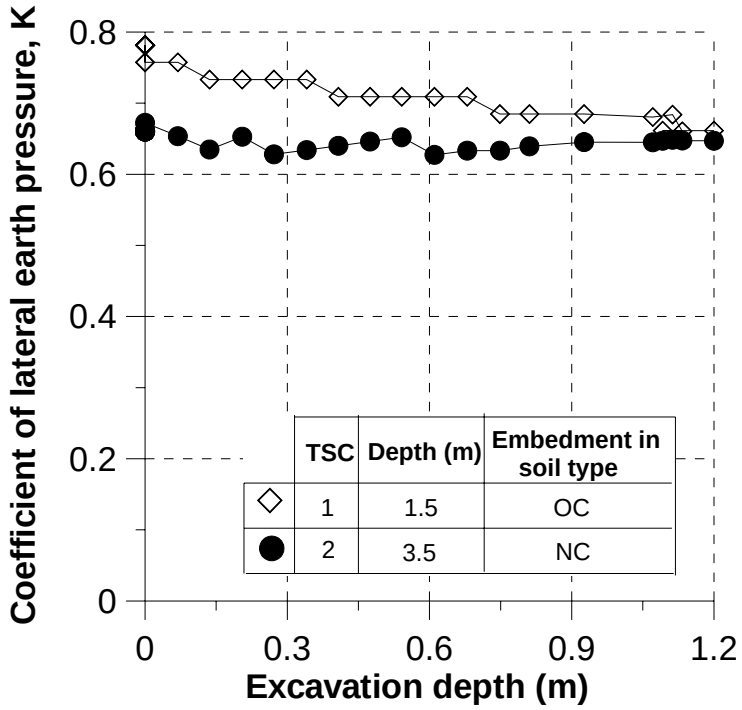

Figure 4.12 Mobilisation of effective lateral earth pressure, K, of soil behind a stable retaining wall during excavation

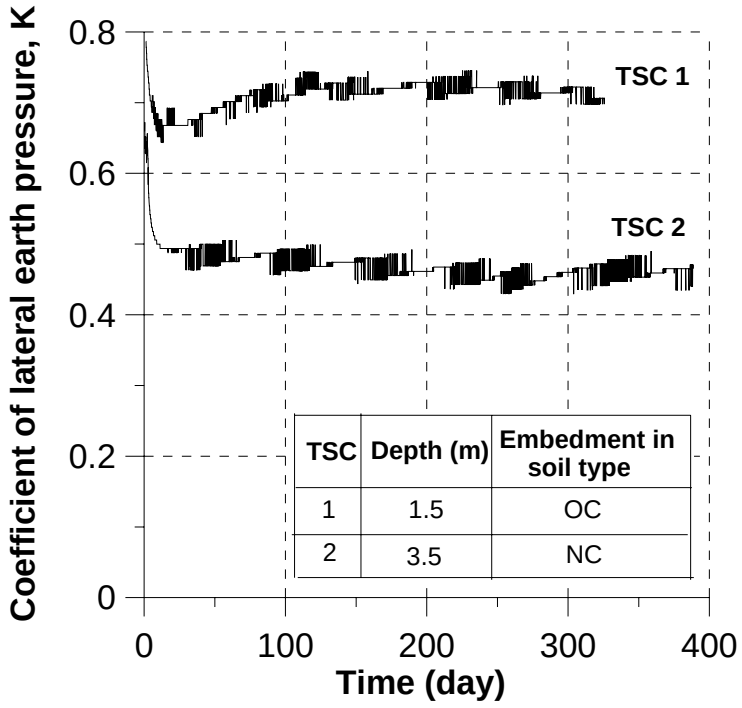

Figure 4.13 Mobilisation of effective lateral earth pressure, K of soil behind a stable retaining wall over time after excavation

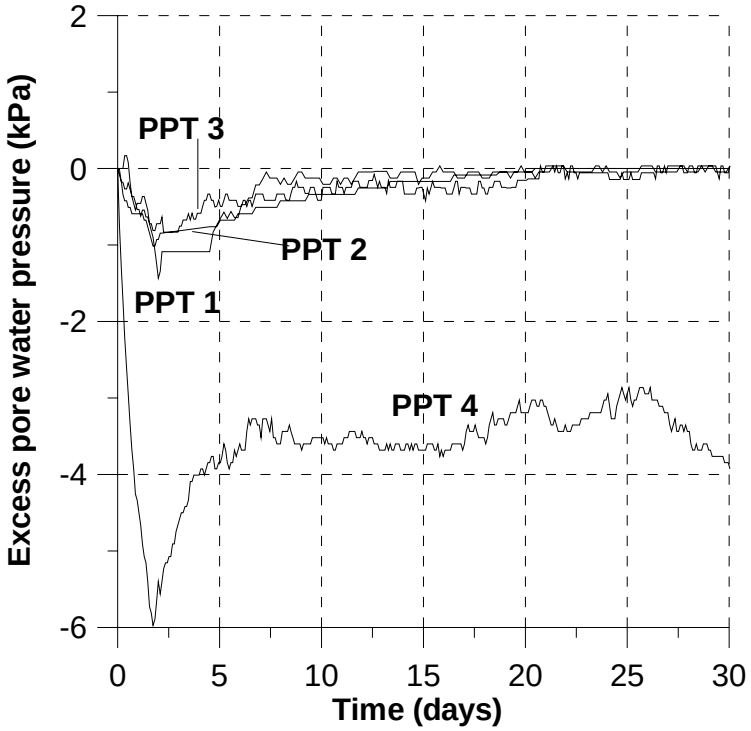

Figure 4.14 Variation of excess pore water pressure with time over first 30 days of test

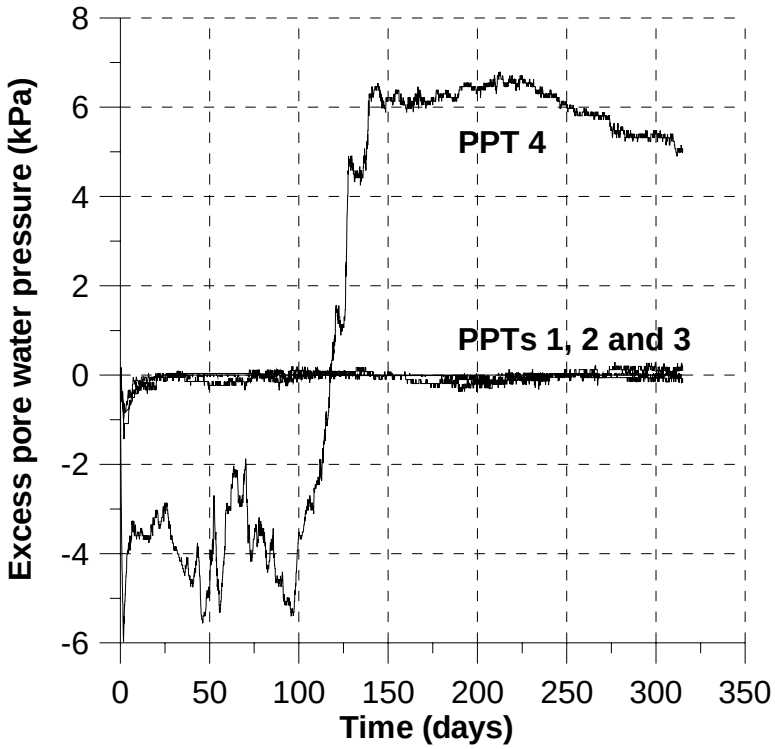

Figure 4.15 Variation of long-term excess pore water pressure with time

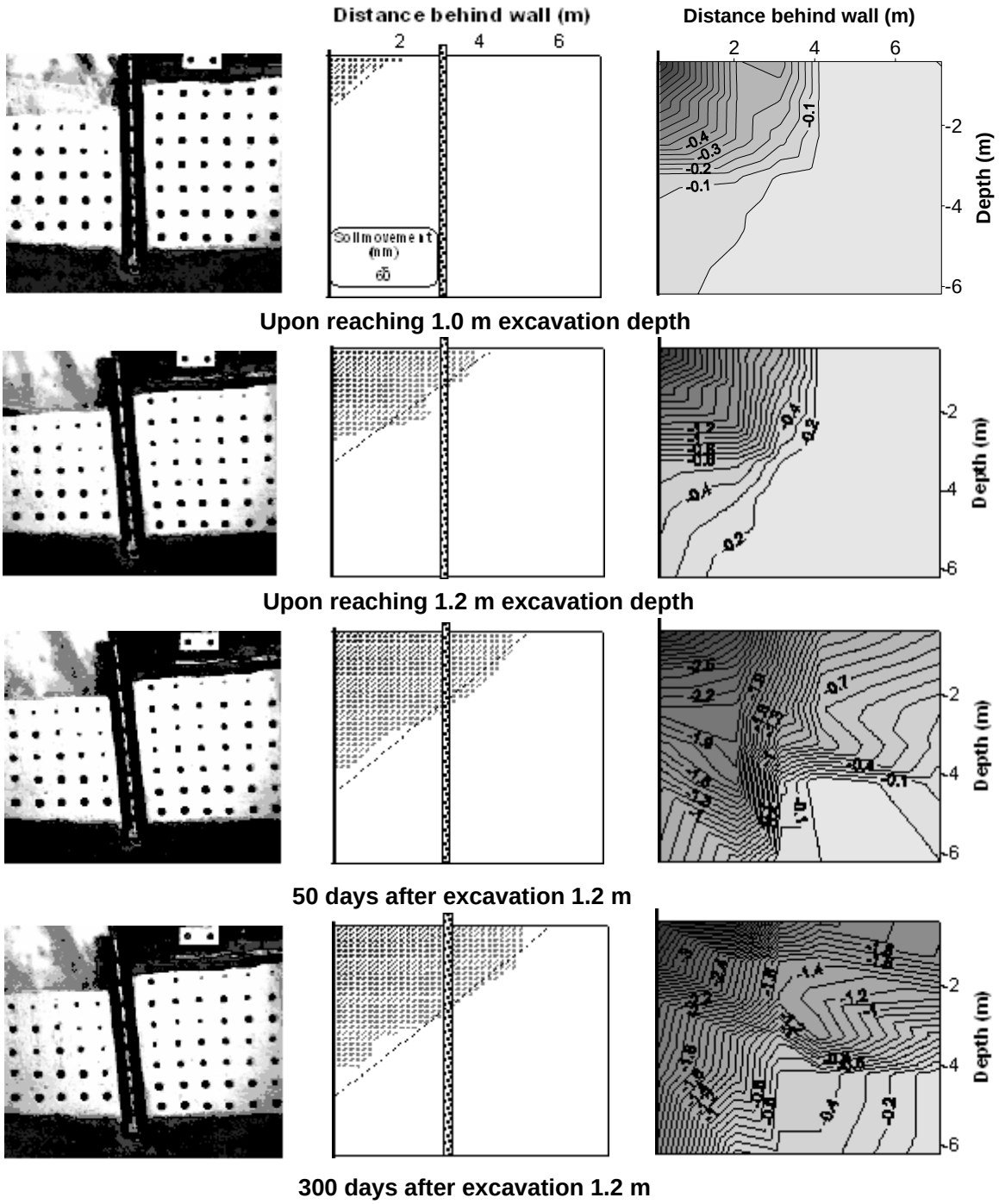

Figure 4.16 Development of soil movements in Test 2: (a) Photographs, (b) soil movement vectors and (c) shear strains

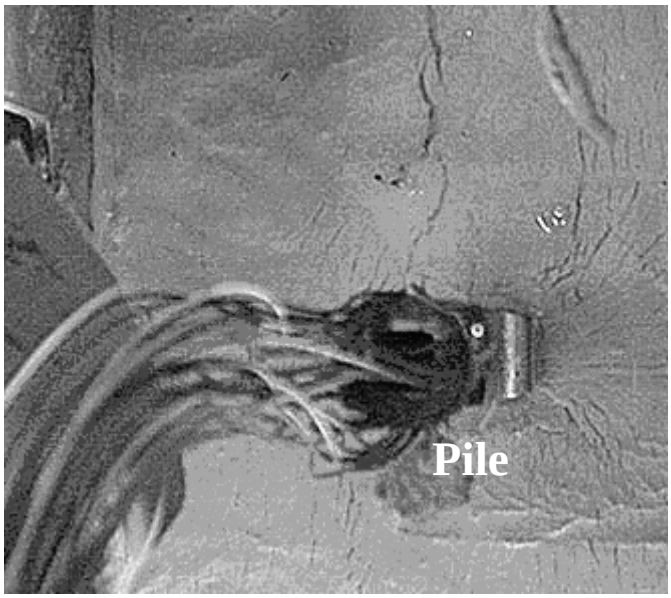

Figure 4.17 Development of fissures around pile (plan view)

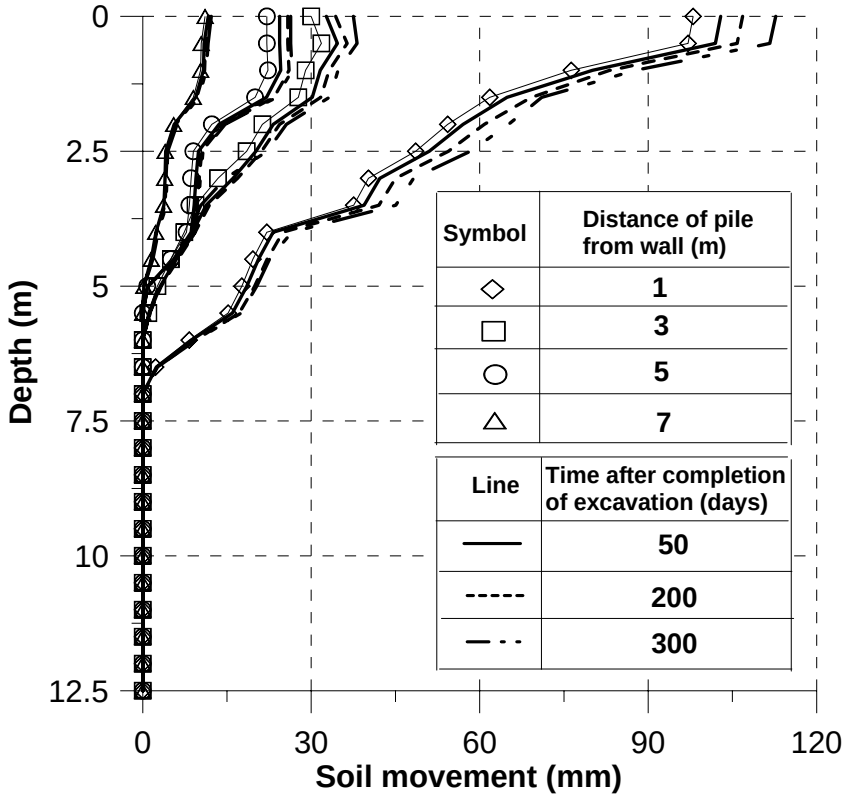

Figure 4.18 Measured free-field lateral soil movement profiles

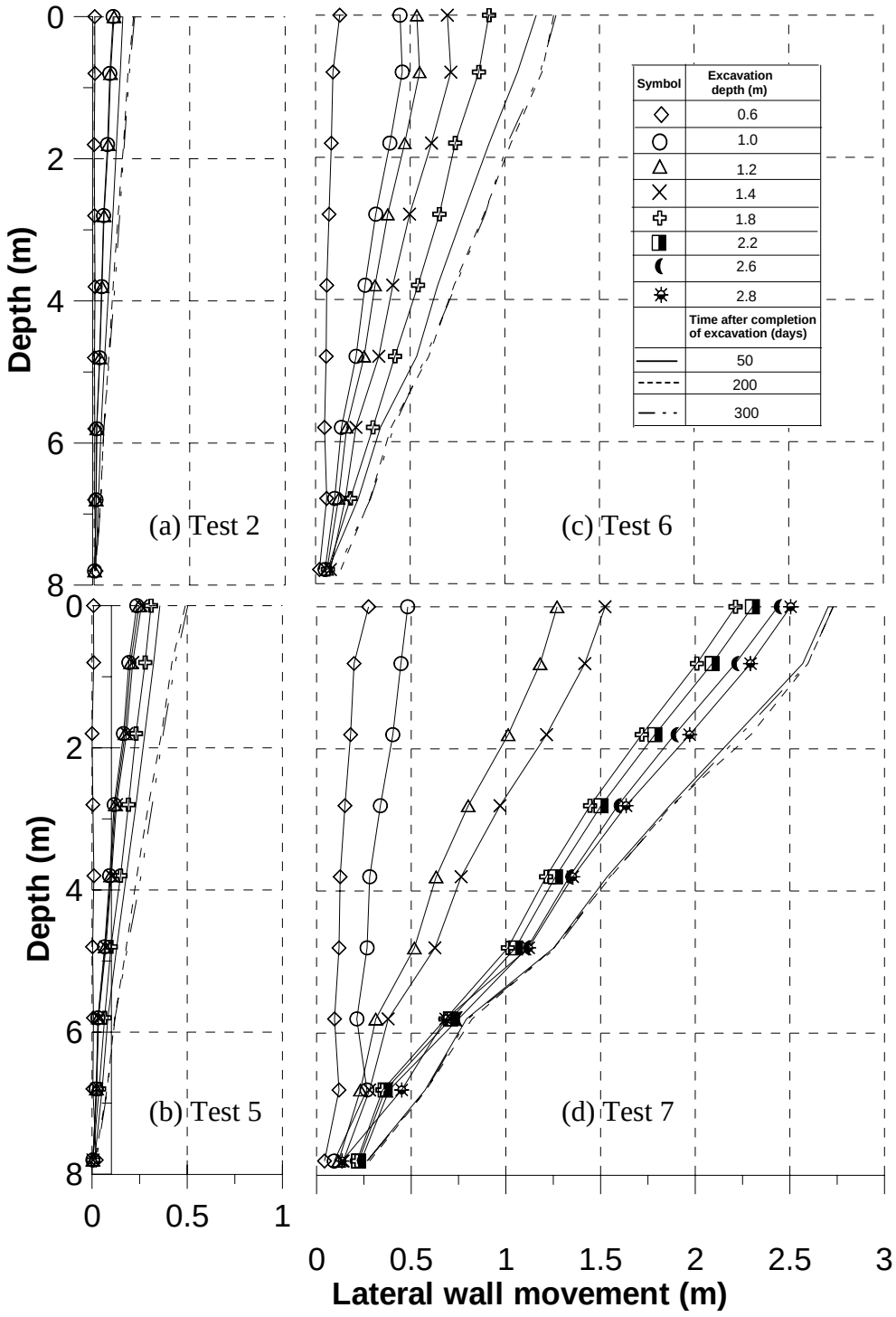

Figure 4.19 Measured lateral wall movement profiles during excavation for (a) Test 2, (b) Test 5, (c) Test 6 and (d) Test 7

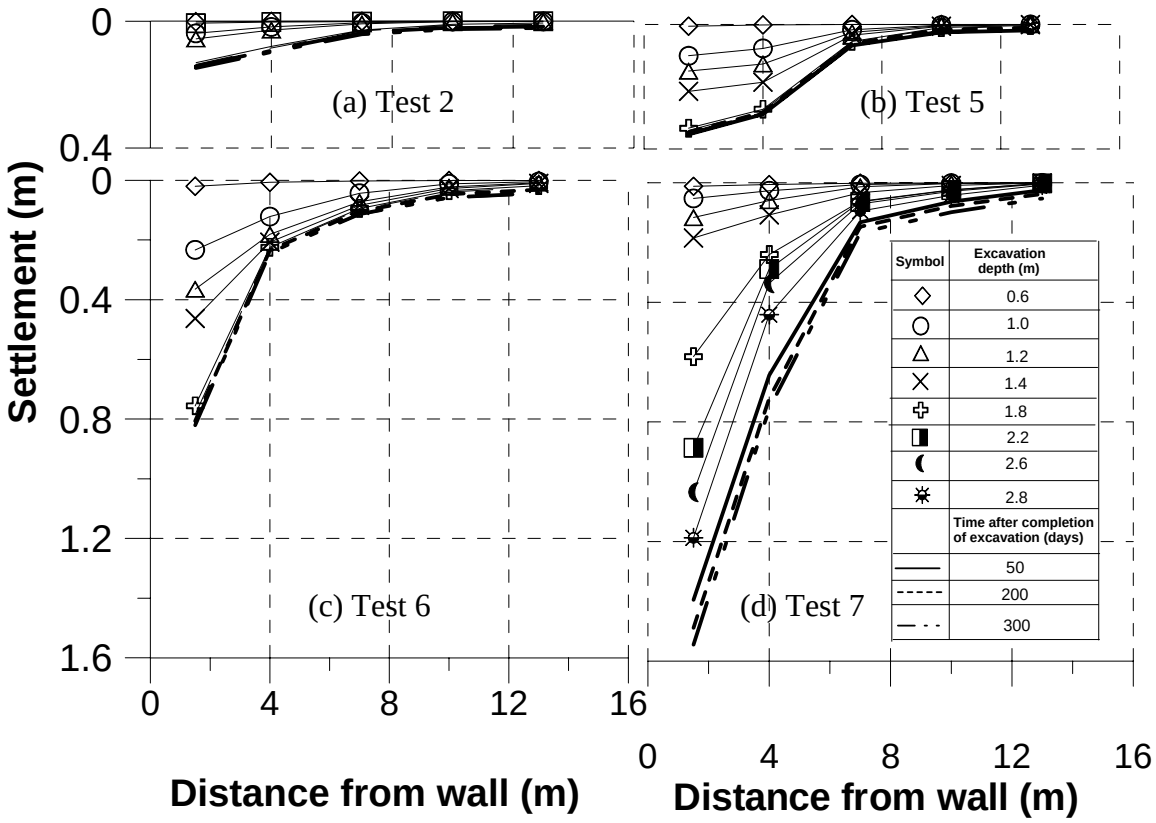

Figure 4.20 Measured surface settlement troughs behind wall during and after excavation for (a) Test 2, (b) Test 5, (c) Test 6 and (d) Test 7

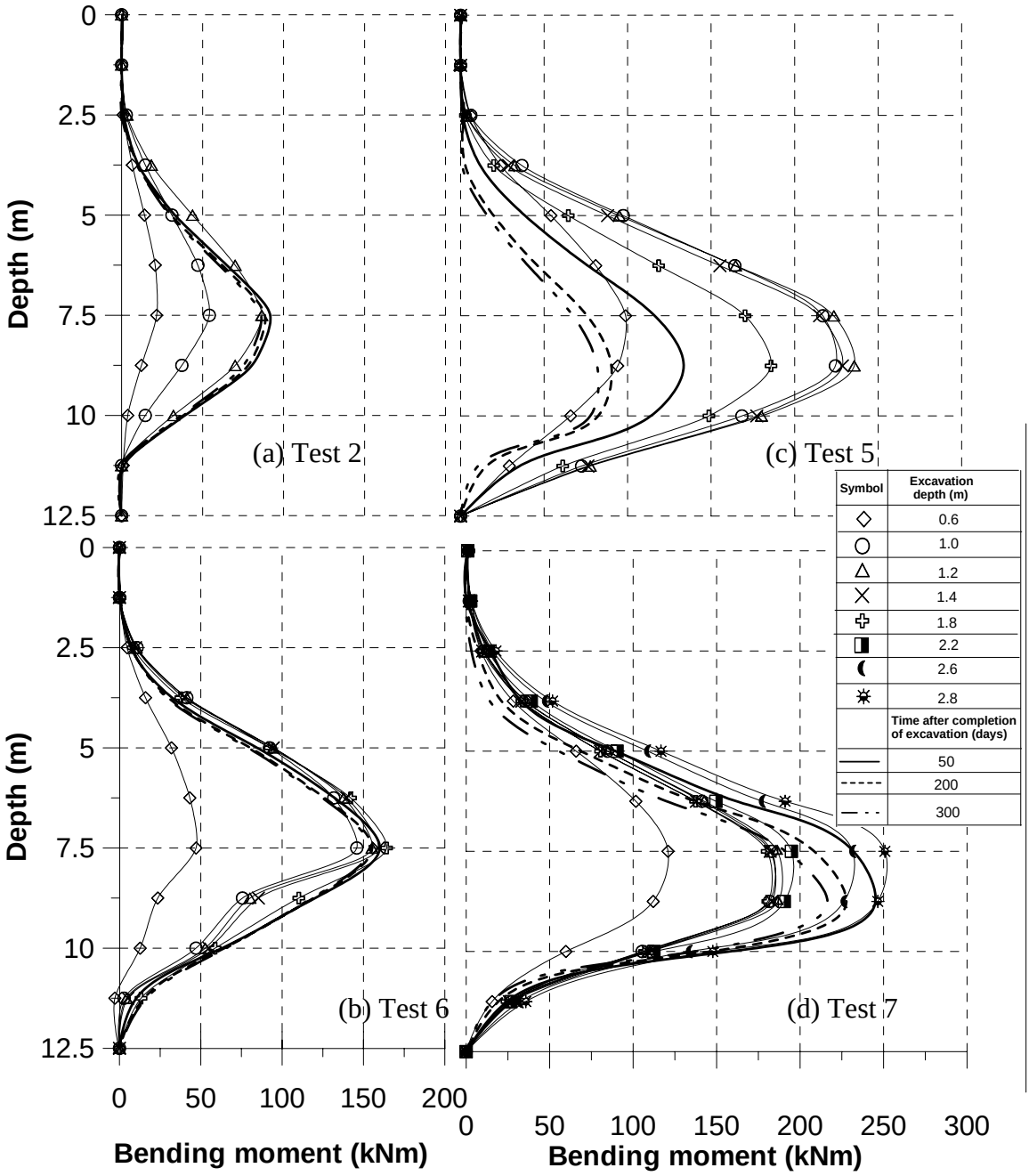

Figure 4.21 Measured pile bending moment profiles during excavation for (a) Test 2, (b) Test 5, (c) Test 6 and (d) Test 7

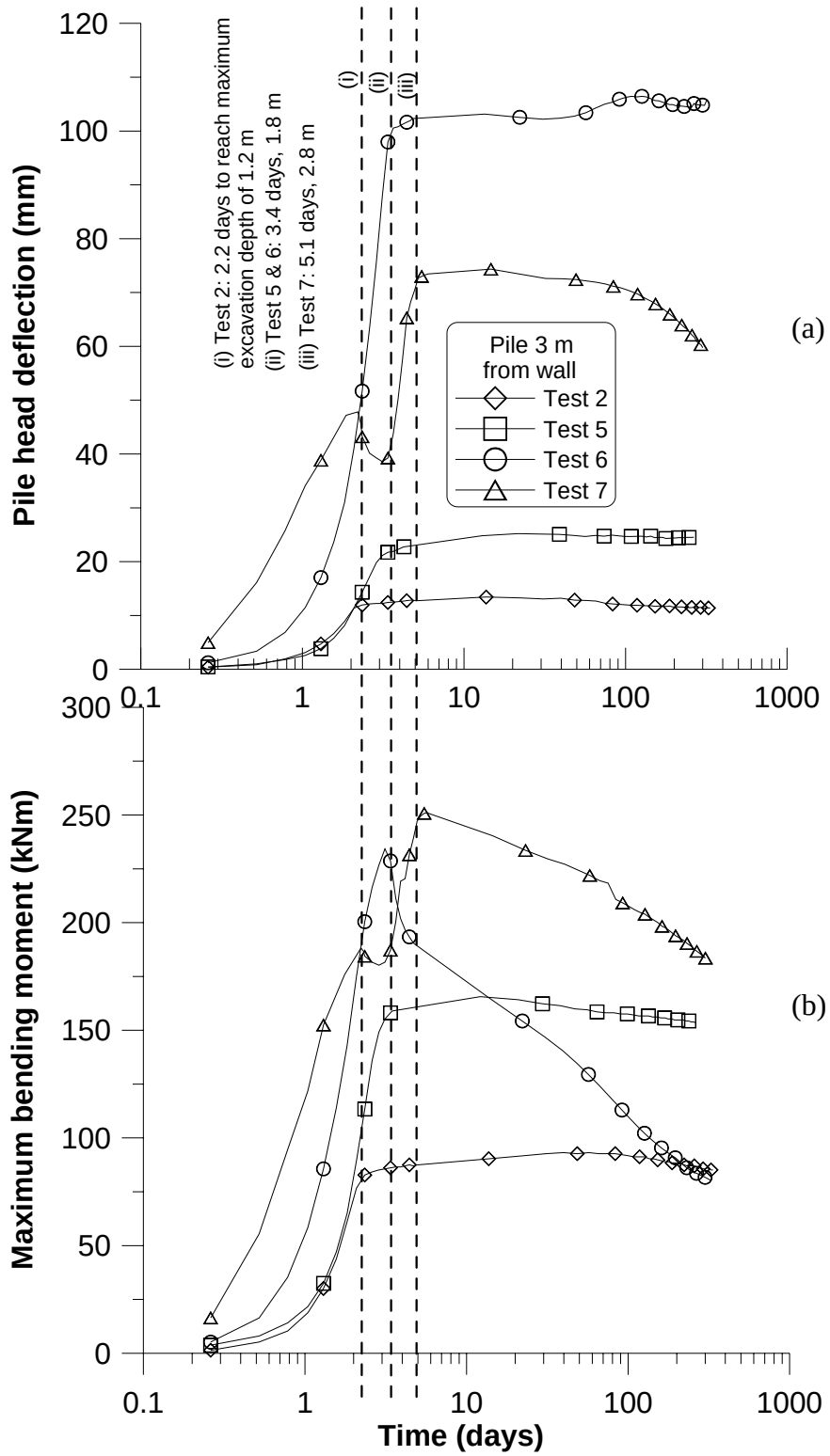

Figure 4.22 Development of maximum induced pile (a) head deflection and (b) bending moment during and after excavation

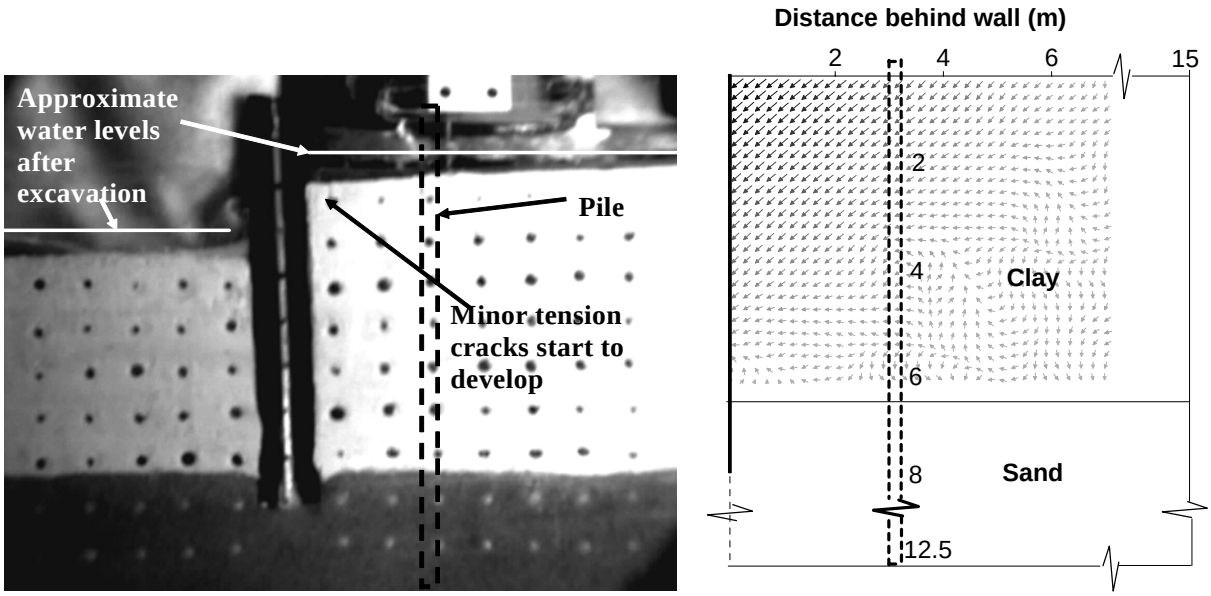

(a) Test 5

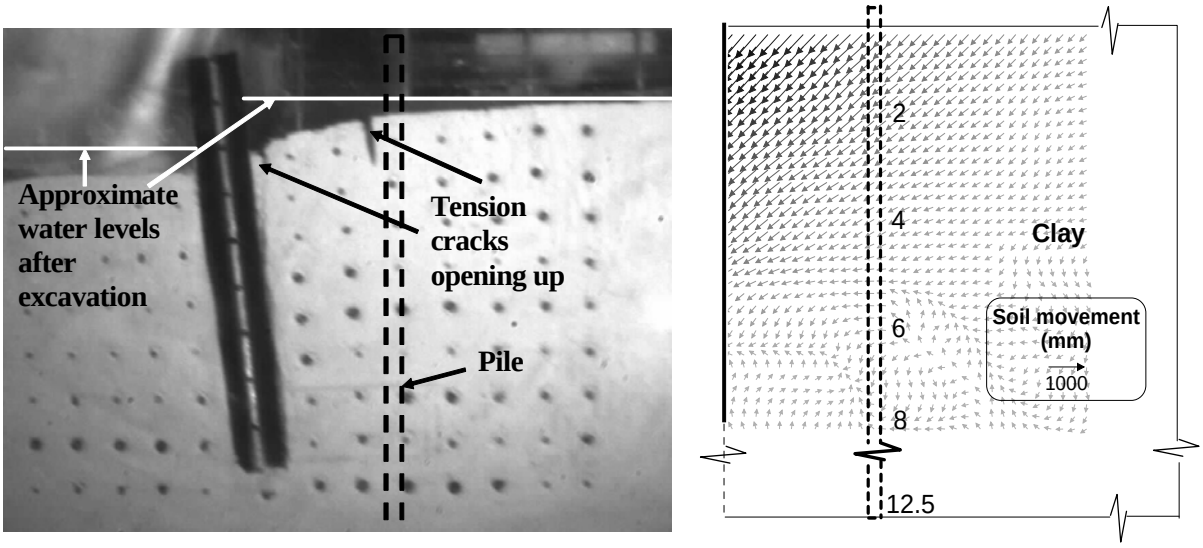

(b) Test 6

Figure 4.23 Resultant soil movements at the end of excavation: (a) Test 5 and (b) Test 6

(a)

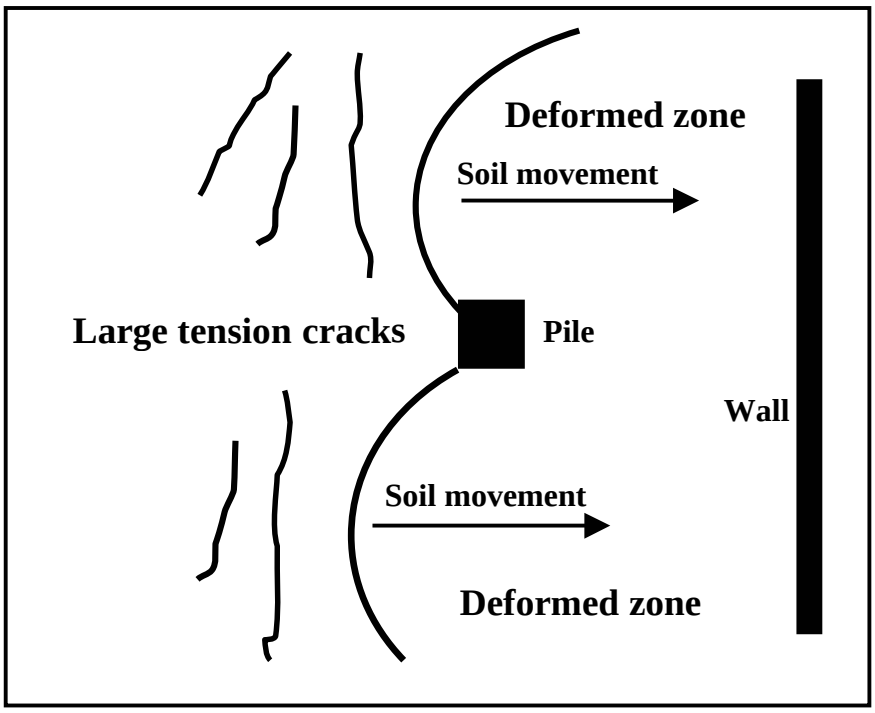

(b)

Figure 4.24 (a) Photograph and (b) sketch of soil movement on ground surface after end of Test 6

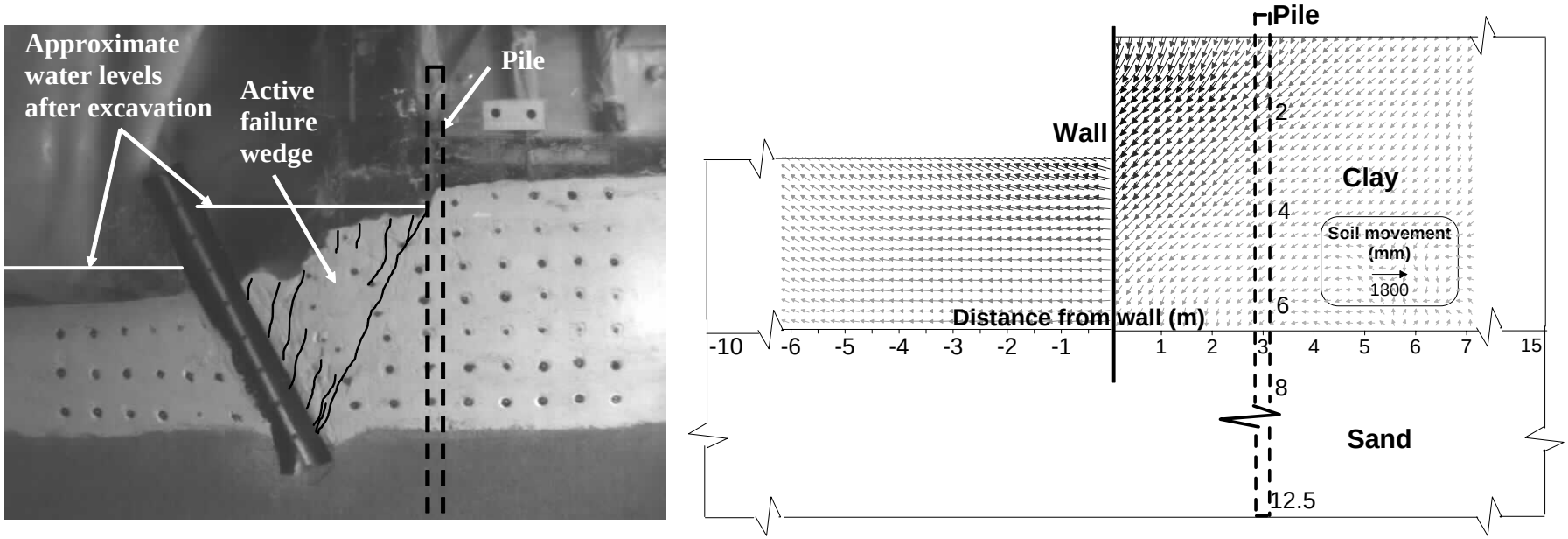

Figure 4.25 Resultant soil movements at the end of excavation for Test 7

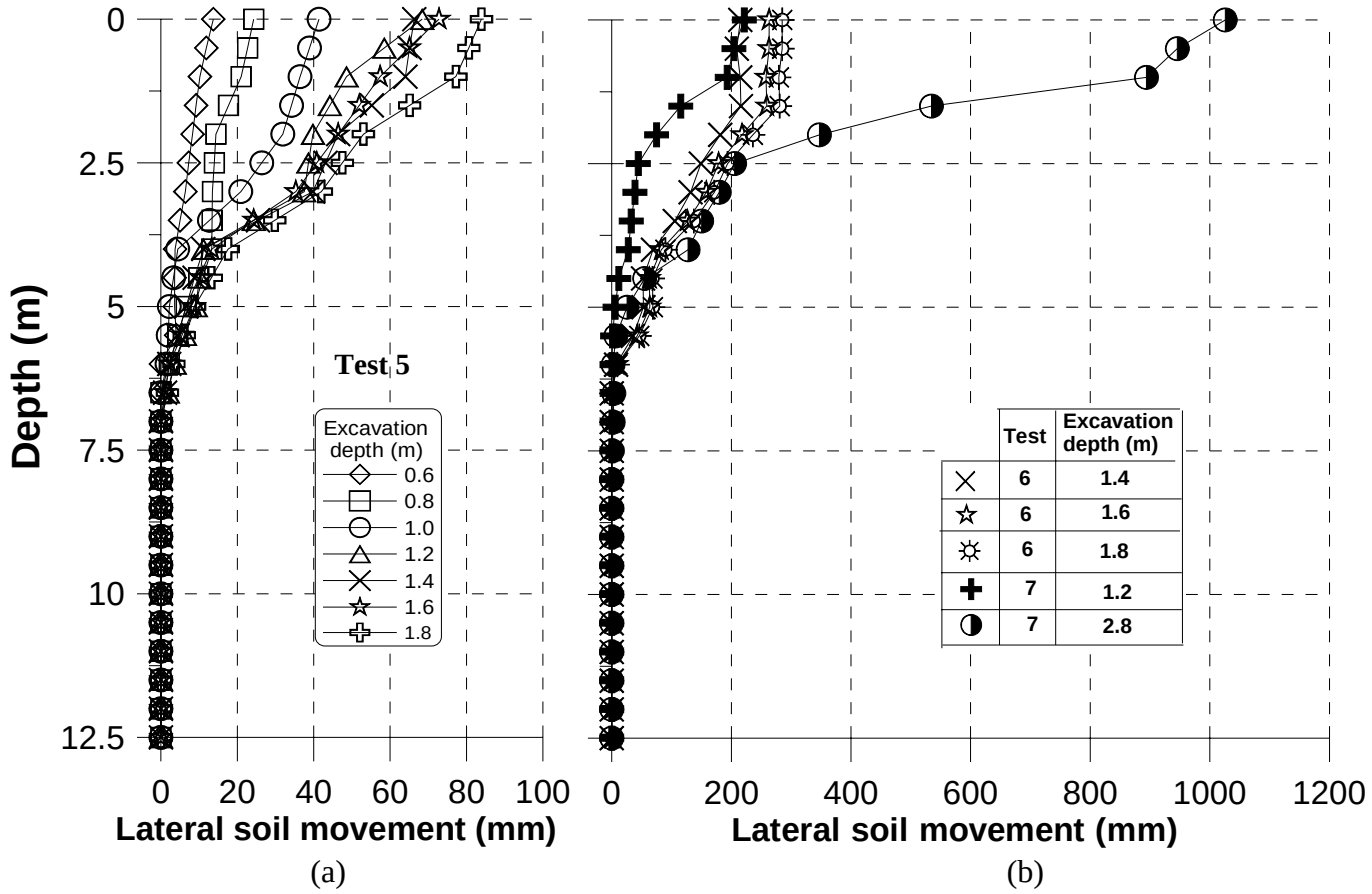

Figure 4.26 Measured lateral soil movement profiles for (a) Test 5 and (b) Tests 6 & 7

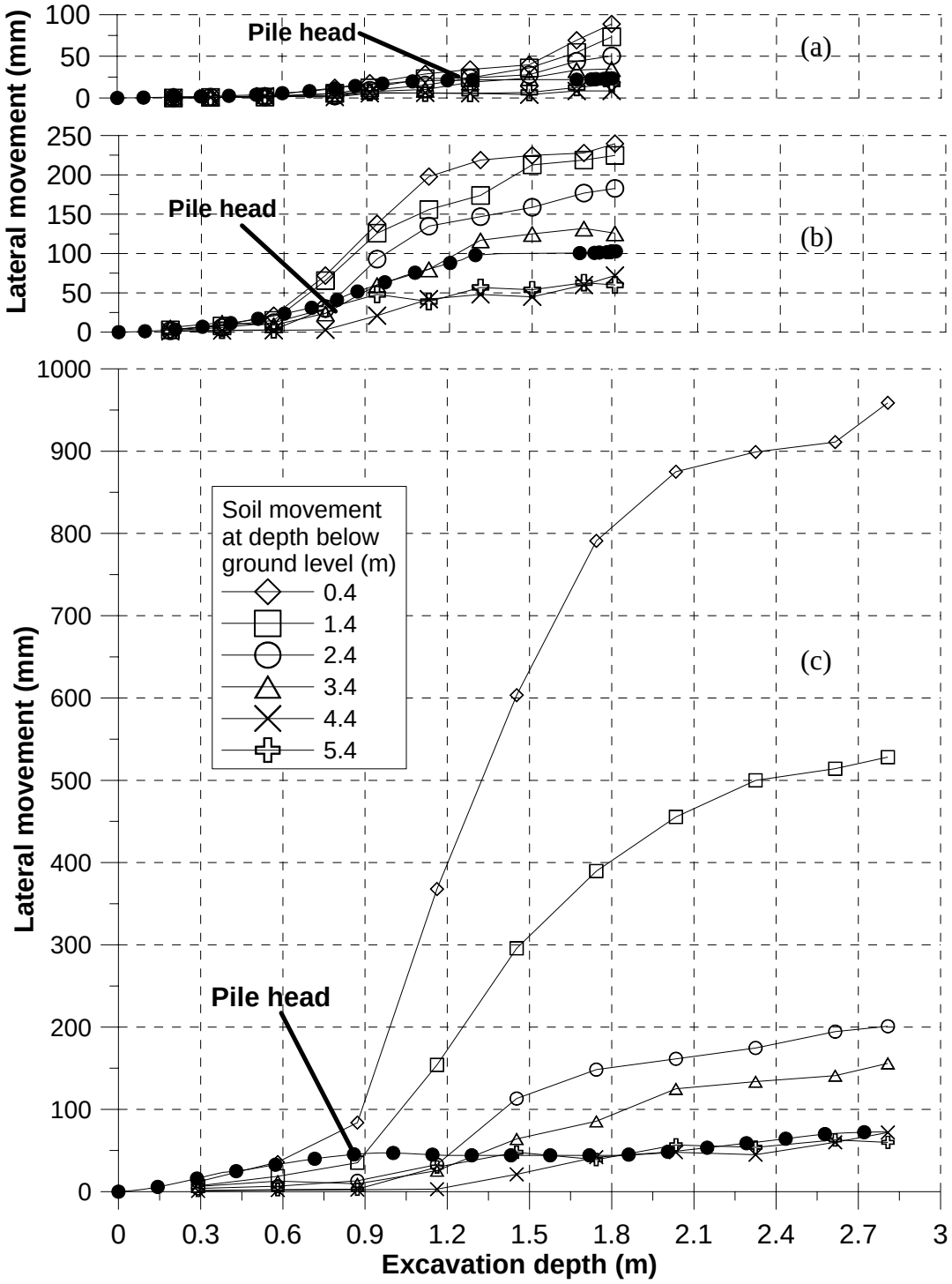

Figure 4.27 Variations of free field soil movement at 3 m from wall and pile head deflection with excavation depth for (a) Test 5, (b) Test 6 and (c) Test 7

CHAPTER FIVE

BEHAVIOUR OF PILE GROUP ADJACENT TO EXCAVATION IN CLAY

5.1 INTRODUCTION

In practice, piles are normally installed in groups and the behaviour of piles in a group is influenced by the pile head condition, size of pile group and centre-to-centre spacing of piles. Piles in a group can be either free-head or capped-head. By capping a pile group, considerable interaction among individual piles in the group may also occur through the pile cap. In order to examine the group interaction effect, centrifuge model tests were performed on pile groups of various sizes, head conditions and configurations. These included tests on free- and capped-head pile groups consisting of two, four and six individual piles. All tests involved a stable wall with the exception of one test involving a collapsed wall. This chapter presents the experimental results of pile group tests and comparisons of results are made with those of single pile tests presented in Chapter 4.

5.2 TEST PROGRAM

All the centrifuge tests were performed at 50g. Unless otherwise stated, the test results are presented in prototype scale hereinafter. The schematic configurations for all the pile group tests are shown in Figure 5.1. The tests involved free-head and

capped-head 2-, 4- and 6-pile groups behind a stable wall having the same maximum excavation depth of 1.2 m. In addition, a test involving a 4-pile group behind a collapsed wall had been carried out with a maximum excavation depth of 1.8 m.

In tests involving capped-head pile groups, the cap was connected to the individual pile heads at about 200 mm above the ground level to avoid interaction between the pile cap and the soil following the approach by Bransby and Springman (1997). It should be noted that the first level of strain gauges on the piles coincided with the ground surface. In addition, the maximum induced pile bending moment presented hereinafter refers to the maximum bending moment values achieved at all times during the tests.

The behaviour of free-head (Tests 8 and 10) and capped-head (Tests 9 and 11) 2-pile groups are arranged in a line perpendicular to the wall and located at various distances behind a stable wall will be first presented. Leung et al. (2003) established that it is not necessary to investigate 2-pile groups with piles aligned parallel to the wall as the individual pile responses are essentially identical.

To further investigate the behaviour of a larger pile group, tests on free-head (Test 12) and capped-head (Test 13) 4-pile groups were carried out. Owing to symmetrical arrangement of a 4-pile group, only two piles, that is one front pile and one rear pile, were instrumented to monitor their responses. The results will then be compared with those of single pile and 2-pile group tests. To further investigate the pile group behaviour, two capped-head 6-pile group tests were carried out in two different configurations. In Test 15, a pair of piles is arranged in three rows at 3 m (front, F), 5 m (middle, M) and 7 m (rear, R) behind the wall, hereinafter denoted as the 2x3 configuration. In Test 16, three piles were arranged in two rows at 3 m (F) and 5 m (R) behind the wall, hereinafter denoted as the 3x2 configuration. Peripheral piles

(P) are piles that are located at the edge of a pile group and are more exposed to the excavation-induced lateral soil movement. Centre piles (C) are the ones that are located in between two peripheral piles and thus are somewhat shielded. The identity of the individual piles in Tests 15 and 16 is also shown in Figure 5.1.

5.3 FREE-HEAD PILE GROUP RESPONSES BEHIND A STABLE WALL

To compare the pile group test results with those of single free-head piles, the pile head deflection and bending moment of Tests 1, 2 and 3 presented in Chapter 4 are also shown in this section. It should be noted that the variations of excavation depth and wall head deflection with time for the single pile and pile group tests behind a stable wall are essentially identical and these are represented by Figures 4.7(a) and (b). The final excavation depth was 1.2 m.

5.3.1 Pile responses over time

Figures 5.2 and 5.3 show the variations of pile head deflection and maximum induced pile bending moment with time, respectively, for free-head pile groups (Tests 8, 10 and 12) and single piles (Tests 1, 2 and 3). It is noted that owing to space constraints in the model container, only the pile head deflection of the rear pile in the free-head pile group can be measured using the laser displacement transducers. Figure 5.2(a) shows a comparison between the pile head deflection of Tests 2 and 8.

The free-head piles are located 3 m behind the wall and the maximum induced pile head deflection is reached at about 50 days after the end of excavation for both the tests. However, for Tests 10 (2-pile group) and 12 (4-pile group) having the rear piles located 5 m behind the wall, the pile head deflection in both tests continues to increase during the entire test duration as shown in Figure 5.2(b). This phenomenon is

consistent with that observed for a single pile located 5 m (Test 3 shown in Figure 5.2(c)) behind the wall, as discussed in detail in Section 4.6.1.

Figure 5.3 shows the development of maximum induced pile bending moment over time for both single pile (Test 1) and that of the front pile of a free-head 2-pile group (Test 8) located at 1 m behind a stable wall. In both tests, the maximum bending moment value is reached 4 days after the completion of excavation. Subsequently, the bending moment is observed to reduce with time. This phenomenon is consistent with the earlier finding made in Section 4.6.2.2 that for a pile that is substantially embedded within the largely plastically deformed soil region, there would be a relaxation of induced pile bending moment and pile head deflection once the soil within the deformation zone has weakened after excavation.

In the case of a single pile or an individual pile in a free-head pile group located 3 m behind the wall, the maximum bending moment is achieved at about 50 days after the completion of excavation as shown in Figure 5.4(a). If these piles are located 5 m behind the wall, the maximum bending moment appears to increase continuously with time for the entire test duration, as shown in Figure 5.4(b). It is noted that the induced maximum pile bending moment is inversely related to the number of piles in a pile group. As the number of piles increases, the induced pile bending moment becomes smaller and the changes in the pile responses with time become less prominent. In general, the time dependent pile head deflection and maximum bending moment show similar behaviour for both single pile and individual piles in a free-head pile group at the same distance behind a stable wall.

5.3.2 Free-head 2-pile group (Tests 8 and 10)

In Test 8, the front and rear piles of the free-head 2-pile group are located 1 m and 3 m behind the wall, respectively. On the other hand, the free-head front and rear piles of Test 10 are positioned at 3 m and 5 m behind the wall. The pile bending moment profiles described hereinafter relates to the maximum induced pile bending moment values obtained from the respective tests.

. Figures 5.5, 5.6(a) and (b) show the induced pile bending moment profiles obtained from Tests 8 and 10 and those of single piles located 1 m, 3 m and 5 m behind the wall, respectively. It is noted that the shape of the pile bending moment profiles for all the tests is similar. For piles located 3 m and 5 m behind the wall, the maximum bending moment is located about 7.5 m below the ground level. However, if the pile is 1 m behind the wall, the maximum pile bending moment is observed to be located at 8.75 m below the ground level. This is attributed to the greater and deeper soil movement experienced by the pile due to the development of the 45^{o} wedge of significant soil movement behind the wall after excavation as shown in Figure 4.16.

By comparing the responses of the rear pile from Test 8 and the front pile from Test 10 with both piles located 3 m behind the wall, the measured bending moment of the latter pile is greater. This observation is similar to that noted by Lim (2001) for pile groups in sand and illustrates that the front pile is capable of shielding or shadowing the rear pile from the detrimental effects of excavation-induced soil movement. Thus it is important to note the relative position of an individual pile within a group as it would affect the response of the respective pile.

5.3.3 Free-head 4-pile group (Test 12)

Test 12 was conducted as a free-head 4-pile group test where pairs of front and rear piles are positioned at 3 m and 5 m behind the wall, respectively, as shown in Figure 5.1. The induced bending moment profiles of the front and rear piles are shown together with those of single pile (Test 2) and 2-pile group (Test 8) in Figure 5.6. It is evident that the trend of induced pile bending moment profiles for all free-head pile groups is similar. Figure 5.6 reveals that as the number of piles in a group increases, smaller bending moment is induced on the piles. The induced bending moment on a single pile located 3 m behind the wall is about 5 % higher than that of the corresponding pile in a 2-pile group but is about 30 % higher than that in a 4-pile group. The corresponding differences are 5 % and 25 % for a pile located at 5 m behind the wall. This observation again confirms that the shadowing effect of front piles over the rear piles increases with increasing number of piles in a group.

Chen and Martin (2002) noted that soil arching would occur between two front piles upon excavation. They defined soil arching as the transfer of stress from the yielding part of a soil mass to adjoining less-yielding or restrained parts of a soil mass. They then analysed the soil arching phenomenon using the finite difference code FLAC (Fast Lagrangian Analysis of Continua). By analyzing the rotation of the principal stresses directions shown in Figure 5.7, Chen and Martin (2002) verified that soil arching exists. Within each arching zone, the tangential direction and the radial direction are the direction of major and minor principal stresses, respectively. Figure 5.8 shows a photograph of top view of the ground surface taken after Test 12. The phenomenon of soil arching and separation is evident and this suggests that the clay in this region may have yielded. This is consistent with the finding of Martin and Chen (2002) shown in Figure 5.9. It is believed that the development of this yield or plastic

zone starts at both sides of the pile and extends to the front of the pile when the soil deformation increases due to excavation.

Figure 5.10 shows the variations of lateral soil movement at different depths at 3 m behind the wall and the pile head deflection with excavation depth for Test 12. When the surrounding soil moves more than the pile head, it is thought that the near surface effect causes the soil at the upper 2 m to move more than the pile head than the underlying soil layers. Such near surface effect has also been observed by Randolph and Houlsby (1984), Poulos (1995a) as well as Chen and Martin (2002). This subsequently results in the development of an equilateral triangular arch, as reported by Adachi (1989) and shown in Figure 5.11. The arch is formed between the front piles when the yielded soil gets detached from its surrounding. The detached soil is then forced to squeeze into the row of piles but without significantly increasing the pressure acting on the piles (Chen and Martin, 2002). This is verified in the present study as the rate of increase of measured pile bending moment is noted to decrease towards the end of the 1.2 m excavation, as shown in Figure 5.12.

Chen and Martin (2002) further studied the effect of pile spacing on the formation of an arch under undrained condition. It was highlighted that the development of an arch was limited by the pile spacing, with no visible arching for pile spacing less than 2 or greater than 4 times the pile diameter. As the 0.63 m square piles are spaced at 2.0 m in the present study, the pile spacing is about 3.2 times pile width. Thus soil arching is expected.

5.4 CAPPED-HEAD PILE GROUP RESPONSES BEHIND A STABLE WALL

This section presents the centrifuge results for various capped-head 2-, 4- and 6-pile groups.

5.4.1 Pile responses over time

The development of pile cap deflection with time for Tests 9, 11, 13, 15 and 16 is shown in Figure 5.13. Since the pile groups are capped, the deflection of each individual pile head is identical. The pile cap deflection for Test 9, which consists of a 2-pile group with front and rear piles located 1 m and 3 m behind the wall, respectively, shows some fluctuations over time due to signal interference during data acquisition. Nevertheless, the general trend of this result shows that the pile cap deflection reduces with time after excavation. In contrast, for Test 11, which consists of a 2-pile group with front and rear piles at 3 m and 5 m behind the stable wall, respectively, the pile cap deflection remains fairly unchanged after achieving its peak value at about 50 days after the start of excavation. For Test 13 (4-pile group), Test 15 (6-pile group, 2x3) and Test 16 (6-pile group, 3x2), where the front peripheral piles (FP) are located at 3 m behind the wall, the pile cap deflection increases continuously until the end of the tests.

Figures 5.14(a) and (b) show the development of maximum positive and negative pile bending moments for the front and rear piles in a capped-head pile group, respectively. For clarity, the simplified figures located at the right hand side of Figures 5.14(a) and (b) are shown to illustrate the locations of the maximum positive and negative pile bending moment for the front and rear piles, respectively. For the front piles, the maximum negative and positive pile bending moment values are typically

located about 6 and 14 pile widths below the ground level, respectively. On the other hand, for the rear and middle piles, the maximum negative and positive pile bending moment values are located at the pile head and about 12 pile widths from the ground level, respectively.

For Test 9 where a substantial portion of the front pile (1 m behind the wall) is embedded within the largely plastically deformed soil region as described in Section 4.6.2.2, there would be a relaxation of induced pile bending moment once the soil within the deformation zone has weakened after excavation. As such, the maximum negative and positive pile bending moment values are observed to reduce after excavation (see Figure 5.14(a)). This phenomenon is consistent with that of a single pile located at the same distance behind the stable wall shown in Figure 4.7. Since the front and rear piles are connected via a rigid pile cap, the rear pile located at 3 m behind the stable wall is dragged along, thus sharing the same behaviour as the front pile, where both the maximum negative and positive pile bending moment values reduce after excavation (see Figure 5.14(b)). Such reduction in pile bending moment for piles located at 3 m behind a stable wall has not been observed previously in the single pile tests (see Figure 4.7) and the free-head pile group test (see Figure 5.3(a)). Besides, the pile cap deflection also shows similar trend over time as discussed earlier (see Figure 5.13). These observations reveal that the interaction between piles in a capped-head pile group is considerably larger than the free-head pile group as the rear piles would jointly resist the excavation-induced soil movement through the pile cap.

In general, the maximum positive bending moment of the front (FP and FC) and rear (RP and RC) piles at 3 m and 5 m behind the stable wall for Tests 11, 13, 15 and 16 is reached about 50 days after the completion of excavation, as shown in Figures 5.14(a) and (b), respectively. Thereafter, the positive bending moment values

decrease with time. This is similar to the observation made for Tests 2 and 3 involving a single pile at identical distances behind the wall as shown in Figure 4.7(d). It has been discussed in Section 4.6.2 that such pile responses are influenced by the progressive wall and soil deformations with time.

In contrast, the negative bending moment values of the front (FP and FC) and middle (MP) as well as the rear (RP and RC) piles at 3 m and 5 m behind the stable wall for Tests 11, 13, 15 and 16 are observed to reduce gradually after the end of excavation, as shown in Figures 5.14(a) and (b), respectively. These maximum negative bending moments are located at the individual pile heads. Therefore, comparison of the development of the maximum negative bending moment values is made to that of the pile cap deflection. It has been described earlier that the pile cap deflection for Tests 11, 13, 15 and 16 is observed to increase continuously until the end of the tests. As the pile deflection profiles are obtained by integrating the spline functions for the bending moment profiles twice with two known boundary conditions, it is therefore acknowledged that the pile head deflection is directly proportional to the bending moment. In other words, if the pile head deflection increases, so would the bending moment at the pile head or the maximum negative pile bending moment. However, such observation is not observed in this study. Instead, as the pile cap deflection values increase over time, the maximum negative pile bending moment values are noted to reduce, thus suggesting relaxation in the pile cap fixity. A reasonable postulation to this observation is the inability of the rigid pile cap to provide full fixity or restraint to the pile heads. This will be further investigated in Chapter 6.

5.4.2 Capped-head 2-pile group (Tests 9 and 11)

Test 9 was carried out on two capped-head piles at 1 m (front pile) and 3 m (rear pile) behind the wall. It is observed from Figure 5.15 that the magnitude of the pile group deflection is lower than that of single piles and free-head pile group located at the same distance behind the wall.

The pile bending moment profiles of Test 9 as well as those of corresponding free-head single piles are shown in Figure 5.16. It is noted that the bending moment profiles for both capped-head and free-head piles are quite different. For the capped-head pile groups, positive and negative bending moments are recorded as opposed to only the positive bending moment recorded by the free-head pile groups. The location of the maximum positive bending moment for both piles is noted to be about 8.75 m below the ground surface. When compared to the respective single piles, it is noted that the magnitude of maximum positive bending moment for the capped-head piles has reduced, especially for the front pile. Nevertheless, negative pile bending moment is induced in the upper portion of both piles due to the restraint provided by the pile cap. The maximum negative bending moment is noted to be at about 3.75 m depth and at the ground surface for the front and rear piles, respectively. With the presence of pile cap, the individual piles in a group are “forced” to act in unison when subject to different magnitudes of soil movement. The induced bending moment on the front pile, which experiences greater soil movement, is expected to be moderated by the rear pile via the rigid pile cap. This is due to the shadowing effect of the front pile over the rear pile first reported by Lim (2001) as well as the pile-pile cap interaction when the pile group is subject to lateral soil movement.

In order to further evaluate the above findings, Test 11 was carried out as a capped-head 2-pile group with the front and rear piles located 3 m and 5 m behind the

wall, respectively. The bending moment profiles of these piles are also observed to be much smaller than those of single piles at the same distance from the wall, as shown in Figure 5.17. It is noted that the location of maximum positive pile bending moment for the front and rear piles are about 8.75 m and 7.5 m, respectively.

The results of Tests 9 and 11 reveal that for the front piles located 1 m and 3 m behind the wall, respectively, the maximum positive pile bending moment is located at 8.75 m depth. However, if the rear pile is located 5 m behind the wall, the maximum moment location shifts up to about 7.5 m depth. This is attributed to the wedge of significant soil movement behind the wall intercepting the pile at a higher elevation. For the front and rear piles in both tests, the maximum negative bending moment is noted to be about 3.75 m below and at the ground surface level, respectively.

A summary of the measured maximum induced pile bending moment is shown in Figure 5.18. It is evident that the front pile would shield the rear pile from the soil movement and thus results in a smaller measured positive bending moment along the rear pile. With the presence of pile cap, the rear pile generates a greater negative bending moment at the pile cap level than the front pile due to pile-soil interaction.

5.4.3 Capped-head 4-pile group (Tests 13)

Figure 5.19 shows the comparison of pile bending moment for a capped-head 2-pile group (Test 10) and a capped-head 4-pile group (Test 13), with the front and rear piles located 3 m and 5 m behind the wall, respectively. By comparing the maximum positive and negative bending moment for the front pile, a difference of 22 % and 9 % is noted for Tests 10 and 13, respectively. However, for the rear pile, the corresponding difference is 20 % and 17 %. Therefore, the ability of a larger pile group to reinforce the surrounding soil undergoing lateral movement due to excavation could

be noted and this is consistent to the observations made for free-head pile groups described earlier.

When comparing the maximum positive pile bending moment between free-head (see Figure 5.6) and capped-head pile groups (see Figure 5.19), the magnitudes for individual piles are larger for a free-head pile group than those of a capped-head pile group. However, negative bending moment is developed at the pile head due to restraint provided by the rigid pile cap. It can be surmised that the presence of a rigid cap can effectively reduce the maximum bending moment on individual piles in a group as the rigid cap forces the individual piles to react in unison to counter resist the detrimental lateral soil movement. Soil arching is also observed to be similar to that of Test 12.

The measured pile head deflections for Tests 12 and 13 are summarized in Figure 5.20. It is again demonstrated that a reduction in pile head deflection can be achieved by connecting individual piles to a rigid pile cap.

5.4.4 Capped-head 6-pile group (Tests 15, 2x3 configuration)

Owing to symmetrical arrangement of the 2x3 pile group configuration, only one of each of the three pairs of piles located at 3 m (front), 5 m (middle) and 7 m (rear) were instrumented. Figure 5.21 shows the bending moment profiles of the three instrumented piles. It is observed that the bending moment profile of the front pile is similar to all other front piles in the capped-head 2-pile and 4-pile group tests. It is also noted that the middle and rear piles demonstrate similar pile bending moment profiles.

By comparing the bending moment profiles of each pile, it is observed that as the distance between the pile and the wall increases, the depth to maximum positive pile bending moment reduces. Such results are consistent with those of single piles

described in Section 4.6. The pile cap deflection is observed to be smaller than that of a capped-head 4-pile group in Test 13 as shown in Figure 5.20.

Soil arching is also observed in Test 15. Similar to Test 12, soil arching is only observed between the pair of front piles located 3 m behind the wall. This shows that relatively large soil deformation is experienced by the piles located 3 m behind the wall. The relatively smaller soil deformation at 5 m behind the wall is not large enough to cause soil arching between that row of piles.

5.4.5 Capped-head 6-pile group (Tests 16, 3x2 configuration)

In the case of a 3x2 capped-head 6-pile group configuration, four instrumented piles were used to capture the pile group behaviour. The positions of the instrumented piles are shown in Figure 5.1. Figure 5.22 shows the measured bending moment for the four instrumented piles. The induced pile bending moment profiles are consistent to those of typical front and rear piles. Again, the elevation of maximum positive pile bending moment for the front piles is deeper than that of rear piles. This observation is similar to that of the 2x3 capped 6-pile group configuration. It is also observed that the induced bending moment for the front peripheral (FP) pile is greater than that of the front centre (FC) pile at the same distance of 3 m behind the wall. Similarly, the bending moment developed in the rear peripheral (RP) piles is also greater than that of the rear centre (RC) pile at the same distance of 5 m behind the wall.

The above observation suggests that peripheral piles can shield the centre piles from excavation-induced soil movement. For the 3x2 pile group configuration of Test 16, relatively larger pile bending moment is induced as compared to that of the 2x3 configuration of Test 15, for the corresponding peripheral piles at the same distance from the wall. Therefore, it is surmised that a capped 3x2 pile group configuration is subjected to larger overall forces than a capped 2x3 pile group as the former is in fact

located closer to the wall. Figure 5.20 shows a comparison of the measured pile cap deflection for Tests 15 and 16. The 2x3 6-pile group shows a greater pile cap deflection than the 3x2 6-pile group. Such observations were also noted by Lim (2001). However, careful observation of the photographs taken after the test reveals that only slight soil arching was observed in Test 16. This could be due to the greater reinforcing effect provided by the 3x2 pile group configuration as opposed to that of 2x3 configuration.

5.5 CAPPED-HEAD PILE GROUP BEHAVIOUR BEHIND A COLLAPSED WALL

Test 14, which consisted of a capped-head 4-pile group, was carried out to investigate the behaviour of pile group behind a collapsed wall. The front and rear piles are located 3 m and 5 m behind the wall, respectively and are floating in thick clay layer, without any toe embedment in sand. The excavation depth is 1.8 m and the wall would subsequently fail upon excavation as the calculated factor of safety using the limit analysis (Bolton and Powrie, 1987) is about 0.95. The results will then be compared with Test 6 from Chapter 4, on a single pile with a similar test setup.

The development of pile cap deflection and maximum pile bending moment for Test 14 are shown in Figures 5.23 and 5.24, respectively. It is evident that the movement of the wall as well as the induced pile bending moment is dependent upon excavation depth and time. This is consistent with the earlier findings for single piles as described in detail in Section 4.7. The long term pile head deflection and front as well as rear pile bending moment demonstrate distinct peaks at the onset of wall collapse as shown in Figures 5.23 and 5.24(a) and (b), respectively. These peak values would then reduce significantly over time. Such pile behaviour is similar to that

demonstrated by the single pile located 3 m behind a collapsed wall in Test 6 (see Figures 4.22(a) and (b)). The reduction in the pile bending moment after excavation may be associated to the failure of the largely deformed soil to resist the excavation-induced soil movement as described in Section 4.7. The similarity between the front and rear pile behaviour is believed to be influenced by the rigid pile cap. This illustrates the ability of a capped-head pile group in resisting further deformation when subjected to excavation-induced soil movement as described earlier.

The measured front and rear pile bending moment profiles are shown in Figures 5.25 and 5.26. For the 4-pile group in Test 14, the pile bending moments remain unchanged only after the excavation has exceeded 1.6 m. This is different from Test 6 where the bending moment reaches a maximum at a shallower excavation depth of 1.4 m. Thus, this demonstrates that a capped-head pile group is capable of resisting excessive soil movement behind a collapsed wall more effectively than a single free-head pile.

Figure 5.25(a) reveals that the induced bending moment is generally much greater for the upper portion of the front pile. This may be attributed to the presence of a wedge of significant soil movement, somewhat similar to that observed for Test 6 as shown in Figure 4.23(b). It is interesting to note that since most of the rear pile is located outside the wedge of significant soil movement, it too demonstrates limiting pile responses as shown in Figures 5.26. Therefore, the observed limiting bending moment for both front and rear piles reveals that the front pile, which experiences larger soil movement, is assisted by the rear pile through the pile cap to resist the soil movement. This demonstrates the interaction between the front and rear piles to jointly resist the excavation-induced soil movement. As such, the pile head deflection as well as the front and rear positive pile bending moment are smaller than those of a single

pile located behind a collapsed wall in Test 6, if Figures 5.23 and 5.24 are compared with Figure 4.22(a) and (b), respectively.

5.6 COMPARISON OF PILE GROUP BEHAVIOUR IN SAND AND CLAY

Lim (2001) performed centrifuge tests on free- and capped-head pile groups in sand. Only tests involving pile groups behind a stable wall had been carried out. The final excavation depth was 4.5 m. The similarities and differences between the behavior of pile groups in clay and sand are discussed hereinafter.

5.6.1 Similarities

When piles are installed in a group in either sand or clay, the front piles would shield the rear piles from the detrimental effects of excavation-induced soil movement and hence relatively smaller bending moment is induced in the rear piles. However, the rear piles would generate a greater negative bending moment at the pile cap level than the front piles due to pile-soil interaction when the rear piles are dragged forward by the front piles which are subject to greater soil movement.

When the size of pile group increases, the reinforcement and shadowing effects provided by the larger number of piles becomes more significant and hence, smaller bending moment is induced on the rear piles. The relative position of an individual pile in a group is also important. Peripheral piles can effectively shield the centre piles at the same distance behind the wall from the full exposure of soil movement and thus, smaller bending moment is developed in the shielded piles. Besides that, both tests in sand and clay evidently show that a capped 3x2 pile group configuration is subjected to larger overall forces than a capped 2x3 pile group as the former is in fact located nearer to the wall and excavation area.

5.6.2 Differences

As discussed in Section 4.8.2 for single piles, pile groups installed in sand do not demonstrate any time-dependent effect. On the contrary, if a pile group is embedded in clay, time dependent pile bending moment is observed due to progressive deformation of the wall and soil over time.

For piles embedded in clay, soil arching is observed to occur between piles that are close enough to the wall when the clay deforms during excavation. Besides that, soil "separation" is also noted to occur in front of a pile group after excavation. However, such observations are not noted in tests conducted in sand.

Similar to the case of a single pile, the induced front and rear pile bending moment would reduce after excavation due to development of tension cracks and slip plane if the wall subsequently collapses after excavation. Such behaviour is not observed in tests carried out in sand.

5.7 SUMMARY

This chapter presents centrifuge model test results of free- and capped-head 2-, 4- and 6-pile groups in clay behind a wall that remains stable after excavation. It is found that the induced maximum bending moment is always smaller than that of a corresponding single pile at identical location. If the free-head piles are located at the same distance, the measured bending moment is higher if it serves as the front pile as opposed to the rear pile of the pile group. In a pile group, each individual pile will provide shadowing and reinforcing effects to the other piles nearby. The degree of shadowing effect experienced by each individual pile depends on its relative position with its surrounding piles.

For instance, it is observed that the induced bending moment for the front peripheral (FP) pile is greater than that of the front centre (FC) pile at the same distance behind the wall. Similarly, the bending moment developed at the rear peripheral (RP) piles is also greater than that of the rear centre (RC) pile at the same distance behind the wall. As the pile group gets larger, the shadowing and reinforcing effects will also become more prominent.

The immediate effect of pile shadowing and reinforcing effect is to limit the detrimental effects of excavation-induced soil movement on the pile group. By capping a pile group, the individual piles are forced to interact in unison when subjected to different magnitudes of soil movement, depending on the distance of the piles from the excavation. The induced bending moment of the front pile, which experiences greater soil movement, is expected to be moderated by the rear pile via the pile cap. The interaction between the front and rear piles induces negative bending moment at the restraint pile head, but reduces the magnitude of bending moment developed along the pile and the pile group deflection.

Soil arching and "separation" of soil have been observed to occur between the front piles of a pile group when the soil deforms during excavation in the 4- and 6-pile groups. The arch is formed between the rows of piles when the yielded soil gets detached from its surrounding. The detached soil is then forced to squeeze into the row of piles but without significantly increasing the pressure acting on the piles.

Generally, the observed long term maximum positive bending moment would increase after excavation until about 50 days later and subsequently reduce. It is thought that progressive wall and soil deformations are the reasons for such observed time dependent pile behaviour. On the contrary, the maximum negative bending moment generally reduces slightly over time after excavation. This behaviour could be

the result of the pile-pile cap interaction as the maximum negative pile bending moment is located nearer to the pile cap.

A test involving a 4-pile group in clay behind a wall that subsequently collapses upon excavation has also been carried out. The pile bending moments remain unchanged and reduce only after excavation exceeds 1.6 m. It is thought that the limiting soil pressure that can be exerted on the piles have been reached at this stage. The long term pile maximum positive and negative bending moments display distinct peaks and would reduce after the completion of excavation. Such pile behaviour is consistent to that observed for the case of a single pile case located behind a collapsed wall.

This chapter has successfully provided experimental evidences that the soil surrounding the piles would resist the detrimental effects caused by excavation by initiating some resisting mechanisms such as soil arching and load-sharing amongst individual piles in a group. These experimental observations have instilled greater confidence level of the centrifuge experiments that have been performed so that the numerical back-analyses described in the next chapter can be “calibrated” to incorporate such soil behaviour, which otherwise could not be ascertained to have existed.

Test number	Plan	Elevation	Parameter (m)	Pile head condition
8	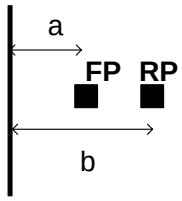	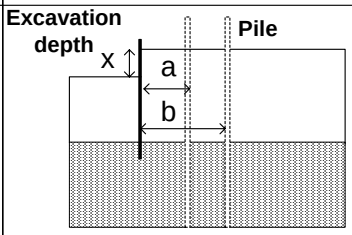	a = 1 b = 3 x = 1.2	Free
9	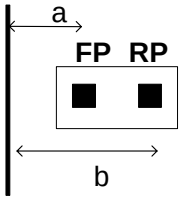	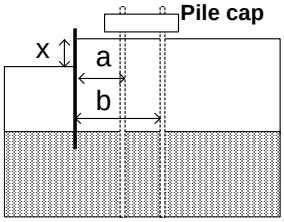	a = 1 b = 3 x = 1.2	Capped
10	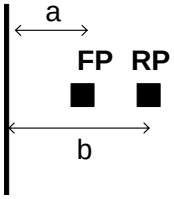	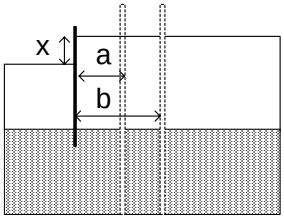	a = 3 b = 5 x = 1.2	Free
11	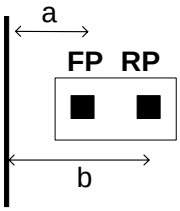	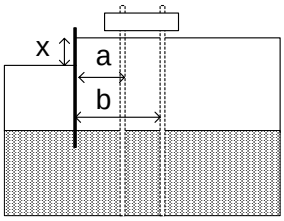	a = 3 b = 5 x = 1.2	Capped
12	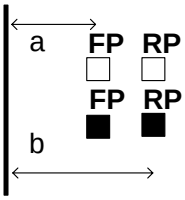	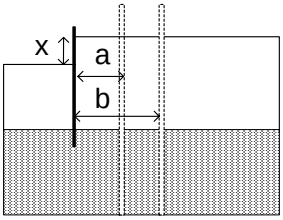	a = 3 b = 5 x = 1.2	Free

□ Uninstrumented pile
■ Instrumented pile

Legend:
FP: Front peripheral
RP: Rear peripheral

Figure 5.1 Test program of pile group

Test number	Plan	Elevation	Parameter (m)	Pile head condition
13	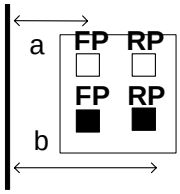	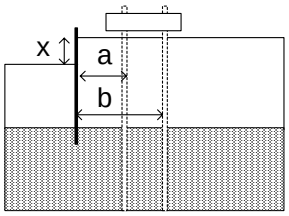	a = 3 b = 5 x = 1.2	Capped
14	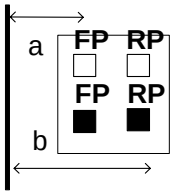	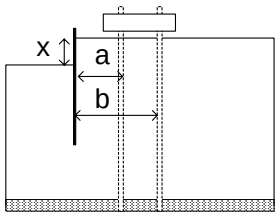	a = 3 b = 5 x = 1.8	Capped (Collapsed wall)
15	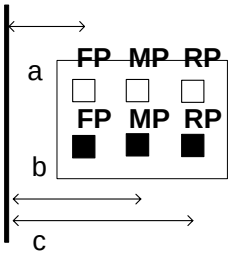	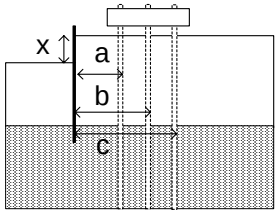	a = 3 b = 5 c = 7 x = 1.2	Capped
16	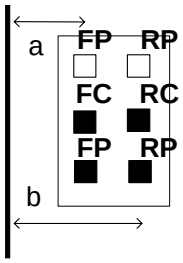	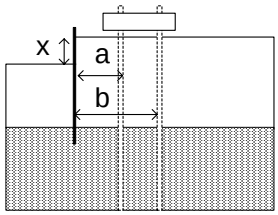	a = 3 b = 5 x = 1.2	Capped

□ Uninstrumented pile
■ Instrumented pile

Legend:
FP: Front peripheral
FC: Front centre
RP: Rear peripheral
RC: Rear centre
MP: Middle peripheral

Figure 5.1 (continued) Test program of pile group

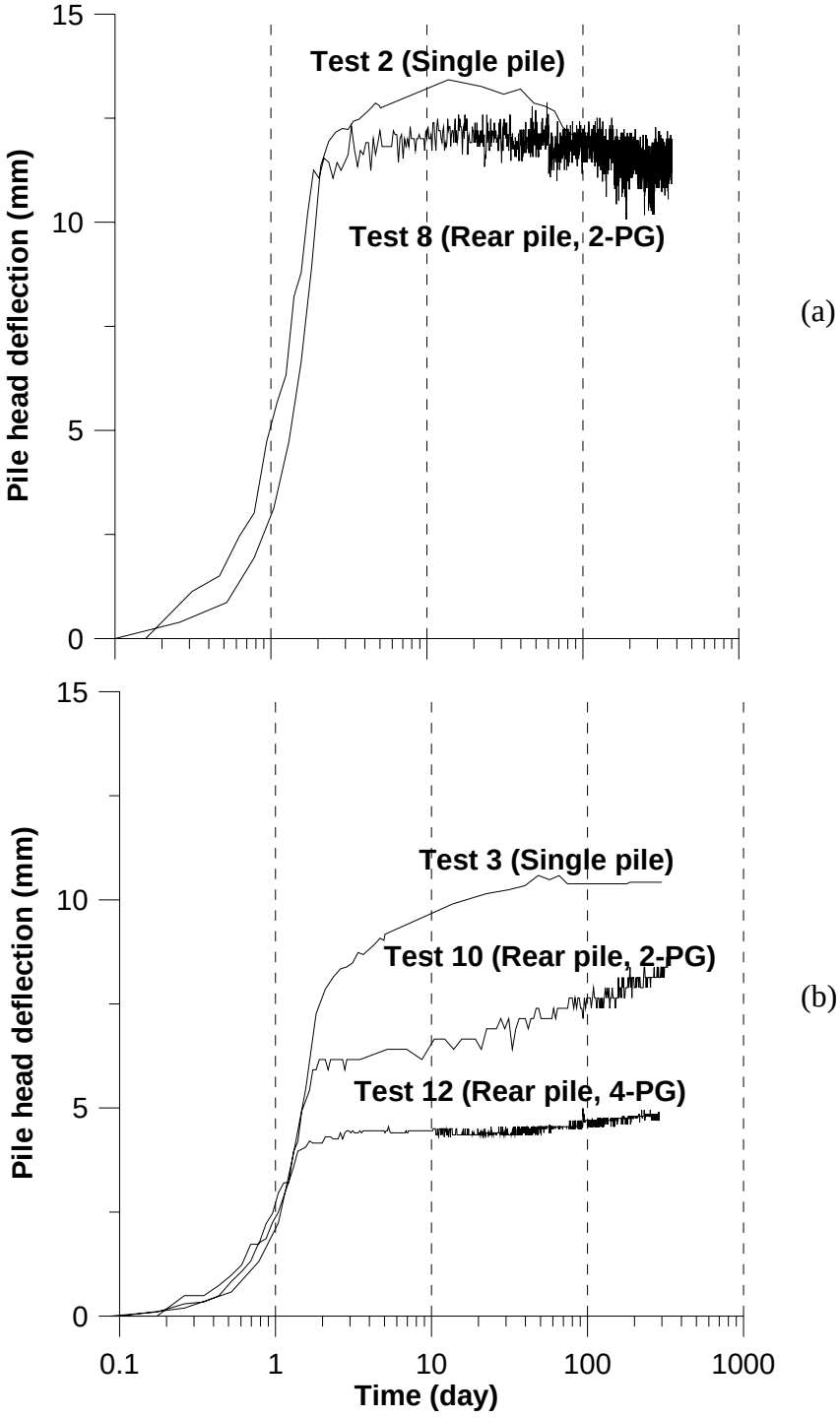

Figure 5.2 Variations of pile head deflection for free-head piles located at (a) 3 m and (b) 5 m behind a stable wall

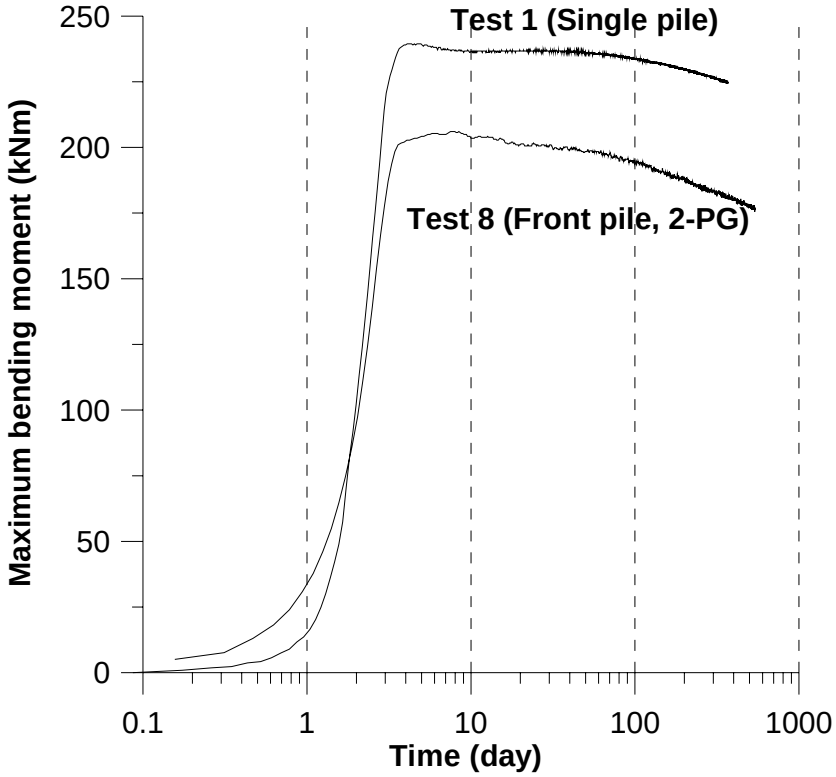

Figure 5.3 Variations of pile bending moment for free-head piles at 1 m behind a stable wall

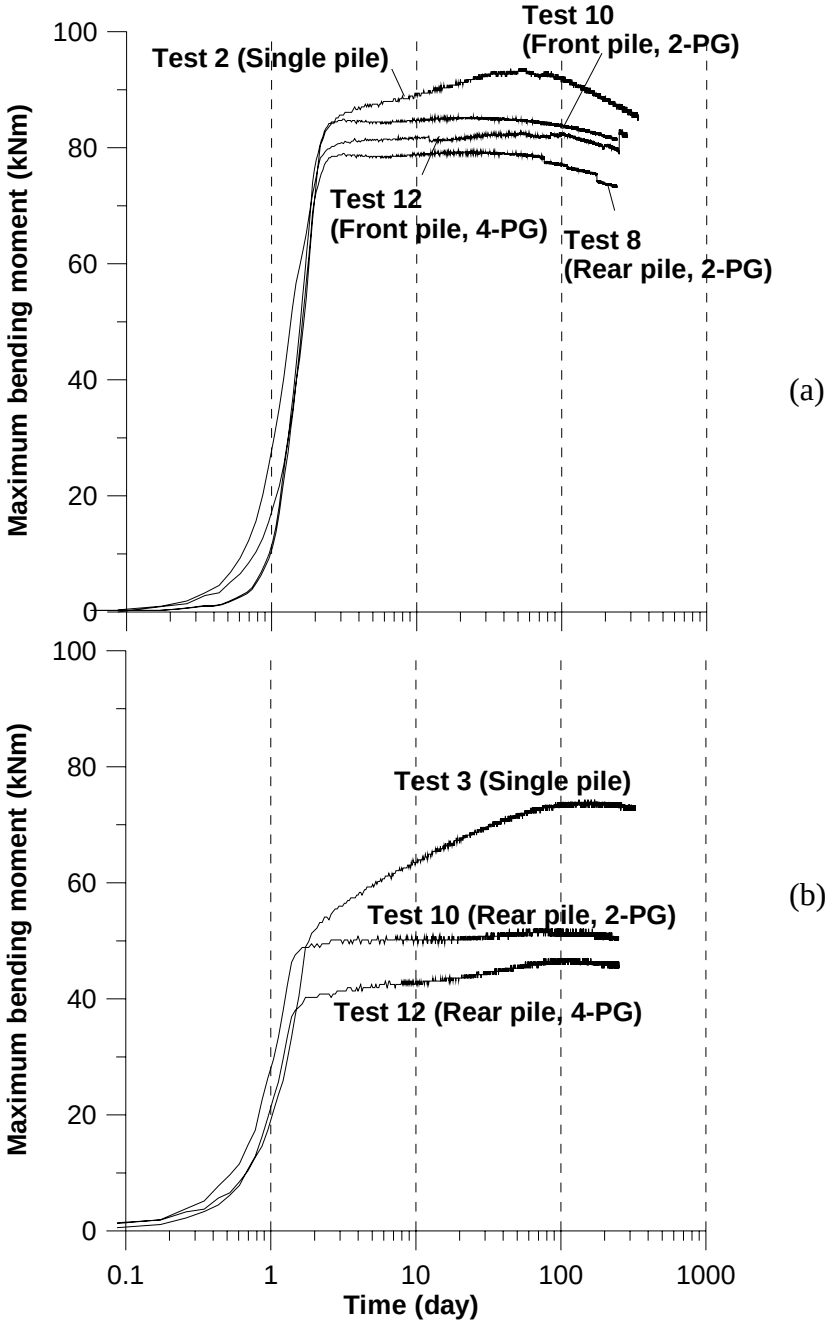

Figure 5.4 Variations of pile bending moment for free-head piles at (a) 3 m and (b) 5 m behind a stable wall

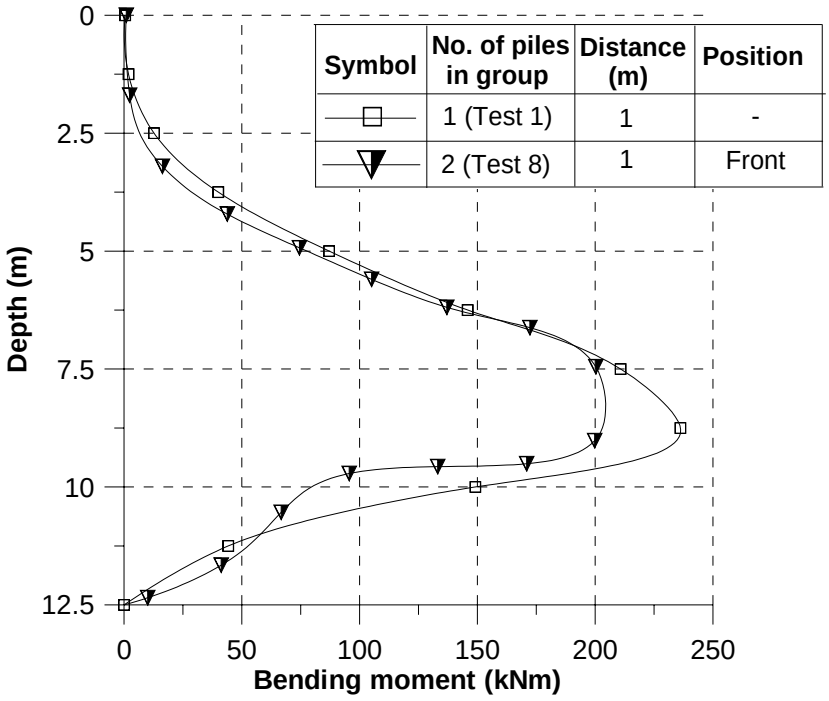

Figure 5.5 Measured maximum induced bending moment profiles for free-head piles at 1 m behind a stable wall

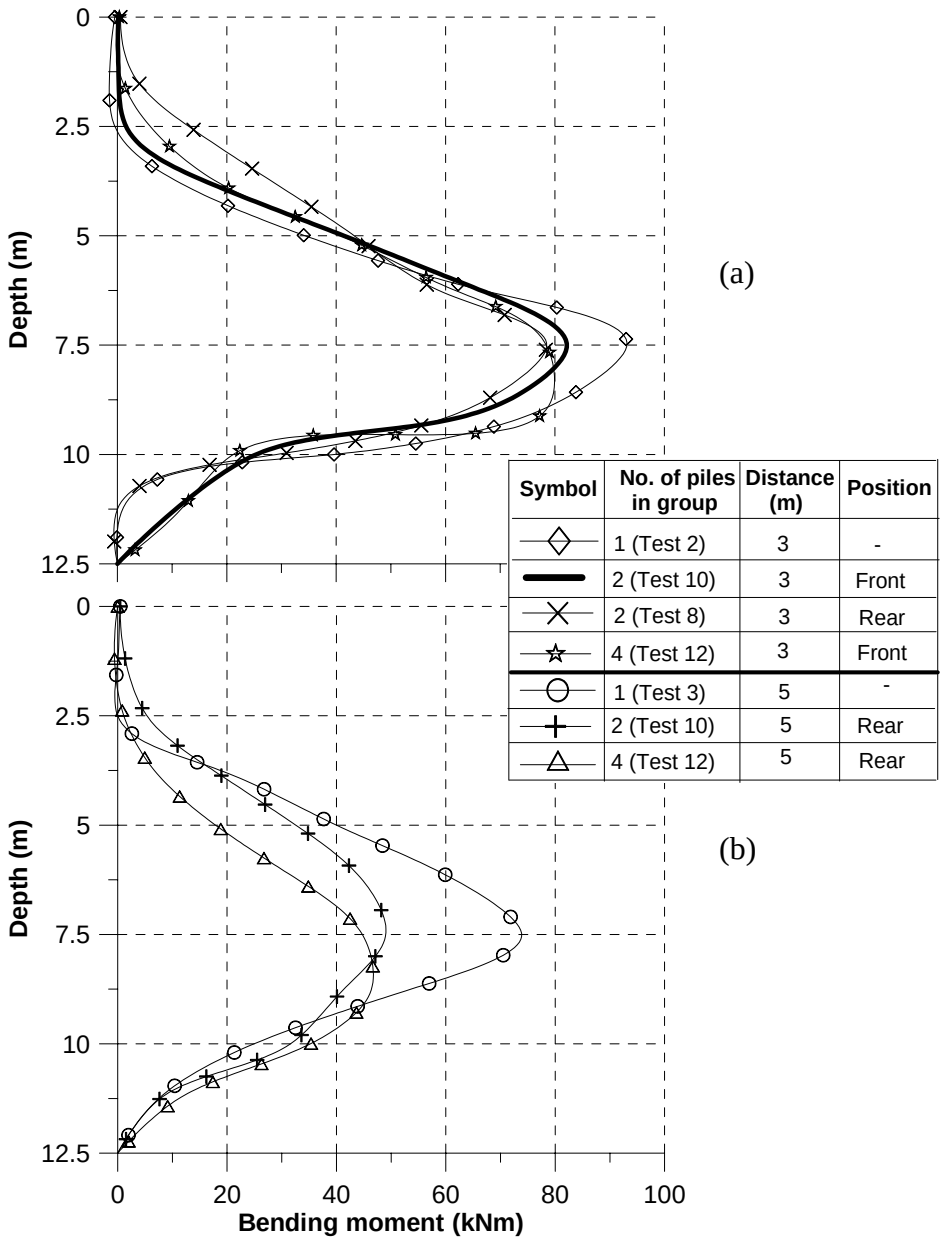

Figure 5.6 Measured maximum induced bending moment profiles for free-head piles at (a) 3 m and (b) 5 m behind a stable wall

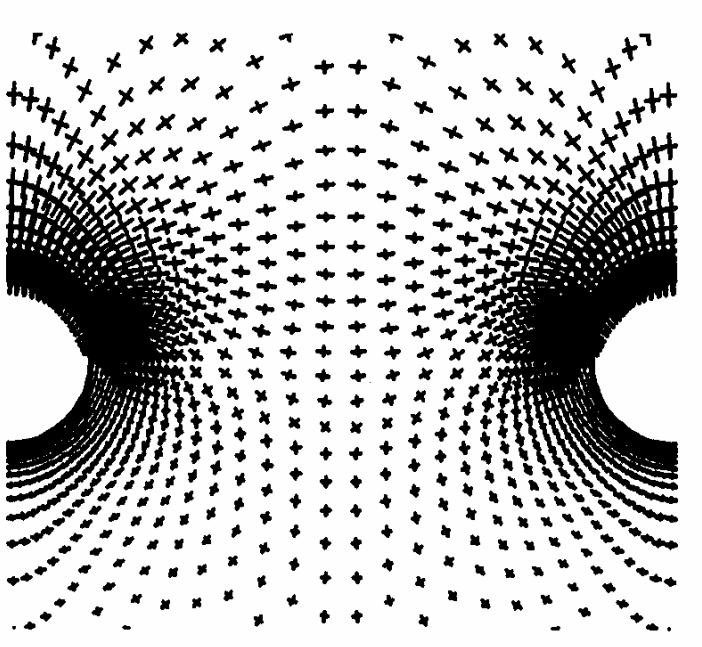

Figure 5.7 Arching effect is depicted by the rotation of the principal stresses directions under undrained condition (after Chen and Martin, 2002)

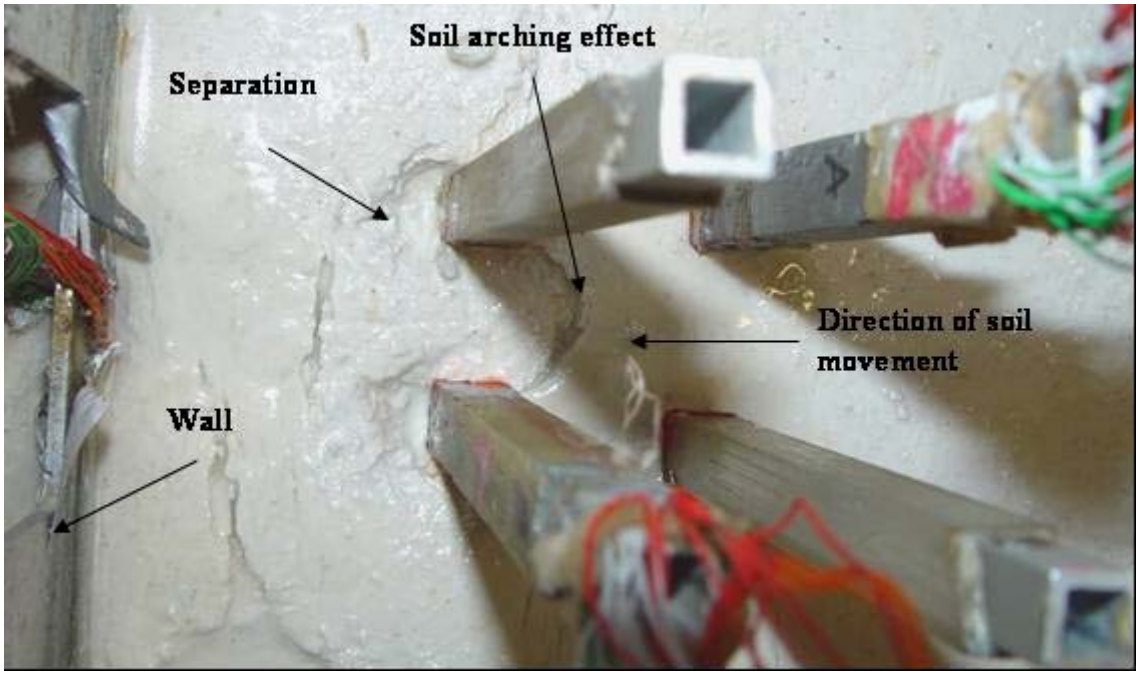

Figure 5.8 Soil arching and separation noted in Test 12

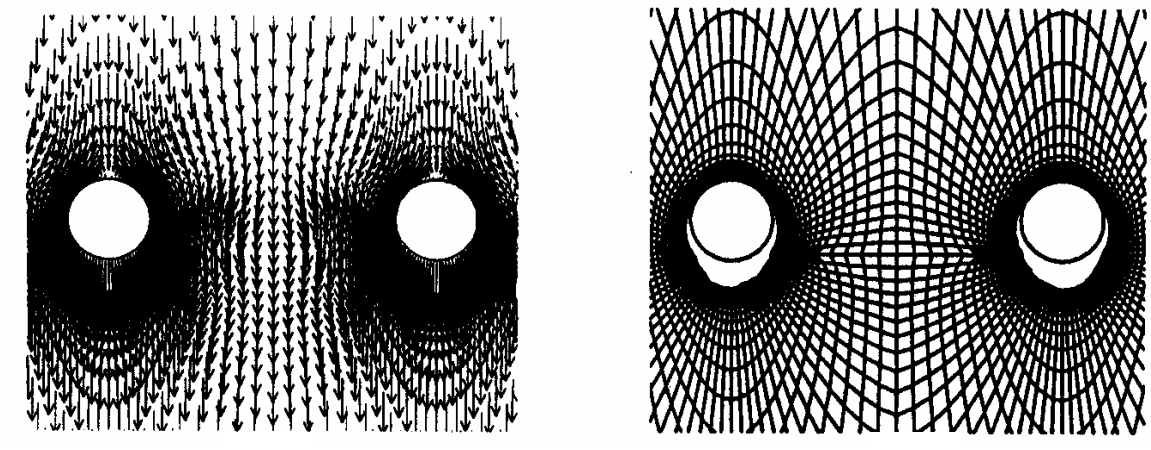

(a) (b)

Figure 5.9 Deformation of pile/soil interface with separation under undrained condition as depicted by (a) displacement vectors and (b) exaggerated grid distortion (after Chen and Martin, 2002)

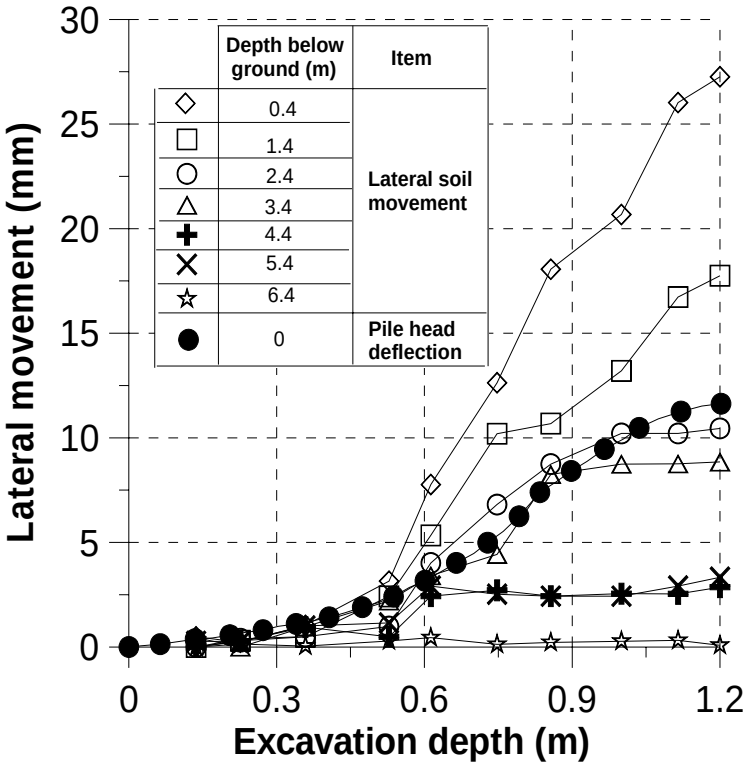

Figure 5.10 Measured free-field soil movements at different depths and pile head deflection at 3 m behind the wall for Test 12

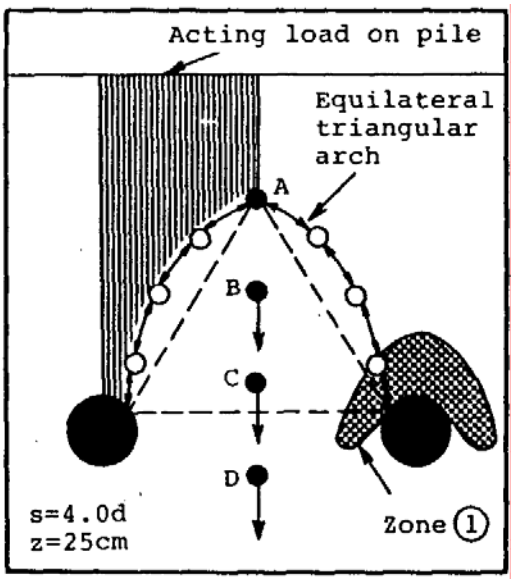

Figure 5.11 Measured free-field soil moving ahead of pile (after Adachi et al., 1989)

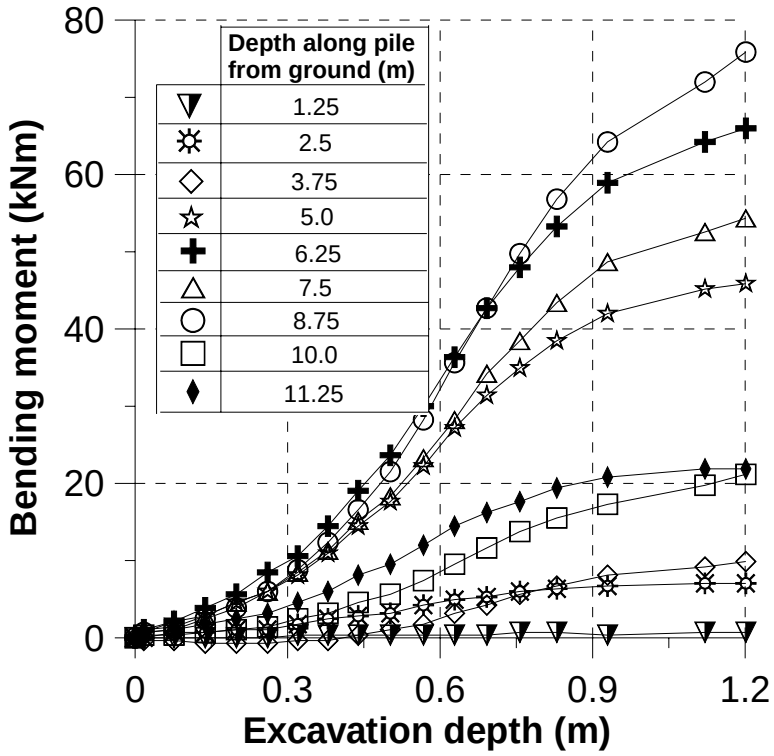

Figure 5.12 Development of pile bending moment for front pile of Test 12

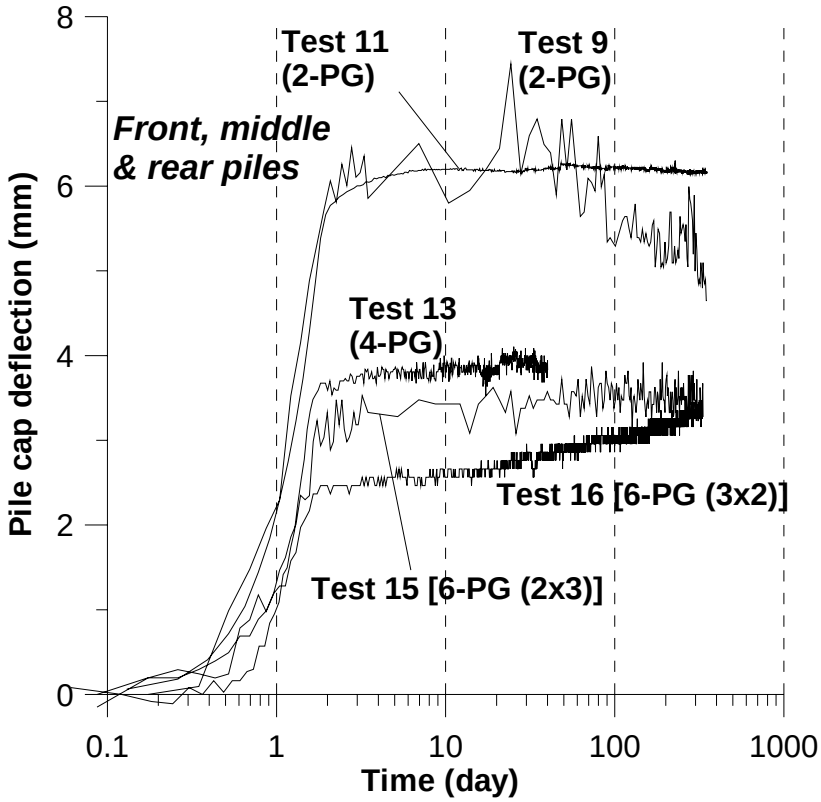

Figure 5.13 Variations of pile cap deflection during and after excavation for front, middle and rear piles of various capped-head pile groups

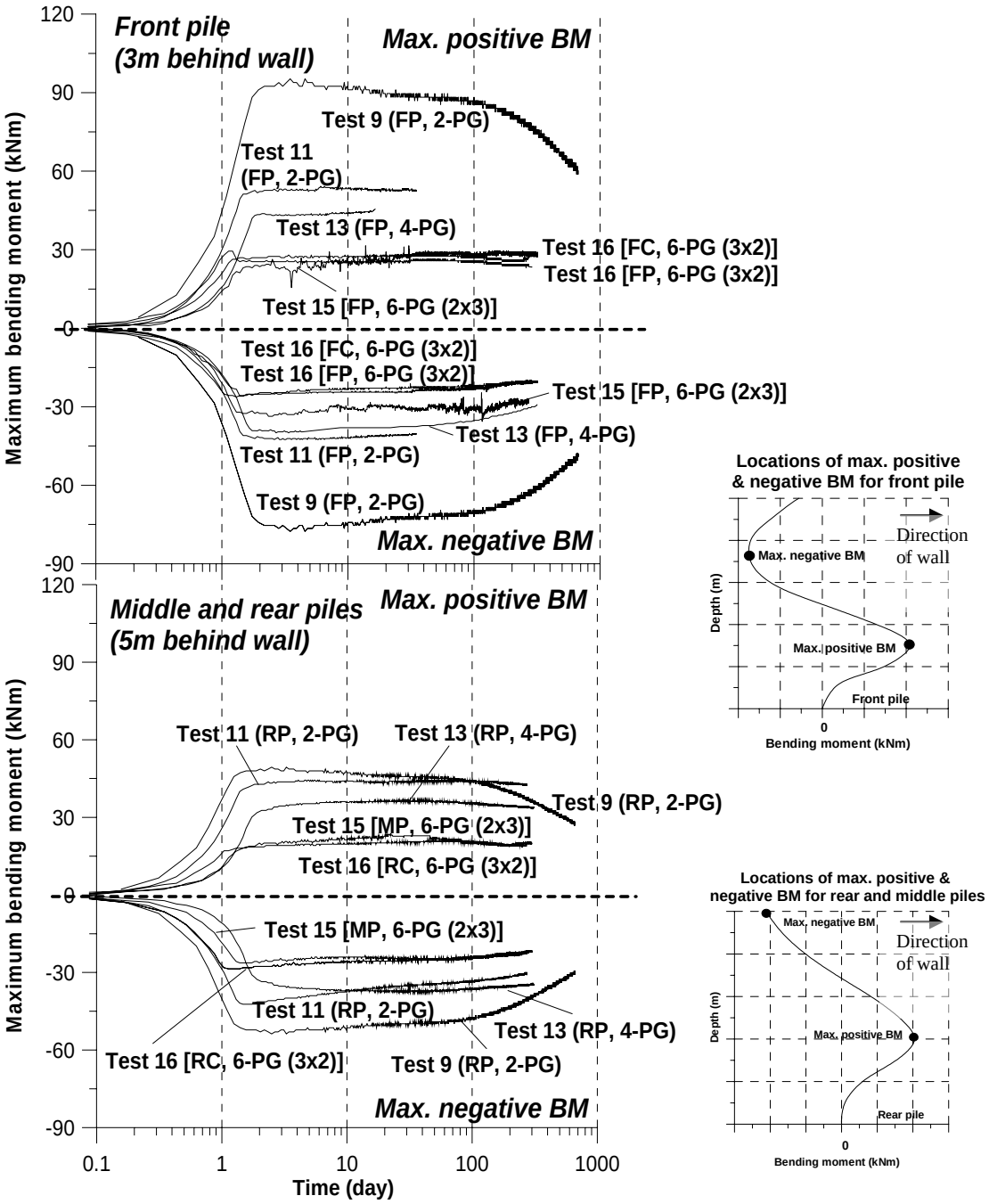

Legend:
FP: Front peripheral
FC: Front centre
RP: Rear peripheral
RC: Rear centre
MP: Middle peripheral

Figure 5.14 Variations of maximum pile bending moment during and after excavation for (a) front and (b) middle and rear piles of various capped-head pile groups

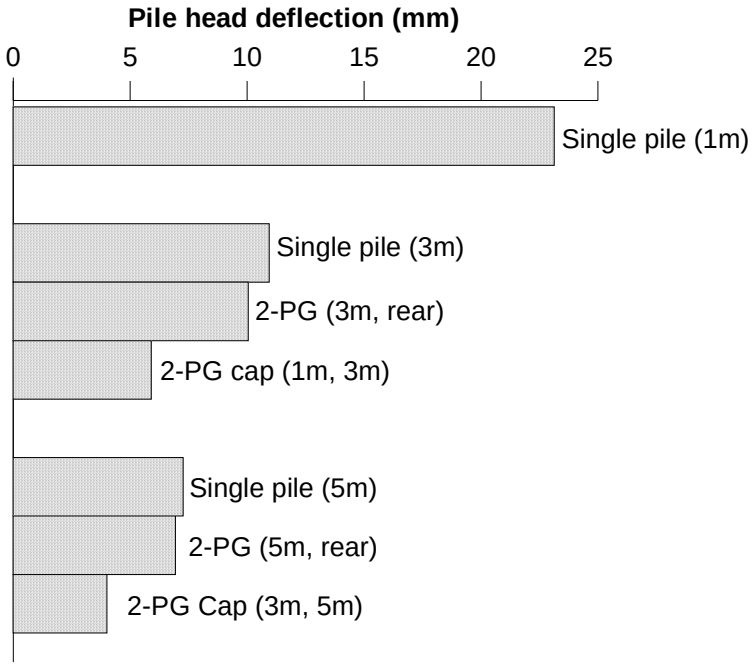

Figure 5.15 Measured pile head deflection for single piles and 2-pile groups

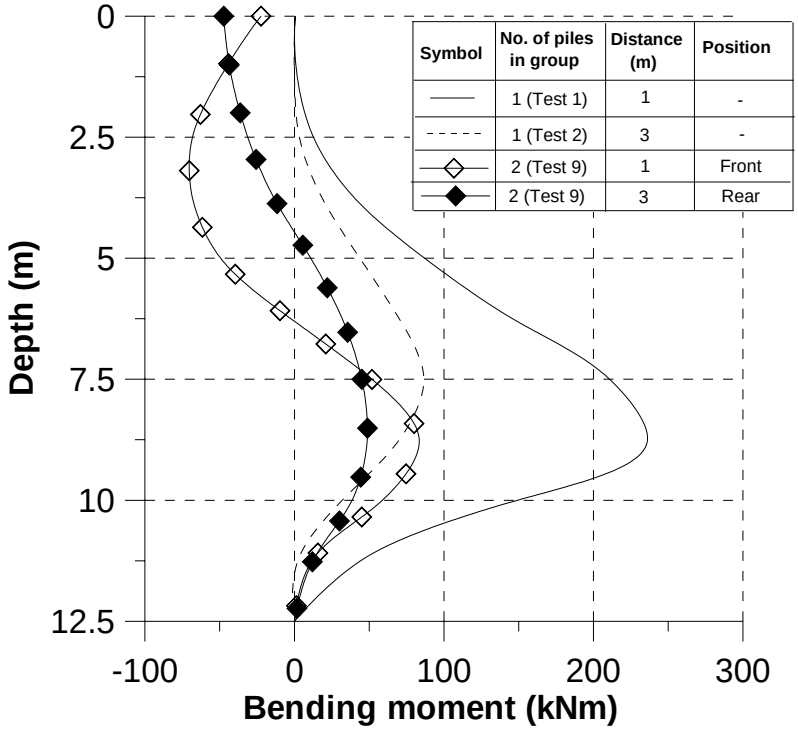

Figure 5.16 Measured maximum induced bending moment profiles for free-head single piles and capped-head 2-pile group at similar locations

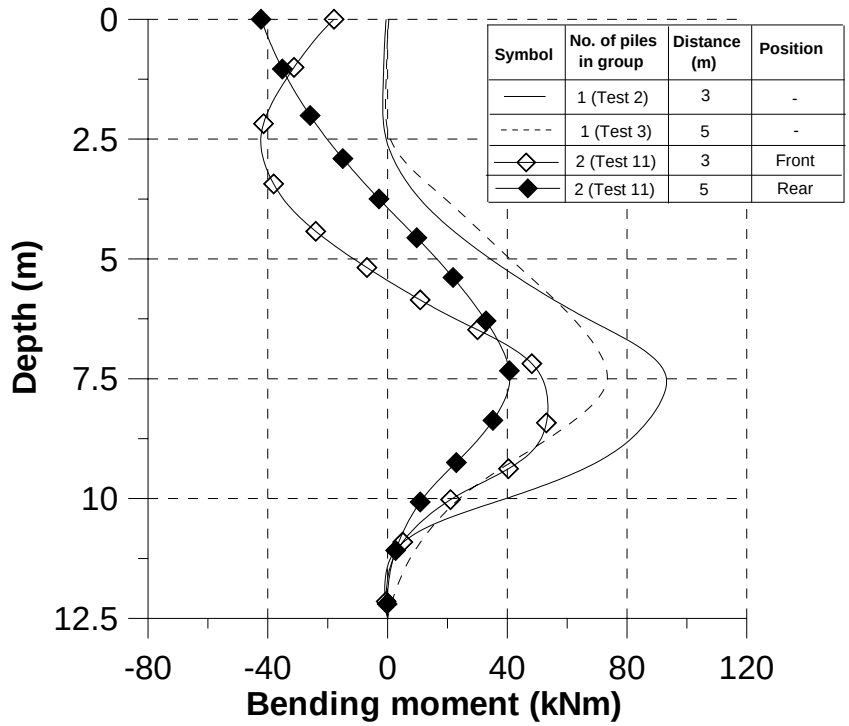

Figure 5.17 Measured maximum induced bending moment profiles for free-head single piles and capped-head 2-pile group at similar locations

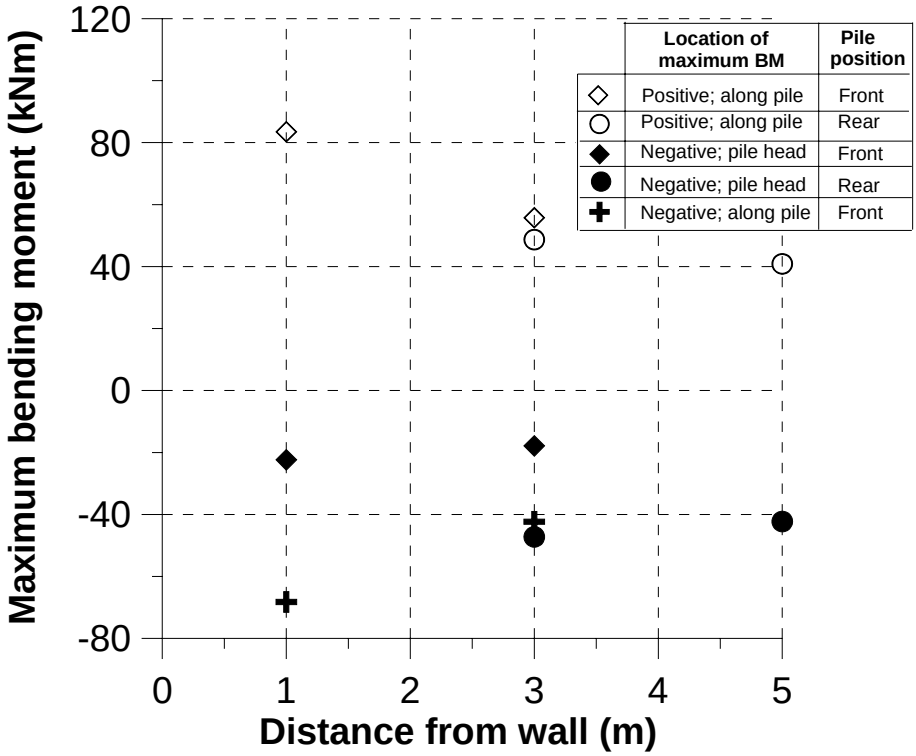

Figure 5.18 Variation in maximum induced pile bending moment with distances from wall for Tests 9 and 11

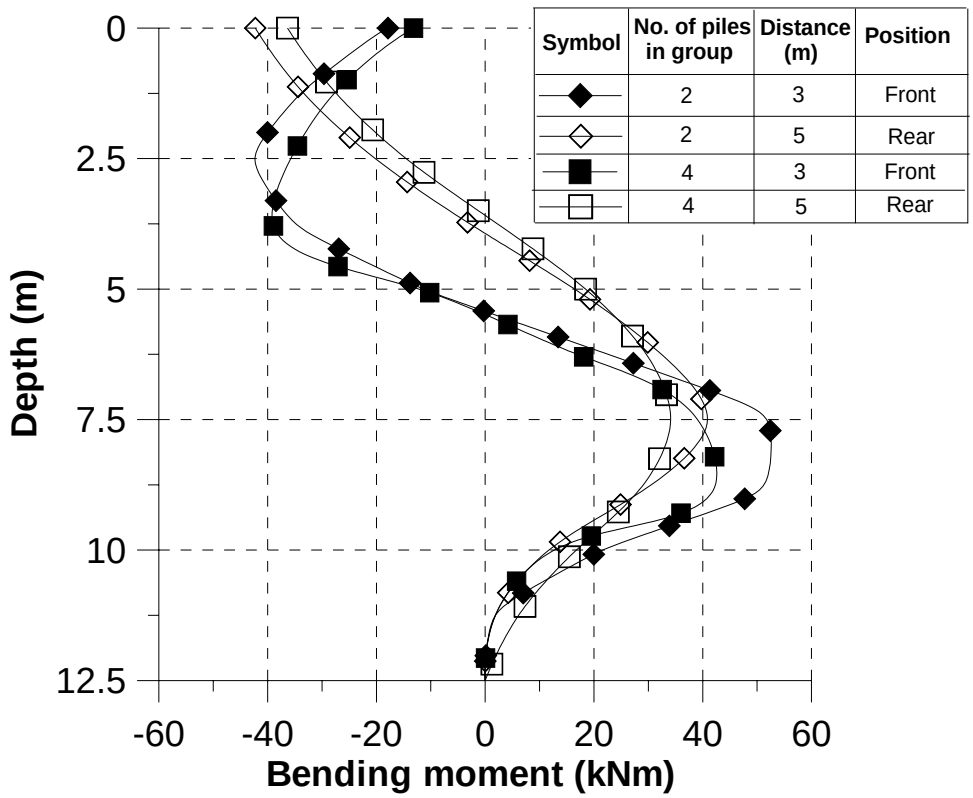

Figure 5.19 Measured pile bending moment profiles for capped-head 2- and 4-pile groups at similar locations (Tests 11 and 13)

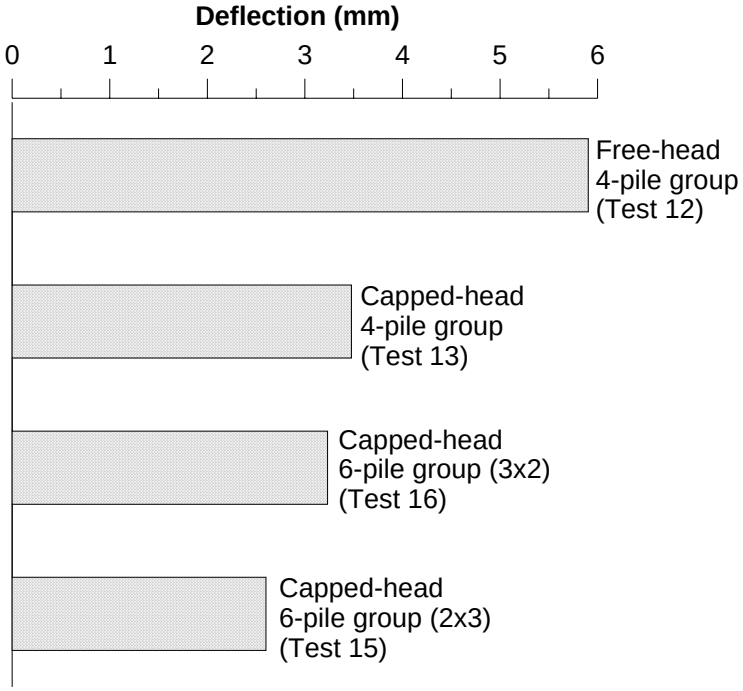

Figure 5.20 Measured pile head deflection for free- and capped-head 4- and 6-pile groups

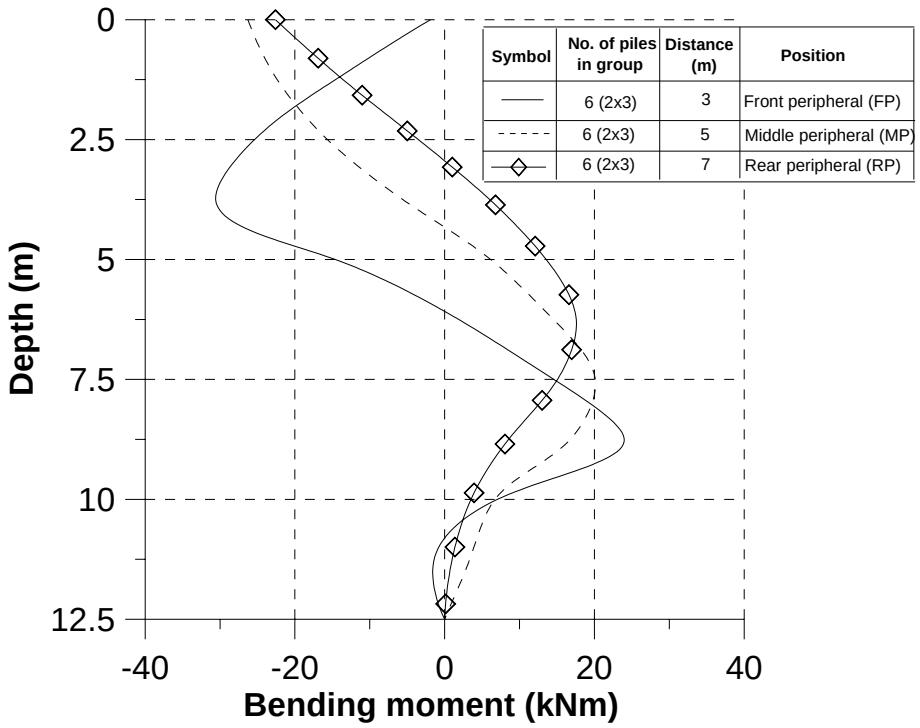

Figure 5.21 Measured pile deflection profiles for a 2x3 capped-head 6-pile group (Test 15)

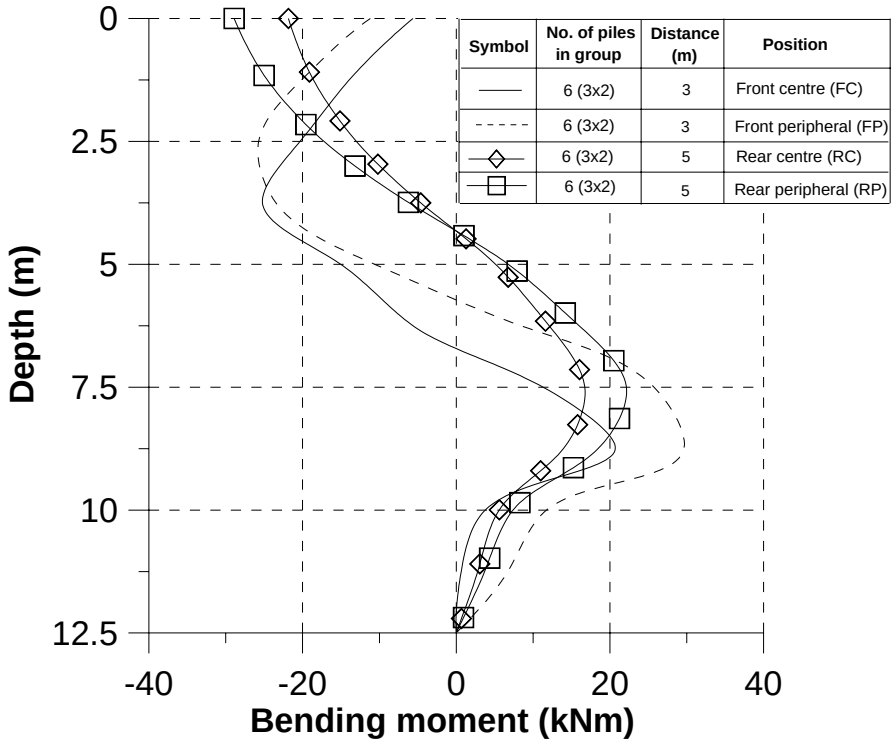

Figure 5.22 Measured pile bending moment profiles for a 3x2 capped-head 6-pile group (Test 16)

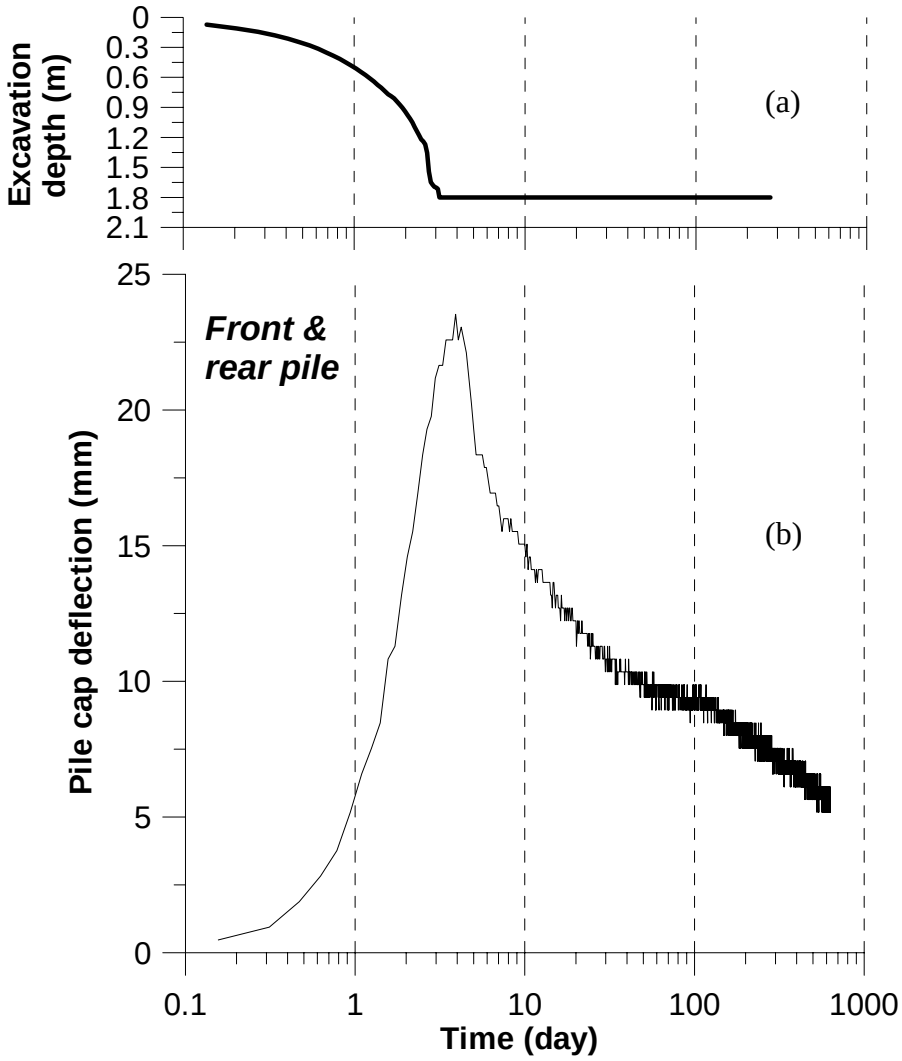

Figure 5.23 Variations of (a) excavation depth and (b) pile cap deflection for a 4-pile group behind a collapsed wall (Test 14)

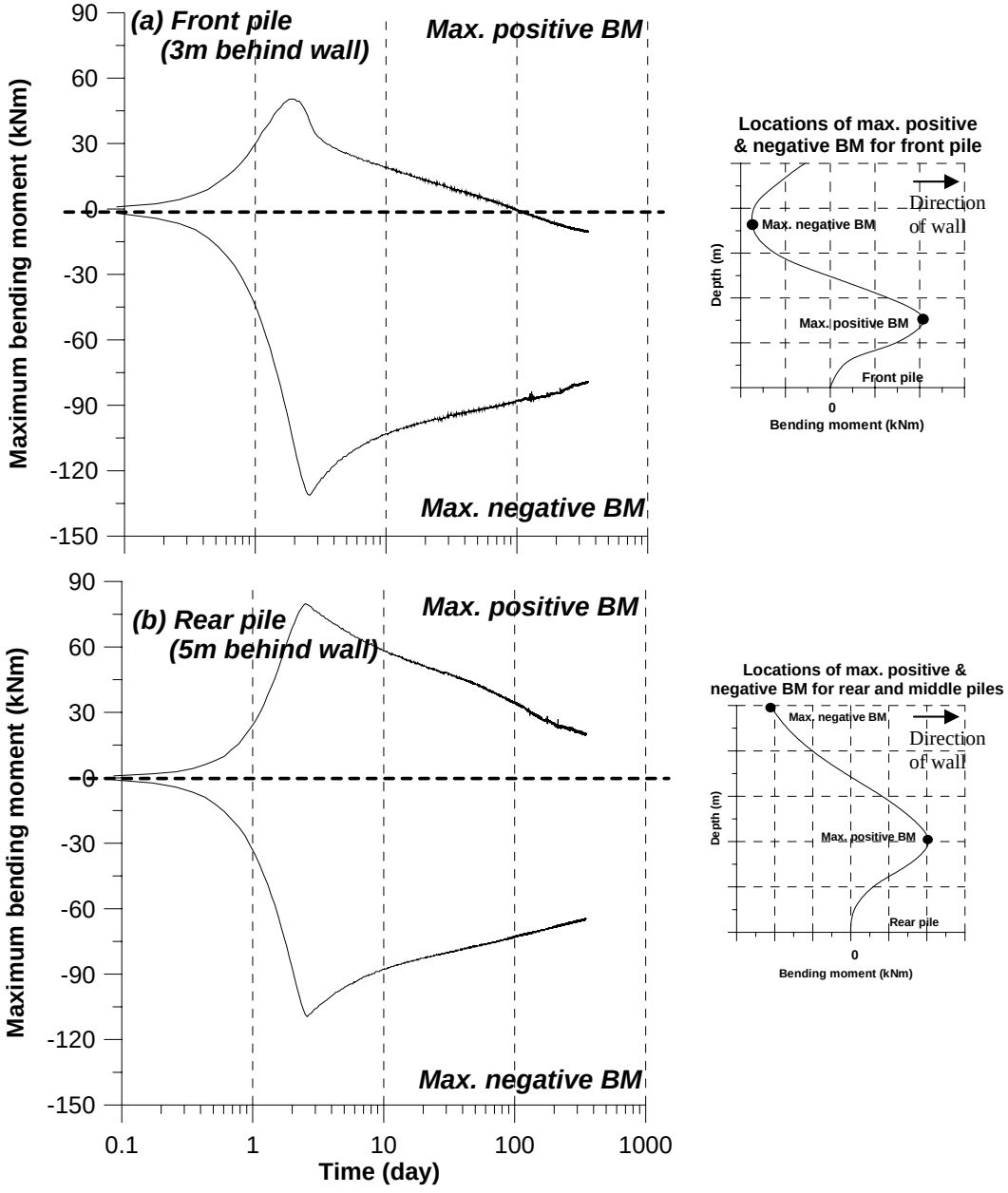

Figure 5.24 Variations of maximum positive and negative bending moment for (a) front and (b) rear pile of a capped-head 4-pile group behind a collapsed wall (Test 14)

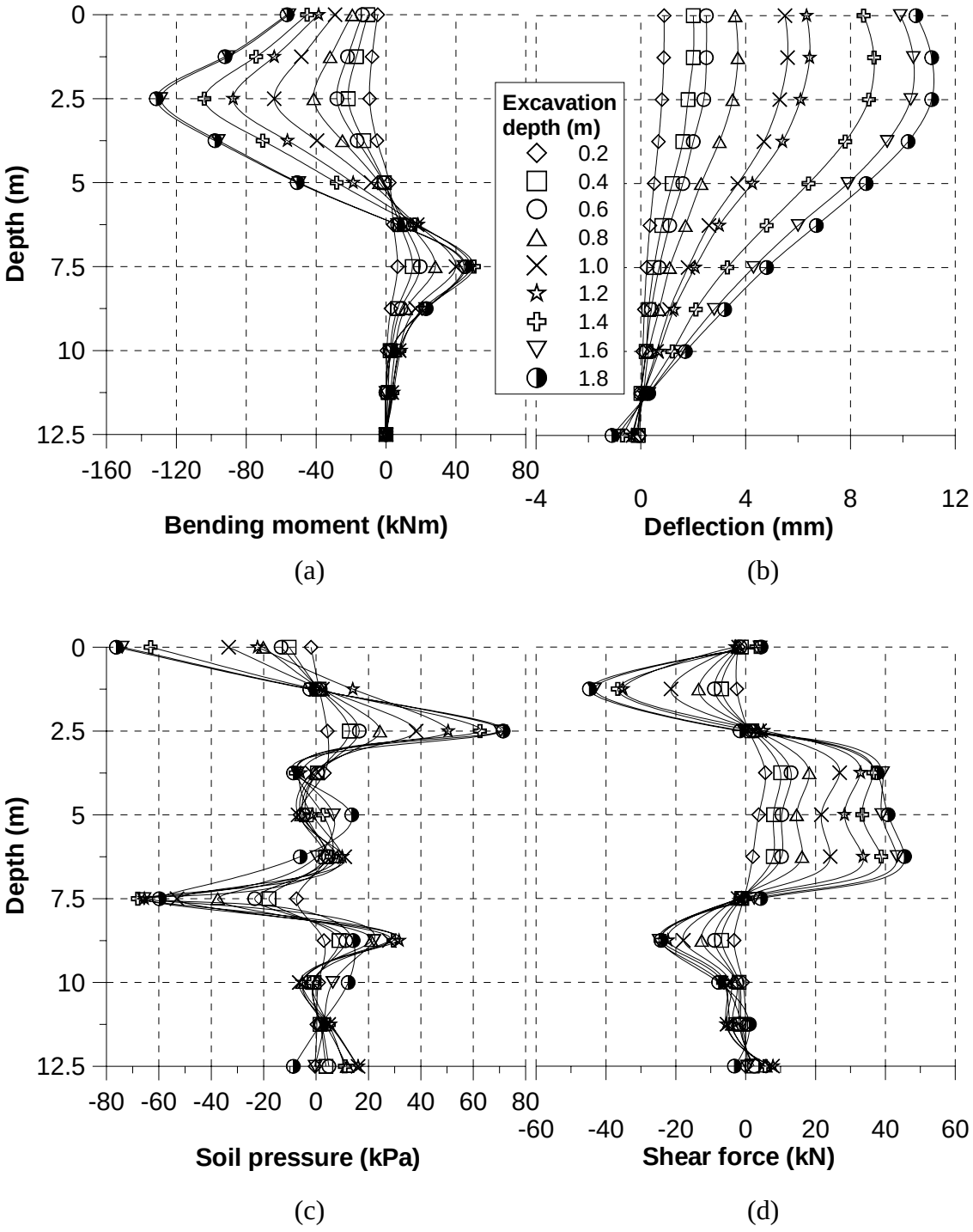

Figure 5.25 Measured front pile (a) bending moment, (b) deflection, (c) soil pressure and (d) shear force for Test 14

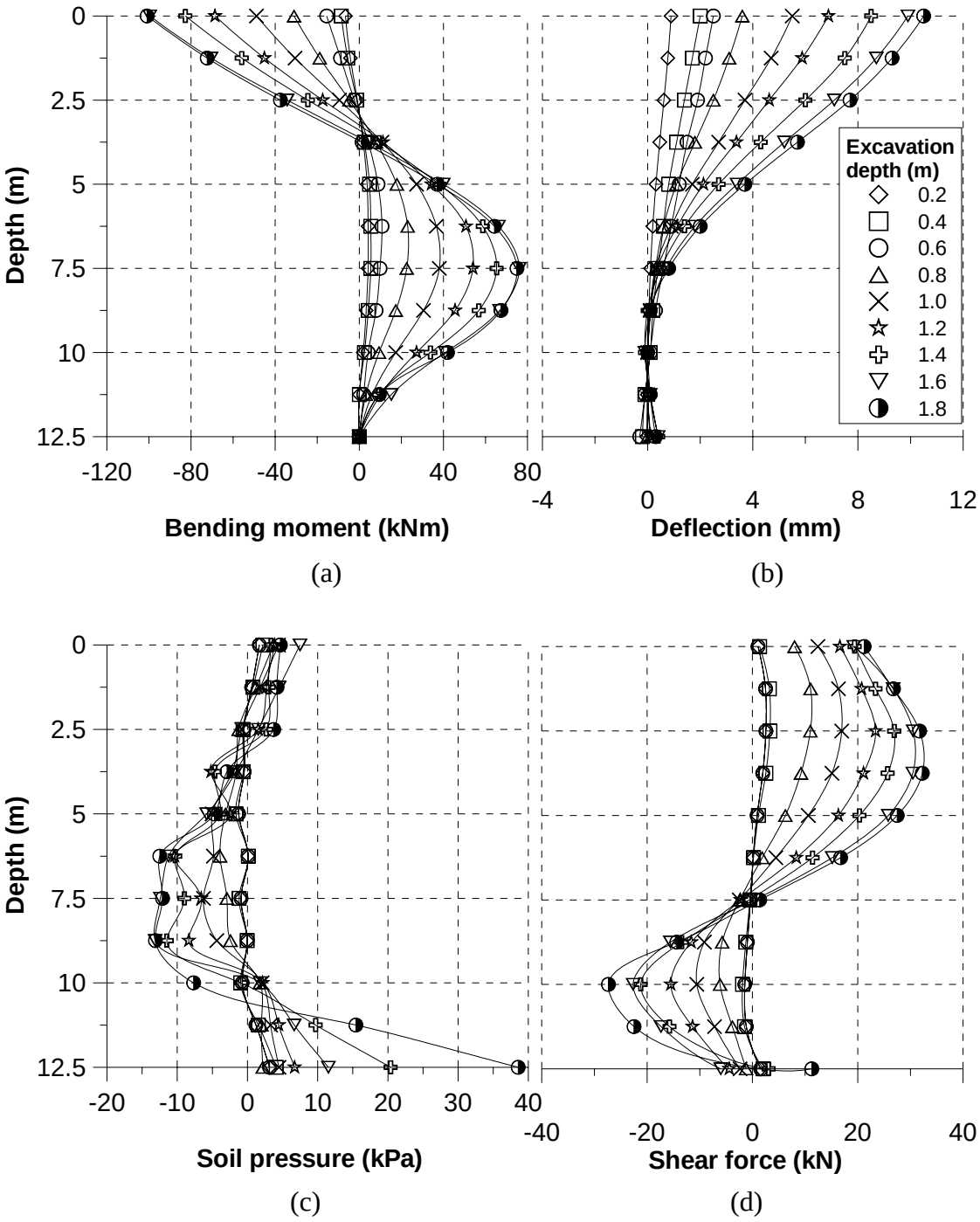

Figure 5.26 Measured rear pile (a) bending moment, (b) deflection, (c) soil pressure and (d) shear force for Test 14

CHAPTER SIX

NUMERICAL ANALYSIS OF CENTRIFUGE TEST RESULTS

6.1 INTRODUCTION

A numerical method of analysis has been proposed by Chow and Yong (1996) to analyze the responses of single piles subject to lateral soil movement. The concept of the method is based on the finite element method where the pile is represented by beam elements and the soil is idealized using the modulus of subgrade reaction. The non-linearity of the soil behaviour can be incorporated by limiting the soil pressure that can act on the pile. Chow (1996) presented a numerical model using a hybrid method of analysis to analyse pile groups subject to lateral soil movement. This hybrid method is an extension of the Chow and Yong (1996) method used for the analysis of single pile subject to lateral soil movement. In this hybrid method, the pile-soil interaction forces acting on the piles and the soil are first considered separately and then combined by considering equilibrium and compatibility.

The numerical method had been used by Shen (1999), Law (2000) and Lim (2001) to analyse centrifuge test results in sand. They found that reasonably good match could be achieved, provided appropriate soil parameters were adopted. This approach is used in the present study to analyse the single pile and pile group responses in clay behind stable and collapsed retaining walls.

6.2 METHOD OF ANALYSIS

The method of analysis for a single pile and a group of piles subject to excavation-induced soil movement is presented in this section.

6.2.1 Analysis for single pile

The method of analysis for a single isolated pile subject to lateral soil movement is described by Chow and Yong (1996). In this method, the pile is modelled as a series of linear elastic beam elements. The behaviour of pile subject to lateral soil movement is analyzed using the finite element method where the soil is idealized using the modulus of subgrade reaction. The analysis requires knowledge of the flexural rigidity, E_pI_p, of the pile, the distribution of the lateral soil stiffness, K_h, with depth and the limiting soil pressure, p_y, with depth. The limiting soil pressure is necessary to allow for local failure, thus permitting non-linear soil behaviour to be incorporated. The free-field soil movement is required as input data. Detailed description of this method can be found in Chow and Yong (1996).

6.2.2 Analysis for piles in a group

Chow (1996) extended the above method to analyse pile groups subject to lateral soil movement. The method of modeling the pile and the soil response at the individual piles are similar to that described for a single pile in Section 6.2.1. The pile-soil interaction forces acting on the piles and the soil are first considered separately and then combined by considering equilibrium and compatibility.

The load-deflection relationship of the piles in a group is given by:

$$\lfloor K_p \rfloor \{y_p\} = \{P_p\} \tag{6.1}$$

where $[K_p]$ = assembled stiffness matrix of all the beam elements forming the piles, $\{y_p\}$ = vector of pile deflection and rotation of the pile nodes and $\{P_p\}$ = vector of pile-soil interaction forces acting on the pile.

The soil response at the individual piles is modelled using the modulus of subgrade reaction. The lateral soil pressure, p_s, acting on the pile is given by:

$$p_s = k_h(y_s - y_o) \tag{6.2}$$

where k_h = modulus of subgrade reaction of the soil, y_s = soil deformation at the pile-soil interface and y_o = lateral soil movement. The lateral force of the soil, P_s, acting on the pile at a particular node is given as:

$$P_s = K_h l(y_s - y_o) \tag{6.3}$$

where $K_h = k_h d$ is the lateral soil stiffness per unit length of the pile and l is the pile element length associated with that node.

The relative lateral soil movement at the pile-soil interface at a particular node i of a pile due to its own interaction forces and at other nodes in the pile group may be obtained by using the principle of superposition from:

$$y_{si} - y_{oi} = \sum_{j=1}^{j=N} f_{ij} P_{sj} \tag{6.4}$$

where y_{si} = lateral soil deformation at the pile-soil interface at node i, y_{oi} = lateral soil movement at node i in the absence of the piles, f_{ij} = flexibility coefficient denoting lateral deformation of the soil at node i due to a unit pile-soil interaction lateral force acting at node j, P_{sj} = pile-soil interaction lateral force acting at node j and N = total number of nodes.

Eq. (6.4) is written for each of the nodes leading to the following flexibility relationship of the soil:

$$\{y_s\} - \{y_o\} = [F_s]\{P_s\} \tag{6.5}$$

where $\{y_s\}$ = vector of soil deformation at the pile nodes, $\{y_o\}$ = vector of lateral soil movement at the pile nodes in the absence of the piles, $[F_s]$ = soil flexibility matrix and $\{P_s\}$ = vector of pile-soil interaction forces acting on the soil.

The following stiffness relationship of the soil is obtained when the flexibility equation in Eq. (6.5) is inverted:

$$\{P_s\} = [F_s]^{-1}(\{y_s\} - \{y_o\}) = [K_s](\{y_s\} - \{y_o\}) \tag{6.6}$$

where $[K_s]$ is the stiffness matrix of the soil.

Equilibrium of the interaction forces acting at the pile-soil interface yields:

$$\{P_s\} = -\{P_p\} \tag{6.7}$$

and the compatibility of the deformation of the pile and the soil (assuming linearity) yields:

$$\{y_s\} = \{y_p\} \tag{6.8}$$

The following stiffness relationship of the pile group system can be obtained by using the above equilibrium and compatibility conditions together with Eqs. (6.1) and (6.6):

$$([K_p] + [K_s])\{y_p\} = [K_s]\{y_o\} \tag{6.9}$$

The vector $[K_s]\{y_o\}$ represents the induced lateral forces acting on the piles resulting from the lateral soil movement. The pile deformation, $\{y_p\}$, is obtained by solving Eq. (6.9). Subsequently, by differentiating the pile deformation profile, $\{y_p\}$, the shear force and bending moment profiles can be obtained. Similar to the case for the method of analysis for single pile, the non-linear behaviour of soil can be incorporated by limiting the soil pressure that can act on the pile.

Law (2000) modified the computer program to handle different magnitudes of soil movement according to the pile location. This enables the program to be more flexible and versatile in solving problems involving a group of piles at various positions when subject to lateral soil movements. Law (2000) also modified the

program so that a capped-head pile group can be modelled. The pile cap is simulated by introducing beam elements into the method of analysis to "tie" the pile heads in a group together. Therefore, the bending rigidity of the pile cap, $(EI)_{cap}$, has to be included as part of the input data.

6.3 SOIL PARAMETERS

6.3.1 Lateral soil stiffness

The modulus of subgrade reaction, k_h, for horizontal loading, is a conceptual relationship between the soil pressure, p, and the deflection, ρ, which is widely used in the analysis of laterally loaded piles. In more general terms, the modulus of subgrade reaction is the slope (tangent or secant line) or ratio of the applied pressure, p, to the corresponding soil deformation, ρ. Hence, the modulus of subgrade reaction, k_h, can be written as:

$$p = k_h \rho \tag{6.10}$$

where k_h has a unit of kN/m^3.

The lateral soil stiffness per unit length of the pile is given as:

$$K_h = k_h d \tag{6.11}$$

where k_h is the modulus of subgrade reaction. The K_h parameter can be approximately related to the Young's modulus of the soil, E_s as follows (Poulos & Davis, 1980 and Chow & Yong, 1996):

$$K_h \approx E_s \tag{6.12}$$

For clay, it is assumed that the E_s is related to the undrained shear strength, c_u, as follows (Poulos and Davis, 1980):

$$E_s = (150 - 400)c_u \tag{6.13}$$

Hence,

$$K_h = (150 - 400)c_u \tag{6.14}$$

Since this study involves a layer of sand underlying the clay, the relevant input involving sand is also presented. Shen (1999) reported that for Toyoura sand, the Young's modulus is normally assumed to be proportional to depth, z:

$$E_s = mz \tag{6.15}$$

where m is the proportional factor in MN/m^3.

Shen (1999) used the relationship from Adachi et al. (1994) to describe the correlation between cone resistance, q_c, and depth, z, for the sand. It was established that:

$$q_c = 2.8z \tag{6.16}$$

where q_c is in MPa and z in m, fits his data well. Webb et al. (1990) showed that the E_s can be related to q_c by the relation:

$$E_s = (1.5 - 2.5)q_c \tag{6.17}$$

Substituting Eq. (6.16) into Eq. (6.17) yields:

$$E_s = (4.2 - 7)z \tag{6.18}$$

Substitution of Eq. (6.18) into Eq. (6.12) leads to:

$$K_h = (4.2 - 7)z \tag{6.19}$$

In this study, the K_h was chosen so that when used in conjunction with the properties derived for clay, the calculated bending moment matches the measured bending moment, which led to:

$$K_h = 5.6z \qquad (in\ MPa) \tag{6.20}$$

where z is the depth in m. Eq. (6.20) is then used in all the subsequent back-analyses.

6.3.2 Undrained shear strength

As described in Section 4.5, a bar penetrometer or T-bar was used to determine the continuous undrained shear strength profile of the clay before and after excavation in separate tests. The measured undrained shear strength will be used as input for all subsequent back-analyses performed hereinafter.

6.3.3 Limiting soil pressure

Poulos (1994) stated that limiting soil pressure can be employed to account for the non-linear pile-soil response. Thus accurate limiting soil pressure can result in a good theoretical prediction of the response of a pile subject to lateral soil movement. This is especially true for the case where lateral soil movement is sufficiently large to cause the soil to flow past the pile without exerting any additional pressure on it.

In general, for piles embedded in cohesive soils, the limit yield pressure due to relative pile-soil displacement can be written as:

$$p_y = Kc_u \tag{6.21}$$

where K is a limit yield pressure coefficient. For a laterally loaded single pile in cohesive soils, Broms (1964a) suggested a simplified and conservative distribution of soil resistance, p_y, as:

$$p_y = 2\left(1+\frac{z}{d}\right)c_u \le 9c_u \tag{6.22}$$

However, in the present study, the limiting soil pressure for a pile embedded in moving soil is not available and needs to be evaluated.

De Beer (1977) described active piles as piles that are being loaded laterally at the pile head that results in surrounding lateral soil movement. On the contrary, passive piles are piles subject to externally imposed lateral soil movements that result in induced forces on the piles. Researchers including Viggiani (1981) and Maugeri

(1994) (see Table 2.2) established that the magnitude of K on a passive pile subject to lateral soil movement should be lesser than that of a laterally loaded pile (K = 9 as described by Broms (1964a)). However, Poulos and Chen (1997) proposed a K value of 9 for piles subject to excavation-induced soil movement (see Table 2.2), which is similar to that for a laterally loaded pile. Goh et al. (1997) (see Table 2.2) also proposed the same K value for piles supporting an embankment, which has contrasting loading condition as the former involves stress relief while the latter involves increasing loading condition. However, for the analysis of piles used for landslide stabilization, Chow (1996) suggested that for sliding soil above the slip surface, K=3 – 4 and for the stable soil below the slip surface, K= 8 – 12. The lower value of K in the sliding zone is thought to be due to its proximity to the ground surface and the weakening of soil due to sliding movements. Since the findings on the K values remain inconsistent, it is hoped that the back-analysis would provide further understanding on the K values of a passive pile.

As mentioned earlier, since this study involves an underlying sand layer where the pile is embedded in, the limiting soil pressure for sand is presented here for completeness. Broms (1964b) proposed that the ultimate soil pressure for cohesionless soils as:

$$p_y = 3\sigma_v' K_p \tag{6.23}$$

where σ_v' = effective vertical overburden pressure

$K_p = (1 + \sin\phi') / (1 - \sin\phi')$

ϕ' = angle of internal friction

6.3.4 Free-field lateral soil movement

Free-field soil movement refers to the soil movement that occurs solely due to excavation without the presence of piles. The free-field soil movement in the present study is obtained by monitoring the movement of soil markers placed behind the perspex side face of the container using the image processing technique described in Chapter 3. Such technique has also been used by Almeida et al. (1985), Bolton & Powrie (1987, 1988), Bransby & Springman (1997) and Kongsomboon (2002). The measured average free-field lateral soil movement profiles used for the analyses of pile behaviour behind a stable and a collapsed retaining wall are shown in Figures 4.26(a) and (b), respectively.

6.4 PREDICTION OF PILE RESPONSES IN THE CASE OF A STABLE RETAINING WALL

Both free and capped pile groups have been analysed. Individual free-head piles are free to deflect and rotate when subject to excavation-induced soil movement. In contrast, capped pile groups would deflect in unison and ideally, the rotation of each individual pile head should be zero if a fully-fixed pile cap that prevents rotation can be successfully achieved. For the case of a pile group, the individual piles are located at pile spacing to pile width ratio of 3.2 from one another. Comparisons will then be made with the measured centrifuge experiment data.

6.4.1 Single pile

Centrifuge tests have been carried out on single piles with free-head condition only. The centrifuge test results are back-analyzed using the numerical method described in Section 6.2. The corresponding lateral soil movement profiles at the pile

locations (Figures 4.26(a) and (b)) are used as input in the analysis. The lateral soil stiffness, K_h of the clay is evaluated using Eq. (6.14). Since the normally consolidated clay in the present study is relatively soft as measured by the T-bar tests, $K_h = 150\ c_u$ is used. Eq. (6.22) is used to calculate the limiting soil pressure, p_y, for the clay. For the underlying sand layer, Eqs. (6.20) and (6.23) are used to calculate the lateral soil stiffness, K_h, and limiting soil pressure, p_y, respectively.

In practice, the maximum pile bending moment and deflection profiles are the most important results as excessive induced bending moment can fail a pile structurally while a large pile deflection can threaten its serviceability. It has been established from earlier chapters that the pile response is time dependent. In the numerical back-analysis, the measured lateral soil movement profile corresponding to the measured peak pile bending moment profile at the pile location is used as the input. The input soil strength values are based on the measured soil strength profile prior to excavation. A comparison of the predicted and measured maximum induced pile bending moment profiles and the corresponding pile deflection, shear force and soil pressure profiles are shown in Figure 6.1 for Tests 1, 2, 3 and 4, where the single pile is located 1 m, 3 m, 5 m and 7 m behind the wall respectively. In general, there is reasonably good agreement between the predicted and measured pile bending moment, deflection, shear force and soil pressure profiles. However, for Test 1 with the pile located 1 m behind the wall, the predicted pile responses are about 25 % higher than the measured values using the pre-excavation soil strength profile.

The T-bar penetrometer test was carried out to determine the undrained shear strength profiles of the clay at various distances behind the wall. The in-flight T-bar tests were conducted before and after the excavation. Figure 4.4 reveals that after excavation, the soil at 1.5 m behind the wall has experienced a substantial reduction in

the undrained shear strength for the top 1.2 m depth. This reduction could be attributed to the large stress relief in the soil caused by excavation due to significant soil movement at the pile location, as shown in Figure 4.16. Figure 4.4 also shows that the soil at 3 m or beyond behind the wall has not weakened upon excavation. It is hence proposed that the post-excavation soil strength profile should be employed in the back-analysis if the pile is located within 2 m of the wall.

For further analysis of Test 1 results, the reduced soil strength profile obtained after excavation is used in Eq. (6.22) and this yields a smaller limiting soil pressure profile to better reflect the situation of large strain soil deformation. The revised predicted pile responses for Test 1 (denoted by a dashed line marked with crosses) are also given in Figure 6.1. It is evident that the revised predicted pile responses give a substantially better agreement with the measured pile responses.

It should be noted that Eq. (6.22) is primarily used to estimate the limiting soil pressure for a conventional laterally loaded pile and hence may not be appropriate for the present case involving large soil deformation for the case of an excavation. The results of the above re-analysis using the post-excavation soil strength profile for Test 1 is consistent with the findings of Viggiani (1981) and Maugeri (1994) (see Table 2.2) who reported that the p_y/c_u ratio for passive piles in the case of excavation and landslide is generally much lower than that for active laterally loaded piles. The large strain soil deformation situation will be further investigated later when addressing the pile behaviour due to excavation-induced soil movement behind a collapsed wall.

6.4.2 2-pile group

Numerical back-analysis involving free- and capped-head 2-pile group tests are presented in this section.

6.4.2.1 Free-head

Tests 8 and 10 involve free-head 2-pile groups arranged in a line in the direction of the soil movement as shown in Figure 5.1. In Test 8, the piles are located 1 m (front) and 3 m (rear) behind the wall, while for Test 10, the piles are located 3 m (front) and 5 m (rear) behind the wall. The centrifuge test results reported in Section 5.4 revealed that the front pile would shield the rear pile from the excavation-induced soil movement. In addition, the reinforcing effect would increase as the number of piles in a group increases. However, the free-field soil movements measured at some distance away from the pile group are likely to neglect such pile shadowing, reinforcing and soil arching effects that have been observed to occur around the pile groups. To tackle the pile shadowing, reinforcing and soil arching effects in the back-analysis, a semi-empirical method is introduced by means of the application of a soil movement moderation factor, k_s. Lim (2001) and Maugeri et al. (1994) realised the occurrence of such phenomena and introduced their own correction factors. It is found that in the present study, a soil moderation factor of 0.8 is found to be the most appropriate for a 2-pile group in clay.

Figures 6.2(a) and (b) show the comparison between the predicted and measured bending moment and deflection profiles between the front (1 m behind wall) and rear (3 m) piles for Test 8, respectively. Similar to the single pile case at 1 m behind the wall (Test 1) reported earlier, there is an over-prediction of the front pile responses if the pre-excavation undrained shear strength of the soil is adopted in the analysis. If the

post-excavation strength is used instead, better pile bending moment and deflection profiles are obtained as shown in Figures 6.2(a) and (b).

The comparisons between the predicted and measured pile bending moment and deflection profiles for the 3 m (front) and 5 m (rear) piles for Test 10 are shown in Figures 6.3(a) and (b), respectively. For consistency, the same moderation factor of 0.8 has been used for Tests 8 and 10 and hence, the predicted pile behaviour at 3 m from the wall show identical response, regardless of the pile being a front or rear pile. The fair agreement between the predicted and measured pile responses reveals that the same moderation factor of 0.8 can be used for a 2-pile group free head group with piles having the same centre-to-centre spacing. The pre-excavation soil strength can be used provided that the piles are located at least 2 m away from the wall.

6.4.2.2 Capped-head

Tests 9 and 11 involved capped-head 2-pile groups arranged in a line in the direction of soil movement. In Test 9, the capped-head front and rear piles are located 1 m and 3 m behind the wall, respectively. In Test 11, the capped-head front and rear piles are located at 3 m and 5 m behind the wall, respectively. The bending rigidity of the pile cap, $(EI)_{cap}$, is determined to be 1.2×10^7 kNm^2. The Young's Modulus of aluminium, E, is 7.2×10^3 MPa. Being a rectangular section, the moment of inertia of the pile cap, I, equals to $bh^3/12$ where b is the breath and h is the thickness of the pile cap. The breath of the pile cap is the dimension perpendicular to the direction of the soil movement. The same soil movement moderation factor of 0.8 is also applied.

The predicted and measured pile bending moment and deflection profiles for the capped-head front (1 m behind wall) and rear (3 m) piles of Test 9 are shown in Figures 6.4(a) and (b), respectively using the pre-excavation soil undrained shear strength for the calculation of soil limiting pressure, p_y, as given in Eq. (6.22). The

overall pile group responses are over-predicted. The over-prediction of the responses of the entire pile group can be attributed to the interaction between the front and rear piles via the pile cap with the soil around the front pile (1 m behind the wall) experiencing significantly greater stress relief and reduction in soil strength upon excavation than the rear pile (3 m behind the wall).

For further analysis, the post-excavation soil strength is used in calculating the limiting soil pressure, p_y, as given in Eq. (6.22). The results show that better prediction of the pile group bending moment and deflection profiles are obtained, except for the predicted bending moment at the pile head as shown in Figures 6.5(a) and (b). For the over-prediction of the pile head bending moment and deflection, it is suspected that the pile cap could not provide full restraint to the pile heads. Such problem has also been observed by Lim (2001). In order to provide a better understanding on the effect of the rotational behaviour of the pile head, the stiffness matrix that governs the load-deformation behaviour of the pile cap in the numerical method is studied further. The pile cap and the piles can be thought of beam elements akin to a 2-D rigid-jointed structure, for example, a portal frame, where the structure lies in the vertical x-y plane and subject to loads acting in the same plane. Ideally, the connections between the pile heads and pile cap should be fixed against vertical displacement and also that rotation of the pile heads with respect to the pile cap should be perpendicular to each other but are allowed to displace in the horizontal x-direction in response to the lateral soil movement. The ability of the pile cap to achieve such criteria will be evaluated subsequently. The general force-deformation relationship for the beam elements subject to external forces and bending moments are given by:

$$\begin{matrix}\begin{bmatrix} F_{a1} \\ F_{n1} \\ M_1 \\ F_{a2} \\ F_{n2} \\ M_2 \end{bmatrix} & = & \left(\frac{EI}{L}\right) & \begin{bmatrix} \frac{A}{I} & 0 & 0 & -\frac{A}{I} & 0 & 0 \\ 0 & \frac{12}{L^2} & -\frac{6}{L} & 0 & -\frac{12}{L^2} & -\frac{6}{L} \\ 0 & -\frac{6}{L} & 4 & 0 & \frac{6}{L} & 2 \\ -\frac{A}{L} & 0 & 0 & \frac{A}{I} & 0 & 0 \\ 0 & -\frac{12}{L^2} & \frac{6}{L} & 0 & \frac{12}{L^2} & \frac{6}{L} \\ 0 & -\frac{6}{L} & 2 & 0 & \frac{6}{L} & 4 \end{bmatrix} & \times & \begin{bmatrix} \Delta_{a1} \\ \Delta_{n1} \\ \theta_1 \\ \Delta_{a2} \\ \Delta_{n2} \\ \theta_2 \end{bmatrix} & + & \begin{bmatrix} F_{fa1} \\ F_{fn1} \\ M_{f1} \\ F_{fa2} \\ F_{fn2} \\ M_{f2} \end{bmatrix} \end{matrix} \qquad (6.24)$$

(a) (b) (c) (d) (e)

Vector (a) represents the resultant forces of the beam element, vector (b) is the common stiffness constant, matrix (c) is the global stiffness matrix relating the force-deformation relationship of the beam element, vector (d) denotes the deformation of the beam element and vector (e) represents the externally applied forces acting on the beam element. The matrices in Eq. (6.24) can be further simplified since only the rotational component is of interest. Therefore, Eq. (6.24) reduces to:

$$\begin{bmatrix} M_1 \\ M_2 \end{bmatrix} = \left(\frac{EI}{L}\right) \begin{bmatrix} 4 & 2 \\ 2 & 4 \end{bmatrix} \times \begin{bmatrix} \theta_1 \\ \theta_2 \end{bmatrix} \qquad (6.25)$$

Since it is suspected that rotation occurs at the pile head as the measured bending moment at the pile head is over-predicted as shown in Figures 6.5(a) and (b), the diagonal elements which represent 4EI/L in the stiffness matrix in Eq. (6.25) are multiplied by a reduction factor, k_c, of less than unity. Thus, Eq. (6.25) can be re-written as:

$$\begin{bmatrix} M_1 \\ M_2 \end{bmatrix} = \left(\frac{EI}{L}\right) \begin{bmatrix} 4k_c & 2 \\ 2 & 4k_c \end{bmatrix} \times \begin{bmatrix} \theta_1 \\ \theta_2 \end{bmatrix} \qquad (6.26)$$

In doing so, the pile cap is now modelled as if it is incapable of providing full rotational restraint to the pile heads. It is found that in this study, k_c is noted be about 0.02 so that the predicted pile head bending moment gives reasonable prediction of the

measured pile head bending moment as shown in Figure 6.6(a). As a comparison, if full rotation is allowed at the pile cap (k_c=0) using the numerical method, the pile head shows that no bending moment is developed as shown in Figure 6.7(a). This shows that relaxation in the rotational degree-of-freedom is the cause of over-prediction of the pile head negative bending moment in Test 9. However, it is also observed that the deliberate relaxation of the rotational degree-of-freedom at the pile heads does not influence the maximum positive and negative bending moments along the pile. As such, this back-analysis method highlights the modelling limitation of the pile cap.

From Figure 6.7(b), both the predicted and measured pile deflection profiles show negligible movement below 9 m depth, revealing that the embedment of the pile into the sand layer is effective in preventing the pile toe movement, thus the validation of a fixed pile toe. For the front pile, negative bending moment is developed at the pile head. Maximum negative and positive pile bending moment are developed at 3.5 m and 8 m below the ground level, respectively. However, for the rear pile, the maximum negative pile bending moment is developed at the pile head, while the maximum positive pile bending moment occurs at approximately 8 m depth.

Figures 6.8(a) and (b) show the derived typical shear force and soil pressure profiles for both the capped front and rear piles of Test 9, respectively, when the post-excavation undrained shear strength is used in computing p_y. It is noted that shear force is produced at the pile head due to the restraint imposed by the pile cap that causes the front pile to drag and pull the rear pile in the direction of the soil movement. The predicted and measured soil pressure acting on the piles generally show fair agreement. Both the predicted and measured pile responses show similar trends and are in fair agreement if the post-excavation undrained shear strength is used computing p_y in the analysis.

Since Test 11 involves front and rear piles at 3 m and 5 m behind the wall, no reduction in undrained shear strength after excavation was observed earlier. Therefore, this pre-excavation soil strength profile is used in the analysis. As for the pile cap rotational stiffness, a similar k_c=0.02 used in Test 9 is adopted to maintain consistency. Figures 6.9(a) and (b) show the predicted and measured pile bending moment and deflection profiles for both capped head front (3 m from wall) and rear (5 m from wall) piles for Test 11, respectively. It is observed that the predicted pile responses are slightly higher than the measured pile responses. The locations of the minimum and maximum pile bending moment are also well-predicted. It is observed that the measured maximum positive pile bending moment and pile head deflection are greater for the front pile in Test 9 than those of the rear pile in Test 11. This is because the capped- pile group in Test 9 is located nearer to the excavation and as a result there is a greater interaction in the pile group due to larger soil movement.

6.4.3 4-pile group

Numerical back-analysis involving free- and capped-head 4-pile group tests are presented in this section.

6.4.3.1 Free-head

In order to account for the pile shadowing, reinforcing and soil arching effects, a soil movement moderation factor has to be adopted to moderate the effect of free-field soil movement on a pile group as discussed earlier. For a larger 4-pile group, the pile shadowing, reinforcing and soil arching effects are expected to be more pronounced. By back-analyses, it is found that, a soil moderation factor of 0.7 is found to be most appropriate for a 4-pile group in clay.

Figures 6.10(a) and (b) show the bending moment and deflection profiles for both the free-head front and rear piles of Test 12. The front and rear piles are located 3 m and 5 m behind the wall, respectively. It is observed that for both the front and rear piles, the locations of the maximum pile bending moments have been well-predicted. Nonetheless, the numerical method slightly under-predicts the front pile head deflection.

6.4.3.2 Capped-head

For the capped-head 4-pile group (Test 13), the bending rigidity of the pile cap, $(EI)_{cap}$, is calculated to be 1.95×10^7 kNm^2. Similarly, the same soil movement moderation factor, k_s, of 0.7 and reduction factor, k_c, for pile cap rotational stiffness of 0.02 are adopted for consistency. As shown in Figures 6.11(a) and (b), the numerical method slightly under-predicts the measured bending moment of the front pile located 3 m behind the wall. However, for the rear pile which is located 5 m behind the wall, the predicted maximum negative bending moment is smaller than the measured values but the predicted maximum positive moment is greater than the measured value. Nevertheless, Figure 6.11(b) shows that the predicted pile deflection profiles generally agree well with the measured ones.

6.4.4 6-pile group

Only capped head 6-pile group tests have been performed. The two tests involve piles arranged in (i) three rows with two piles per row (2x3) in Test 15 and (ii) two rows with three piles per row (3x2) in Test 16. For case (i), the three rows of piles are located 3 m , 5 m and 7 m behind the wall; while for case (ii), the two rows of piles are located 3 m and 5 m behind the wall. The pile group layout for Tests 15 and 16 are shown in Figure 5.1.

6.4.4.1 Capped-head

The ideal bending rigidity of the pile cap, $(EI)_{cap}$, for the 6-pile groups arranged in 2x3 (Test 15) and 3x2 (Test 16) formations is 1.95×10^7 kNm^2 and 3.6×10^7 kNm^2, respectively. By back-analyses, it has been found in this study that a soil movement moderation factor of 0.5 is found to be most appropriate for a 6-pile group in clay. The same reduction factor, k_c, for pile cap rotational stiffness of 0.02 is also adopted for consistency.

Figures 6.12(a) and (b) show the predicted and measured pile bending moment and deflection profiles for the 3x2 arrangement of the 6-pile group (Test 15) at 3 m, 5 m and 7 m behind the wall, respectively. It is observed that the pile head deflection is generally under-predicted. Nevertheless, the predicted and measured pile bending moment profiles seem to show better agreement than the deflection profiles. The peripheral pile bending moment profiles at 3 m and 7 m behind the wall are similar to those of a typical front and rear pile as observed in the 2- and 4-pile groups earlier. It is interesting to note that the bending moment profile of the middle peripheral pile at 5 m behind the wall assumes similar shape of a typical rear pile.

For Test 16, the same soil movement moderation factor of 0.5 and reduction factor, k_c, for pile cap rotational stiffness of 0.02 are also adopted for consistency. The predicted and measured pile bending moment and deflection profiles for the 2x3 arrangement of the 6-pile group at 3 m and 5 m behind the wall are shown in Figures 6.13(a) and (b), respectively. It is also observed that the bending moment profiles and the locations of the maximum positive and negative bending moment have been well-predicted. Nevertheless, the pile group deflection is slightly under-predicted.

6.5 PREDICTION OF PILE RESPONSES IN THE CASE OF A COLLAPSED RETAINING WALL

This section describes the back-analysis of a single pile and also that of a pile group in the case of a collapsed wall. Comparisons with existing established limiting soil pressure / undrained shear strength ratio, K, are also made.

6.5.1 Single pile

In Section 6.4.1, it has been established that the pile bending moment and deflection could be reasonably well predicted using the numerical method if the single pile is located at 3 m or more behind the wall. However, if the pile is located very close to the wall at 1 m away, the pile responses are well over-predicted especially at greater excavation depths due to significant soil movement at the pile location. As the soil movement for Tests 5, 6 and 7 are significantly large for a great distance behind the wall due to the collapse of the wall (see Figures 4.23 and 4.25), the numerical method would also grossly over-predict the pile bending moment and deflection. It is anticipated that under large soil movement, the soil pressure acting on the pile may have reached its limiting values. The numerical back-analyses for a single pile that experiences substantial lateral soil movement are carried out hereinafter.

6.5.1.1 Pre-excavation undrained shear strength

As a first attempt, the pre-excavation undrained shear strength profile at the pile location of 3 m behind the wall is used as the input soil strength parameters in the back analyses. The limiting soil pressure coefficient K is defined as the ratio of limiting soil pressure p_y and c_u. The following K values (Poulos and Davis 1980) are adopted in the back analysis:

$$K = p_y/c_u = 2(1+z/d) \leq 9 \qquad (6.27)$$

where z is the depth below the ground and d is the pile diameter or width.

Figure 6.14 shows a comparison of the measured and calculated maximum induced pile bending moments and pile head deflection for Test 5. The maximum induced pile bending moment occurs at about 7.5 m depth, as shown in Figure 4.21(b). There is a reasonably close agreement between the measured and calculated pile responses up to an excavation depth of about 1.8 m, after which the calculated pile bending moments and deflections considerably overestimate the measured pile responses. The calculated and measured pile responses for Test 6 (measured peak pile responses at 1.4 m excavation depth) and Test 7 (measured pile responses at excavation depths of 1.2 m and 2.8 m) plotted in Figures 6.15, 6.16(a) and 6.16(b), respectively, reveal that the calculated pile bending moments are much larger than the measured values. The above findings are similar to those established in the back-analyses of the earlier stable wall study in Section 4.6 and this confirms that the use of pre-excavation undrained shear strength profiles would over-predict the induced pile bending moments when the magnitude of lateral soil movement is large. It is believed that under large soil movements, the soil pressures acting on the pile may have reached their limiting values.

6.5.1.2 Post-excavation undrained shear strength

Figure 4.5 shows that the undrained shear strength of the top soil had significantly weakened after excavation. In view of the over-prediction of pile responses at large soil movements using the pre-excavation undrained shear strength, the second attempt in the back analyses is to employ the post-excavation undrained shear strength profiles as the input soil strength values. The calculated pile bending moments and deflections using the post-excavation strength profiles for Tests 5, 6 and 7 are also shown in Figures 6.14, 6.15 and 6.16, respectively. It is evident that the

agreement between the calculated and measured pile bending moments are considerably better. However, the calculated pile deflections are lower than the measured values. In practice, the correct prediction of pile bending moment is the most critical issue as this concerns the structural capacity and integrity of the pile. The under-prediction of pile deflection is probably due to the presence of tension cracks and the formation of active failure wedge in the tests (see Figures 4.23(b) and 4.25), which could not be modeled in the numerical analysis. The under-prediction is especially severe for Test 7. Figure 4.19(d) clearly shows that after an excavation depth of 1.4 m in Test 7, the wall rotation in the underlying sand layer increases considerably implying a reduction in effectiveness of the wall 'key-in' in the sand layer. This in turn causes a bigger pile rotation in the underlying sand layer and such phenomenon could not be accounted for in the numerical analysis.

As mentioned earlier, the maximum soil pressures acting on the pile is likely to be reached at large soil movements. At this juncture, it is worthy to evaluate the actual magnitudes of soil pressures on the pile. The method of deriving the soil pressure profiles is the same used for the earlier stable wall study. As an example, Figure 6.17 shows the soil pressure profiles of Test 6 that are deduced from the corresponding bending moment profiles shown in Figure 4.21(c). It is evident that the limiting soil pressures p_y along the upper portion of the pile have been reached at an excavation depth of 1.2 m. Thereafter the soil pressures do not increase further with increasing excavation depth.

Using the p_y values derived from the experimental data for the 3 tests and the post-excavation undrained shear strength profiles, the variation of limiting soil pressure coefficient K with depth for the 3 tests can be derived and shown in Figure 6.18(a). It is noted that the back-analyzed K value increases from zero at the ground

surface to a maximum value of around 8 at about 2 m depth. The theoretical K values determined using Equation 2 are also plotted in Figure 6.18(a) for comparison. It is evident that the theoretical and back-analyzed K values are reasonably close. This verifies that the post-excavation undrained shear strength values should be adopted in order to obtain a more accurate prediction of induced pile bending moments.

6.5.1.3 Pre-excavation undrained shear strength with back-analysed limiting soil pressure

In most practical cases, the post-excavation undrained shear strength profiles are not available. In view of this, the back-analyzed K values with respect to the pre-excavation undrained shear strength profiles for the 3 tests are also determined and shown in Figure 6.18(b). As expected, the back-analyzed K values are much lower than the theoretical K values shown in Figure 6.18(a). An envelope of limiting K values is hence plotted and indicated by the dash line in Figure 6.18(b). The maximum back-analyzed K value of 6 is close to the K values proposed by a number of researchers (for example, Maugeri, 1994; Moser, 1973) for piles subject to lateral soil movement. The above finding illustrates that the reduction of K from a value of 9 for conventional laterally loaded piles to a lower value of 6 for piles subject to excavation-induced soil movements is attributed to the reduction in the undrained shear strength upon excavation. It should be noted that the magnitude of 6 is merely a back-analyzed value and may not be applicable to other situations with different wall, soil or pile conditions.

The third and final attempt in the back analyses is to employ the pre-excavation undrained shear strength profiles but adopting the envelope of K values deduced from Figure 6.18(b). The calculated pile bending moments and deflections for Tests 5, 6 and 7 shown in Figures 6.14, 6.15 and 6.16, respectively, again reveal much better

agreement with the measured pile responses. It should be noted that the calculations obtained using the post-excavation undrained shear strength profile and pre-excavation undrained shear strength profile with reduced K values are identical. This is as expected as the two approaches essentially use the same back-analyzed limiting soil pressures.

Some researchers (Viggiani, 1981; Maugeri, 1994; Pan et al., 2002) established that the magnitude of K on a conventional laterally loaded pile should be greater than that on a pile subject to lateral soil movement. However, others (Chen and Poulos, 1994) suggested that the K values for the above two situations could be similar with a K value of 9 proposed for piles subject to excavation-induced soil movement (Poulos and Chen, 1997) and for embankment piles (Goh et al., 1997). The results of the present study help to clarify the above contrasting proposals of K values. The results of the back analyses reveal that if only pre-excavation undrained shear strength profiles are available, an appropriate reduction in the K value should be adopted in order to obtain a more accurate prediction of pile responses behind an excavation with large soil movements.

6.5.2 Pile group

The experimental set up of Test 14 is similar to that of Test 6, except that the former consists of a capped head 4-pile group with front and rear piles located 3 m and 5 m behind the wall while the latter consists of a single pile at 3 m behind the wall.

The method of analyses established in Section 6.5.1 above is adopted. The free-field soil movement profiles used is similar to that of Test 6 and shown in Figure 4.26(b). Using the simplified envelope of limiting soil pressure distribution (Figure 6.15(b)) and the reduced c_u values after excavation (Figure 4.5), the predicted front and rear pile responses are shown in Figures 6.19(a) and (b). The predicted pile responses

show fair agreement with the measured values, suggesting that the limiting soil pressure envelope developed for a single pile can also be used for a group of pile behind a collapsed wall. It is also interesting to note that when prediction is made at excavation depth of 1.8 m, the greater soil movement (see Figure 4.26(b)) has no effect on the pile responses as the soil limiting pressure has been reached. As such, it is not necessary to use the soil moderation factor as for the case of pile groups located behind a stable wall. This finding reiterates the postulation that once soil limiting pressure has been reached, the pile responses will not increase further. This is consistent with the findings made for the case of a single pile located behind a collapsed wall (Test 6).

6.6 DISCUSSION ON SOIL LIMITING PRESSURE ON PILES

The postulation of using lower limiting soil pressure on piles generally works well in this study as large strain soil deformation or soil "flow" had occurred behind the collapsed wall during and/or after the excavation process. This is somewhat analogous to the effect of landslide or in the case of a slope failure. In all these cases, both sliding and stable zones exist within the soil. From Figures 4.23(b) and 4.25, it is evident that behind an excavation in clay, a zone of significant soil movement is formed at an angle of 45^{o} propagating from a distance of about 6.5 m behind the wall to the depth of the clay-sand interface. When a shear plane or a plane of weakness starts to form within the soil mass, the soil located in the failure zone would weaken and may be detached from its original soil mass in the form of tension cracks. Therefore, lateral stress relief or reduction in confining stress occurs within the affected soil mass, thus reducing the magnitude of soil pressure that can be exerted on the pile.

It must be mentioned that for the case of a collapsed wall for both the single pile and pile group, the usage of the soil moderation factor is not as important as for the case of a stable wall. This is so because the very large soil movements associated with the collapse of the wall is taken care of by the appropriate soil limiting pressure. Once the limiting soil pressure has been reached, any increase in the lateral soil movement will not increase the induced forces on the piles anymore. As such, this study highlights the fact that for large strain soil deformation as in the case of a collapsed wall, the governing parameter is the limiting soil pressure, p_y, that can act on the pile as opposed to the case of a stable wall, where the governing parameter is the lateral soil stiffness, K_h.

6.7 GENERAL COMPARISON WITH TESTS DONE IN SAND

Lim (2001) and Law (2000) used the numerical methods as described in Section 6.2 to predict the responses of single piles and pile groups due to excavation in sand. It was concluded that the numerical method was capable of predicting reasonably well the shape and locations of the maximum bending moment values. However, the magnitudes of the pile bending moment are not predicted satisfactorily as shown from Figures 6.20 to 6.24. They reported that this could be due to experimental errors caused by the difficulties in constructing the pile caps to fully constrain the pile head movement in the centrifuge model tests. Further investigation shows that the pile caps used were too thin and could only be used to clamp the individual piles in a single direction. Both of these construction methods used in the study are thought to be unable to provide the necessary restraint mechanism to the pile heads and hence the measured magnitudes of the pile responses do not agree with the predicted values.

In view of these deficiencies, the pile caps used in this study are made thicker and can be clamped to the individual piles in both directions. Besides that, the undrained shear strength profiles of the clay have been appropriately measured using in-flight T-bar tests before and after the excavation process. As the important parameters involved have been properly quantified and correctly accounted for, it is not surprising that the measured and predicted pile responses show better agreement in terms of magnitudes and shapes of the pile responses (for example, from Figures 6.11 to 6.13) than the predictions made by Lim (2001) and Law (2000) for tests conducted in sand.

The similarity for both the numerical prediction between sand and clay tests is the adoption of soil moderation factors to account for the pile reinforcing, shadowing and soil arching effects.

6.8 SUMMARY OF FINDINGS

The numerical methods proposed for the analysis of a single pile and a pile group subjected to excavation-induced soil movement can generally provide fair prediction when compared to centrifuge test results. This is so provided that the soil undrained shear strength can be appropriately measured using an in-flight bar penetrometer or T-bar.

When piles are installed in a group, each individual pile will provide shadowing and reinforcing effects to other adjacent piles. Therefore, it is intuitively correct that as the pile group gets larger, the shadowing and reinforcing effects will also become more prominent. The immediate effect of pile shadowing and reinforcing effect is to limit the detrimental effects due to excavation-induced soil movement. Since the input data involves measured free-field soil movement, a soil moderation

factor has to be established to account for the pile shadowing and reinforcing effects. Besides that, soil arching effect is also observed to occur at the surface of the OC crust of the kaolin clay for the pile groups. This soil arching effect will also contribute to the moderation of the excavation-induced soil movement. By back-analysis, the magnitude of soil moderation factor is established to be 0.8 for a 2-pile group, 0.7 for a 4-pile group and 0.5 for a 6-pile group in clay.

It should be noted that the reduction factor, k_c, for pile cap rotational stiffness may not be similar because different pile caps were used for different pile groups but generally k_c serves as a reasonable approximation. By allowing some rotation at the pile head and adopting lateral soil movement moderation factors in all the numerical analyses, consistently fair agreement of the pile responses between the numerical predictions and centrifuge test results can be achieved. Therefore, the centrifuge tests and numerical methods can be used to complement each other well to provide a better understanding on pile-soil interaction behaviour.

The present study on the case of a collapsed wall establishes that due to soil stress relief after excavation, the soil pressure acting on the pile is found to be lower than those on a conventional laterally loaded pile. Based on the findings of the numerical back-analysis, a simplified envelope of K values having a maximum value of 6 with respect to original soil strength prior to excavation is proposed to estimate the magnitude of bending moment induced on the pile in this study.

This Chapter has also highlighted the importance of understanding and estimating the soil limiting pressure due to the collapse of a retaining wall caused by excavation. It brings to light that for soil undergoing large strain deformation, the governing parameter is the limiting soil pressure, p_y, as opposed to the case of a stable wall, where the lateral soil stiffness, K_h, is the governing parameter. Such knowledge

will lead to the understanding that when designing landslide or creeping slope stabilizing piles, increasing the number of less reinforced piles will be far more beneficial than having a smaller number of highly reinforced piles.

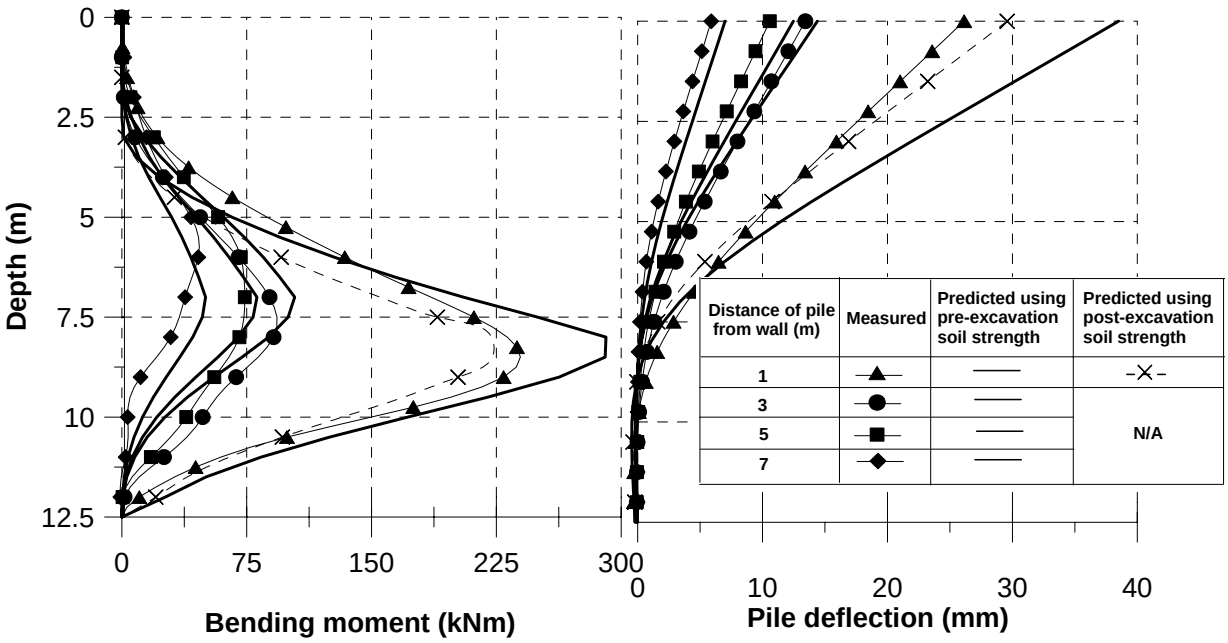

(a) (b)

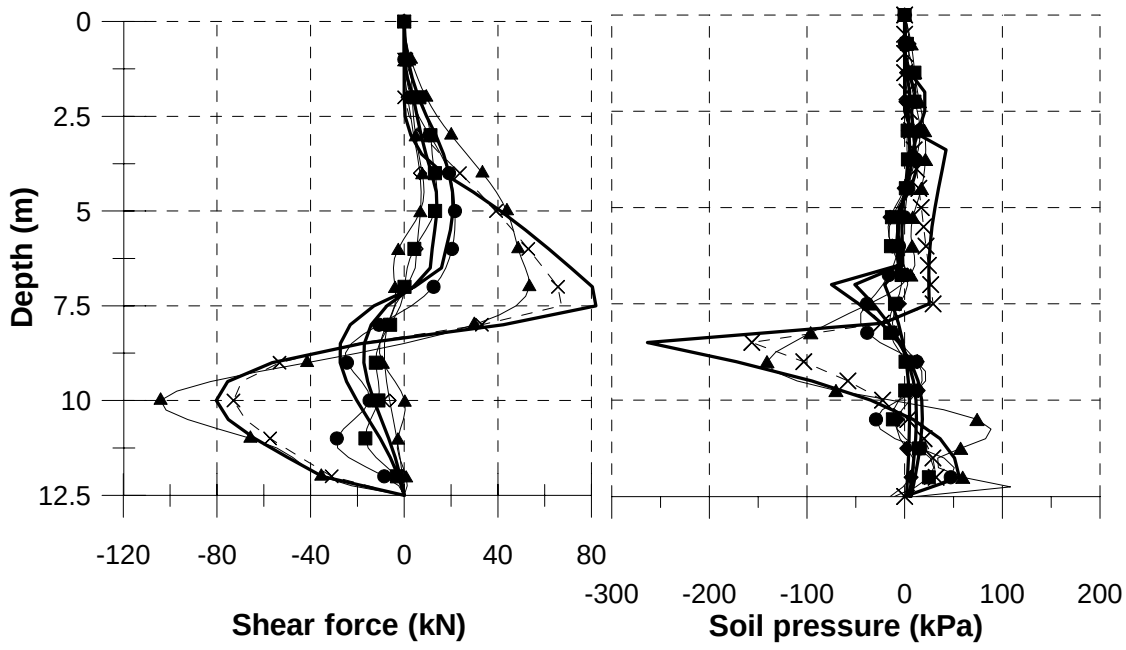

(c) (d)

Figure 6.1 Comparison of measured and predicted maximum induced pile (a) bending moment, (b) deflection, (c) shear force and (d) soil pressure profiles

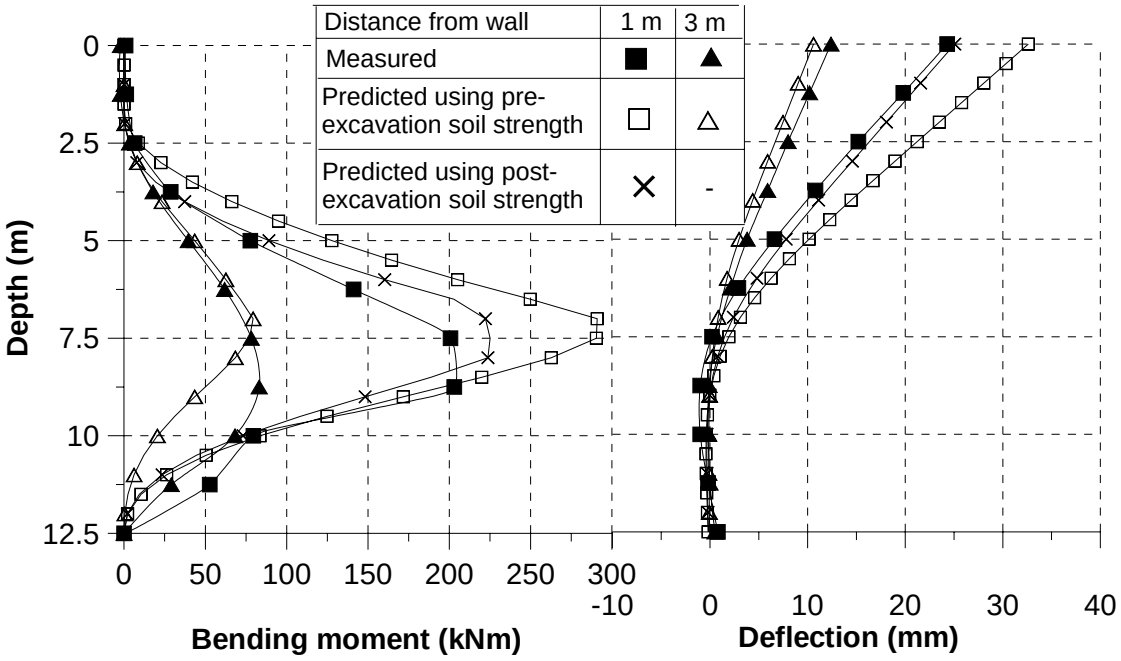

(a) (b)

Figure 6.2 Predicted and measured pile (a) bending moment and (b) deflection profiles (Test 8)

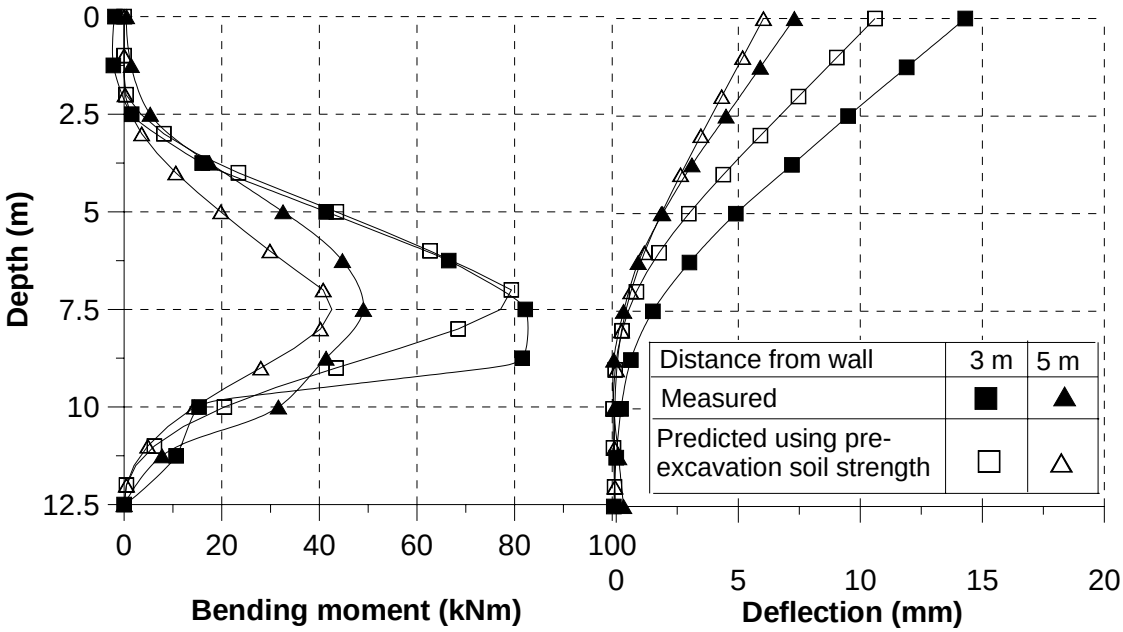

(a) (b)

Figure 6.3 Predicted and measured pile (a) bending moment and (b) deflection profiles (Test 10)

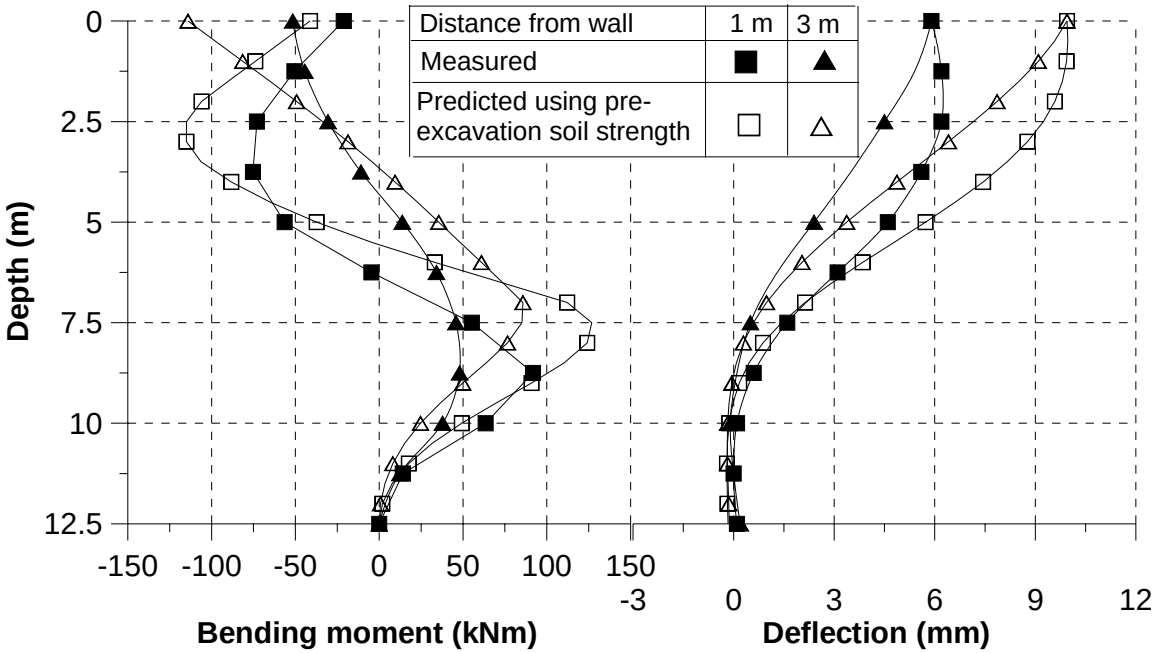

Figure 6.4 Predicted and measured pile (a) bending moment and (b) deflection profiles (Test 9) using pre-excavation of undrained shear strength and without reduction in pile head rotation stiffness

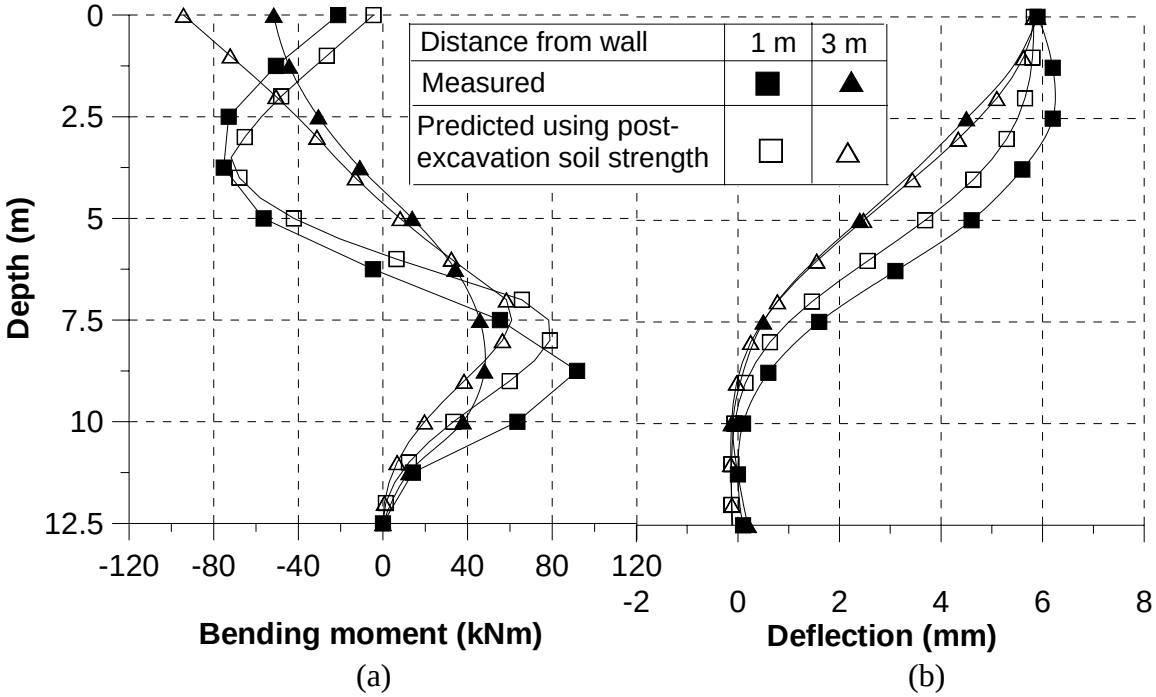

Figure 6.5 Predicted and measured pile (a) bending moment and (b) deflection profiles (Test 9) using post-excavation undrained shear strength and without reduction in pile head rotation stiffness

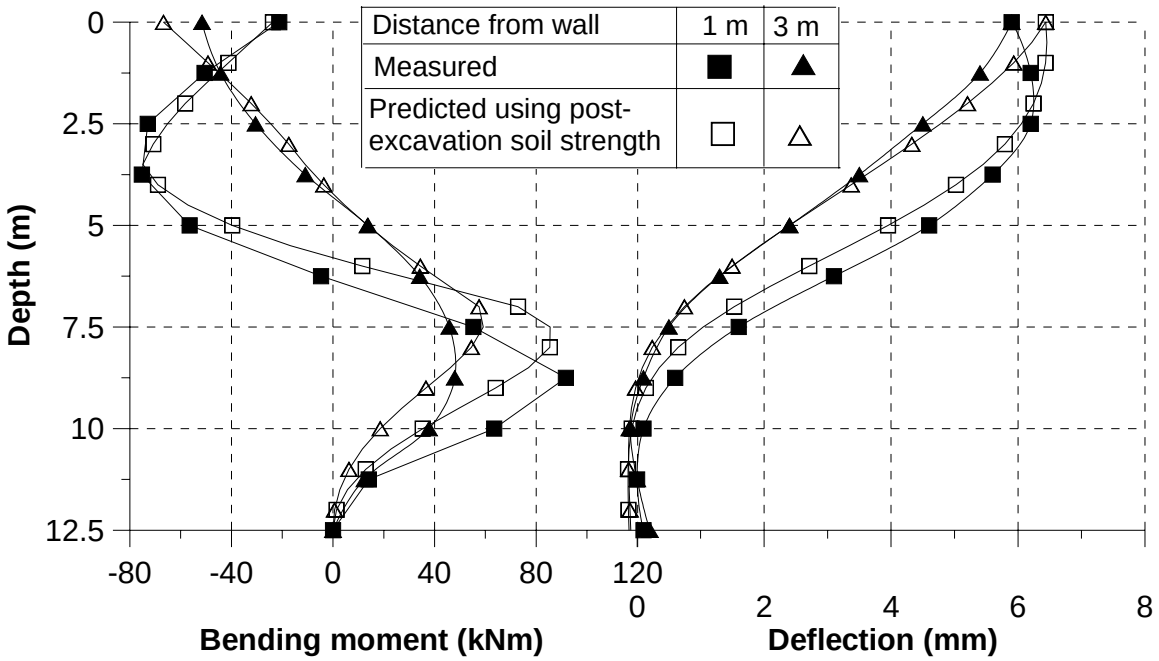

(a) (b)

Figure 6.6 Predicted and measured pile (a) bending moment and (b) deflection profiles (Test 9) using post-excavation undrained shear strength and reduction in pile head rotation stiffness (k_c=0.02)

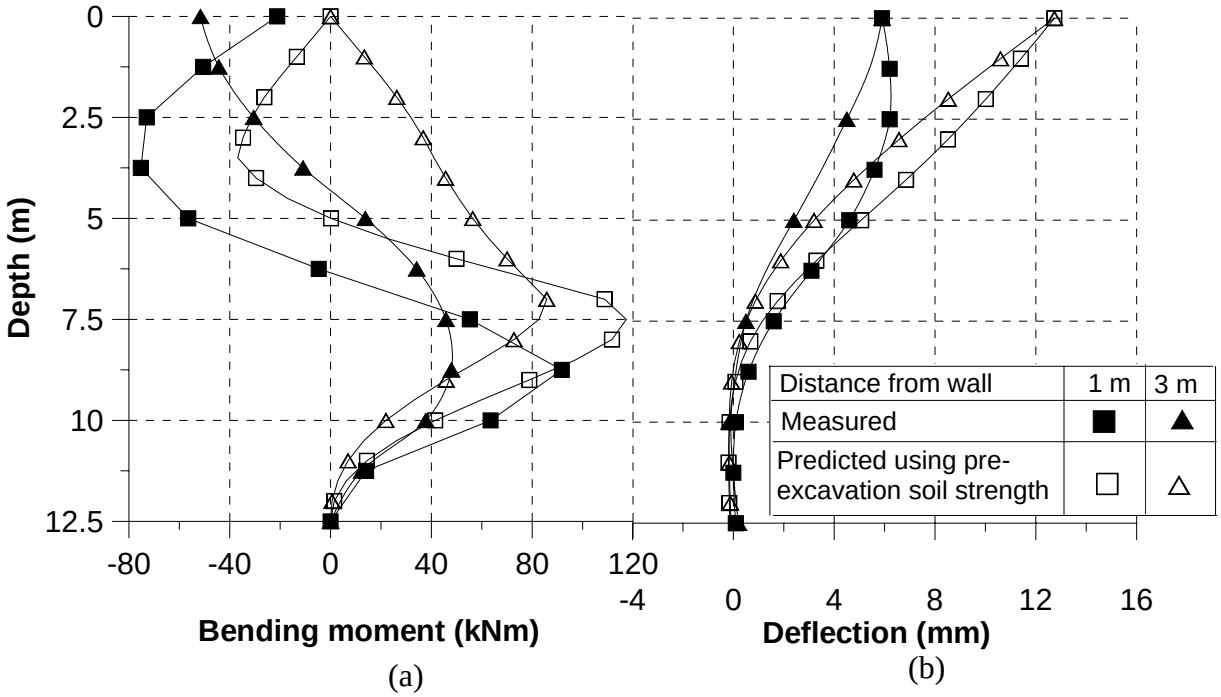

(a) (b)

Figure 6.7 Predicted and measured pile (a) bending moment and (b) deflection profiles (Test 9) using post-excavation undrained shear strength and allowing full pile head rotation (k_c=0)

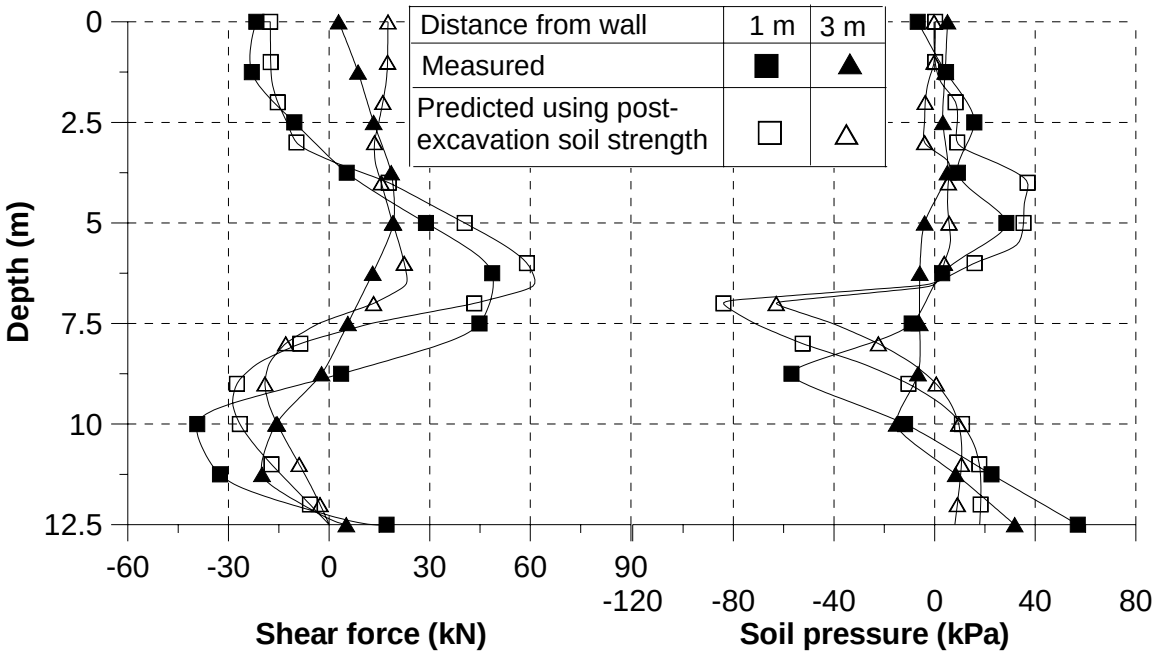

(a) (b)

Figure 6.8 Predicted and measured pile (a) shear force and (b) soil pressure profiles (Test 9) using post-excavation undrained shear strength and reduction in pile head rotation stiffness (k_c=0.02)

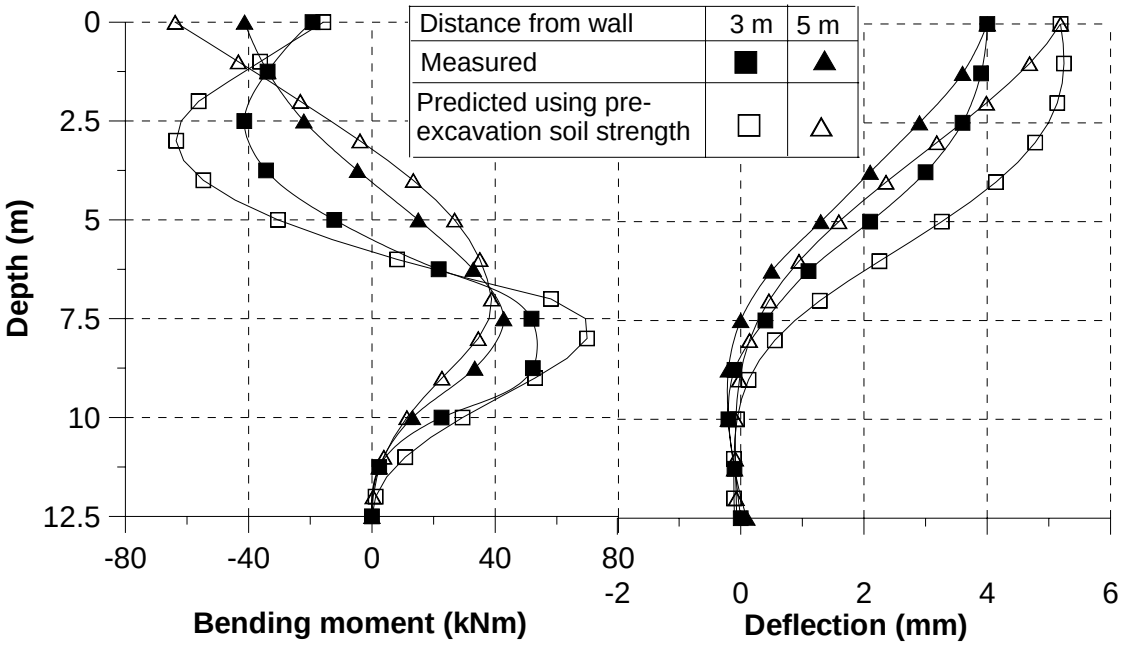

(a) (b)

Figure 6.9 Predicted and measured pile (a) bending moment and (b) deflection profiles (Test 11)

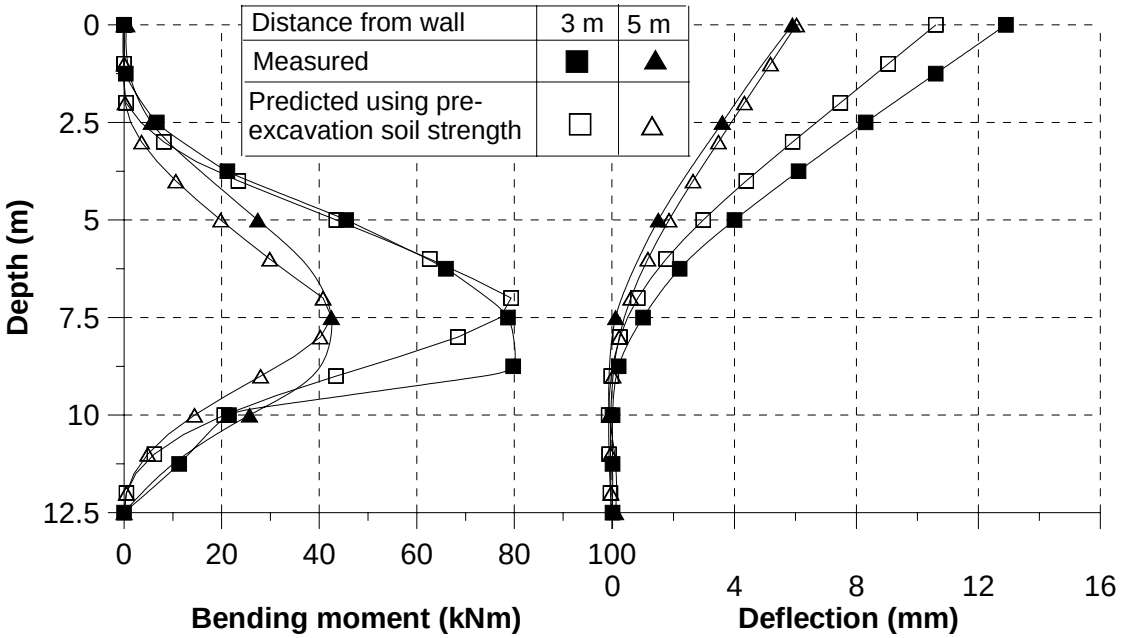

(a) (b)

Figure 6.10 Predicted and measured pile (a) bending moment and (b) deflection profiles (Test 12)

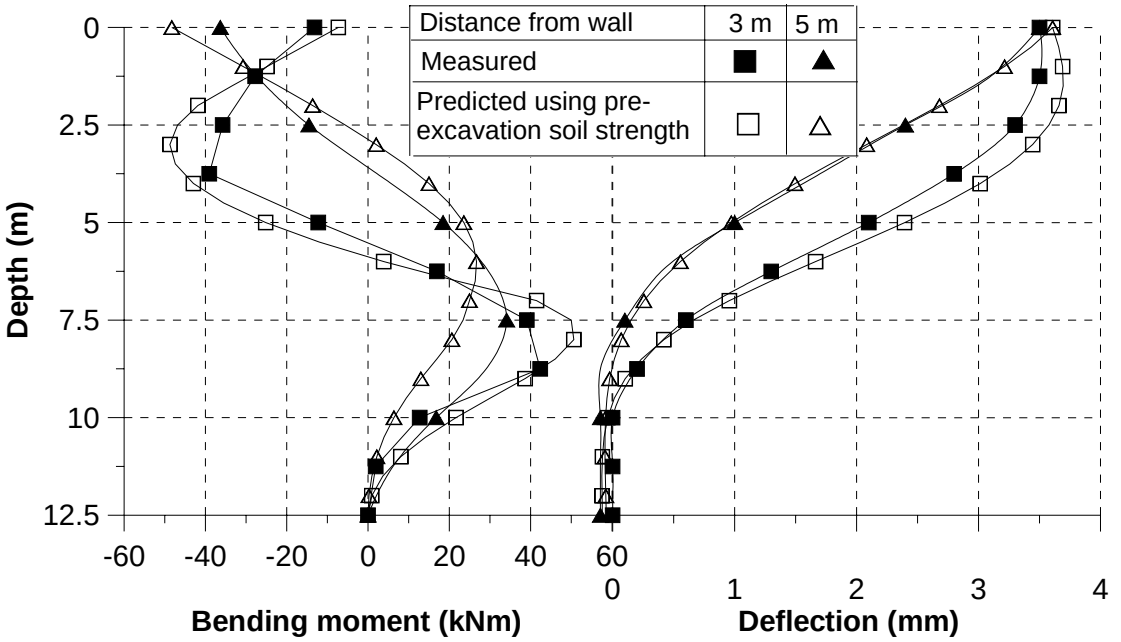

(a) (b)

Figure 6.11 Predicted and measured pile (a) bending moment and (b) deflection profiles (Test 13)

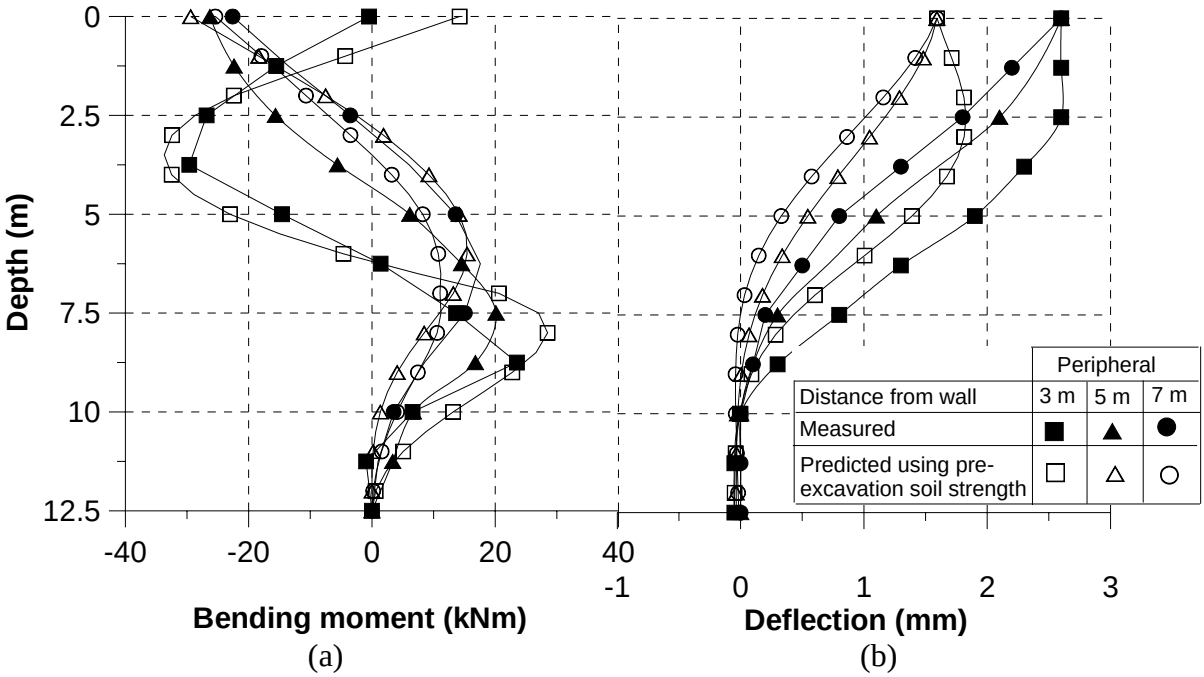

Figure 6.12 Predicted and measured pile (a) bending moment and (b) deflection profiles (Test 15)

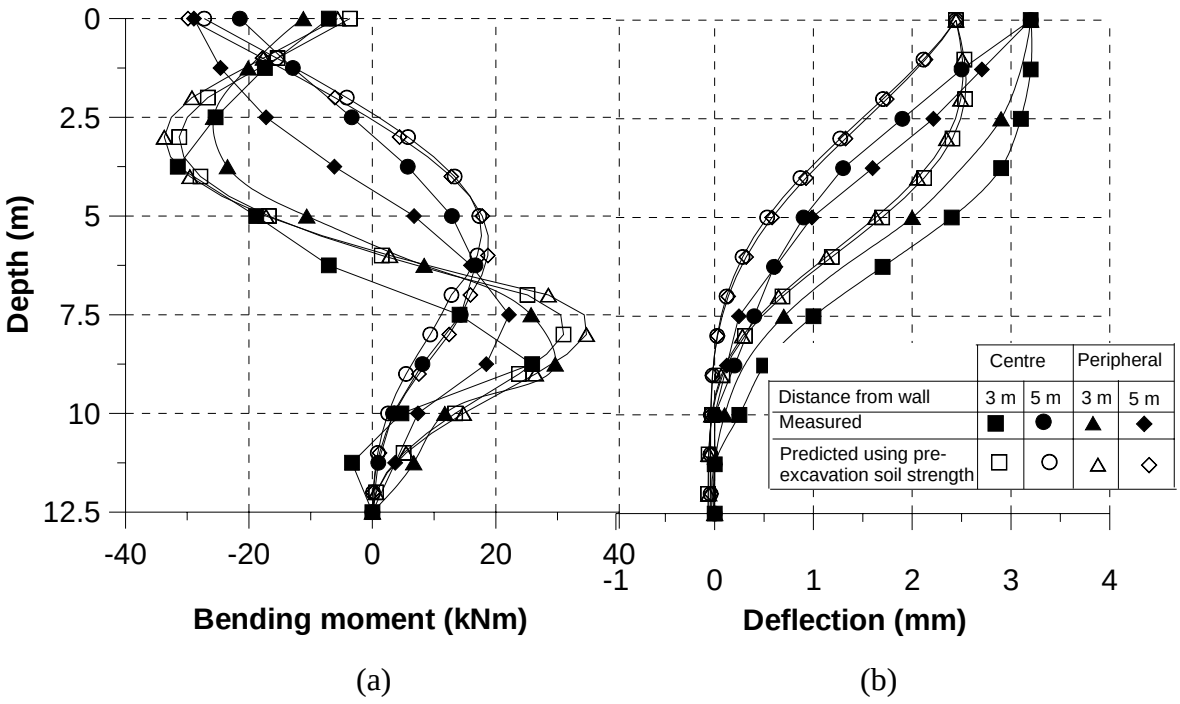

Figure 6.13 Predicted and measured pile (a) bending moment and (b) deflection profiles (Test 16)

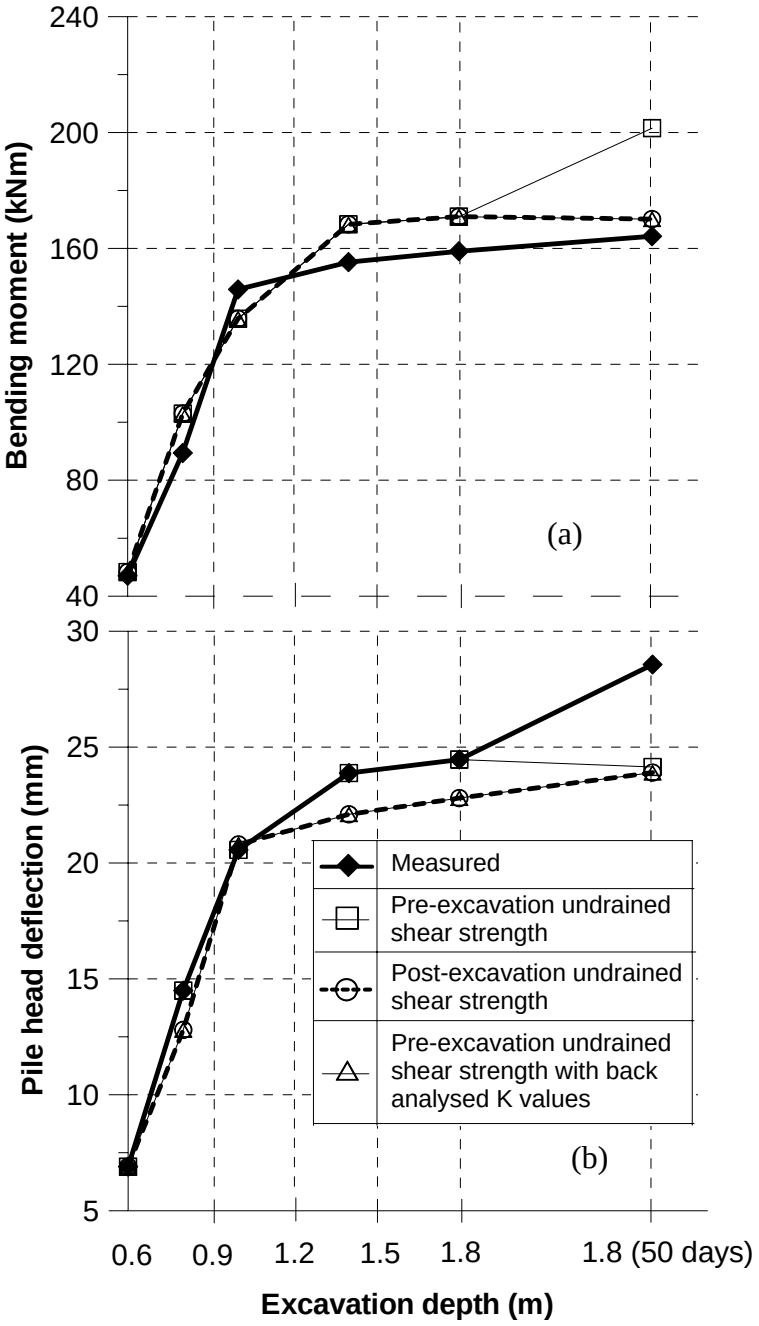

Figure 6.14 Variation of measured and calculated (a) bending moment and (b) pile head deflection with excavation depth for Test 5

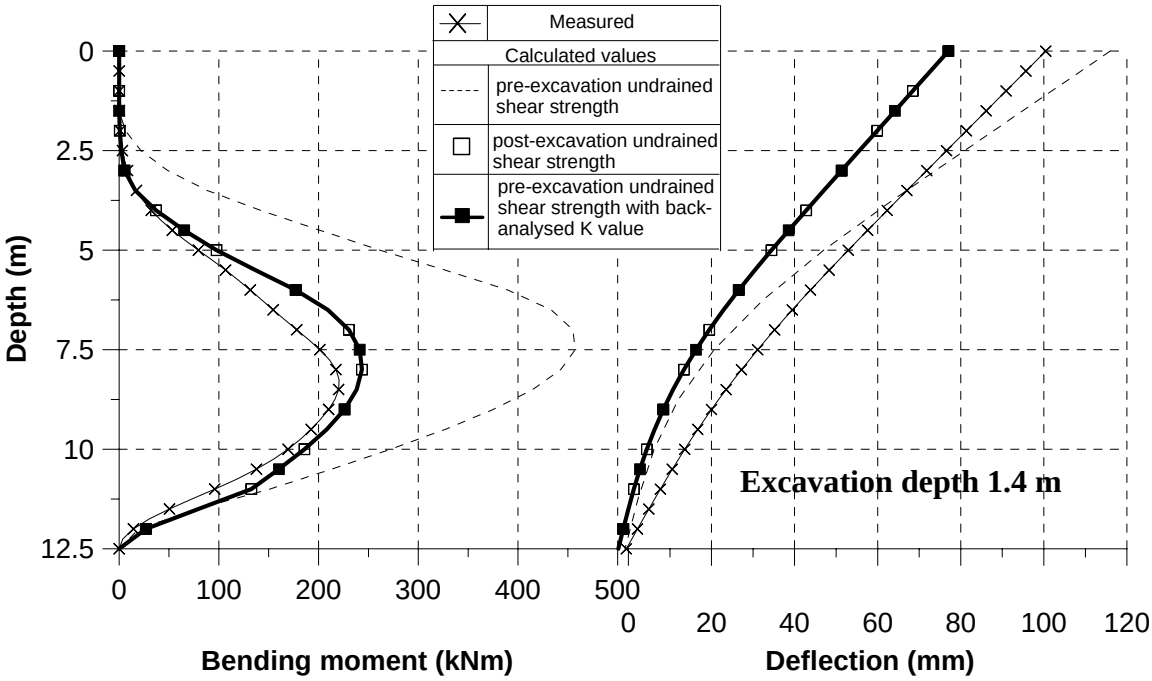

Figure 6.15 Comparison of measured and calculated pile (a) bending moment and (b) deflection profiles for Test 6 at excavation depth of 1.4 m

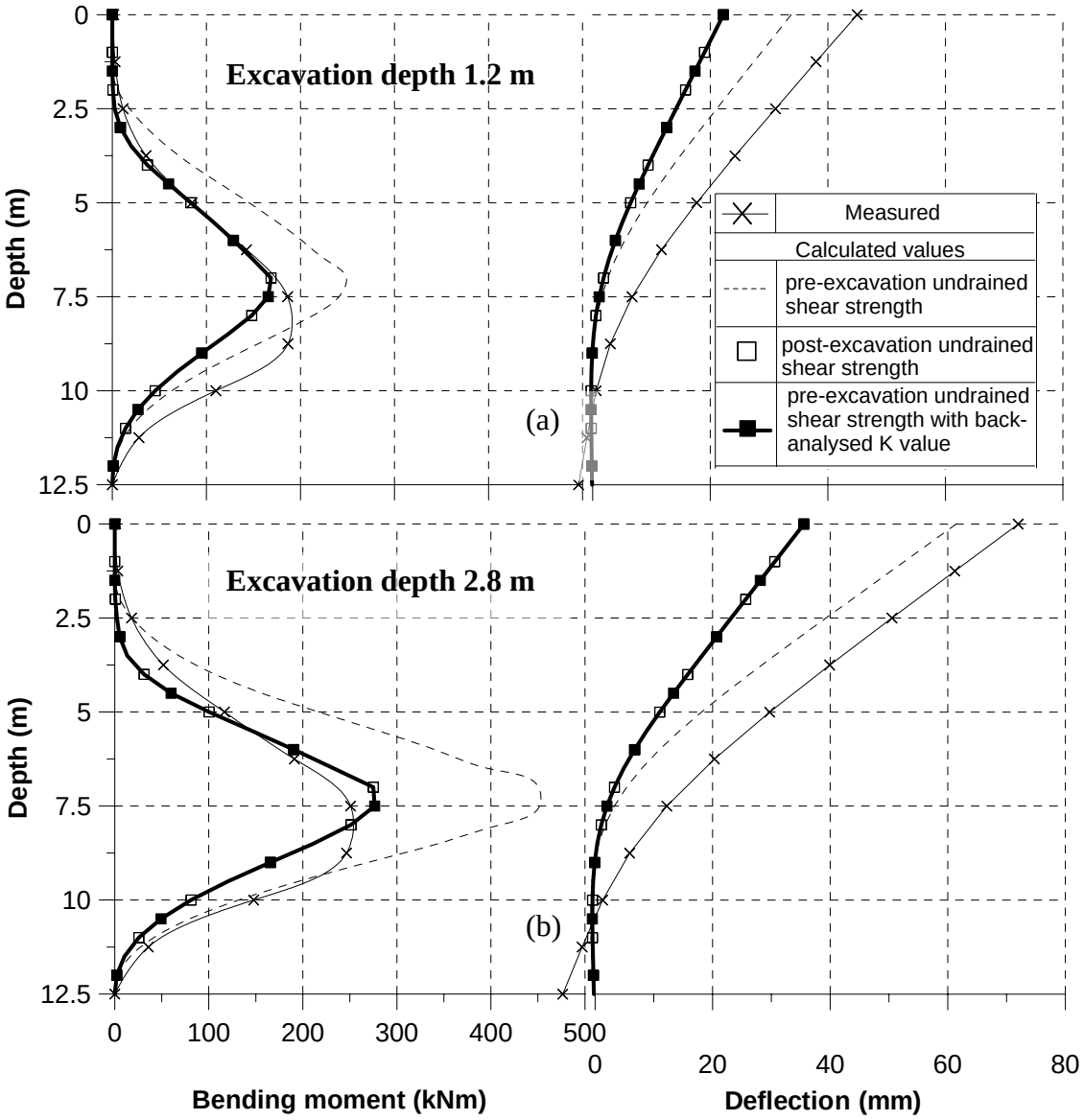

Figure 6.16 Comparison of measured and calculated pile (a) bending moment and (b) deflection profiles for Test 7 at excavation depth of (a) 1.2 m and (b) 2.8 m

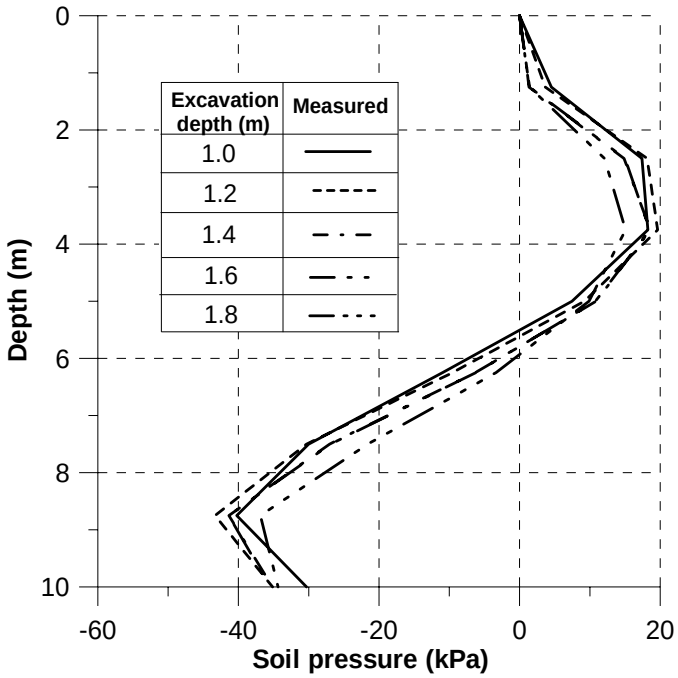

Figure 6.17 Limiting soil pressure deduced from pile bending moments (Test 6)

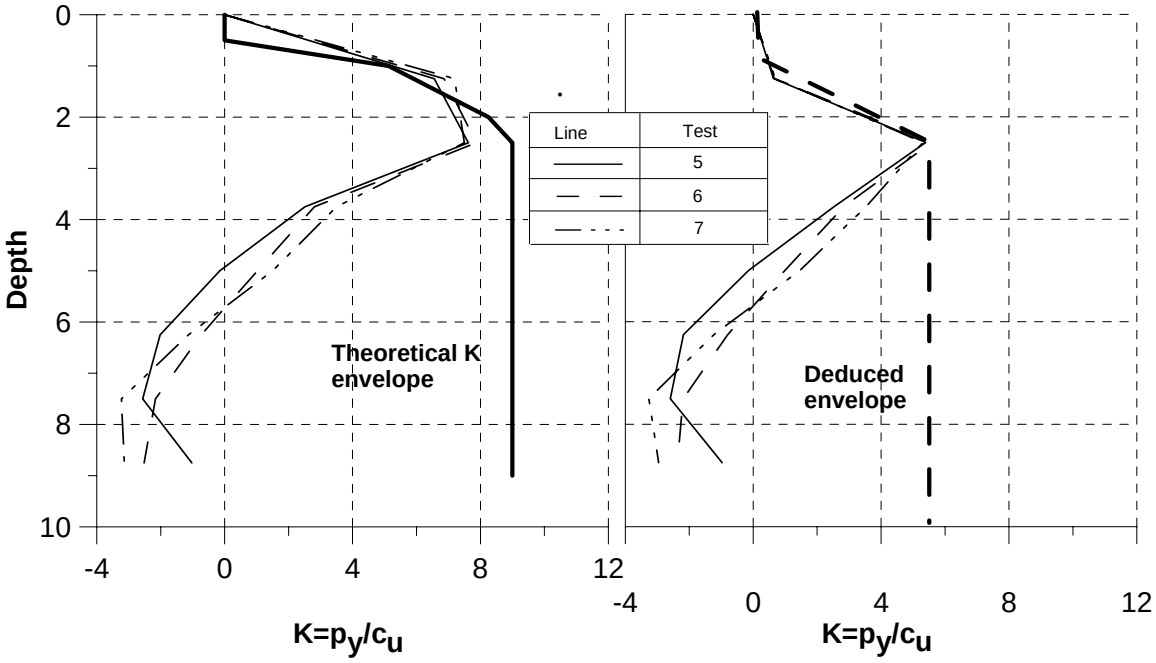

(a) Post-excavation undrained shear strength

(b) Pre-excavation undrained shear strength

Figure 6.18 Variation of K value with depth using (a) post-excavation and (b) pre-excavation undrained shear strength

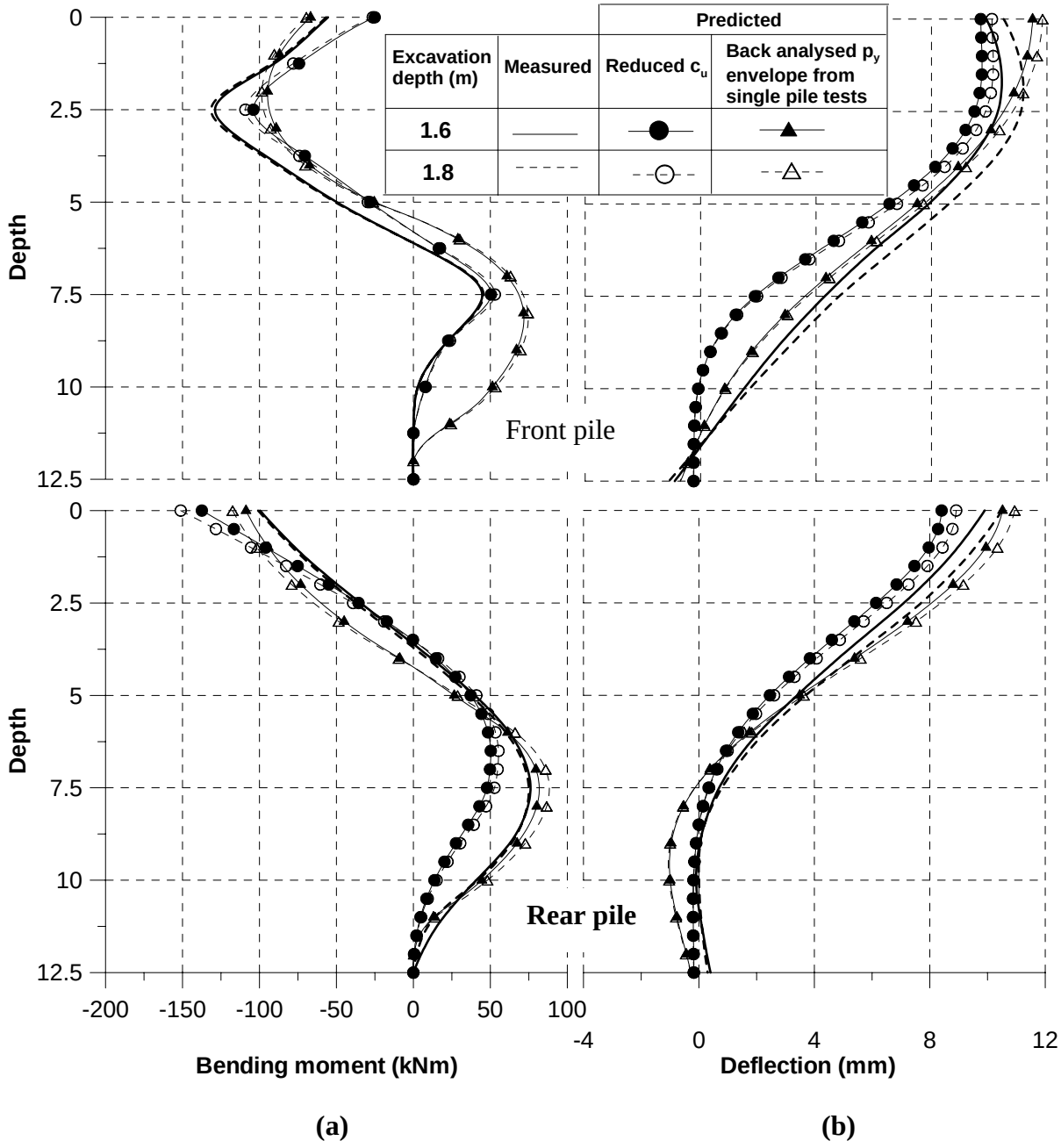

Figure 6.19 Predicted and measured pile (a) bending moment and (b) deflection profiles for capped front and rear piles (Test 14) using two different methods

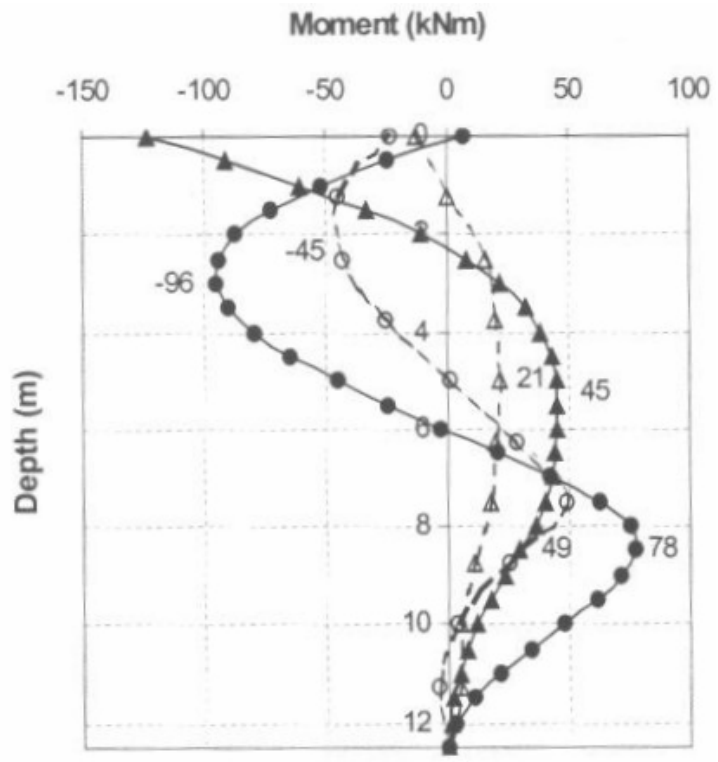

Figure 6.20 Predicted and measured 4-pile group bending moment profiles for capped front and rear piles (after Law, 2000)

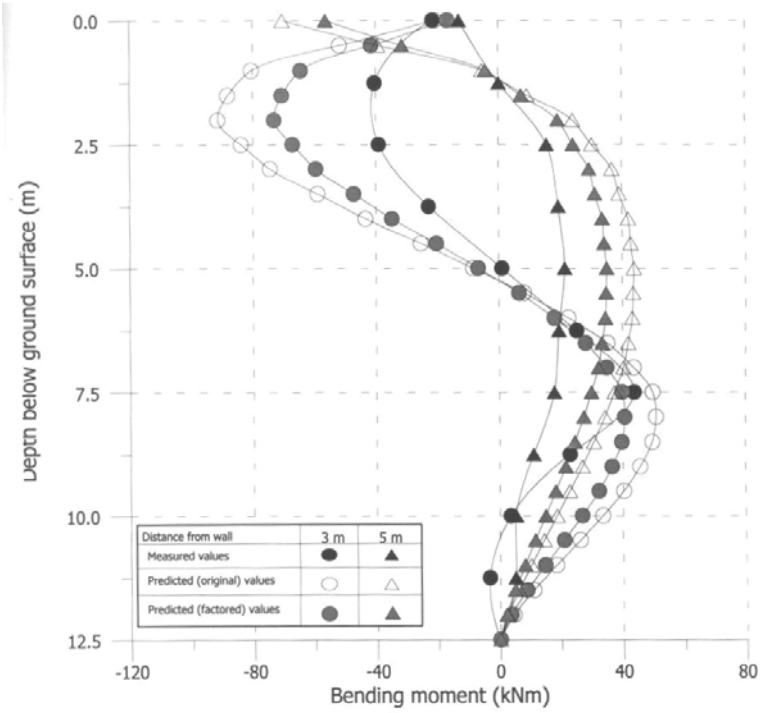

Figure 6.21 Predicted and measured 4-pile group bending moment profiles for capped front and rear piles (after Lim, 2001)

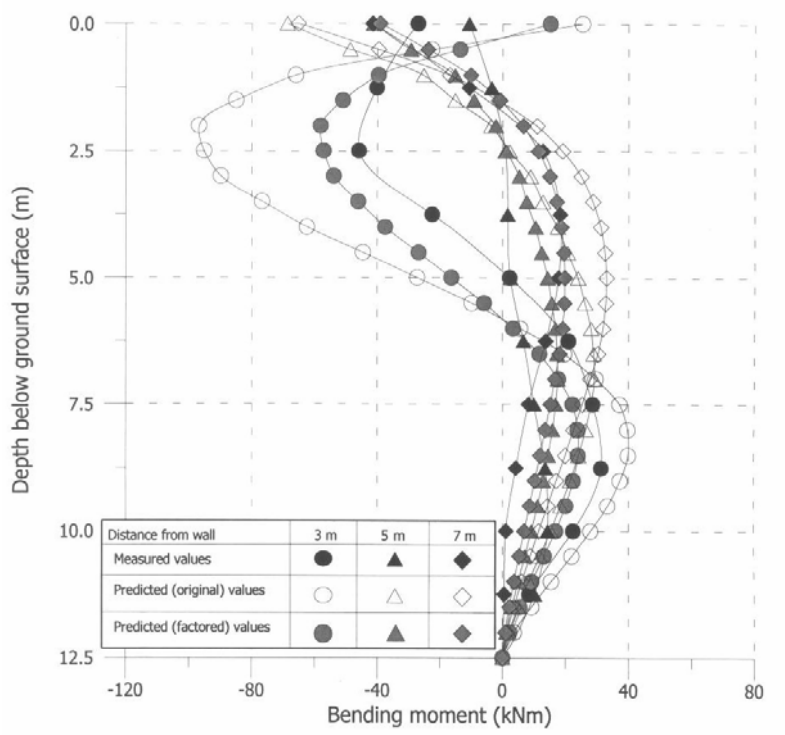

Figure 6.22 Predicted and measured 6-pile group (2x3) bending moment profiles for capped piles (after Lim, 2001)

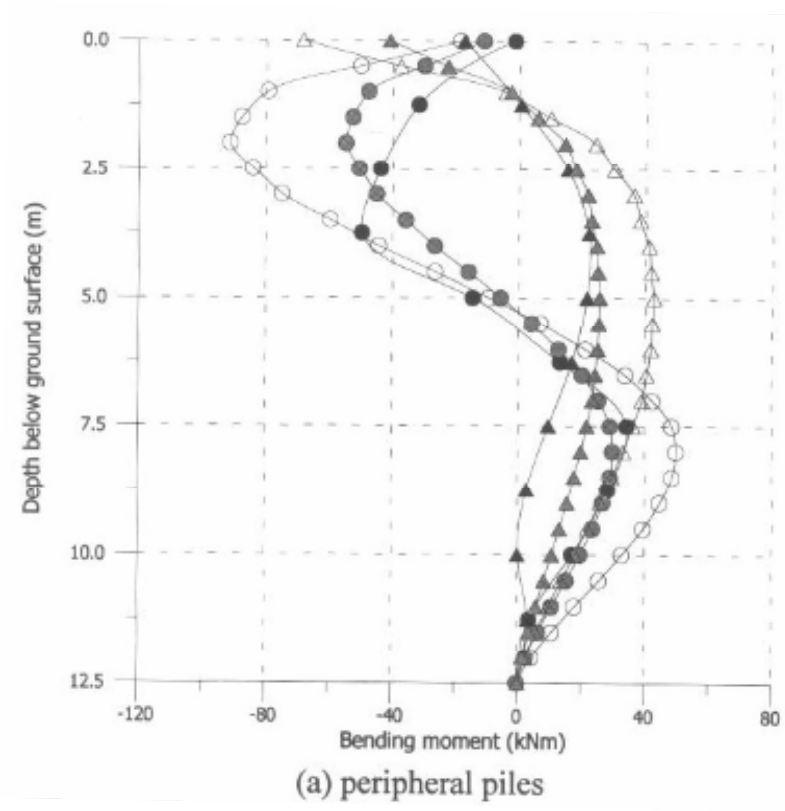

Figure 6.23 Predicted and measured 6-pile group (3x2) bending moment profiles for capped peripheral piles (after Lim, 2001)

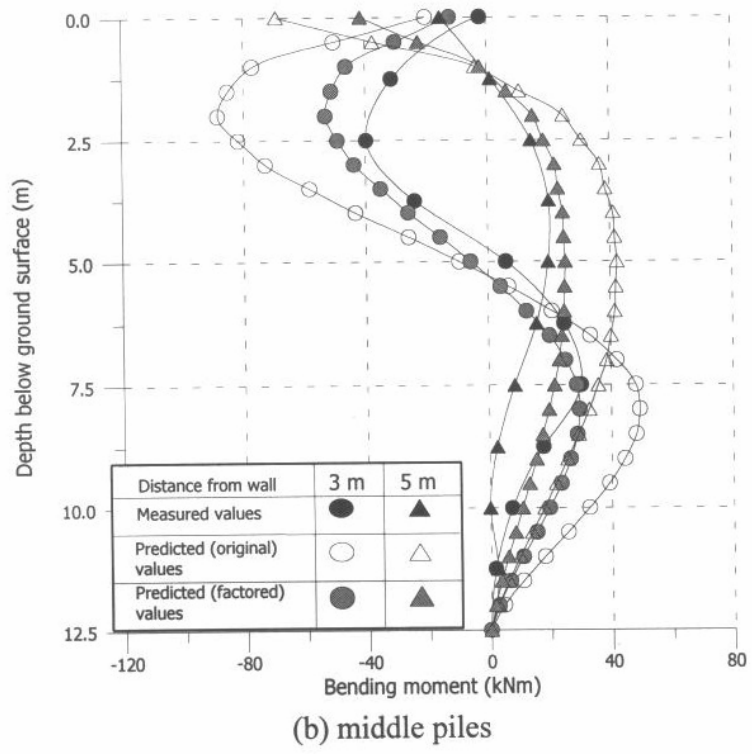

Figure 6.24 Predicted and measured 6-pile group (3x2) bending moment profiles for capped middle piles (after Lim, 2001)

CHAPTER SEVEN

FIELD STUDY

7.1 INTRODUCTION

A proposed 8-storey industrial building with one-level basement carpark is to be constructed at a site bounded by two existing 5-storey buildings the East and South directions. In order to construct an underground storage tank, a temporary open-cut excavation of a 1V:2.5H slope was proposed. The excavation was to be carried out in front of a 4-pile group. This case provided an excellent opportunity to carry out a detail field study to supplement the earlier centrifuge model studies and numerical back-analyses to obtain a further understanding on the pile behaviour due to excavation-induced soil movement in clay.

Owing to some unforeseen situations, excessive soil movement had taken place during the slope excavation and caused failure of the instrumented pile group. This pre- and post-failure pile behaviour of the unintended failure has provided valuable field data for analysis. It is hoped that from this field study, the effects of soil "flow" on the pile as well as the behaviour of a capped-head pile group as observed in the centrifuge tests in Chapter 4 can be further evaluated. In addition, the field data can also be used to further investigate the magnitude of limiting soil pressure on the pile obtained from the numerical back-analyses performed in Chapter 6.

7.2 CHARACTERISTICS OF SITE

The site plan and layout is shown in Figure 7.1. The location of the instrumented 900-mm 4-pile group is also shown in the figure.

7.2.1 Soil investigation works

The soil investigation work consists of:

(i) 4 boreholes made using rotary wash boring. Borehole 1 (BH 1) was located within the excavation area, see Figure 7.1.

(ii) Standard Penetration Tests (SPT) with split spoon samplers were carried out to obtain disturbed samples for index property tests.

(iii) Undisturbed sampling of soil specimens at 1.5 m to 3.0 m intervals using thin wall samplers for trixial compression tests.

(iv) Ground water level and pore water pressure measurement using water standpipe and piezometer.

(v) Vane shear tests carried out in borehole to determine the in-situ strength of the soft marine clay.

7.2.2 Geological formation

The geological formation of the site belongs to the Alluvial Member of Kallang Formation and Old Alluvium. According to Moh (2001), the former can be described as sediments consisting of pebbles, sand, clay or peat. This layer is usually normally or lightly over-consolidated. On the contrary, Old Alluvium typically consists of loose coarse quartz-feldspar sand and gravel with lightly cemented sandstone-conglomerate. The top 8 m of this layer are usually deeply weathered.

7.2.3 Subsoil conditions

Figure 7.2 shows the subsurface profile close to the instrumented piles. It can be subdivided into 6 layers with the top fill layer (denoted by Layer 1a) of between 0.5 m and 1.5 m thick. Beneath the fill is the very soft, greenish grey marine clay (Layer 1) with thickness ranging between 7.5 m and 9 m. The SPT N values for this layer are less than 4. Layer 2 is about 5 m thick and consists of loose, clayey sand as well as medium stiff sandy clay with SPT N values between 4 and 10. Subsequently, medium dense clayey sand (Layer 3) with SPT N values between 10 and 30 of about 2 m thick can be found. Layer 4, which is about 10 m thick, consists of dense, clayey sand with SPT N values ranging between 30 and 50. This is followed by an 8-m thick very dense clayey sand and hard silty clay (Layer 5) with SPT N values ranging between 50 and 100. The hard stratum, or Layer 6, consists of dense sand and stiff clay, having SPT N values of in excess of 100. The physical properties of the soils are partially shown in Table 7.2.

A water standpipe was located in front of the sheet piles as shown in Figure 7.1. The groundwater table was observed to be about 1 m below the ground level prior to the commencement of excavation. The geotechnical parameters of the subsoils such as undrained shear strength, N values and effective strength parameters (c’ and ϕ’) are summarized in Table 7.2.

7.3 INSTRUMENTATION PROGRAM AND LAYOUT

The instrument layout plan is shown in Figure 7.1. The instruments consisted of resistance-type strain gauges and inclinometers so that pile bending moment and soil deflection profiles could be measured, respectively. Resistance-type strain gauges were employed, as they were more economical than the commonly used vibrating wire

strain gauges. To ensure that the resistance-type strain gauges function well under harsh and damp conditions during the estimated monitoring period of about 3 months, they were properly waterproofed using resin. The wires connecting the strain gauges were buried underground leading to the strainmeter. The strainmeter was programmed to acquire the strain gauge data at specified intervals automatically.

Since the 4-pile group was symmetrical, it was necessary to instrument only two piles perpendicular to the excavation boundary. Therefore, only the front (nearer to excavation) and rear (further from excavation) piles were instrumented. Owing to concerns over the effects of year-end Singapore monsoon rainstorms at the site, the engineers decided to bring the excavation schedule forward. As such there was a shortage of strain gauges. Hence only a limited number of strain gauges were installed in the two instrumented piles, as shown in Figure 7.3. Figure 7.4 shows the plan and elevation views of the instrumented piles in relation to the excavation, respectively. The centre-to-centre pile spacing is 2.5 m and hence the pile spacing/diameter ratio is approximately 2.8.

7.4 PROPOSED METHOD AND SEQUENCE OF EXCAVATION

The proposed sequence of excavation to reach the soffit level of the underground storage tank can be divided into four stages as follows:

Stage 1

The 900-mm diameter bored piles would be installed first as shown in Figure 7.5(a). Subsequently, sheet piles would be installed behind the proposed excavation area to prevent water from seeping in. Then, the 4-pile group (PG A) would be capped by a 1.5 m thick pile cap.

Stage 2

Excavation would then be carried out to reach the soffit of the basement slab forming a slope with a maximum gradient of 1V:2.5H as shown in Figure 7.5(b). Then, the 4-pile group (PG B) would be capped with a 1.5 m thick pile cap.

Stage 3

Further excavation was proposed to reach the soffit of the proposed underground storage tank at the same gradient as in Stage 2. The soffit of the storage tank would be reached after an excavation of about 5.2 m from the existing ground level. Subsequently, the 4-pile group (PG C) and the single pile (SP 1) would be capped with 1.5 m thick pile caps as shown in Figure 7.5(c). These piles were designed to support the proposed underground storage tank.

Stage 4

The basement slabs and walls of the underground storage tank would then be cast as shown in Figure 7.5(d). The cut slope would be backfilled to the existing ground level. Finally, the sheet piles behind the excavation would be extracted from the ground.

7.5 ACTUAL EXCAVATION AND CONSTRUCTION EVENTS

The early arrival of year-end monsoon rain prevented the Contractor from executing the excavation works according to the proposed method given in Section 7.4. Table 7.3 entails the actual construction and excavation sequence over the 3-month monitoring period. Although the original design called for an open-cut, sheet piles and struts were subsequently installed when large soil movement was recorded,

in particular after the occurrence of the slope failure next to the instrumented pile group. The alignment and location of these sheet piles are shown in Figure 7.1. Some of the major construction events are highlighted as follows:

a) 1-5 Dec 2002 - Installation of strain gauges and inclinometers in the instrumented bored piles.

b) 11 Dec 2002 - Excavation approached the instrumented piles.

c) 12 Dec 2002 - Slope failed next to the instrumented piles due to heavy rain overnight.

d) 17-21 Dec 2002 - Installation of cantilever sheet piles to prevent further slope movement.

e) 20-30 Dec 2002 - Excavation was carried out in front of sheet piles. Further soil movement was recorded.

f) 28 Dec 2002 - 2 Jan 2003 - Installation of strut to reduce sheet pile deflection.

g) 3-10 Jan 2003 - Excavation continued. Further soil movement was recorded.

h) 9 Jan-12 Feb 2003 - Construction of pile cap for piles supporting water tank, casting of basement slab and waterproofing of storage tank wall.

i) 13-25 Feb 2003 - Back filling of cut slope, extraction of sheet piles and compaction.

Snapshots of the excavation process are shown in Figures 7.6. Figure 7.7 shows the actual excavation and construction sequence as described from points (c) to (h) above. The unintended soil failure at the site provided valuable field data on the behaviour of a 4-pile group subject to excavation-induced soil movement.

7.5.1 Measured in-pile and in-soil inclinometer readings

The in-pile inclinometer in the instrumented rear pile (see Figure 7.3) was monitored daily since the start of the excavation. Unfortunately, due to some ground resistance during installation, the in-soil inclinometer (see Figure 7.1 for location) was

only successfully installed on 17 Dec 2002. Therefore, the soil movement that occurred during the slope failure on 12 Dec 2002 was not recorded. However, the pile deflection profile was available. For a clearer presentation, only the measured pile deflection and their corresponding soil movement profiles that occurred during major construction events are presented here. Owing to the presence of the 1.5 m thick pile cap, the top of the pile was restrained from deflecting freely, as shown in Figure 7.8. The worst pile deflection profile was recorded after the completion of the excavation works on 7 Feb 2003. After 13 Feb 2003, the back-filling of the slope and compaction of the backfill had caused the pile to move backwards and hence a reduction in the pile deflection profile. The corresponding soil movement profiles are shown in Figure 7.9.

Figure 7.10 shows the measured lateral pile deflection and soil movement at various depths over the excavation period. It is noted that prior to 26 Dec 2002, the lateral pile deflection is generally greater than the lateral soil movement. After 26 Dec 2002, the latter exceeded the former significantly, especially for the top 7.5 m of the soil, primarily of soft marine clay. This happened during the excavation in front of the slope. This revealed that the unstrutted sheet piles, which were only installed when the soil movement was noted to be as large as 270 mm at the ground surface on 28 Dec 2002, were ineffective.

A drop in the ground water level was noted within the excavation area as indicated by the water standpipe readings shown in Figure 7.11.

7.6 PILE BENDING MOMENT

Bending moment in deep foundation can be estimated using the curvature of the deflection curve obtained from in-pile inclinometer readings. Inclinometer tubes are normally made of PVC and would deflect according to the lateral displacement

curvature. The toe of the inclinometer casing should be embedded into a hard layer or grouted to prevent any toe movement. However, if this cannot be achieved, then the displacement should be referred to the top of the inclinometer tube, which must be surveyed very accurately so that the boundary condition can be accurately established. The use of inclinometer provides a continuous set of deflection data, recommended at every 0.5 m elevation or less. The bending moment profile can then be deduced from the deflection data.

Alternatively, the bending moment at a given pile elevation can be obtained from strain gauges mounted in pairs at each elevation at opposite sides of the reinforcement cage of the pile. The difference in the elongation strains divided by the distance between these two strain gauges at the same elevation gives the measure of curvature. However, in any case, if only one strain gauge at a particular elevation functions properly, then the curvature is calculated using the measured strain divided by the distance from that strain gauge to the neutral axis of the section. Unless many levels of strain gauges are used, a continuous profile of the bending moment cannot be obtained.

The following sections discusses the available pile capacity, the calculation of suitable moment of inertia for the pile and finally the computation of the pile bending moment from the measured inclinometer and strain gauge readings.

7.6.1 Pile capacity

The cracking moment, M_{cr} is calculated based on:

$$M_{cr} = f_{ct}Z \tag{7.1}$$

where f_{ct} is the tensile strength of concrete in flexure or the modulus of rupture of concrete and equals to $0.623f'^{0.5}_{c}$ (in MPa), f'_c is the characteristic strength of concrete (in MPa), Z is the section modulus ($=I_g/y$), I_g is the gross moment of inertia and y is the distance from the centroid of the section to the extreme fibre in tension. For the 900-

mm diameter bored pile, the cracking moment is calculated to be 264 kNm. The cracking moment is the minimum bending moment required to initiate a crack in the pile. Since concrete is weak in resisting tension, steel is an important element that can increase the bending moment capacity of the pile.

When a pile reaches its ultimate capacity, the concrete in compression will be crushed and the steel reinforcement will yield causing the load carrying capacity of the pile to decrease significantly resulting in structural distress. The ultimate bending moment capacity of a pile can be calculated using the moment interaction diagram proposed by Mohammad and Merrony (1996), as shown in Figure 7.12. The ultimate bending moment capacity, M_{ult}, of this 900-mm diameter bored pile with nominal 0.5 % steel reinforcement works out to be about 520 kNm, which is just about two times the cracking moment, M_{cr}, of the pile. In comparison, the ultimate bending moment capacity for the 1075-mm diameter bored pile with 3 % steel reinforcement used by Chandrasekaran et al. (1999) was about 3000 kNm. The reason behind this superior ultimate bending moment capacity is the much higher percentage of steel provided, as Chandrasekaran et al. (1999) anticipated additional bending moment due to soil movement. It is evident that the engineers had not designed the 900-mm bored piles against any soil movement, as the large soil movement caused by the slope excavation at the site was not anticipated.

7.6.2 Average moment of inertia

A pile develops bending moment when subject to lateral soil movement. If the bending moment exceeds the cracking moment, M_{cr} of the pile, cracks would start to develop. In the presence of cracks, the tensile stress is assumed to be resisted completely by the reinforcement. Nevertheless, the depth and width of cracks may vary, depending on the bending moment distribution along the pile. However, there

may also be some sections along the pile where the M_{cr} is not exceeded and hence, cracks are not formed. For instance, the concrete between cracks may still be capable of carrying some tension. As a result, the actual effective moment of inertia, I_e, will be somewhat in between the uncracked, I_g, and the fully cracked, I_{cr} values. Branson (1977) mentioned that in such a situation, the moment of inertia used to represent the entire pile would be the average effective moment of inertia, I_e. The significance of using an average I_e value for the entire pile length is to ensure a smooth bending moment profile. Such a method has also been used by Reese (1997) to analyse the cracking behaviour of laterally loaded piles. The method used by Reese (1997) employed the average observed deflection, the applied loading and iteration to find the values of the average EI and the corresponding values of maximum bending moment that fitted the results. In such computations, the value of EI was changed for the entire pile for ease in the computations.

A fundamental assumption of bending theory for a simple beam is that plane sections remain plane. This means that traverse planes of a beam, which are flat before any load is applied remain flat after the bending moment is applied, that is, they simply rotate slightly but do not distort. Values of the ultimate strain of concrete and steel have to be selected to reflect their failure because the non-linear stress-strain curves for these materials do not indicate a condition for collapse. Therefore, it is often assumed that concrete fails in compression when it reaches the ultimate compressive strain of 0.003. For the reinforcing steel, the ultimate value of strain is 0.015. Steel is assumed to have a linear stress-strain relation until the yield stress is attained and beyond which, the stress in the steel remains constant as the strain increases or strain hardening is neglected. This results in a linear variation of strain with distance from the neutral axis, with no limit to the amount of plastic deformation in both tension and compression.

The following paragraphs present the application of simple beam theory to calculate the I_g, I_{cr} or I_e based on existing simple design charts.

MacGregor (1988) did a comparison between circular and rectangular reinforced concrete columns by using the conservation of area method. An axial load-bending moment interaction diagram as shown in Figure 7.13 is used to describe the behaviour of both columns under similar loading conditions. It was shown that a discrepancy of only 5 % was observed in the case of pure bending (no axial force) for the two different sections. Nevertheless, discrepancies may arise due to the eccentricity ratio of the column when axial load is present. Therefore, the assumption of area conservation to transform a circular section to a rectangular one so that the beam theory can be used for the case of pure bending (no axial load) is acceptable for this study.

For a fully cracked section, the stresses in the steel and concrete are assumed to be proportional to the strains. The cracked moment of inertia, I_{cr} of a rectangular section is given by Kong and Evans (1987) as:

$$I_{cr} = bd^3\left[\frac{1}{3}\left(\frac{x}{d}\right)^3 + \alpha_e\rho\left(1-\frac{x}{d}\right)^2 + \alpha_e\rho'\left(\frac{x}{d}-\frac{d'}{d}\right)^2\right] \qquad (7.2)$$

where

$$\frac{x}{d} = -\alpha_e(\rho+\rho') + \sqrt{\alpha_e^2(\rho+\rho')^2 + 2\alpha_e\left(\rho+\frac{d'}{d}\rho'\right)}$$

$$\alpha_e = \frac{E_s}{E_c} \text{ (modular ratio)}$$

$$\rho = \frac{A_s}{bd} \text{ (ratio of compression steel)}$$

$$\rho' = \frac{A_s'}{bd} \text{ (ratio of tension steel)}$$

d = effective depth

d' = depth from compression zone to centroid of compression steel

x = depth of neutral axis

b = width of concrete section

Alternatively, readily available design charts such as that shown in Figure 7.14 can also be used to evaluate I_{cr}.

For an uncracked section, since the pile is only reinforced with 0.5 % steel, it can be considered as a lightly reinforced pile. Branson (1977) indicated that for lightly reinforced concrete structure, the gross moment of inertia, I_g of the section can be used. As such, the gross moment of inertia, I_g for a circular section is given by:

$$I_g = \frac{\pi d^4}{64} \tag{7.3}$$

Nonetheless, if in any case that a heavily reinforced section (e.g. 3 % steel) is used, it would be more accurate to use the uncracked moment of inertia, I_{uncr} (Branson, 1977). Based on the conservation of area method, the I_{uncr} for a circular pile can be approximated (Kong and Evans, 1987):

$$I_{uncr} = \frac{1}{12}bh^3 + bh\left(x - \frac{h}{2}\right)^2 + \alpha_e A_s'\left(x - d'\right)^2 + \alpha_e A_s\left(d - x\right)^2 \tag{7.4}$$

where h = total depth of the concrete section and the other symbols remain similar as above.

Finally, for an intermediately cracked section, the effective moment of inertia, I_e is given by Branson (1977) and ACI (1989):

$$I_e = \left(\frac{M_{cr}}{M}\right)^4 I_{uncr} + \left[1 - \left(\frac{M_{cr}}{M}\right)^4\right] I_{cr} \le I_{uncr} \tag{7.5}$$

By adopting Eqs. (7.2) and (7.3), the I_{cr} and I_g of pile is calculated to be 0.00607 m^4 and 0.03221 m^4, respectively for the 900-mm bored piles. The Young's modulus, E_c, for Grade 35 concrete is 32000 MPa.

In structural engineering, the distribution of load on a beam can be readily calculated and thus, the applied moment, M, or moment diagram can be produced for the entire span of the beam so that standard equation like Eq. (7.5) can be used to calculate I_e. However, in this study, the applied moment, M, is unknown and thus Eq. (7.5) cannot be used. Nonetheless, it has been established earlier that the pile is lightly reinforced and the M_{ult} is only twice the M_{cr}. Figure 7.15, which is derived from Eq. (7.5) by Branson (1977), shows the generalized moment of inertia against bending moment relation in the cracking range. By using I_g/I_{cr} of 4.0 (since I_g/I_{cr} = 5.0 is not available in Figure 7.15), the M/M_{cr} ratio is about 3.0, if I_e/I_g = 0.25 is assumed. Had I_g/I_{cr} of 5.0 been used instead, the M/M_{cr} ratio was expected to be approximately 2.6. The M/M_{cr} ratio will be subsequently checked. From the computed ratio I_e/I_g = 0.25, I_e has a value of 0.00805 m^4, which is reasonably close to that of I_{cr} whose value is 0.00607 m^4. This is consistent to the observation that the pile is lightly reinforced and that the M_{ult} is only twice the M_{cr}. Hence, in this study, I_e can be approximated (without large errors) to be equal to I_{cr} and be used as the average moment of inertia for the calculation of pile bending moment, if and only if the M_{cr} of the pile is exceeded in cases where the soil movement profiles are severe. This simple analytical method by Branson (1977) only serves as a good first approximation of I_e and hence, further validation using numerical method is necessary. Errors in using constant values of I_e in the regions of low values of bending moment are thought to be small (Reese, 1997). This method is particularly suitable for the first approximation in this study

because in both Eq. (7.5) and in the field work, axial load is absent and hence, the computation is more straightforward.

7.6.3 Calculation of pile bending moment

Since the strain gauges were fastened to the opposite faces of the reinforcement cage and perpendicular to the excavation face through proper installation procedure, the output readings of the strain gauges give the strain readings directly. As strain is a function of the stress and the Young's modulus of steel, E_{st}, the curvature, ψ of the pile can be obtained from the sum (if different signs) or difference (if similar signs) in the strains in tension, ε_t, and compression, ε_c, steel reinforcement divided by the distance between them:

$$\psi = \frac{\varepsilon_t - \varepsilon_c}{d - d'} \tag{7.6}$$

Such a method was also used by Poh et al. (1999). Hence, with the curvature and the flexural rigidity, E_cI of the pile known, the bending moment can be calculated based on Macaulay's method:

$$M = \psi E_c I \tag{7.7}$$

where E_c = Young's modulus of concrete and the moment of inertia, I can be either the I_g, I_{cr} or I_e depending on the degree of cracking of the pile. In computing the bending stiffness, the value of E_c is assumed to remain constant (Reese, 1997).

Inclinometer readings can be employed to obtain the bending moment profile. Poh et al. (1999) established that high order polynomials are necessary to fit the measured deflection profiles. To obtain a good fit between the measured and fitted deflection profiles, a 7^{th} order polynomial function is used in the present study. Differentiating the pile deflection profile twice would give the curvature along the pile.

With the curvature along the length of the pile known, the bending moment profile can then be computed using Eq. (7.1).

A sensible way to start predicting the condition of the pile is to use the gross moment of inertia, I_g, as the first approximation. Since all the pile deflection profiles are similar in trend as shown in Figure 7.8, a trial and error process is performed to obtain the minimum pile deflection profile that initiates cracking or when the pile M_{cr} is reached. This minimum pile deflection profile and its fitted 7^{th} order polynomial function are shown in Figure 7.16. When the fitted 7^{th} order polynomial function is differentiated twice, the corresponding pile bending moment profile is obtained as shown in Figure 7.17. At this stage, the pile bending moment at depth 12.5 m just reaches its M_{cr} value. As the top of the piles are tied to the pile cap with relatively high percentage of steel, the negative bending moment at the pile cap level is smaller in absolute magnitude than the maximum positive bending moment that developed along the lower part of the pile, where the steel reinforcement of the pile is nominal.

Unfortunately, the first measured pile deflection profile obtained was on 11 Dec 2002 (see Figure 7.8), at the time when the excavation had already begun. Therefore, at this particular point in time, the pile has already cracked as the deflection profile measured on 11 Dec 2002 is much greater than the minimum value for crack initiation, as shown in Figure 7.16. This again verifies the earlier assumption that the pile is a lightly reinforced one, whose cracking resistance due to soil movement is very low.

In order to show that there exists different degrees of cracking along the length of the pile as described above and that an average I_e is necessary to compute a smooth bending moment profile, the ratio of the back-analysed bending moment, M and the cracking moment, M_{cr} is plotted against the ratio of the measured deflection, D and the

initial deflection at the onset of cracking, D_i (Figure 7.18) at different depths along the pile for the selected back-analysed pile responses between 11 Dec 2002 and 17 Jan 2003. Three typical zones can be evidently identified as shown in Figure 7.18. Zone 1 is identified as the zone where the pile experiences no cracking at all and hence the assumption of gross moment of inertia, I_g, for the pile is valid. This coincides with data points measured at depth of 15 m for the medium dense clayey sand layer with SPT blow counts of between 10 and 30. The higher resistance of the sand and attenuated lateral soil movement might have prevented the pile from being deflected excessively.

The measured data points in Zone 2 are obtained from the pile responses at depths of 3 m, 5 m and 9 m below the ground surface. It is evident that these data points are somewhat nestled between the two extremes of Zones 1 and 3. These depths are dominated by the soft marine clay, whose soil resistance is relatively smaller than that of sand. The rate of increase of the M/M_{cr} ratio is not as high as that noted in Zone 1, suggesting that cracking of the pile might be on-going and hence, an effective moment of inertia, I_e would best present this zone.

Zone 3 represents the measured data points obtained from the pile responses at depth of 12.5 m, which coincides with the location of maximum pile bending moment. As such the M/M_{cr} and D/D_i ratios are the greatest compared to those in Zones 1 and 2. The M/M_{cr} ratio for Zone 3 is about 2.6, which is consistent to the earlier assumption made in Section 7.6.2. Thus the assumption of a fully cracked pile having a fully cracked moment of inertia, I_{cr} can be justifiably used at this depth along the pile.

The pile behaviour at different degrees of cracking as observed in Figure 7.18 shows similar trend to that postulated by the European Concrete Committee (see Figure 7.19) and is described in greater detail by Branson (1977). This chart is typically known as the bilinear moment-deflection curve, which suggests that while the

moment capacity of the pile reduces at increasing load levels, the pile deflection increases corresponding to the increasing degree of cracking of the pile. This would transform the pile from an initially uncracked one (Zone 1 of Figure 7.18) when there is no cracking to that of an intermediately cracked pile (Zone 2) and finally to a fully cracked pile (Zone 3) when large degree of cracking has occurred.

As described earlier, the significance of using an average moment of inertia for the entire pile length is to ensure a smooth bending moment profile. Therefore, I_{cr} is adopted as the average moment of inertia as described in Section 7.6.2. and is used for all the subsequent back-analyses. The results of the pile deflection and the corresponding calculated bending moment profiles on 4 occasions are shown in Figure 7.20. The measured pile deflection profiles obtained from in-pile inclinometer installed in the rear piles reveal that the pile deflected considerably above 14 m depth. For the rear pile, the bending moment profile obtained from the inclinometer deflection profile and from strain gauges at 4 elevations shows reasonable agreement. For the front pile, only the bending moment obtained from the strain gauges is shown as no inclinometer has been installed.

7.7 NUMERICAL PREDICTION

The numerical method by Chow and Yong (1996) described in Chapter 6 is used to further evaluate the field data. The soil properties used in the numerical analysis are shown in Table 7.2. As discussed in Section 6.5.1, the limiting soil pressure/soil strength ratio, K, of 6 is used because the post-excavation soil undrained shear strength is not available. The stiffness rigidity of the pile cap is calculated to be 2.7×10^7 kNm^2. The fully cracked moment of inertia, I_{cr}, is used as discussed before, since the piles are nominally reinforced and experience large deflection and soil movement. Therefore,

the fully cracked bending rigidity, EI_{cr}, of the pile is 133422 kNm^2. The input soil movement profiles are obtained from the in-soil inclinometer readings.

Figure 7.20 show the comparison between the measured and predicted bending moment and deflection profiles of the piles. It is noted that the shapes of the measured and predicted bending moment profiles and the elevation of their maximum values are similar. Unfortunately, the strain gauges in both piles are several metres above the maximum bending moment elevation. Figure 7.10 shows that after 26 Dec 2002, the soil at 10 m below the ground surface had moved ahead of the pile. This suggests a typical soil "flow" phenomenon where the soil pressure is approaching its limiting values, similar to that reported in Chapter 4. Therefore, limiting soil pressure, p_y, given in Table 7.2 for the clay layer based on the recommendation of Chapter 6 are used in the numerical back-analysis.

Figure 7.20(a) shows a fair agreement between the predicted and measured pile responses on 28 Dec 2002. This date coincides with excavation around the piles to facilitate the installation of the pile caps. Figure 7.7 reveals that at this stage, the excavation has reached about 5 m below the existing ground level. Figure 7.20(b) shows the predicted and measured pile responses on 31 Dec 2002 when excavation progressed further, but with a strut put in place at the top of the sheet pile to prevent further soil movement. Unfortunately, the strut was not stiff enough to prevent further soil movement. As a result, the soil moved considerably till a greater depth inducing a larger bending moment and deflection on the pile. The predicted and measured pile responses also show reasonable agreement (see Figure 7.20(b)) at this stage.

Figure 7.9 reveals that on 6 Jan 2003, a substantial increase in lateral soil movement was recorded when excavation depth reached 6.0 m (see Figure 7.7). This caused the partially embedded pile cap and the top of the piles to be further loaded by

the moving soil. As the current numerical method cannot model the embedded reinforced pile cap, it is not surprising that the negative pile bending moment of the rear pile at the pile cap elevation cannot be predicted accurately as shown in Figure 7.20(c). Additional soil movement was also recorded during the casting of the pile cap on 17 Jan 2003 (see Figure 7.9). Similarly, the measured pile responses are well under-predicted especially at the pile cap level of the rear pile and at depths of between 5 and 10 m of the front pile. The measured pile deflection profiles are also well under-predicted. Therefore, it can be surmised that the numerical method underestimates the maximum negative and positive bending moment values at the pile cap level and at depth of about 12.5 m, respectively. This could be due to the presence of reinforcement provided for connecting the pile top to the pile cap that could not be directly modelled in the numerical analysis.

Figure 7.21 shows the comparison between the measured and predicted maximum pile bending moment of the rear pile over the excavation period. As mentioned before, the rear pile had already cracked prior to the start of acquiring the in-pile inclinometer data. After 26 Dec 2002, the pile experienced increasingly large soil movement as shown in Figure 7.10. This helps to suggest that after 26 Dec 2002, the extent of cracking along the pile had increased. This is supported by the fact that when I_{cr} is used in the numerical analysis after 26 Dec 2002, consistent predictions that yield about 18 % difference of the measured values are observed, as shown in Figure 7.21. The figure also shows that the ultimate pile bending moment has been exceeded after 31 Dec 2002. This signifies that the instrumented piles have been damaged by excessive soil movement during the excavation. Thus, these piles are deemed unfit to carry the design column loads and a replacement pile group is deemed necessary.

By comparing Figures 7.10 and 7.21, it is evident that after 5 Jan 03 the rate of increase of pile bending moment actually reduces, despite the pile experiencing increasing soil movement. This observation is consistent to that made in Chapter 5 that as the soil starts to yield or approaches failure, the development of the pile bending moment would not increase further as its limiting soil pressure values is being reached due to progressive stress relief caused by excavation.

7.8 SUMMARY

This field study involving an instrumented pile group behind an excavation that subsequently failed has shed some light on the importance of designing piles to withstand the detrimental effects of lateral soil movement on piles. The pre- and post-failure pile behaviour of the unintended failure has provided valuable data necessary for analysis and further understanding.

This field study has demonstrated that the extent of the cracked section along a pile depends on the soil condition and pile embedment depth when plotted using the bi-linear moment-deflective curve method proposed by Branson (1977). For the case of pure bending as in this case study, the conservation of area method can be used to transform a circular section to a rectangular one such that the readily available design charts for the more common rectangular beam section can be utilized. Therefore, the gross, I_g and fully cracked I_{cr} moment of inertia can be determined. This is necessary as further development of cracks along a pile would transform the pile from an initially uncracked pile to that of an intermediately cracked pile and finally to a fully cracked pile when large degree of cracking has occurred. It has also been demonstrated that the calculation of the average effective moment of inertia, I_e can be complicated, but necessary, in order to obtain a smooth pile bending moment profile. The numerical

analysis has been deployed to back-analyse the field results and it has been found that the measured and predicted pile bending moment and deflection profiles are generally consistent in trend. Therefore, the findings of this field study complement those of centrifuge experiments reported in Chapters 4 and 5 and numerical back-analyses presented in Chapter 6 as all the results reveal that the development of pile bending moment is influenced by the limiting soil pressure associated with the progressive stress relief due to excavation.

Table 7.1 Soil physical properties for BH 1 (after Moh, 2001)

Borehole No.	Sample No.	Depth (m) From	Depth (m) To	Specific Gravity	Liquid Limit (%)	Plasticity Index	Natural Moisture Content (%)	Total Unit Weight (kN/m³)	Grain Size (%) (ASTM) Gravel	Sand	Silt	Clay	Unified Classification	Soil Layer No.
BH-1	UD-1	3.00	3.70	-	-	-	99.3	13.86	-	-	-	-	-	1
	UD-2	5.00	5.80	-	119	89	84.0	14.69	4		24	72	CH	1
	UD-3	7.50	8.40	2.73	-	-	28.3	18.59	0	69	31		-	2
	UD-4	10.50	11.40	-	37	19	24.7	18.18	0	69	10	21	SC	2
	S-3	12.00	12.45	-	-	-	22.6	20.03	0	68	32		-	3
	UD-5	13.50	13.90	-	-	-	15.6	19.70	0	82	18		-	4
	S-6	19.00	19.45	-	-	-	17.8	21.30	32		32	36	-	4
	S-8	23.00	23.45	2.72	-	-	15.7	21.77	20		41	39	-	5
	S-9	25.00	25.45	-	-	-	25.7	20.66	0	78	22		-	5
	S-12	31.00	31.45	-	-	-	12.6	21.68	2	75	23		-	6

Table 7.2 Geotechnical parameters of subsoil layers

Layers	Depth m	c_u vane kPa	w %	LI	γ kN/m3	Effective parameters c' kPa	Effective parameters ϕ' deg	SPT	E_{sand} kPa	K_h kPa	p_y kPa
Fill	0.1				18.00	0.10	28	1	1500	1500	6.81
	0.5				18.00			1	1500	1500	29.10
	1				18.00			1	1500	1500	68.05
	1.5				18.00			1	1500	1500	102.08
Marine clay	2	10.30	99.30	0.78	13.86	0.10	23	0		3605	61.80
	2.5	10.30	99.30	0.78	13.86			0		3605	61.80
	3	10.30	99.30	0.78	13.86			0		3605	61.80
	3.5	10.30	99.30	0.78	13.86			0		3605	61.80
	4	10.30	99.30	0.78	13.86			0		3605	61.80
	4.5	10.30	99.30	0.78	13.86			0		3605	61.80
	5	10.30	99.30	0.78	13.86			0		3605	61.80
	5.5	10.70	84.00	0.61	14.69			0		3745	64.20
	6	10.70	84.00	0.61	14.69			0		3745	64.20
	6.5	10.70	84.00	0.61	14.69			0		3745	64.20
	7	10.70	84.00	0.61	14.69			0		3745	64.20
	7.5	13.30	28.30	-0.02	18.59			0		4655	79.80
Med stiff	8				18.59	2.00	30	5	7500	7500	647.28
sandy clay	8.5				18.59			6	9000	9000	675.11
	9				18.59			7	10500	10500	730.02
	9.5				18.59			7	10500	10500	758.98
	10				18.59			7	10500	10500	808.68
Loose medium	10.5					5.00	30	10	15000	15000	790.97
clayey sand	11							12	18000	18000	828.63
	11.5				18.18			14	21000	21000	859.27
	13				20.03			18	27000	27000	965.73
	13.5				20.03			22	33000	33000	1017.71
	14							25	37500	37500	1054.62
Dense	14.5				20.00	10.00	33	38	57000	57000	1538.51
clayey sand	15							38	57000	57000	1555.46
	15.5				20.00			38	57000	57000	1616.09
	16							29	43500	43500	1659.15
	16.5							29	43500	43500	1711.00
	17				20.00			29	43500	43500	1758.62
	19				20.00			29	43500	43500	1970.25
Very dense	21				21.00	10.00	35	36	54000	54000	2598.51
clayey sand	23.5				21.00			52	78000	78000	2943.49
	24				21.00			58	87000	87000	3041.63
	26				21.00			64	96000	96000	3203.49
	28				21.00			64	96000	96000	3449.15
	30				21.00			64	96000	96000	3662.06
	31				21.00			64	96000	96000	3840.25
Very dense clayey sand	36.42				21.00	15.00	35	100	150000	150000	4059.75

Table 7.3 Schedule of actual construction and excavation process

No.	Activity	30-Oct-02	Dec-02																												
		5-Dec-03	1	2	3	4	5	6	7	8	9	10	11	12	13	14	15	16	17	18	19	20	21	22	23	24	25	26	27	28	29	30	31
1	Installation of strain gauges in bored piles and laying of cables underground.																														
2	Excavation starts from easterly to westerly direction - Excavation approaches the instrumented piles																														
3	Heavy rain causes slope failure next to the instrumented piles																														
4	Areas affected by slope failure are backfilled with sand																														
5	Installation of sheet piles at the toe of the slope to facilitate excavation for piles																														
6	Excavation in front of the sheet piles at the toe of slope																														
7	Installation of struts after excavation of approximately 1.0m																														

No.	Activity	Jan-03																													
		1	2	3	4	5	6	7	8	9	10	11	12	13	14	15	16	17	18	19	20	21	22	23	24	25	26	27	28	29	30	31
7	Installation of struts after excavation of approximately 1.0 m																														
8	Locating and further excavation for installed piles at toe of slope																														
9	Localised excavation to recover pile head and hacking of pile head to appropriate cut-off level																														
10	Slope surface is sprayed with lean concrete																														
11	Construction of pile cap for piles at toe of slope																														

No.	Activity	Feb-03																											
		1	2	3	4	5	6	7	8	9	10	11	12	13	14	15	16	17	18	19	20	21	22	23	24	25	26	27	28
11	Construction of pile cap for piles at toe of slope																												
12	Casting of basement slab and waterproofing of tank wall																												
13	Back filling																												
14	Extraction of sheet piles																												
15	Compaction prior to placement of lean concrete on backfilled material																												

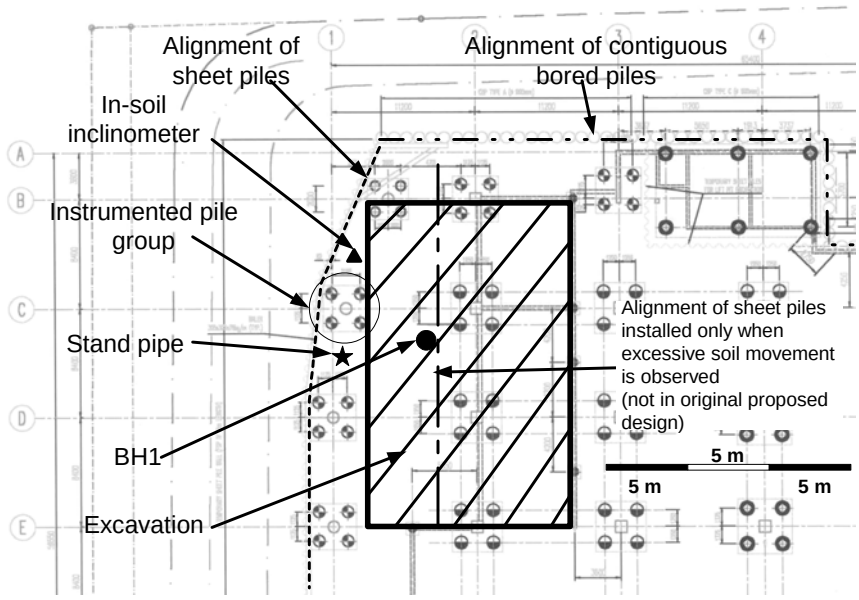

Note: BH4 is located 50 m to the east of BH 1 and not shown for clarity

Figure 7.1 Location of instruments and piling layout

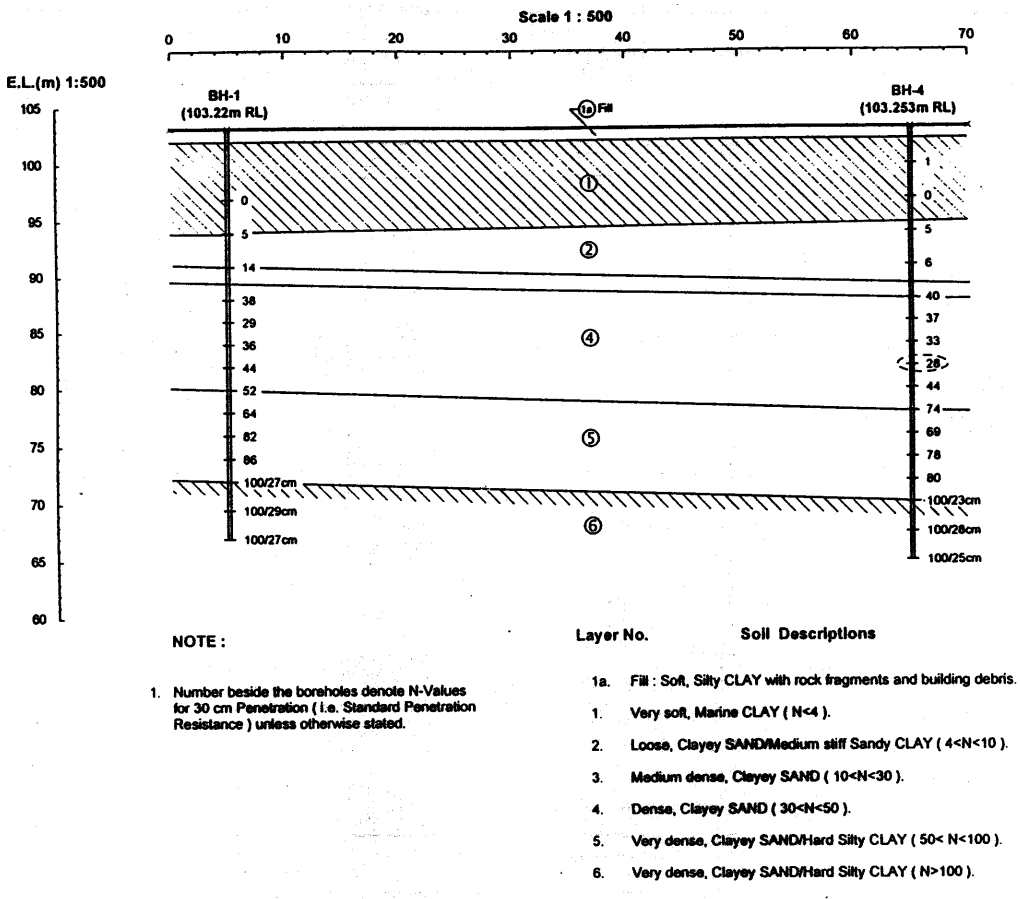

Figure 7.2 Subsurface profile (after Moh, 2001)

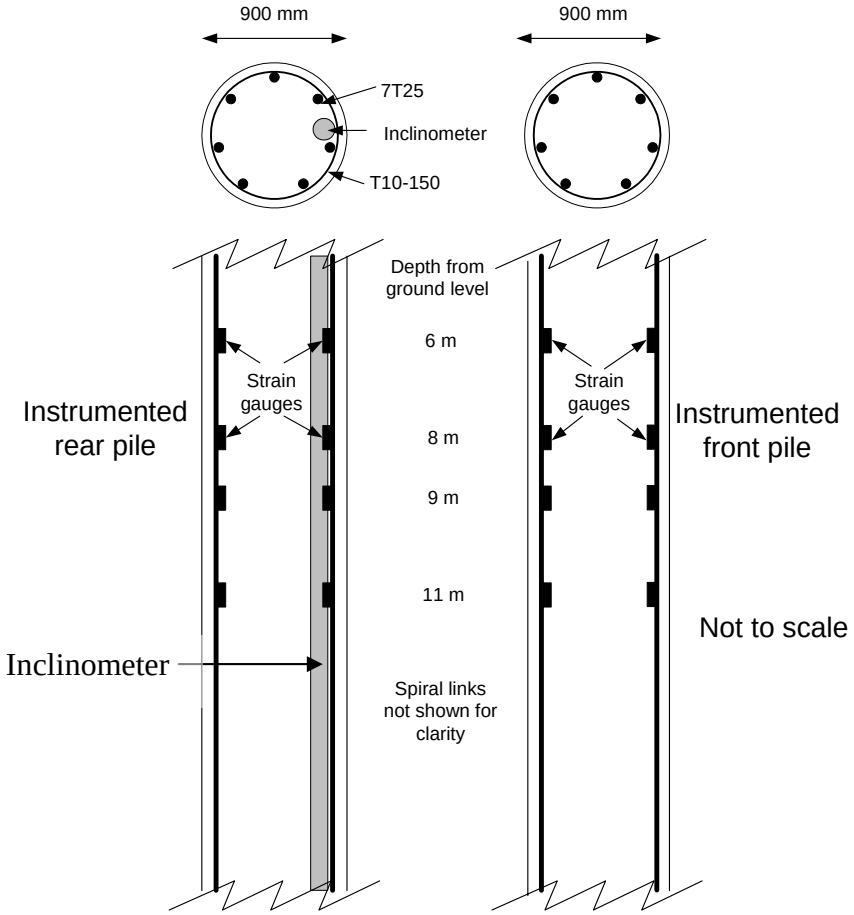

Figure 7.3 Layout of instruments attached to reinforcement cages of bored piles

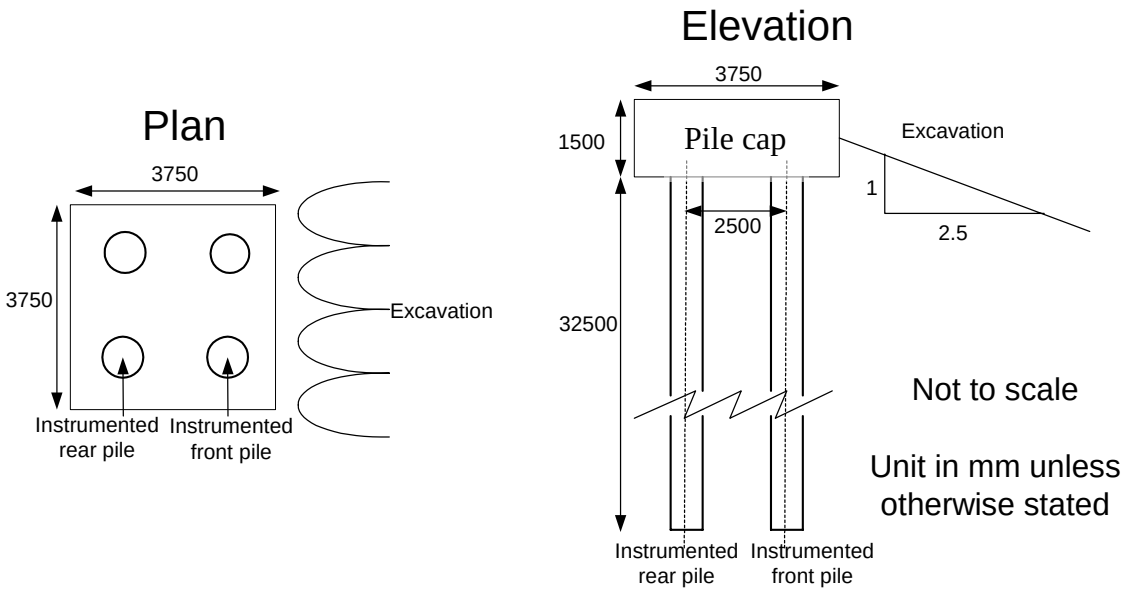

Figure 7.4 Plan and elevation views of instrumented pile group

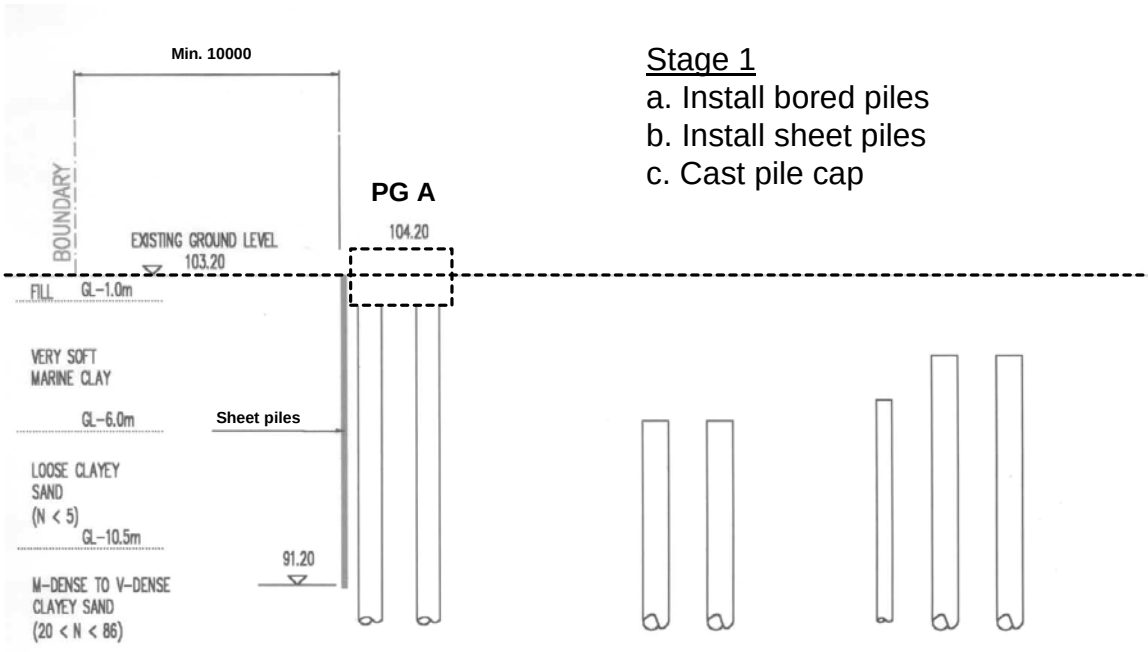

(a) Stage 1

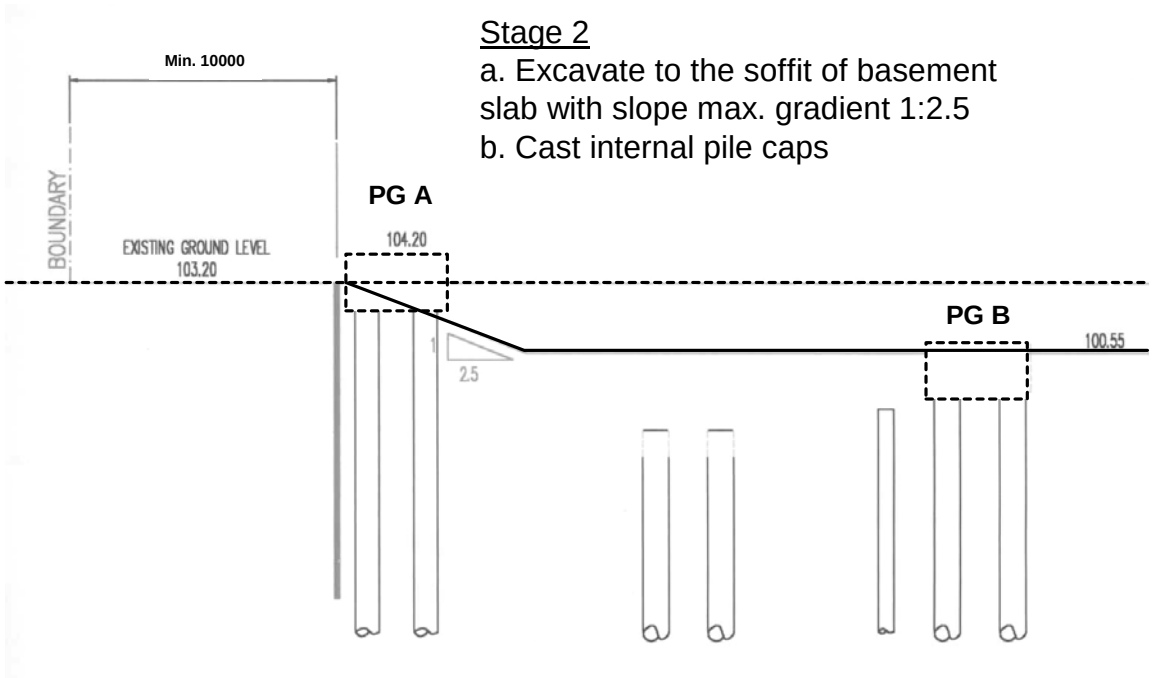

(b) Stage 2

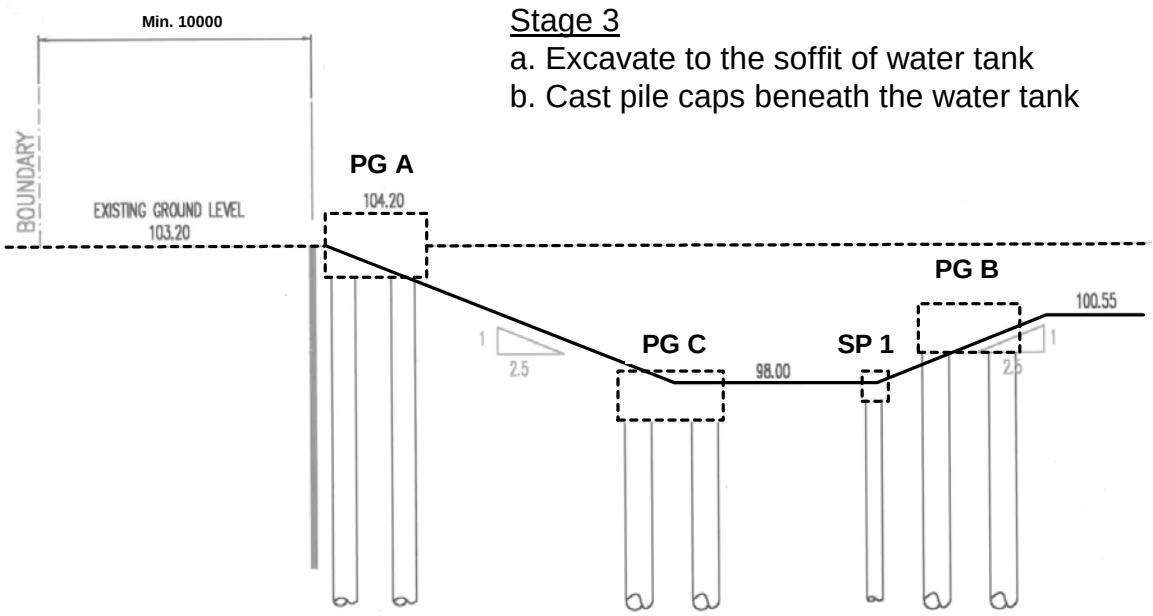

(c) Stage 3

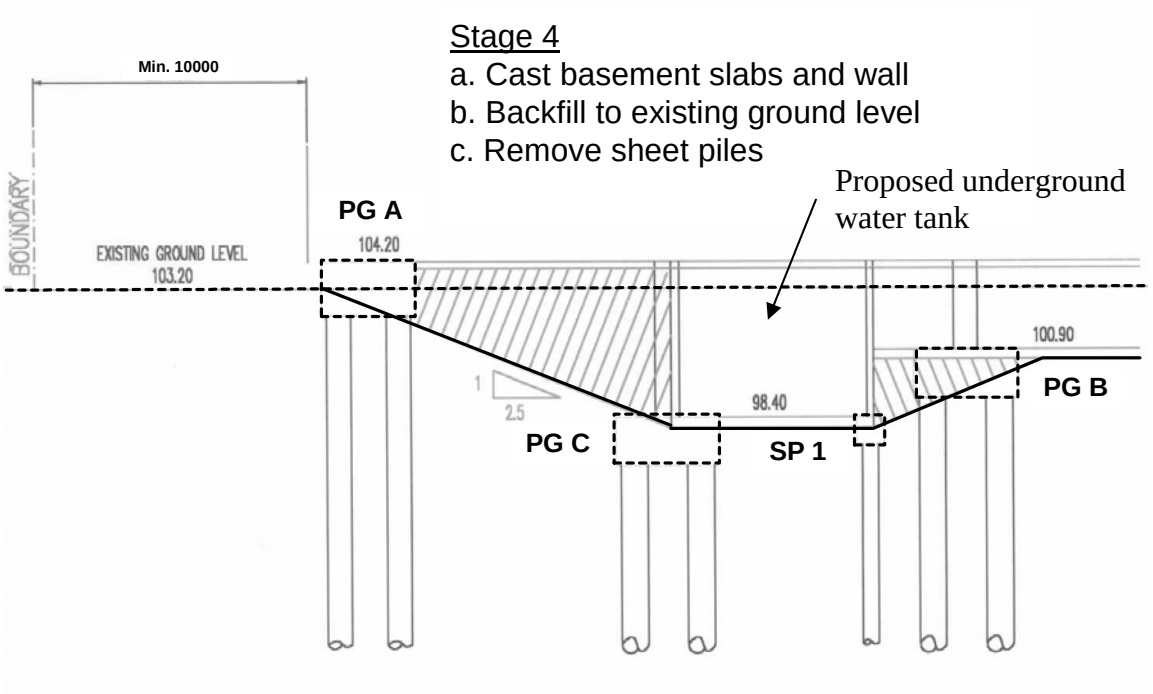

(d) Stage 4

Figure 7.5 Proposed excavation sequence

(a) Lowering of reinforcement cage into the ready-to-cast bored pile (5 Dec 2002)

(b) Slope failure next to instrumented pile group (12 Dec 2002)

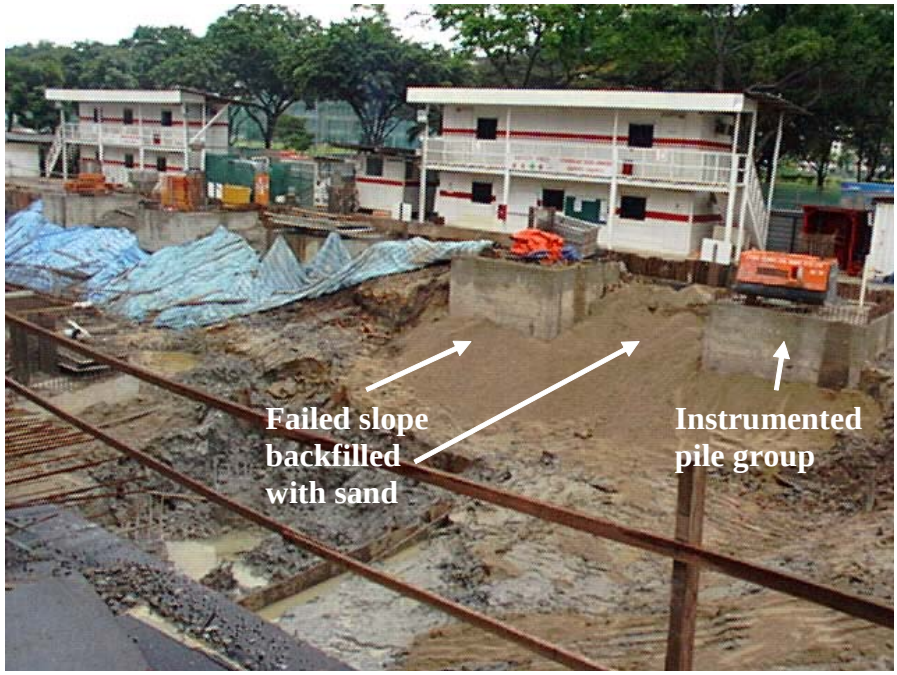

(c) Failed slope being backfilled temporarily with sand (13 Dec 2002)

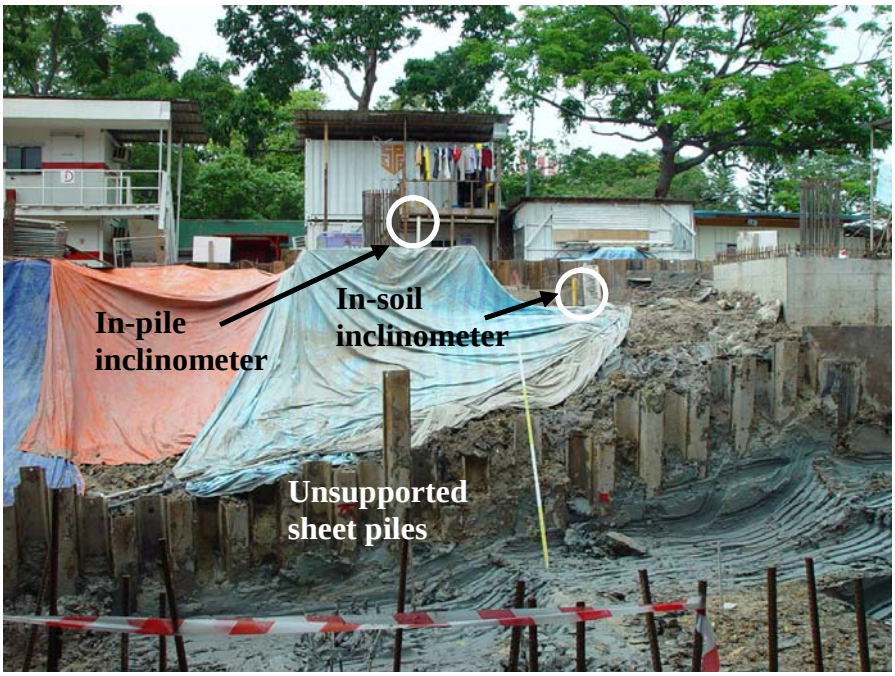

(d) Excavation in front of sheet piles at toe of slope (20 – 30 Dec 2002)

(e) Deflected sheet piles due to excessive soil movement (26 Dec 2002)

(f) Another view of deflected sheet piles due to excessive soil movement (26 Dec 2002)

(g) Installation of struts when soil movement is uncontrollable (28 Dec 2002 – 2 Jan 2003)

(h) Casting of pile caps for underground water storage tank (9 – 17 Jan 2003)

Figure 7.6 Photographs of major events at site

Excavation period	Excavation sequence
12 Dec 02	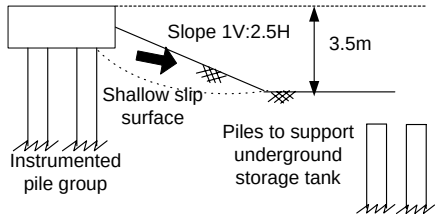
12 - 17 Dec 02	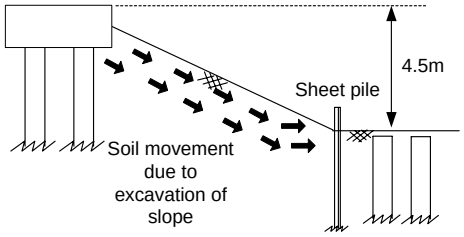
20 - 30 Dec 02	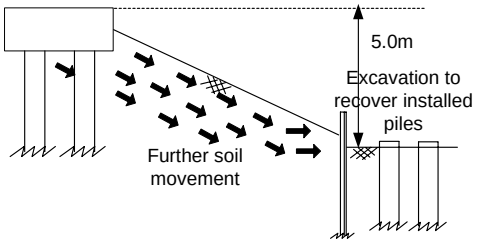
28 Dec 02 - 2 Jan 03	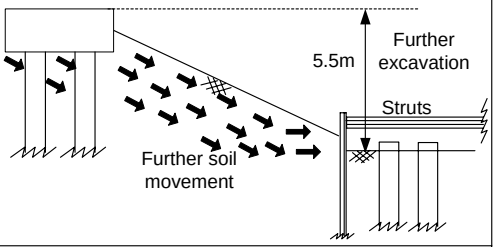
3 - 10 Jan 03	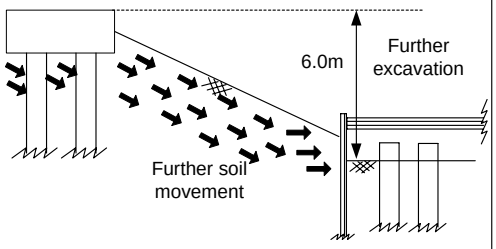
9 Jan - 12 Feb 03	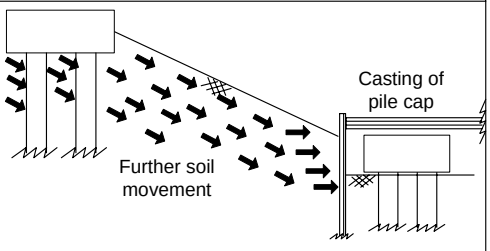

Figure 7.7 Actual excavation and construction sequence

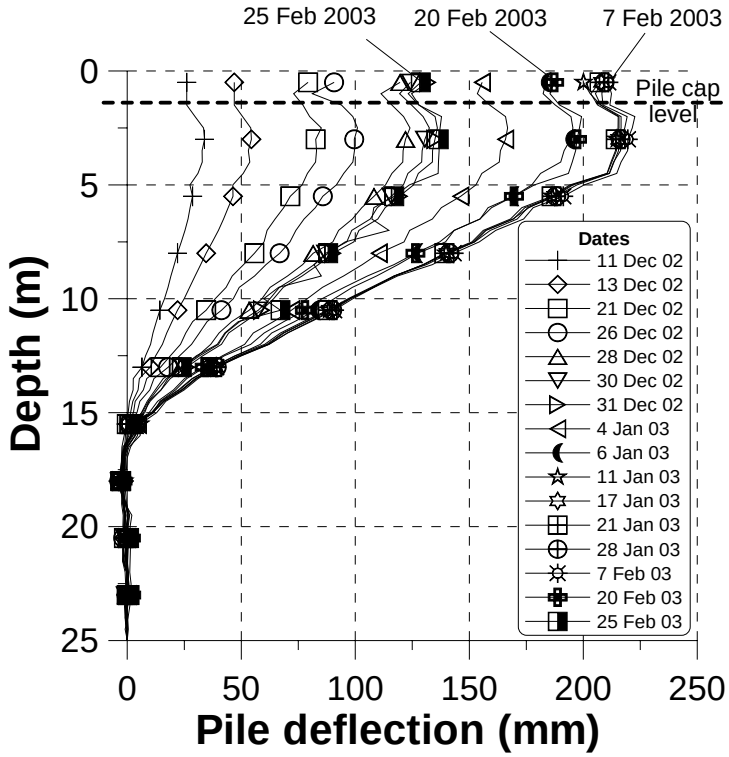

Figure 7.8 Measured deflection profiles of rear piles

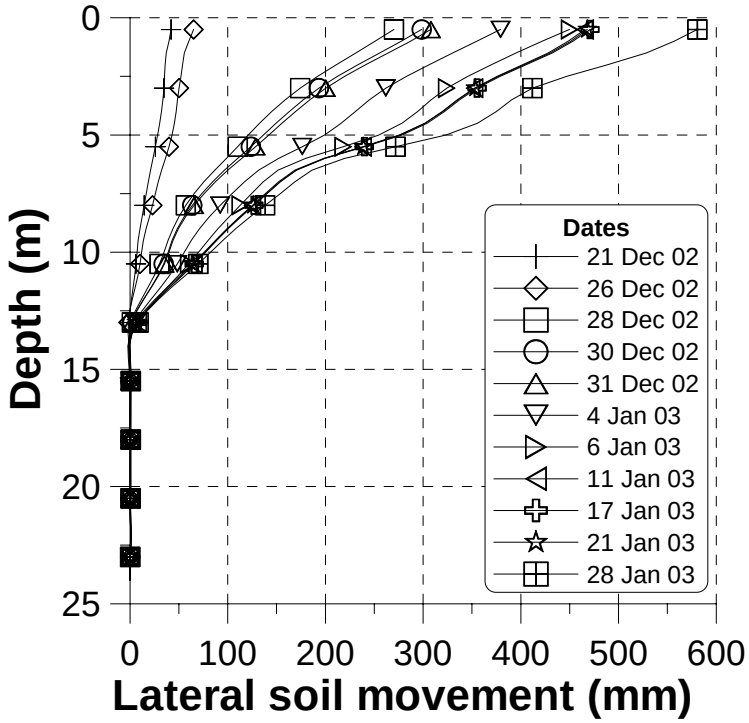

Figure 7.9 Measured lateral soil movement profiles

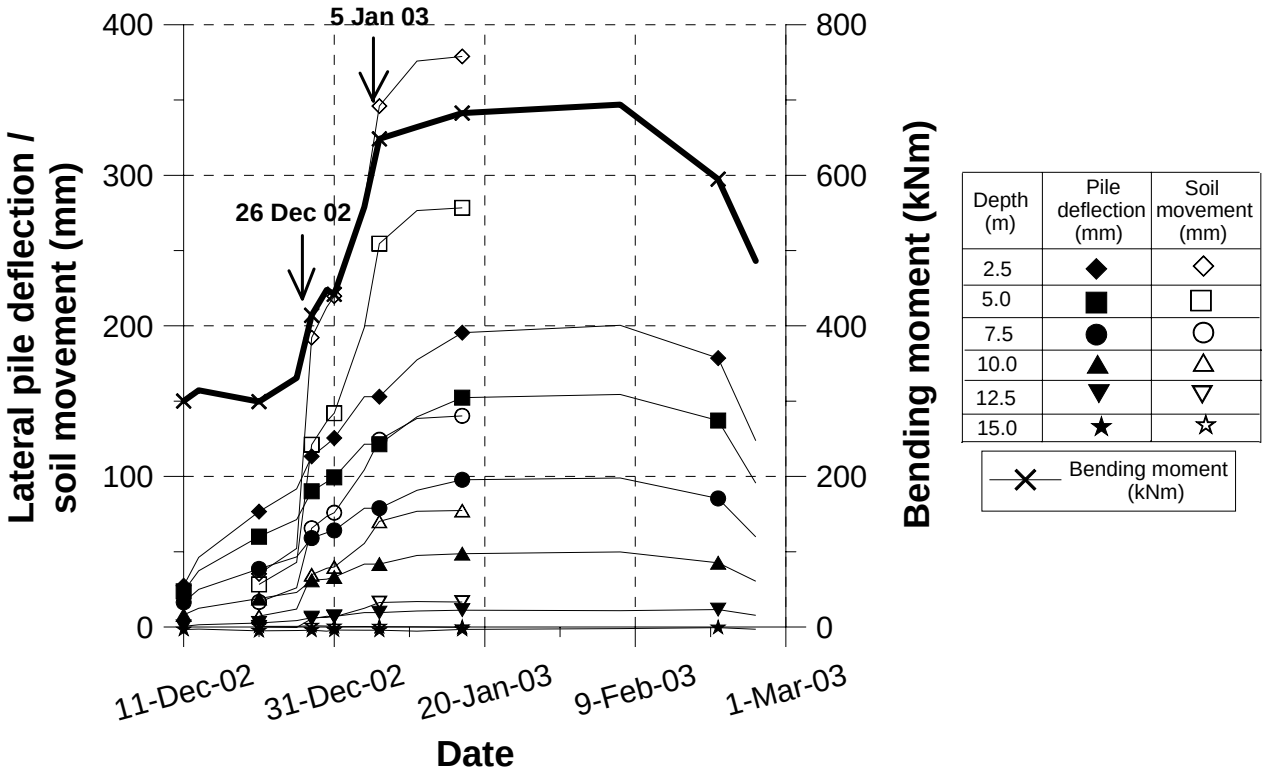

Figure 7.10 Measured lateral pile deflection and soil movement over time

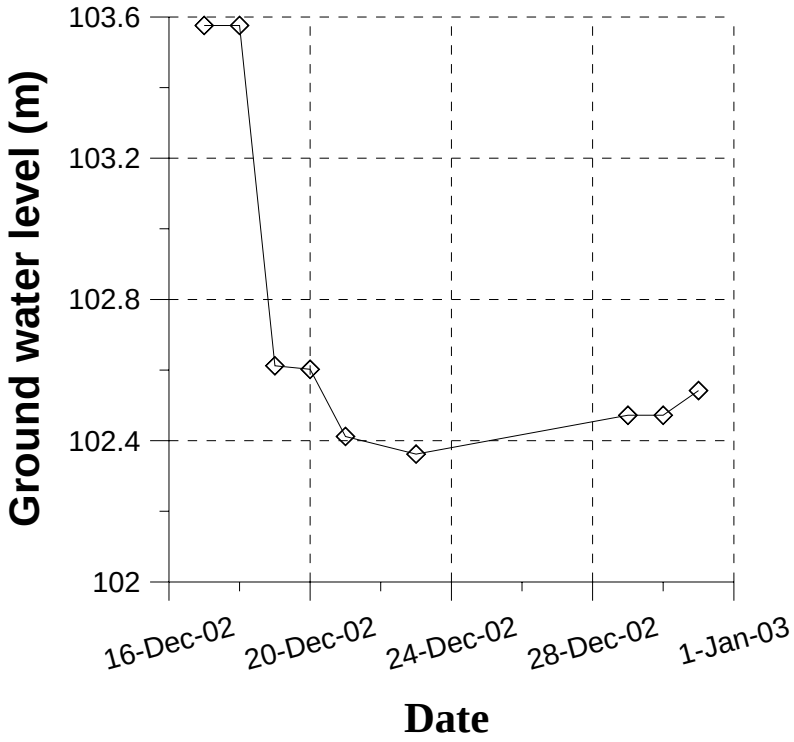

Figure 7.11 Ground water level variation before and after start of excavation

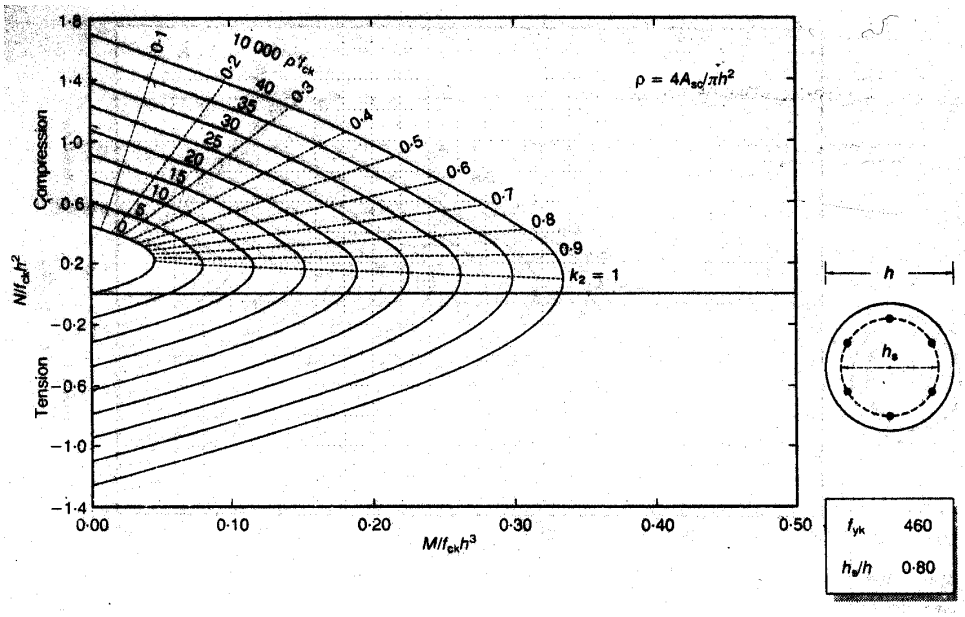

Figure 7.12 Moment interaction diagram for a circular column (after Muhammad and Merrony, 1996)

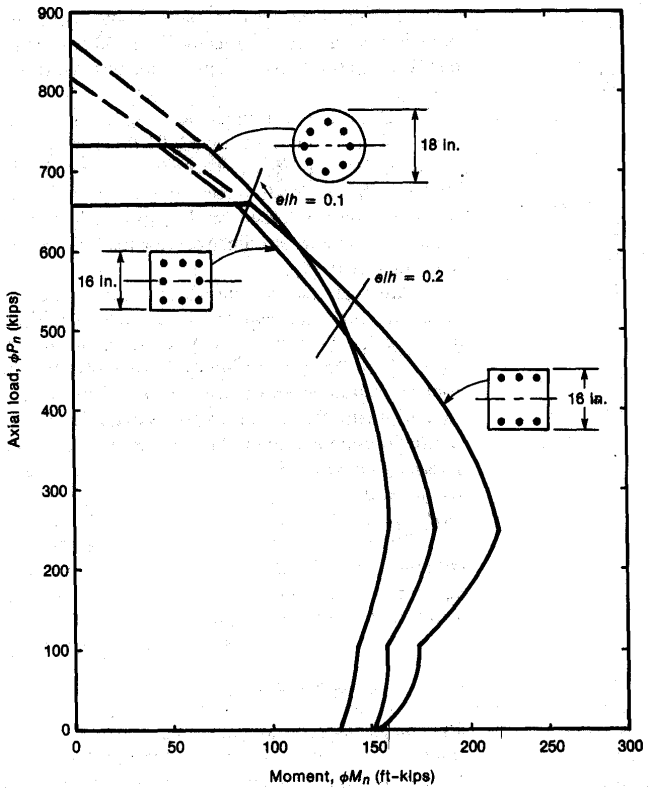

Figure 7.13 Effect of column type on shape on interaction diagram (after MacGregor, 1988)

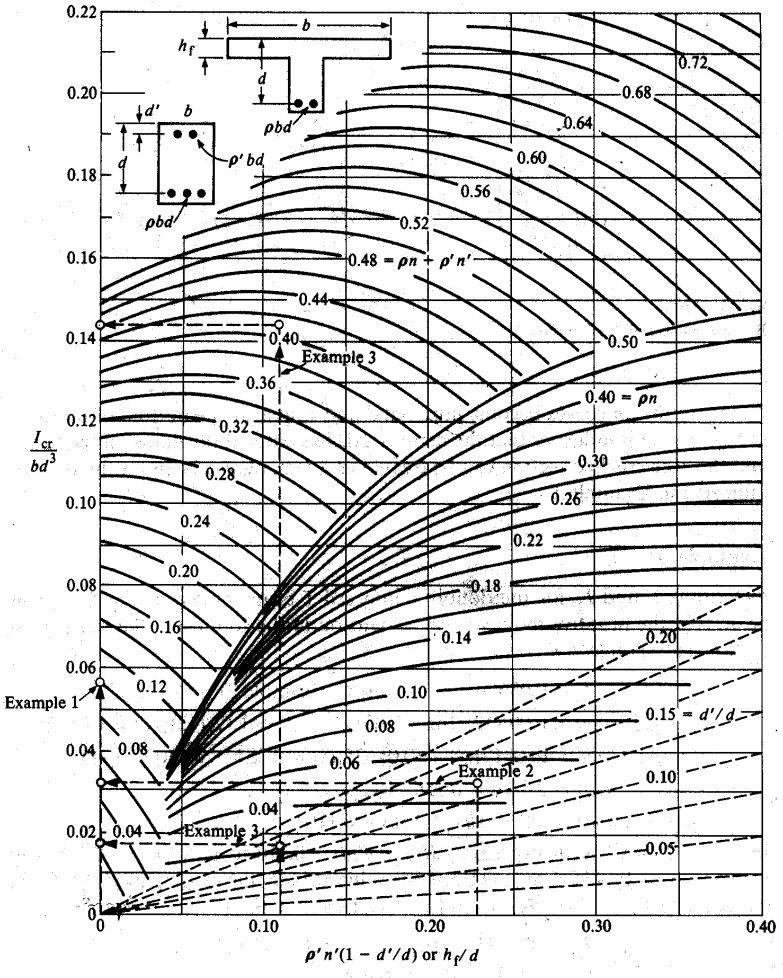

Figure 7.14 Design chart for a cracked section moment of inertia (after Lutz, 1973)

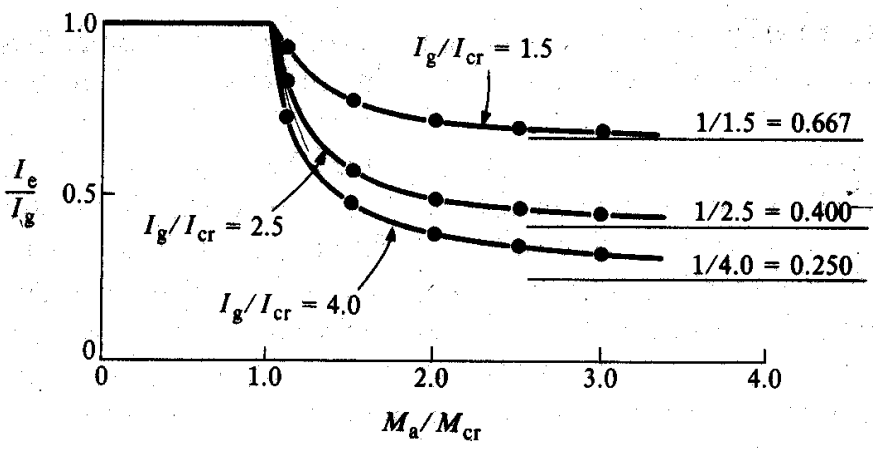

Figure 7.15 Generalised effective moment of inertia versus bending moment relation in the cracking range (after Branson, 1977)

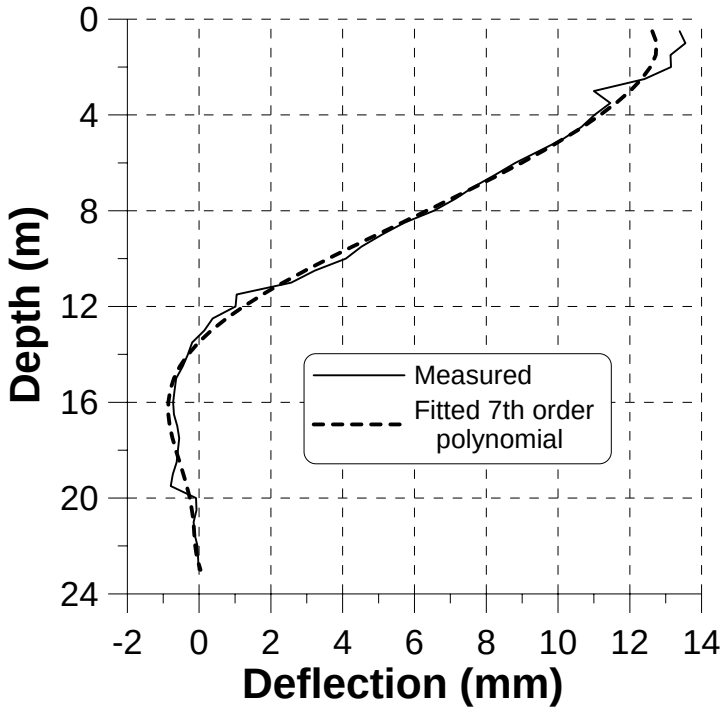

Figure 7.16 Minimum pile deflection profile to initiate cracking

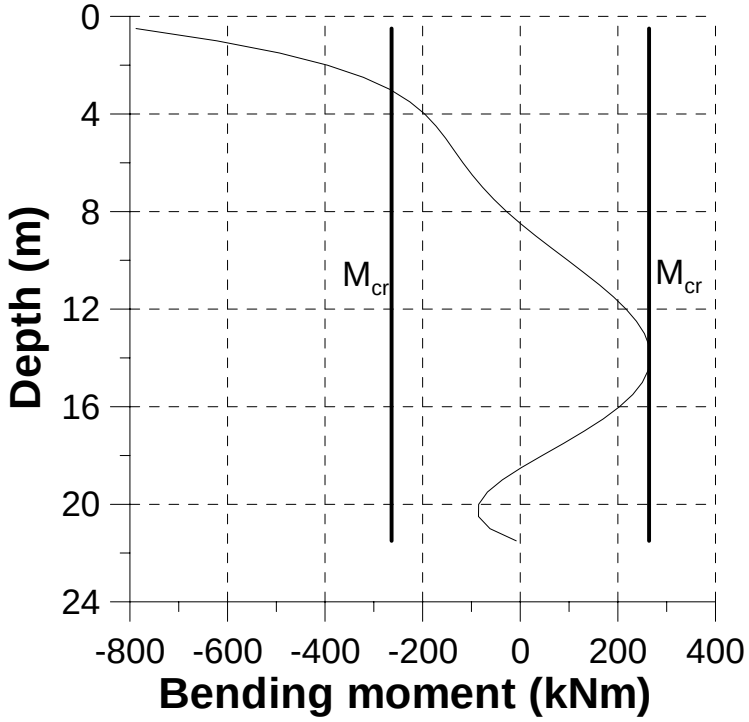

Figure 7.17 Minimum bending moment profile to initiate cracking

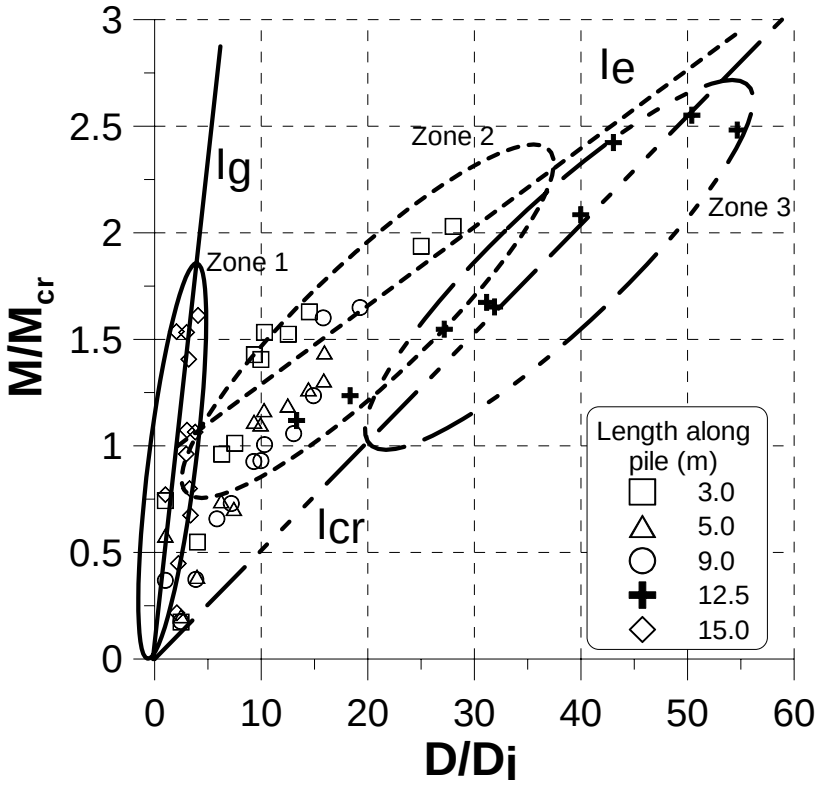

Figure 7.18 Measured bi-linear moment-deflection curve

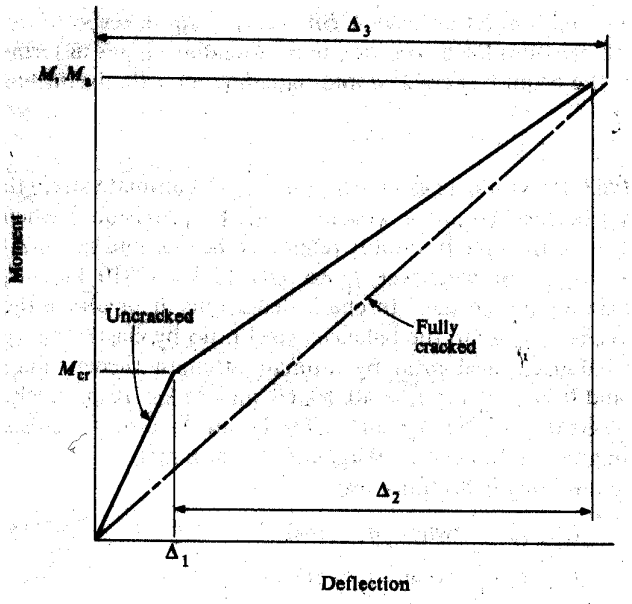

Figure 7.19 Bi-linear moment-deflection curve (after Branson, 1977)

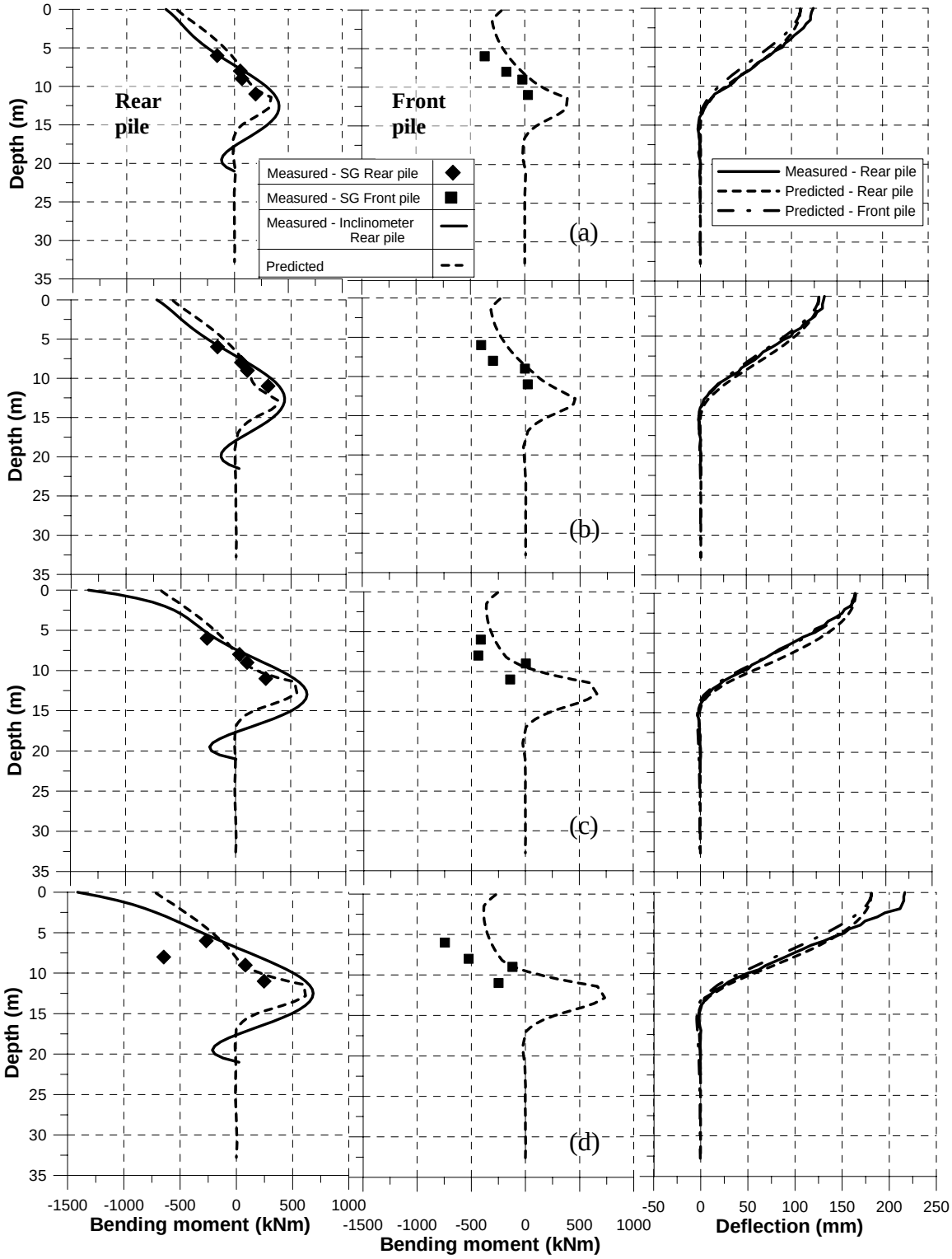

Figure 7.20 Measured and predicted bending moment and deflection profiles of piles on (a) 28 Dec 2002, (b) 31 Dec 2002, (c) 6 Jan 2003 and (d) 17 Jan 2003

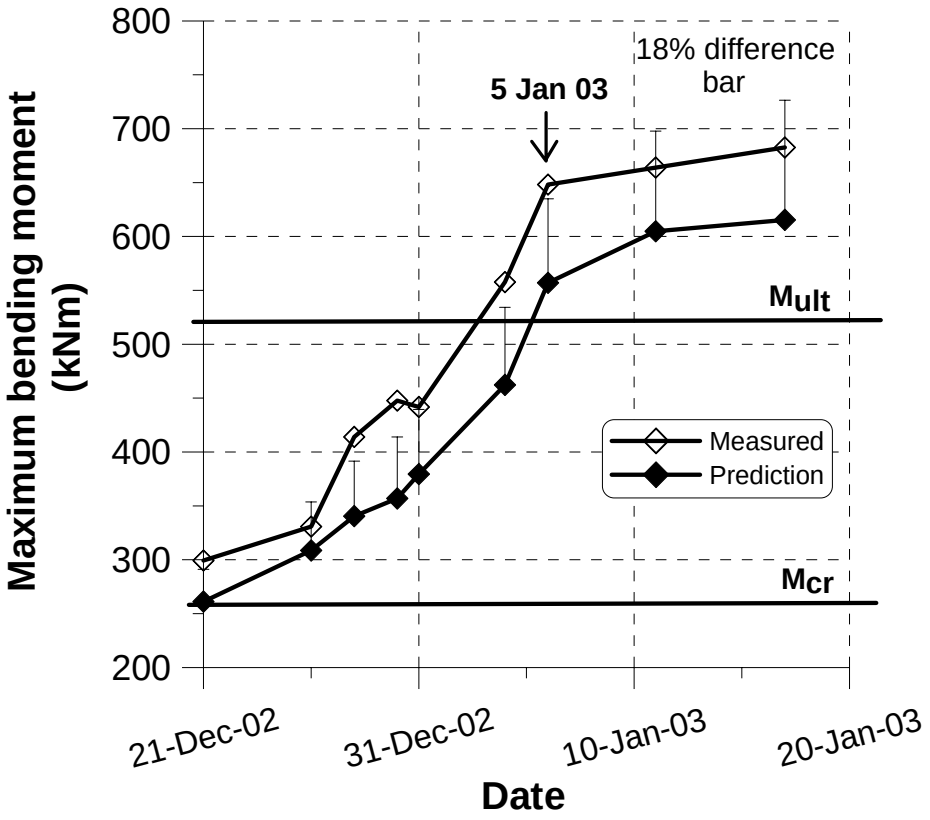

Figure 7.21 Development of measured and predicted pile maximum positive bending moment of rear pile over time

CHAPTER EIGHT

CONCLUSIONS

8.1 CONCLUDING REMARKS

Centrifuge model tests have been carried out to investigate the effects of excavation-induced soil movement on a free-headed single pile as well as free- and capped-head pile groups adjacent to an unstrutted excavation in clay behind a stable and a collapsed retaining wall. In conjunction with the model study, in-flight T-bar tests have been performed to obtain the undrained shear strength profiles before and after the excavation process. An image processing technique has also been used to measure the lateral soil movement profiles at different locations and times with reasonably good accuracy and sensitivity of displacement magnitudes. The measured free-field soil movement at the pile location and measured soil strength profile are adopted as input parameters for an existing finite element program to back analyze the measured pile responses. A field case study on a pile group subject to excavation-induced soil movement has also been carried out. The pre- and post-failure behaviour of the instrumented pile group has provided valuable data for a further understanding of the effects of soil movement on piles and also for comparison between field measurements and those predicted using the above mentioned numerical method. The findings of the studies are given as follows:

8.1.1 Single piles behind a stable retaining wall

It has been established that the development of induced pile bending moment and deflection is time dependent due to the progressive wall and soil movements after excavation. For single piles located close to the wall and much of the pile lies within the large soil deformation zone, the induced pile bending moment and deflection increase with time after excavation has been completed. However, there is relaxation in the induced pile bending moment and deflection once the soil in the deformation zone has weakened. On the other hand, for single piles located further behind the wall, the induced pile bending moment and deflection increase continuously with time. This suggests that the soil surrounding the pile may not have weakened and are still capable of offering further resistance against increasing soil movement.

It has been found that for single piles located at 3 m or more behind the stable wall, reasonably good pile responses can be predicted using an existing finite element program developed at the National University of Singapore. On the other hand, for a single pile located very close to the wall, the predicted pile bending moment and deflection are about 25% higher than the measured responses. This case is re-analyzed using the measured reduced soil strength after excavation and a much better agreement between the predicted and measured pile responses can be obtained. This supports the finding of Hull et al. (1991) that the limit soil pressure/soil strength ratio for pile subject to soil movement is significantly less than that of conventional laterally loaded piles, in particular when the magnitudes of soil movement are large as in the case of the pile located at 1 m from the wall.

8.1.2 Single piles behind a collapsed retaining wall

The performance of a single pile behind retaining walls having various degrees of instability has also been investigated. It is found that the wall would continue to move after excavation for stable and marginally stable walls, demonstrating similar time dependent phenomenon as stable walls. The wall movement would in turn cause soil movement behind the wall and this time dependent effect becomes more prominent with increasing excavation depth or decreasing wall stability. For tests experiencing wall collapse, the pile bending moment would start to reduce even before the excavation has been completed. For a pile located within the zone of significant soil movement, there is lateral soil stress relief due to excavation and the soil surrounding the piles would experience a reduction in strength that results in the relaxation of induced pile bending moment and soil pressure. This observation is reinforced by the image processing results, which reveal the occurrence of soil "flow" past the pile and tension cracks on the ground surface.

The existing numerical method is used to back-analyse the maximum pile bending moments and head deflections obtained from the centrifuge tests. In order that the performance of the pile subject to large soil movement could be reasonably well predicted, it is established that appropriate limiting soil pressure on the pile should be adopted. The limiting soil pressure derived from the measured pile bending moment profile reveals that the ratio of limiting soil pressure over soil strength proposed by Poulos and Davies (1980) is appropriate provided that the reduced soil strength profile due to stress relief upon excavation is adopted in the back-analysis. As only the soil strength profile prior to excavation is known in most practical cases, a simplified envelope of limiting soil pressure/original soil strength ratio is proposed. The induced bending moment on a pile subject to large soil movement can also be reasonably well

predicted using this proposed envelope with limiting soil pressure/original soil strength ratio established to be about 6 in this study. This finding illustrates that the reduction of K from a value of 9 for conventional laterally loaded piles to a lower value of 6 for piles subject to excavation-induced soil movements is attributed to the reduction in the undrained shear strength upon excavation. It should be noted that the magnitude of 6 is merely a back-analyzed value and may not be applicable to other situations with different wall, soil or pile conditions. The results of the present study help to clarify the above contrasting proposals of K values. The results of the back-analyses reveal that if only pre-excavation undrained shear strength profiles are available, an appropriate reduction in the K value should be adopted in order to obtain a more accurate prediction of pile responses behind an excavation with large soil movements.

8.1.3 Pile groups located behind a stable retaining wall

Centrifuge model tests involving free- and capped-head 2-, 4- and 6-pile groups in clay behind a wall that remains stable after excavation have been carried out. It is found that the induced maximum bending moment is always lower than that of a corresponding single pile at identical location. If the piles are located at the same distance behind the wall, the measured bending moment is higher if the piles serve as the front piles as opposed to the rear piles of the pile group. The induced bending moment of the front pile, which experiences greater soil movement, is moderated by the rear pile via the pile cap. The interaction between the front and rear piles induces negative bending moment at the restraint pile head, but reduces the magnitude of bending moment developed along the pile and the pile group deflection.

In a pile group, each individual pile will provide some shadowing and reinforcing effects on piles nearby. The degree of shadowing experienced by each individual pile depends on its relative position with its surrounding piles. It is observed that the

induced bending moment for the front peripheral (FP) pile is greater than that of the front centre (FC) pile at the same distance behind the wall. Similarly, the bending moment developed at the rear peripheral (RP) piles is also greater than that of the rear centre (RC) pile at the same distance behind the wall.

Soil arching effect and "separation" of soil are observed to occur between the front piles of a pile group when the soil deforms during excavation in the 4- and 6-pile groups. An arch is formed between the row of piles when the yielded soil gets detached from its surrounding. The detached soil is then forced to squeeze into the row of piles hence without significantly increasing the pressures acting on the piles.

Generally, the observed long term maximum positive bending moment would increase after excavation until about 50 days later and subsequently reduce. This behaviour is consistent to that observed for single piles. On the contrary, the maximum negative bending moment generally reduces slightly over time after excavation. This behaviour could be the result of the pile-pile cap interaction as the maximum negative pile bending moment is located close to the pile cap.

In the numerical back-analysis, the soil moderation factor, whose magnitude depends on the size of the pile group, has been proposed to account for the shadowing and reinforcing effects. Soil arching moderates the detrimental effects of excavation-induced soil movement on a pile group. It is acknowledged that as the pile cap is incapable of providing full fixity to the individual pile heads, a reduction factor for pile cap rotational stiffness is thus necessary. By adopting a consistent set of lateral soil movement moderation factor as well as reduction factor for pile cap rotational stiffness in the numerical back-analyses, the pile responses can be predicted reasonably well.

8.1.4 Pile group located behind a collapsed retaining wall

A test involving a 4-pile group in clay behind a wall that subsequently collapses after excavation has also been carried out. The long term front and rear pile bending moment and head deflection demonstrate distinct peaks at the onset of wall collapse. These peak values would then reduce significantly over time and similar observation is also noted for a single pile. The observed limiting bending moments for both front and rear piles suggest that the front pile, which experiences larger soil movement, is assisted by the rear pile through the pile cap to resist the soil movement. This further illustrates the interaction between the front and rear piles to jointly resist the excavation-induced soil movement. For the case of a pile group, the bending moment and head deflection of both the front and rear piles are smaller than those of a single pile. Thus a capped-head pile group could resist the excessive soil movement behind a collapsed wall more effectively than a single pile.

In the numerical back-analysis, fair agreement between the predicted and measured pile responses can be obtained when both the simplified envelope of limiting soil pressure distribution and the measured reduced undrained shear strength values after excavation are adopted. Therefore, the limiting soil pressure envelope developed for a single pile can also be used for a group of pile behind a collapsed wall. It is found that despite experiencing greater soil movement, both the front and rear pile responses remain unchanged suggesting that the soil limiting pressures have been reached. As such, the adoption of soil moderation factor is not necessary in the numerical analysis as the pile responses are governed by the soil limiting pressures that can be developed when the wall collapses. This is consistent to the findings deduced for a single pile located behind a collapsed wall.

8.1.5 Field study

This field study involving an instrumented pile group behind an excavation that subsequently failed has highlighted the importance of designing piles to withstand the detrimental effects of lateral soil movement on piles. The pre- and post-failure pile behaviour of the unintended failure has provided valuable data necessary for analysis and further understanding.

It is found that the measured and predicted pile bending moment and deflection profiles are generally consistent in trend. For the case of pure bending, the conservation of area method can be used to transform a circular section to a rectangular one such that the readily available design charts for the more common rectangular beam section can be utilized. Therefore, the gross, I_g and fully cracked I_{cr} moment of inertia can be determined. It has also been demonstrated that the calculation of the average effective moment of inertia, I_e can be complicated. Nevertheless, a simple analytical method by Branson (1977) based on beam theory can be used as a first approximation. The numerical analysis has been shown to explain the field results to provide a better understanding of the development of the moment of inertia, I, from an initially uncracked section to a fully cracked section. An average effective moment of inertia, I_e, can be approximated to represent the various degrees of cracking along the length of the pile so that a smooth pile bending moment profile can be obtained.

8.2 RECOMMENDATIONS FOR FURTHER STUDIES

This research has provided an insight into the fundamental behaviour of piles subject to excavation-induced soil movement in clay behind an unbraced excavation. The combination of centrifuge modeling, numerical back-analysis and field study has successfully highlighted the importance of designing piles against lateral soil

movement. Nevertheless, through the rigorous numerical back-analyses that have been performed, some weaknesses of centrifuge modeling have been observed. Some suggested improvements that can be done are listed as follows:

(i) Full rotational fixity between pile heads and pile cap can be further improved by means of welding instead of clamping the pile heads in both directions.

(ii) Various pile head conditions may be of interest for further research. For example, a fix-fix pile head condition in both translation and rotation should better represent the field condition as pile caps are normally restraint by ground beams. The ground beams may be simulated using steel or aluminium square sections that can be welded to the pile cap.

(iii) Since excavation is normally strutted in practice, it would also be of interest if a strutted excavation can be studied.

(iv) To better reflect the actual function of a load carrying pile group, it is recommended that that an externally applied axial load be used on the pile group.

(v) If a larger pile group is required for a test, a suitable container with width greater than 3 times the width of the pile cap should be used to prevent “near boundary” effects.

REFERENCES

ACI Committee 318 (1989). “Building code requirement for reinforced concrete.” American Concrete Institute, Detroit, Michigan.

Adachi, T., Kimura, M., and Kobayashi, H. (1994). “Behaviour of laterally loaded pile groups in dense sand.” Proc. Int. Conf. Centrifuge 94, Singapore, pp. 509-514.

Allersma, H. G. B. (1991). “Using image processing in centrifuge research.” Proc. Int. Conf. Centrifuge 91, Colorado, pp. 551-558.

Almeida, M. S. S., Davies, M. C. R. and Parry, R. H. G. (1985). “Centrifuge tests of embankments on strengthened and unstrengthened clay foundations.” Geotechnique, Vol. 35, No. 4, pp. 425-441.

Bolton, M. D. and Powrie, W. (1987). “The collapse of diaphragm walls retaining clay.” Geotechnique, Vol. 37, No. 3, pp. 335-353.

Bolton, M. D. and Powrie, W. (1988). “Behaviour of diaphragm walls in clay prior to collapse.” Geotechnique, Vol. 38, No. 2, pp. 167-189.

Bransby, M. F. and Springman, S. M. (1996). “3-D finite element modelling of pile groups adjacent to surcharge loads.” Journal of Computer and Geotechnics, Vol. 19, No. 4, pp. 301-324.

Bransby, M. F. and Springman, S. M. (1997). "Centrifuge modelling of pile groups adjacent to surcharge loads." Soils and Foundations, Vol. 37, No.2, pp. 39-49.

Branson, D. E. (1977). Deformation of concrete structures. McGraw-Hill.

Broms, B. B. (1964a). "Lateral resistance of piles in cohesive soils." Journal of Soil Mechanics and Foundation Engineering Division, ASCE, Vol. 90, No. SM2, pp. 27-63.

Broms, B. B. (1964b). "Lateral resistance of piles in cohesionless soils." Journal of Soil Mechanics and Foundation Engineering Division, ASCE, Vol. 90, No. SM2, pp. 123-156.

Bujang, B. K. H., Craig, W. H. and Merrifield, C. M. (1991). "Simulation of a trial embankment structure in Malaysia." Proc. Int. Conf. Centrifuge 91, Colorado, pp. 51-58.

Bujang, B. K. H. and Faisal, A. (1993). "Pile embankment on soft clay: Comparison between model and field performance." Proc. 3rd Int. Conf. on Case Histories in Geotechnical Engineering, St. Louis, Missouri, pp. 433-436.

Byrne, P. M., Anderson, D. L. and Jansen, W. (1984). "Response of pile and casings to horizontal free-field soil displacements." Canadian Geotechnical Journal, Vol. 21, pp. 720-725.

Chandrasekaran, B., Tang, S. K. and Lim, T. L. (1999). "Behaviour of piled foundation subjected to lateral movements due to deep excavation." Proc. Field Measurements in Geomechanics, Rotterdam, pp. 197-200.

Chen, C. Y. and Martin, G. R. (2002). "Soil-structure interaction for landslide stabilizing piles." Computers and Geotechnics, Vol. 29, pp. 363-386.

Chen, L. T. and Poulos, H. G. (1994). "A method of pile-soil interaction analysis for piles subjected to lateral soil movements." Proc. 8th Int. Conf. on Computing Methods and Advances in Geomechanics, Vol. 3, pp. 2311-2316.

Chen, L. T. and Poulos, H. G. (1997). "Piles subjected to lateral soil movements." Journal of Geotechnical and Geoenvironmental Engineering, Vol. 123, No. 9, pp. 802-811.

Chow, Y. K. (1996). "Analysis of piles used for slope stabilization." Int. Journal for Numerical and Analytical Methods in Geomechanics." Vol. 20, pp. 635-646.

Chow, Y. K. and Yong, K. Y. (1996). "Analysis of piles subject to lateral soil movements." Journal of The Institution of Engineers Singapore, Vol. 36, No. 2, pp. 43-49.

Coutts, D. R. and Wang, J. (2000). "Monitoring of reinforced concrete piles under horizontal and vertical loads due to tunneling." Tunnels and Underground Structures, pp. 541-546.

Craig, W. H. (1995). "Geotechnical centrifuges: past, present and future." Geotechnical Centrifuge Technology, London: Blackie Academic & Professional, pp. 1-18.

Davies, M. C. R. and Jones, A. M. (1998). "Image acquisition using an on-board film camera." Proc. Int. Conf. Centrifuge 98, Tokyo, pp. 67-71.

Davies, M. C. R. and Parry, R. H. G. (1982). "Determining the shear strength of clay cakes in the centrifuge using a vane." Geotechnique, Vol. 32, No. 1, pp. 59-62.

De Beer, E. E and Wallays, M. (1972). "Forces induced in piles by unsymmetrical surcharges on the soil around the piles." Proc. 5th European Conf. on Soil Mechanics and Foundation Engineering, Madrid, Vol. 1, pp. 325-332.

De Beer, E. E. (1977). "Piles subjected to static lateral loads." State-of-the-Art Report, Proc. 9th Int. Conf. on Soil Mechanics and Foundation Engineering, Specialty Session 10, Tokyo, pp. 1-14.

Dewoolkar, M. M., Ko, H. Y. and Pak, R. Y. S. (1998). "Suitability of total stress stress gauges for soil pressure measurements." Proc. Int. Conf. Centrifuge 98, Japan, pp. 129-134.

Ellis, E. A. and Springman, S. M. (1998). "Centrifuge and numerical modeling of piled bridge abutments on soft clay." Proc. Int. Conf. Centrifuge 98, Japan, pp. 557-562.

Ellis, E. A. and Springman, S. M. (2001). "Full-height piled bridge abutments constructed on soft clay." Geotechnique, Vol. 51, No. 1, pp. 3-14.

Finno, R. J., Lawrence, S. A. and Harahap, I. S. (1991). "Analysis of performance of pile groups adjacent to deep excavation." Journal of Geotechnical Engineering, ASCE, Vol. 117, No. 6, pp. 934-955.

Fukuoka, M. (1977). "The effects of horizontal loads on piles due to landslides." Proc. 9th Int. Conf. on Soil Mechanics and Foundation Engineering, Specialty Session 10, Tokyo, pp. 77-80.

Goh, A. T. C., Teh, C. I. and Wong, K.S. (1997). "Analysis of piles subjected to embankment induced lateral soil movements." Journal of Geotechnical and Geoenvironmental Engineering, Vol. 123, No. 9, pp. 792-801.

Hannink, G. and van Tol, A. F. (1988). "Large horizontal displacements of houses in Rotterdam." Proc. 2nd Int. Conf. on Case Histories in Geotechnical Engineering, St. Louis, Missouri, pp. 1409-1415.

Holtz, R. D. and Kovaks, W. D. (1981). An Introduction to Geotechnical Engineering. Prentice-Hall.

Hull, T. S. and McDonald, P. (1992). "Lateral soil movement loading in bridge foundation piles." Proc. 6th ANZ Conf. on Geomechanics, Christchurch, pp. 146-150.

Ismes, V. F. and Taylor, R. N. (1991). "Centrifuge modeling of embankment construction on soft clay foundations." Proc. 16th European Conf. on Soil Mechanics and Foundation Engineering, Vol. 1, pp. 83-86.

Ito, T. and Matsui, T. (1975). "Methods to estimate lateral force acting on stabilizing piles." Soils and Foundations, Vol. 15, No. 4, pp. 43-59.

Jaky, J. (1948). "Pressures in soils." Proc. 2nd Int. Conf. on Soil Mechanics and Foundation Engineering, Vol. 1, pg. 103.

Juneja, A. (2003). "Centrifuge model study of the effects of sand compaction pile installation on soft clay ground." Ph.D Thesis, National University of Singapore.

Kalteziotis, N., Zervogiannis, F., Seve, G. and Berche, J. (1993). "Experimental study of landslide stabilization by large diameter piles." Proc. Geotechnical Engineering of Hard Soils-Soft Rocks, pp. 1115-1124.

Katakami, N., Saitoh, K., Katagiri, M., Satoh Y. and Furuyama, S. (1998). "Lateral resistance behaviour of pile in sandy ground subjected to excavation." Proc. Int. Conf. Centrifuge 98, Tokyo, pp. 527-532.

Kimura, T., Takemura, J., Hiro-Oka, A., Okamura, M. and Park, J. (1994). "Excavation in soft clay using an in-flight excavation." Proc. Int. Conf. Centrifuge 94, Singapore, pp. 649-654.

Kong, F. K. and Evans, R. H. (1987). Reinforced and prestressed concrete. 3rd Edition. Van Nostrand Reinhold (U.K.) Co. Ltd.

Kongsomboon, T. (2002). "Behaviour of an embedded improved soil berm in an excavation." Ph.D Thesis, National University of Singapore.

Law, Y. (2000). "Effect of lateral soil movements on pile groups." Final Year Thesis, National University of Singapore.

Lee, F. H. (1992). "The National University of Singapore Geotechnical Centrifuge – User's Manual." Research Report No. CE 001. Department of Civil Engineering, National University of Singapore.

Lee, F. H., Juneja, A., Dasari, G. R. and Tan, T. S. (2002). "Performance of total stress cells in model experiments in soft clays." Proc. Int. Conf. on Physical Modeling in Geotechnics, pp. 101-106.

Lee, F. H., Tan, T. S. and Yong, K. Y. (1993). "Excavation in residual soils with high permeability." Proc. 11th Southeast Asia Geotechnical Conf., Singapore, pp. 739-744.

Lee, F. H., Tan, T. S., Leung, C. F., Yong, K. Y., Karunaratne, G. P. and Lee, S. L. (1991). "Development of geotechnical centrifuge facility at the National University of Singapore." Proc. Int. Conf. Centrifuge 91, Colorado, pp. 11-17.

Lee, Y. (1995). "Centrifuge modelling of deep excavations." Final Year Thesis, National University of Singapore.

Leung, C. F., Chow, Y. K. and Shen, R. F. (2000). "Behaviour of pile subject to excavation-induced soil movement." Journal of Geotechnical and Geoenvironmental Engineering, Vol. 126, No. 11, pp. 947-954.

Leung, C. F., Lim, J. K., Shen, R. F. and Chow, Y. K. (2003). "Behaviour of pile groups subject to excavation-induced soil movement." Journal of Geotechnical and Geoenvironmental Engineering, Vol. 129, No. 1, pp. 58-65.

Lim, J. K. (2001). "Behaviour of piles subject to excavation-induced soil movement." M.Eng Thesis, National University of Singapore.

Loganathan, N., Poulos, H. G. and Stewart, D. P. (2000). "Centrifuge model testing of tunneling-induced ground and pile deformations." Geotechnique, Vol. 50, No. 3, pp. 283-294.

MacGregor, J. G. (1988). Reinforced concrete: mechanics and design. Prentice Hall.

Marche, R. (1973). Discussion, Specialty Session No. 5, Proc. 8th Int. Conf. for Soil Mechanics and Foundation Engineering, Moscow, Vol. 4.3, pp. 247-253.

Maugeri, M., Castelli, F. and Motta, E. (1994). "Analysis of piles in sliding soil." Proc. 3rd Int. Conf. on Deep Foundation Practice Incorporating Piletalk, Singapore, pp. 191-196.

Matsui, T., Won, P. H. and Ito, T. (1982). "Earth pressures on piles in a row due to lateral soil movements." Soils and Foundations, Vol. 22, No. 2, pp. 71-80.

Menzies, B. (1997). "Applying modern measures." Ground Engineering, Vol. 30, pp. 22-23.

Moh and Associates (S) Pte. Ltd. (2001). Report on soil investigation works for proposed 8-storey industrial development.

Mohammad, F. A. and Merrony, B. (1996). "Design charts for reinforced concrete circular columns in accordance with Eurocode2." Proc. Institution of Civil Engineers, Structure and Buildings, Vol. 110, pp. 71-80.

Moser, A. (1973). Discussion, Specialty Session No. 5, Proc. Int. Conf. on Soil Mechanics and Foundation Engineering, Moscow, Vol. 43, pp. 252-253.

Mroueh, M and Shahrour, H. (1999). "Three-dimensional analysis of the interaction between tunneling and pile foundations." Proc. Numerical Models in Geomechanics – NUMOG VII, pp. 397-402.

Ou, C. Y., Liao, J. T. and Cheng, W. L. (2000). "Building response and ground movements induced by a deep excavation". Geotechnique, Vol. 50, No. 3, pp. 209-220.

Ovesen, N. K. (1979). "The scaling law relationship." Panel Discussion, Proc. 7th European Conf. on Soil Mechanics and Foundation Engineering, Brighton, No. 4, pp. 319–323.

Poh, T. Y., Goh, A. T. C., Wong K. S., Wong, I. H. and Poh, K. B. (1999). "Determination of BM in diaphragm wall." Field Measurements in Geomechanics, pp. 229-234.

Poulos, H. G. (1994). "Piles subjected to externally-imposed soil movements." Development in Geotechnical. Engineering, pp. 491-499.

Poulos, H.G., (1997). "Failure of a building supported on piles." Proc. Int. Conf. on Foundation Failures, Singapore, pp. 53-66.

Poulos, H. G. and Chen, L. T. (1995a). "Design of reinforcing pile to increase slope stability." Canadian Geotechnical Journal, Vol. 32, No. 5, pp. 808-818.

Poulos, H. G. and Chen, L. T. (1995b). “Model tests on single piles subjected to lateral soil movement.” Soils and Foundations, Vol. 35, No. 4, pp. 85-92.

Poulos, H. G. and Chen, L. T. (1996). “Pile response due to unsupported excavation-induced lateral soil movement.” Canadian Geotechnical Journal, Vol. 33, pp. 670-677.

Poulos, H. G. and Chen, L. T. (1997). “Pile response due to excavation-induced lateral soil movement.” Journal of Geotechnical and Geoenvironmental Engineering, Vol. 123, No. 2, pp. 94-99.

Poulos, H. G. and Davis, E. H. (1980). Pile foundation analysis and design. John Wiley & Sons, New York.

Powrie, W. (1985). Discussion. “Performance of propped and cantilevered rigid walls.” Geotechnique, Vol. 35, No. 4, pp. 546-548.

Powrie, W. (1986). “The behaviour of diaphragm walls in clay.” Ph.D Thesis, Cambridge University.

Randolph, M. F. and Houlsby, G. T. (1984). "The limiting pressure on a circular pile loaded laterally in cohesive soil”. Geotechnique, Vol. 34, No. 4, pp. 613-623.

Reese, L. C. (1997). "Analysis of laterally loaded piles in weak rock". Journal of Geotechnical and Geoenviromental Engineering, Vol. 33, No. 11, pp. 1010-1017.

Schmidt, H. G. (1977). "Large diameter bored piles for abutments." Proc. 9th Int. Conf. on Soil Mechanics and Foundation Engineering, Specialty Session 10, Tokyo, pp.107-112.

Schofield, A. N. (1980). "Cambridge geotechnical centrifuge operations." Geotechnique, Vol. 20, No. 3, pp. 227-268.

Shen, R. F. (1999). "Pile behaviour due to excavation-induced soil movement." M.Eng Thesis, National University of Singapore.

Sommer, H. (1977). "Creeping slope in a stiff clay." Proc. 9th Int. Conf. on Soil Mechanics and Foundation Engineering, Specialty Session 10, Tokyo, pp.113-118.

Springman, S. M., Bolton, M. D. and Randolph, M. F. (1991). "Modeling the behaviour of piles subjected to surcharge loading." Proc. Int. Conf. Centrifuge 91, Colorado, pp. 253-260.

Stewart, D. P. (1992). "Lateral loading of piled bridge abutments due to embankment construction." Ph.D Thesis, University of Western Australia.

Stewart, D. P. and Randolph, M. F. (1991). "A new site investigation tool for the centrifuge." Proc. Int. Conf. Centrifuge 91, Colorado, pp. 531-538.

Stewart, D. P., Jewell, R. J. and Randolph, M. F. (1994a). "Design of piled bridge abutments on soft clay for loading from lateral soil movements." Geotechnique, Vol. 44, No. 2, pp. 277-296.

Stewart, D. P., Jewell, R. J. and Randolph, M. F. (1994b). "Centrifuge modeling of piled bridge abutments on soft ground." Soils and Foundations, Vol. 32, No. 1, pp. 41-51.

Tatsuoka, F., Okahara, M., Tanaka, T., Tani, K., Morimoto, T. and Siddiquee, M. S. A. (1991). "Progressive failure and particle size effect in bearing capacity of a footing in sand." Proc. ASCE Geotechnical Engineering Congress 1991, Vol. II (Geotechnical Special Publication 27), pp. 788-802.

Taylor, R. N. (1995). "Centrifuges in modeling: principles and scale effects." Geotechnical Centrifuge Technology, London: Blackie Academic & Professional, pp. 19-33.

Viagianni, C. (1981). "Ultimate lateral load on piles used to stabilize landslides." Proc. 10th Int. Conf. on Soil Mechanics and Foundation Engineering, Stockholm, Vol. 3, pp. 555-560.

Wei, J. (1997). “Centrifuge modeling of deep excavations.” M.Eng Thesis, National University of Singapore.

Weiler, W. A. Jr. and Kulhawy, F. H. (1982). “Factors affecting stress cell measurements in soil.” Journal of Geotechical Engineering Division, ASCE, Vol. 108, No. GT12, pp. 1529-1548.

Zeng, X. and Lim, S. L. (2002). “The influence of variation of centrifugal acceleration and model container size on accuracy of centrifuge test.” Geotechnical Testing Journal, Vol. 25, No. 1, pp. 24-43.